DEPARTMENT OF ELECTRONIC AND ELECTRICAL ENGINEERING
LOUGHBOROUGH UNIVERSITY OF TECHNOLOGY

PERFORMANCE STUDY OF HIGH RESOLUTION ALGORITHMS IN SONAR SIGNAL PROCESSING

BY

SUN CHAO, B.Sc

A doctoral thesis
submitted in partial fulfilment of the requirement for the award of
doctor of philosophy of the Loughborough University of Technology

June 1992

Supervisor : Professor J.W.R. Griffiths, B.Sc. (Eng), Ph.D, F.Eng, F.I.E.E, F.I.O.A.
Department of Electronic and Electrical Engineering

Performance Study of High Resolution Algorithms in Sonar Signal Processing

ABSTRACT

In the last two decades or so there has been great interest in the problem of estimating signal parameters from the measurements at sensor array outputs. The most important parameters are probably the directions-of-arrival (DOAs) at the array from radiating sources in the observed spatial field. This thesis is devoted to the study of algorithms and techniques which have been suggested from different points of view for the same direction estimation problem. Several classes of algorithms are examined which include the conventional beamforming methods, eigenstructure based algorithms, subspace rotation methods, decompositions techniques, and the more recently proposed weighted subspace fitting methods.

The research in this thesis contains three main aspects addressing theoretical analyses, computer simulations, and practical experiments respectively. A set of simulation programs has been developed to evaluate the performance in various scenarios, and Monte Carlo tests have been carried out to support theoretical analyses. The simulation work was carried out on an IBM PC, and the computer language used was MATLAB (Matrix Laboratory), a package especially developed for matrix computations.

A sonar system available in the sonar research group at Loughborough University of Technology (LUT) was modified and used to collect real data for off-line processing so as to demonstrate the algorithm performance in real experimental environments. Two scenarios were examined when the system worked in passive and active modes respectively. In the passive working mode, two emitters were employed to give uncorrelated or strongly correlated signals by using the same or different working frequencies. When working in the active mode, a single sensor was placed on the top of the receiving array which received reflections from two targets in the distance. The data was captured and then saved on floppy disks from the measurement system and processed on PCs.

A large number of results are presented, analysed, and summarized in the thesis, including both computer simulations and practical measurements. This provides a fundamental ground for further work in this and related areas.

ACKNOWLEDGEMENT

I would like to express my sincere gratitude to my supervisor, Professor J.W.R. Griffiths, for his guidance, support and encouragement throughout the research. Although he was ill and away in the last few months of my study, he was still concerned with the progress of my thesis and the appointment of the examiners. I am very grateful for having such a supervisor and hope that he will recover very soon.

Professor C.F.N. Cowan became my supervisor for the last several months of my Ph.D study due to Professor Griffiths' illness. I wish to thank him for his careful reading of my thesis and his editorial comments, and also for his help in arranging the examination.

I would also like to thank the Chinese Government, Sir Y.K. Pao, and the British Council for their financial support. Mrs. Linda Marshall is especially remembered for her encouragement, kindness and help.

I want to say thanks to Mr. Tahseen Ali Rafik who is my colleague in the Research Group. The signal acquisition system in the measurement system for the experiments in this thesis was originally designed and built by him. I am grateful to him for allowing me to use it.

I would like to extend my thanks to Mrs. Sheila Clarson and all the colleagues in the Sonar Research Group and in the Signal Processing Laboratory for their help and friendship, especially to Dr. Guojun Lu whose encouragement will always be remembered.

Mrs. Janet Steveson helped to correct language errors in the thesis. She has always been kind and supportive the discussions over my thesis. Her help is appreciated.

To my beloved husband, LiBin, I will always be greatly indebted. Being away from him made the first two and a half years of my Ph.D study the hardest time in my life. It was his endless love, patience, and encouragement that enabled me to complete my study.

I am very grateful to my parents and my sister and brother for everything they have given to me. I dedicate this thesis to my family.

CONTENTS

LIST OF SYMBOLS AND ACRONYMS

AIC	Akaike Information Criterion
AP	Alternating Projection
CBF	Conventional BeamForming
CFAR	Constant False Alarm Rate
CPDF	Conditional Probability Density Function
CRB	Cramer Rao Bound
Det-ML	Deterministic Maximum Likelihood
DFT	Discrete Fourier Transform
DICANNE	Digital Interference Cancelling Adaptive Null Network Equipment
DOA	Direction of Arrival
ESPRIT	Estimation of Signal Parameters via Rotation Invariance Techniques
FINE	FIrst priNciple Eigenvector
FINES	FIrst priNciple Eigenvectors
IFA	Iterative Filtering Algorithm
IMP	Incremental Multi-stage Parameter estimation
LP	Linear Predication
LR	Likelihood Ratio
LS	Least Squares
MDL	Minimum Description Length
MEM	Maximum Entropy Method (Burg's Method)
MNM	Minimum Norm Method (K-T Method)
MODE	Method of Direction Estimation
MUSIC	MUltiple SIgnal Characterisation (Schmidt's Method)
MD-MUSIC	Multi-Dimensional MUSIC
MVM	Minimum Variance Method (Capon's Method)
SNNR	Signal plus Noise to Noise Ratio
SNR	Signal to Noise Ratio
SR	Subspace Rotation
SSF	SubSpace Fitting

Sto-ML	Stochastic Maximum Likelihood
TAM	Toeplitz Approximation Method (Kung's Method)
TLS	Total Least Squares
WB^2	Wagstaff and Berrou Broadband method
WSF	Weighted Subspace Fitting
w.p.1	with probability one
w.r.t	with respect to

$\mathbf{A}$	array manifold matrix
$\mathbf{A}^+$	pseudo inverse of $\mathbf{A}$, $\mathbf{A}^+ = (\mathbf{A}^H \cdot \mathbf{A})^{-1} \cdot \mathbf{A}^H$
$\mathbf{C}$	pre-conditioning matrix in IMP
$\mathbf{D}$	first derivative matrix of $\mathbf{A}$
$\mathbf{E}$	eigenvector matrix of sample covariance matrix, $\mathbf{E} = [\mathbf{e}_1, \cdots, \mathbf{e}_m]$
$\mathbf{E}_S$	matrix of signal eigenvalues as column vectors
$\mathbf{E}_N$	matrix of noise eigenvalues as column vectors
$\mathbf{E}_S'$	matrix having same elements of $\mathbf{E}_S$ with first row deleted
$\mathbf{E}_N'$	matrix having same elements of $\mathbf{E}_N$ with first row deleted
$\mathbf{G}$	generalised array manifold in ESPRIT
$\mathbf{P}_A$	projection matrix onto column space of $\mathbf{A}$
$\mathbf{P}_A^-$	projection matrix onto null space of $\mathbf{A}$
$\mathbf{R}$	sample covariance matrix
$\mathbf{R}_{XX}$	auto-correlation matrix of subarray X in ESPRIT
$\mathbf{R}_{XY}$	cross-correlation matrix between subarrays X and Y in ESPRIT
$\mathbf{S}$	source covariance matrix
$\mathbf{X}_N$	data matrix of N independent snapshots, of dimension $m \times N$
Φ	diagonal matrix representing the relation between measurements from two subarrays in ESPRIT
$\mathbf{a}$	steering vector (array manifold vector)
$\mathbf{c}$	column vector having first elements of noise subspace eigenvectors
$\mathbf{d}$	searching vector in MNM
$\mathbf{e}_i$	ith eigenvector of sample covariance matrix
$\mathbf{g}$	column vector having first elements of signal subspace eigenvectors, or generalised steering vector in ESPRIT

$\mathbf{n}(t)$	noise measurement of the whole array at time instant t, of dimension $m \times 1$
$\mathbf{s}(t)$	signal sample at time instant t, of dimension $d \times 1$
$\mathbf{x}(t)$	measurement of the whole array at time instant t, of dimension $m \times 1$
$\mathbf{u}_1$	first unit vector, $\mathbf{u}_1 = [1, 0, \cdots, 0]^T$
$\mathbf{w}$	weighting coefficient vector
$L(\theta)$	criterion function in ML estimators
$P(\theta)$	power spectrum of array output
$n_j(t)$	noise measured at jth sensor
$s_i(t)$	ith signal received at array
$\hat{s}_i(t)$	Hilbert transform of $s_i(t)$
$\tilde{s}(t)$	analytical form of $s_i(t)$
$u_i(t)$	amplitude modulation function of $s_i(t)$
$v_i(t)$	phase modulation function of $s_i(t)$
$x_j(t)$	noisy measurement at jth sensor
$y(t)$	array output
c	propagation speed of the wavefront
d	number of signals
$g(\theta)$	direction characteristics of array sensors
l	Euclidean length
m	number of sensors
N	number of snapshots
Δ	inter-element spacing in metric of wavelength or displacement vector in ESPRIT
ω_o	centre frequency of signal
ρ_{ij}	correlation coefficient between $s_i(t)$ and $s_j(t)$
σ^2	noise variance
τ	time delay
$Tr(\mathbf{A})$	trace of $\mathbf{A}$
$det(\mathbf{A})$	determinant of $\mathbf{A}$
$rank(\mathbf{A})$	rank of $\mathbf{A}$
$R(\mathbf{A})$	range of $\mathbf{A}$
$N(\mathbf{A})$	null space of $\mathbf{A}$

CHAPTER 1

INTRODUCTION

The problem of detecting signals in background noise and estimating their properties such as direction, waveform, etc. has attracted great interest in the last several decades. Research in this field is concerned with theoretical studies and practical implementation which have brought up a vast number of algorithms and applications in different practical situations. This thesis discusses the most typical algorithms or methods which represent different underlying philosophies and possess potential use in practice, and presents computer simulation results and practical results of the considered algorithms. In this chapter, we describe briefly the history of array signal processing focusing on the modern period of its development, give the motivation and significance of the research in this thesis, summarize the contributions, and present the organization of subsequent chapters.

1.1 Historical Perspective

Array signal processing has a very long history which dates back at least to 1795 [Pro95]. Arrays of sensors replacing a single sensor provide much better determination of the directions of incident signals and also increase the output signal to noise ratio by a factor proportional to the number of sensors in the arrays. The resolution of a linear array with equispaced omnidirectional sensors is determined by the size of the array which, in turn, is determined by the number of sensors and the inter-element spacing. Two sources can be separated only if their separation is larger than the inverse of the array aperture (this is described as the Rayleigh criterion). To increase the resolution of an array implies either adding more sensors in the array or increasing the inter-element spacing; the former increases cost and the latter causes grating lobes. Also, the physical size of an array is limited by practical considerations. This is the main problem inherent in the conventional beamforming method whose resolution is restricted by the Rayleigh criterion.

The improvement in the array resolution was marked by the method proposed by Burg in 1967 [Bur67, Bur68] which is now commonly known as the Maximum Entropy Method (MEM). This method modifies the zero assumption on the unavailable correlation lags by fitting an AR model to the given data. A spectrum is formed and the directions of sources are determined by locating the peaks in the spectrum.

Capon's method proposed in 1969 [Cap69] is also a modification of the conventional beamforming method. He found that the output of the array in one direction is formed by input in that direction and also contributions from other directions. The aim of Capon's method is to eliminate interferences while maintaining the response in the wanted direction as unity and, therefore, to improve the resolving ability of the array. Again, the estimated directions of sources are found at the maxima of the resulting spectrum.

Both Burg's and Capon's methods provide better resolution than the conventional beamforming method, and the term "high resolution" came into being. However, the underlying structure of the estimation problem was still unexploited. The method that so far attracts most interest, MUSIC, and so-called eigenstructure based methods are in a class of methods which exploit the structure of the problem. Work in this direction was pioneered by Ligget [Lig73], and Brillinger [Bri75] who related the well-studied factor-analysis techniques in statistics with sensor array processing. Pisarenko [Pis73] used the theorem of Caratheodory regarding the trigonometrical moment problem in complex analysis to develop a different method for the same problem. And independently, Berni [Ber75] proposed a similar approach which is more direct and less complicated. Pisarenko's method was refined and generalised by Schmidt [Sch79] and Bienvenu and Kopp [BK80]. In their methods, all those eigenvectors of the covariance matrix corresponding to its smallest eigenvalues are used in constructing the estimator and, therefore, make better use of the available information. Furthermore, the array geometry is released to arbitrary geometries and the sources are not necessarily uncorrelated as long as they are not fully correlated, i.e., coherent.

During the same time, Reddi [Red79] proposed a different method which is applicable only to uniform linear arrays. His method was latterly interpreted by Kumaresan and Tufts [KT83] and modified to be the method known as Minimum Norm Method (MNM) or KT method.

All these methods which have been mentioned so far, except the most basic conventional beamforming method, share one common shortcoming, i.e., they are unable to resolve coherent sources. Multiple dimensional algorithms which search all existing sources

simultaneously can be used for coherent sources at the cost of much higher computation load. As a result of an extensive study of direction-of-arrival estimation techniques, the spatial smoothing technique was suggested by Evans et al [EJS81] and was shown to provide a very attractive solution to coherent problems in the case of a uniform linear array. In this technique, the array is divided into overlapping subarrays, the modified covariance matrix is formed by averaging covariance matrices at each subarray and used to estimate the source directions in conjunction with eigenstructure based algorithms. One disadvantage of this technique is that it reduces the effective aperture of the array significantly. To increase the effective aperture of the array, the modified spatial smoothing technique was suggested by Evans et al [EJS85] with an effort of not having to increase the computational burden significantly. A proof of this modified spatial smoothing technique was provided in [WPMS88] and the conditions under which the modified algorithm may fail were also shown.

Concerning the problem of coherence, the conventional beamforming technique is superior to MEM, MVM, MUSIC, and MNM. This method resolves coherent sources when they are sufficiently separated. As the separation decreases, this method fails to work no matter whether the sources are coherent or not. Recently, a novel method was proposed by Clarke and studied by Mather [Cla87, Cla88, Cla89a,b, Mat89a,b] modifying the conventional beamforming method. The relevant algorithm, the so-called IMP (Incremental Multi-stage Parameter) algorithm, uses the conventional beamscan as its basic processing procedure and adopts adaptive techniques. At each stage of the algorithm, all other sources but the one under refinement are eliminated by putting correspondent projections into their directions. The procedure is repeated alternatively for all sources and the algorithm terminates when some pre-defined criterion is satisfied.

When using the MUSIC method, knowledge of the array geometry is essential although this can be arbitrary. This knowledge is usually obtained by calibrating the array, i.e., measuring the array responses for all possible combinations of parameters and saving these responses in some form for later referencing. In general, array calibration is a time-consuming and difficult task. The ESPRIT (Estimation of Signal Parameter via Rotational Invariance Techniques) algorithm proposed in 1985 [PRK85, RPK86, RK87, RK89, OK90, etc.] avoids this task by setting a constraint on the array. In this method, sensors are replaced by doublets holding a constant displacement vector between two sensors in each pair which possess identical characteristics. Measurements are collected from two subarrays which are composed of one sensor in each doublets. The relative displacement vector in each doublet is used in the final determination of the directions of sources rather than the array manifold.

Concerning the problem of estimation of source parameters, a huge number of methods, algorithms, and techniques have been proposed. Some of them are analyzed and compared mainly with MUSIC, the method which has been taken as the best algorithm for quite a long time. Viberg and Ottersten [VOK89, VO91, OV88, OWVK89, etc.] proposed a framework to include several popular algorithms in a single framework and lead to different algorithms when the data are used in different ways and the searching is implemented in different spaces. The Cramer-Rao Bound (CRB) which gives a lower bound for the covariance matrix of the estimate error of any unbiased estimate is used as a measure for assessment of algorithm performance. Their framework includes one-dimensional searching methods, such as the Conventional BeamForming method (CBF) and the MUlti SIgnal Characterisation method (MUSIC), multidimensional methods such as Maximum Likelihood Method (MLM) and Multi-Dimensional MUSIC (MD-MUSIC), and ML- and Total Least Squares (TLS-) ESPRIT, etc. Based on this framework a new algorithm for sensor array processing is deduced. This is the so-called optimal Weighted Subspace Fitting (WSF) method. The optimal weighting was obtained by minimizing the covariance matrix of the estimate error with respect to (w.r.t.) the weighting matrix, and the resulting method was shown approaching the CRB asymptotically for both uncorrelated and coherent cases. The performance of WSF was proven to be superior to that of MUSIC and other algorithms. But the optimality of the optimal WSF method is achieved at the cost of heavy computational burden.

1.2 · Motivation for the Research in this Thesis and Contributions

One thing is obvious: whether an algorithm is optimal, sub-optimal, or totally inadequate is dependent on the problem which is going to be resolved. An overall optimal algorithm does not exist, at least not so far. Choosing a suitable method for the problem under consideration is of importance and significance especially in practical situations. A basis for doing so is to obtain a comprehensive understanding of the algorithms and their performance under possible conditions. A thorough study of the algorithm performance is possible by means of theoretical analysis and also computer simulations. This will be greatly helpful to practical applications of these techniques.

Many papers have appeared in the literature concerning the analysis and comparison of algorithm performance. But these are by no means exhaustive. Theoretical studies attract much more attention, particularly those algorithms that provide superior resolution and involve complicated mathematical computations. By the use of high speed digital processing

these methods seem to be attractive. However they are impractical for real-time processing in many situations. By comparison the practical considerations of the high resolution methods are mentioned less.

Some modern algorithms do not restrict the sensor array to a uniform linear array or any other regular form, as long as the knowledge of the array geometry is available; in practice, however, the most commonly used array has always been the one of the simplest, the uniform linear array. The array manifold of the uniform linear array has an analytical form which coincidentally is of the Vandermonde form. This property of the array allows more algorithms to be applicable than other array geometries and, at the same time, the applied algorithms can be simplified correspondingly.

The work which has been done in this thesis falls mainly into two categories: computer simulations and practical experiments. In the computer simulation part, many algorithms and methods were analyzed theoretically and simulated on the computer. These algorithms include the Maximum Entropy Method (MEM) and Minimum Variance Method (MVM) belonging to adaptive techniques, Minimum Norm Method (MNM) and the popular MUSIC method representing eigenstructure based methods, and their versions, the ESPRIT technique, the IMP algorithm in the class of deconvolution techniques, and the novel optimal Weighted Subspace Fitting (WSF) method and the multidimensional Maximum Likelihood Method (MLM). A large number of results were obtained and analyzed to give a straightforward understanding and also to support the theoretical calculations. Monte Carlo experiments were carried out to show the asymptotic properties of these methods. Three statistics about the results were examined and presented which are the probability of resolution, bias of the angular estimates, and their standard deviation. The results are given as functions of signal to noise ratios and angular separations, respectively, which are thought as two important parameters in the estimation problem. The correlation between the two sources is also considered by assigning different correlation factors in the simulations which demonstrate the effect of the correlation on the algorithm performance.

In the practical experiment part, an air acoustic sonar array in the research group was modified for the purpose of evaluating different algorithms and methods which have been discussed in the simulation part of the thesis. The sonar array was tested when working in two different modes: first receiving signals radiated from emitters placed at a distance, and then receiving signals reflected from the targets when a single emitter was used at the receiving array. In the first mode, two types of signals were used which worked at different frequencies and the

same frequency, respectively, to imitate weakly correlated sources and strongly correlated sources. When working in the second mode, a single emitter was used at one frequency. For both cases, the separation between the two sources / targets was varied and several measurements under each separation were taken. The measurements were saved for later processing. Estimates of directions of arrival were calculated by using most of the discussed methods and tabulated to show the performance of these methods in practical situations.

Although mathematical modelling provides a better means than ever for the problem under consideration here and analytical expressions show the performance in varying circumstances, computer simulations give a better demonstration of these methods under practical situations. The results from practical measurements are inevitably more powerful in explaining the behaviour of different algorithms in real situations. The work presented in this thesis is by no means exhaustive but it does provide a better reference in selecting a suitable method for practical applications.

1.3 Organization of the Thesis

This thesis includes theoretical analyses of several sensor array processing algorithms, performance comparisons between them, simulation results of these algorithms showing their performance, and practical results obtained from an air sonar system which was available in the research group. Before detailed discussions, a data model is formed as a basis for the later presentation of the algorithms, and a literature survey of high resolution techniques is also presented. The thesis is outlined as follows:

Chapter 2 Problem Formulation and Mathematical Preliminaries

This chapter presents the passive sensor array problem, formulates signal, noise, and array models, and states basic assumptions and definitions. Two fundamental maximum likelihood estimators, deterministic and stochastic estimators, are introduced together with their statistical properties. Some mathematical concepts, such as subspaces, eigen-decomposition of covariance matrices and singular value decomposition of data matrices, are briefly described.

Chapter 3 Literature Survey of Direction-of-Arrival Estimation Techniques

This chapter includes the presentation of typical algorithms and techniques in each stage of

the evolution of sensor array processing which are of interest. Based on the model and assumptions and definitions in the previous chapter, methods such as conventional beamforming, maximum entropy, minimum variance, MUSIC, and minimum norm, etc. are discussed in more detail than those novel methods including ESPRIT, IMP, and WSF which will be discussed later in relevant chapters with numerical examples.

Chapter 4 Performance Comparison of Spectral and Root Versions of MEM, MVM, MUSIC, and MNM

Root versions of single stage spectral methods can only be applied to uniform linear arrays while some of their spectral versions are applicable to arbitrary array geometries. Constrained to uniform linear arrays, this chapter compares, analytically and by simulations, the performance of different versions of these methods.

Chapter 5 ESPRIT Algorithm

LS- and TLS-ESPRIT are two popular versions of the same ESPRIT algorithm with different consideration of the noise terms in the measurements, which have been shown to be asymptotically equivalent. This chapter mainly concerns the properties of the LS-ESPRIT and its performance comparison with the better known MUSIC technique, both spectral and root versions.

Chapter 6 IMP Algorithm

The IMP algorithm is the main topic of this chapter as a representative of the class of decomposition techniques. The implementation of the IMP algorithm is discussed and so is the selection of the subject threshold in terminating the procedure. Numerical examples are presented with convergence plots to illustrate the iterations in this method for different orders of model. Monte Carlo experiments have been carried out to compare the performance of IMP to that of MUSIC showing their similarity under the weak correlation case and the advantages of IMP in the highly correlated case.

Chapter 7 Weighted Subspace Fitting Methods

The more recently proposed weighted subspace fitting methods are analysed in this chapter. Initialisation of the parameter estimates is crucial in this class of methods. The Alternating

Projection method of Ziskind and Wax is employed in the initialisation procedure and the modified Gauss-Newton method in the iterative searching. The implementation of this class of methods is discussed and the method with optimal weighting coefficients is compared with the multidimensional Maximum Likelihood estimator to demonstrate its performance advantage in the asymptotic case.

Chapter 8 Discussion of Computer Simulation Results

A summary of a vast number of results provided in previous chapters is given in this chapter in order to draw a clearer picture about the performance of different methods under consideration in this thesis. This serves as a useful guide when applying these methods to the practical experiments.

Chapter 9 Practical Measurements with Different Algorithms

Based on a sonar system which was available in the research group, tests were carried out in the air to explore the performance of the algorithms that have been simulated in previous chapters in the practical situations. A brief description of the system is given in this chapter and so are the modifications that have been done for the task in this thesis. Several cases which are commonly encountered in practical situations are considered. Measurements from the array outputs were saved on floppy disks and processed off-line. This chapter presents results given by different methods using the collected data and a discussion of these results.

Chapter 10 Conclusion and Suggestion for Further Work

The work covered in this thesis is more theoretical than practical, although some practical experiments have been carried out and the results been analysed. A thorough study of algorithm performance provides a useful foundation for future practical applications in this or related fields. Some suggestions for following work in sonar signal processing are given since possibilities of applying high resolution algorithms in practical systems are getting larger as the development of electronics and mathematical algorithms progresses.

1.4 Notations

In this thesis, a somewhat standard notation is used to make the presentation as clear as possible. Lower case italic roman characters denote scalars. Lowercase bold characters are generally used to represent vectors with elements denoted by subscripted lower case italic characters, e.g., a_i representing the ith element of vector **a**. Upper case bold characters generally refer to matrix and its (i,j) entry is usually denoted by corresponding characters in lower italic case with two subscripts, e.g., a_{ij} is the (i,j) entry of matrix **A**. Operators are usually denoted by superscripts, such as $(\cdot)^*$ denotes the conjugate operator, $(\cdot)^T$ the transpose operator, and $(\cdot)^H$ the conjugate transpose or Hermitian transpose.

Several characters are conventionally used to represent some variables. These will be described in following chapters in relevant places.

CHAPTER 2

PROBLEM FORMULATION AND MATHEMATICAL PRELIMINARIES

Before going into details of algorithms and their performance, the problem to which algorithms and techniques discussed in this thesis are applied is formulated first. The task of this chapter is this problem formulation and associated assumptions and considerations concerning the sensor array, the medium and the sources. Notations and representations are introduced for the convenience of theoretical derivations which will greatly simplify the problem under consideration and provide insight into the underlying signal and noise models and make it possible to understand the problem and its solution more thoroughly.

In this chapter, we present the data model on which the following analysis will be based. In forming this model, the arrays in use, propagation medium, as well as signals and noise are of great significance and some assumptions are essential for the following discussion. We provide, in this chapter, some general assumptions and mathematical representations for signals and noise received at the array under consideration. Specific requirement on array geometries, signals, etc. will be given with the algorithm in need of them.

For most algorithms used to solve the estimation problem, the sensor array may possess an arbitrary configuration and no analytical expression is available for the sensor responses. What is needed in these algorithms concerning the array is an array calibration table. But although most algorithms do not constrain the array geometry, the most commonly used array in practice is the uniform linear array in which sensors are equispaced on a line. Uniform linear arrays are considered in this thesis for analytical simplicity.

Concerning signal waveforms, two main models have appeared in the literature which assume deterministic and stochastic waveforms respectively. These two signal models are suitable

for different applications. Their statistical properties and likelihood functions are discussed, herein, after presenting the more general assumptions on signals : the narrowband signal assumption, and their complex representation.

Generally, the sensor noise is modelled as a Gaussian random process, which is justified by the central limit theorem. Second order moments of sensor noise are given in section 3. Based on the given array, signal and noise models, the problem is formulated in section 4 and the model extension is also given therein. A brief description of some mathematical definitions and theorems are provided in section 5 for convenience in the following discussion. The final section of this chapter, section 6, is devoted to maximum likelihood estimators.

2.1 Arrays

The sensor array under consideration in this thesis is a passive sensor array which only receives signals. This kind of array is often encountered in underwater acoustics as well as many other research fields such as radio or satellite communications, seismic applications, etc.

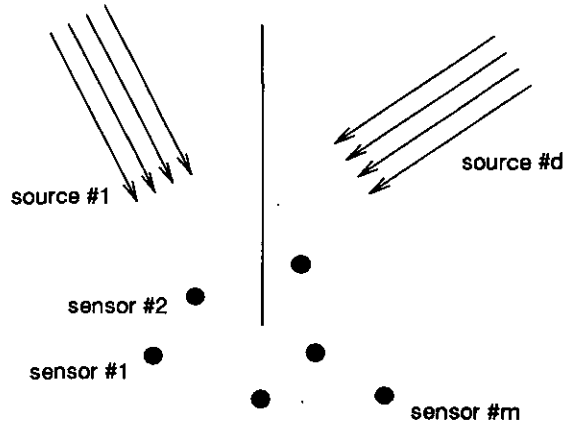

Figure 2.1 A passive sensor array receiving plane waves from far-field point sources

Figure 2.1 depicts a sensor array of m sensors arranged in an arbitrary geometry in a plane, receiving the wavefronts from d point sources which are assumed to be in the far field. The transmission medium is assumed to be homogeneous and isotropic, so the propagation of signals is along straight lines and the wavefronts of signals can be approximated as planar when they arrive at the array. Therefore, the measured output from each sensor is a super-position of

delayed and scaled replicas of the transmitted signals from individual emitters and noise (or is a linear combination of the d incident wavefronts and noise). Let $s_1(t), \cdots, s_d(t)$ denote the d signal waveforms, the measured output of the kth sensor, $x_k(t)$, is modelled by

$$x_k(t) = \sum_{i=1}^{d} g_k(\theta_i) \cdot s_i(t - \tau_k(\theta_i)) + n_k(t) \tag{2.1}$$

where $g_k(\theta_i)$ represents the sensitivity of the kth sensor to the signal in direction θ_i, $\tau_k(\theta_i)$ is the time delay of the ith signal at the kth sensor relative to the reference sensor (or reference point, which is usually the centriod of the array in arbitrary array geometry cases), and $n_k(t)$ denotes an additive noise term. The measured array output is formed by collecting the outputs at m sensors in the m-vector $\mathbf{x}(t)$

$$\mathbf{x}(t) = \begin{bmatrix} x_1(t) \\ x_2(t) \\ \cdot \\ \cdot \\ \cdot \\ x_m(t) \end{bmatrix} = \begin{bmatrix} \sum_{i=1}^{d} g_1(\theta_i) \cdot s_i(t - \tau_1(\theta_i)) \\ \sum_{i=1}^{d} g_2(\theta_i) \cdot s_i(t - \tau_2(\theta_i)) \\ \cdot \\ \cdot \\ \cdot \\ \sum_{i=1}^{d} g_m(\theta_i) \cdot s_i(t - \tau_m(\theta_i)) \end{bmatrix} + \begin{bmatrix} n_1(t) \\ n_2(t) \\ \cdot \\ \cdot \\ \cdot \\ n_m(t) \end{bmatrix} \tag{2.2}$$

and more compactly

$$\mathbf{x}(t) = \mathbf{G} \cdot \mathbf{s}(t) + \mathbf{n}(t) \tag{2.3}$$

where

$$\mathbf{x}(t) = \begin{bmatrix} x_1(t) \\ x_2(t) \\ \cdot \\ \cdot \\ \cdot \\ x_m(t) \end{bmatrix}, \quad \mathbf{G} = \begin{bmatrix} g_1(\theta_1), \cdots, g_1(\theta_d) \\ g_2(\theta_1), \cdots, g_2(\theta_d) \\ \cdot \quad \cdot \quad \cdot \\ \cdot \quad \cdot \quad \cdot \\ \cdot \quad \cdot \quad \cdot \\ g_m(\theta_1), \cdots, g_m(\theta_d) \end{bmatrix}, \quad \mathbf{s}(t) = \begin{bmatrix} s_1(t) \\ s_2(t) \\ \cdot \\ \cdot \\ \cdot \\ s_d(t) \end{bmatrix}, \quad \mathbf{n}(t) = \begin{bmatrix} n_1(t) \\ n_2(t) \\ \cdot \\ \cdot \\ \cdot \\ n_m(t) \end{bmatrix} \tag{2.4}$$

A kind of sensor array with special constraints on the array geometry is most commonly used

in practical applications rather than arrays of arbitrary geometry. They are uniform linear arrays (ULA), in which the sensors are spaced equi-distant spaced on a line. ULA(Δ) is usually used to denote a uniform linear array with inter-element spacing Δ, as shown in figure 2.2.

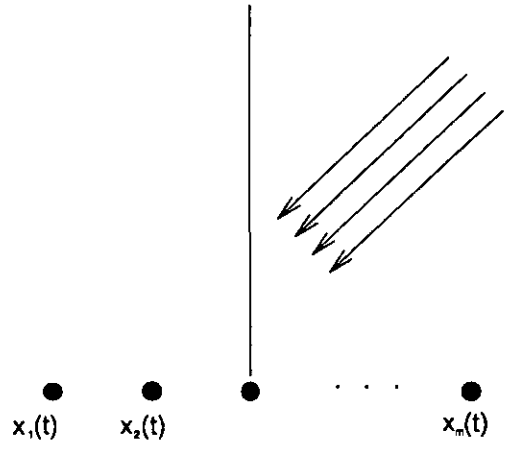

Figure 2.2 A plane wave impinging on a uniform linear array

Let the first sensor be the reference sensor, the time delay of the *i*th signal at *k*th sensor is calculated as

$$\tau_k(\theta_i) = (k-1)\tau_o(\theta_i) = (k-1)\cdot\frac{\Delta}{c}\cdot \mathrm{Sin}\,\theta_i \tag{2.5}$$

where $\tau_o(\theta_i) = (\Delta/c)\cdot \mathrm{Sin}\,\theta_i$ is the time delay of the *i*th signal between two adjacent sensors, and c is the propagation speed of the wavefront. If the array sensors are of identically directional characteristics, $g(\theta)$, then the array output can be rewritten as

$$\mathbf{x}(t) = \begin{bmatrix} x_1(t) \\ x_2(t) \\ \cdot \\ \cdot \\ \cdot \\ x_m(t) \end{bmatrix} = \begin{bmatrix} \sum_{i=1}^{d} g(\theta_i)\cdot s_i(t)) \\ \sum_{i=1}^{d} g(\theta_i)\cdot s_i(t-\Delta\,\mathrm{Sin}\,\theta/c) \\ \cdot \\ \cdot \\ \cdot \\ \sum_{i=1}^{d} g(\theta_i)\cdot s_i(t-(m-1)\Delta\,\mathrm{Sin}\,\theta/c) \end{bmatrix} + \begin{bmatrix} n_1(t) \\ n_2(t) \\ \cdot \\ \cdot \\ \cdot \\ n_m(t) \end{bmatrix} \tag{2.6}$$

Furthermore, if omnidirectional sensors are used in the sensor array, the sensitivity will be equal in all directions for all sensors implying that $g(\theta)$ is constant, which can be taken as unity without loss of generality. Once more, we have the written array output as

$$\mathbf{x}(t)=\begin{bmatrix} x_1(t) \\ x_2(t) \\ \cdot \\ \cdot \\ \cdot \\ x_m(t) \end{bmatrix} = \begin{bmatrix} \sum_{i=1}^{d} s_i(t) \\ \sum_{i=1}^{d} s_i(t-\Delta \operatorname{Sin}\theta/c) \\ \cdot \\ \cdot \\ \cdot \\ \sum_{i=1}^{d} s_i(t-(m-1)\Delta \operatorname{Sin}\theta/c) \end{bmatrix} + \begin{bmatrix} n_1(t) \\ n_2(t) \\ \cdot \\ \cdot \\ \cdot \\ n_m(t) \end{bmatrix} \tag{2.7}$$

2.2 Signals

Concerning signals emitted by far-field sources and received at the sensor array, some assumptions are also necessary.

Assume the signals are narrowband, and have the same known centre frequency, ω_o. Thus, the ith signal can be modelled as a sinusoid with frequency ω_o and slowly time-varying amplitude and phase

$$s_i(t) = u_i(t) \cdot \operatorname{Cos}(\omega_o t + v_i(t)) \tag{2.8}$$

where slowly time-varying functions $u_i(t)$ and $v_i(t)$ modulate the amplitude and phase of $s_i(t)$ respectively. The definition of slowly time-varying, herein, means that the amplitude and phase variations as functions of spatial position for time instant t are negligible over the aperture of the array, i.e.,

$$\begin{aligned} s_i(t-\tau_k(\theta_i)) &= u_i(t-\tau_k(\theta_i)) \cdot \operatorname{Cos}\{\omega_o \cdot (t-\tau_k(\theta_i)) + v_i(t-\tau_k(\theta_i))\} \\ &\approx u_i(t) \operatorname{Cos}\{\omega_o \cdot (t-\tau_k(\theta_i)) + v_i(t)\} \end{aligned} \tag{2.9}$$

For narrowband signals, complex envelope representation is a more suitable form to describe the signals. In this representation, a so-called analytic signal, $\bar{s}(t)$, is constructed by combining

the original real signal $s(t)$ and its Hilbert transform $\hat{s}(t)$ in the following way,

$$\bar{s}(t) = s(t) + j\hat{s}(t) \tag{2.10}$$

where $j = \sqrt{-1}$, and the Hilbert transform $\hat{s}(t)$ of $s(t)$ is defined as

$$\hat{s}(t) = \int_{-\infty}^{\infty} \frac{s(\sigma)}{t-\sigma} d\sigma \tag{2.11}$$

which actually shifts the phase of the signal $s(t)$ by 90°, i.e.,

$$\hat{s}(t) = u(t) \cdot \mathrm{Sin}(\omega_o t + v(t)) \tag{2.12}$$

Thus, the analytic signal $\bar{s}(t)$ can be written in the form of

$$\begin{aligned} \bar{s}(t) &= u(t) \cdot \mathrm{Cos}(\omega_o t + v(t)) + j \cdot u(t) \cdot \mathrm{Sin}(\omega_o t + v(t)) \\ &= u(t) \cdot e^{j(\omega_o t + v(t))} \end{aligned} \tag{2.13}$$

Obviously, the original real signal $s(t)$ can be easily recovered from the analytic signal $\bar{s}(t)$ by taking the real part.

Recalling the narrowband assumptions, for all moderate time delays τ, $u(t) \approx u(t-\tau)$ and $v(t) \approx v(t-\tau)$, so the time delays τ can be simply expressed as a phase shift as

$$\begin{aligned} \bar{s}(t-\tau) &= u(t-\tau) \cdot e^{j(\omega_o \cdot (t-\tau) + v(t-\tau))} \\ &\approx u(t) \cdot e^{j(\omega_o t + v(t))} \cdot e^{-j\omega_o \tau} \\ &= \bar{s}(t) \cdot e^{-j\omega_o \tau} \end{aligned} \tag{2.14}$$

Substituting the complex representation of the signal into equation (2.7)

$$\tilde{\mathbf{x}}(t) = \begin{bmatrix} \sum_{i=1}^{d} \tilde{s}_i(t) \\ \sum_{i=1}^{d} \tilde{s}_i(t) \cdot e^{-j\omega_o \cdot \Delta \sin\theta_i / c} \\ \cdot \\ \cdot \\ \cdot \\ \sum_{i=1}^{d} \tilde{s}_i(t) \cdot e^{-j\omega_o \cdot (m-1) \cdot \Delta \sin\theta_i / c} \end{bmatrix} + \begin{bmatrix} n_1(t) \\ n_2(t) \\ \cdot \\ \cdot \\ \cdot \\ n_m(t) \end{bmatrix}$$

$$= \sum_{i=1}^{d} \mathbf{a}(\theta_i) \cdot \tilde{s}_i(t) + \mathbf{n}(t) \tag{2.15}$$

where

$$\mathbf{a}(\theta_i) = \left[1, e^{-j\omega_o \Delta \sin\theta_i / c}, \cdots, e^{-j\omega_o (m-1) \Delta \sin\theta_i / c}\right]^T \tag{2.16a}$$

and

$$\mathbf{n}(t) = [n_1(t), \cdots, n_m(t)]^T \tag{2.16b}$$

Defining

$$\mathbf{A}(\Theta) = [\mathbf{a}(\theta_1), \cdots, \mathbf{a}(\theta_d)] \tag{2.17}$$

$$\tilde{\mathbf{s}}(t) = [\tilde{s}_1(t), \cdots, \tilde{s}_d(t)]^T \tag{2.18}$$

the measurement model for the passive sensor array narrowband signal processing problem can be represented as

$$\tilde{\mathbf{x}}(t) = \mathbf{A}(\Theta) \cdot \tilde{\mathbf{s}}(t) + \mathbf{n}(t) \tag{2.19}$$

where the complex d-vector $\tilde{\mathbf{s}}(t)$ contains the received signal waveforms, the Θ represents the unknown signal parameter vector. The columns of $\mathbf{A}(\Theta)$, $\mathbf{a}(\theta_i), i = 1, \cdots, d$, are usually referred to as the steering vectors or array manifold vectors. They represent the complex array responses to unit wavefronts from the directions-of-arrival of interest. In more general cases, steering vectors may depend on more than one parameter per source, which might include bearing and elevation angle, range, polarization, centre frequency, etc. Concerning

the DOA estimation problem considered in this thesis, the parameter space of interest is defined as the compact set in which the signal direction θ is allowed to vary, and a more general matrix **A** is defined as the array manifold in the following way.

Definition 2.1 *The array manifold,* **A**, *is defined as the collection of all array response vectors* $\mathbf{a}(\theta)$ *over the parameter space of interest*

$$\mathbf{A} = \{\mathbf{a}(\theta) \mid \theta \in \Theta\} \tag{2.20}$$

In the application of DOA estimation problems, most algorithms require knowledge of **A**. This can be done in two ways, either by analytical calculations or by array calibration. For azimuth only DOA estimation, the array manifold is a one-parameter manifold which may be expressed in an analytical form if the sensor characteristics and the array geometry are known. For more general cases, expressing the array response as a function of the incident angles is impossible, and a procedure usually referred to as array calibration is applied. This is an experimental procedure in which the array outputs, when one source is present, are measured as a function of the parameter to be estimated, collected and stored. This can be a time-consuming task, particularly when the array is large and more than one parameter is to be estimated. However, it does provide an alternative to the incredibly complex modelling for some array geometries.

Besides the knowledge of the array manifold, another factor about the array geometry which must be considered is the array ambiguity. The existence of array ambiguities makes the mapping from the steering vectors to the DOAs not one-to-one, so the DOA estimates will not be unique even when steering vectors are determined. Thus, an assumption is made that ambiguity is not allowed in the array manifold. This can be stated in the following way : For any collection of d distinct DOAs, $\theta_i \in \Theta, i = 1, \cdots, d$, the corresponding steering vectors are linearly independent.

For the uniform linear array, the array manifold is a collection of steering vectors possessing the structure shown in equation (2.16a), which are addressed as Vandermonde vectors. If the DOAs are restricted within $[-\pi/2, \pi/2]$ and the inter-element spacing Δ is less than a half-wavelength, $\lambda/2$, such an array can be shown to be unambiguous.

2.3 Noise

Throughout this thesis, the noise at array sensors is modelled as a zero mean, stationary and white random process with equal variance σ^2 for independent components. This is a natural assumption due to the fact that the sensor noise can often be regarded as a super-position of several "error sources" and the central limit theorem applies. Its distribution is complex Gaussian which implies that its real and imaginary parts are independent, identically distributed Gaussian processes. Such a noise process $\mathbf{n}(t)$ has second moments as follows :

$$\begin{aligned} E[\mathbf{n}(t)\cdot\mathbf{n}^H(s)] &= \sigma^2\mathbf{I}\delta_{t,s} \\ E[\mathbf{n}(t)\cdot\mathbf{n}^T(s)] &= \mathbf{0} \end{aligned} \tag{2.21}$$

For a stationary, temporally and spatially white, complex Gaussian random process, $\mathbf{n}(t)$, with zero mean, the noise covariance is $E[\mathbf{n}(t)\cdot\mathbf{n}^H(t)] = \sigma^2\mathbf{I}$

2.4 Problem Formulation and Model Extension

In preceding sections, we have made appropriate assumptions on array, signal, and noise, and defined models. Now we come to formulate the estimation problem.

The array outputs modelled in (2.19) are simultaneously sampled at N time instants, and the measurements are collected into a data matrix $\mathbf{X}_N$

$$\mathbf{x}(t) = \mathbf{A}(\Theta)\cdot\mathbf{s}(t) + \mathbf{n}(t) \qquad t = 1,\cdots,N \tag{2.22a}$$

$$\mathbf{X}_N = [\mathbf{x}(1), \mathbf{x}(2), \cdots, \mathbf{x}(N)] \tag{2.22b}$$

The tilde in (2.19) representing the complex signals is omitted in the above equations and from now on. These simultaneous measurements at the array output are usually referred to as the snapshots of the array outputs. Given these N observations, the estimation problem generally consists of estimating the following three quantities

1) The number of signals, d
2) The signal parameters, Θ
3) The signal waveforms, $\mathbf{s}(t)$, $t = 1,\cdots,N$

The problem of estimating the number of signals, d, is often referred to as the detection problem. The knowledge of the number of signals present in the scene is crucial in most high resolution algorithms, and many approaches have been suggested [Sch81, WK85, WZ88, VOK91, etc.] for the detection problem in order to ascertain the anticipated performance of estimation algorithms. The problem of most interest in this thesis is the signal parameter estimation problem.

Under the assumption that the signal wavefronts are independent from the noise process, the covariance matrix of the array output is of the form

$$\mathbf{R} = \mathrm{E}[\mathbf{x}(t) \cdot \mathbf{x}^H(t)] = \mathbf{A}(\Theta) \cdot \mathbf{S} \cdot \mathbf{A}(\Theta) + \sigma^2 \mathbf{I} \tag{2.23}$$

which is commonly referred to as the array (or sample) covariance matrix. Strictly speaking, $\mathbf{R}$ coincides with the covariance of the observation vector only when the signals are assumed to have zero mean. Matrix $\mathbf{S}$ in equation (2.23) is defined as

$$\mathbf{S} = \mathrm{E}[\mathbf{s}(t) \cdot \mathbf{s}^H(t)] \tag{2.24}$$

and referred to as the signal (or source) covariance matrix. All of the signals incident onto the array may be uncorrelated, partially correlated or completely correlated (or coherent) with each other. In particular, for two jointly stationary signals $s_i(t), s_j(t)$ (*cf.* eqn.(2.8)), the correlation coefficient between them is defined as

$$\rho_{ij} = \frac{\mathrm{E}[s_i(t) \cdot s_j(t)^*]}{\sqrt{\mathrm{E}[|s_i(t)|^2]\,\mathrm{E}[|s_j(t)|^2]}} \tag{2.25}$$

and from the Schwatz inequality (*cf.* [Cra61]), it is known that $|\rho_{ij}| \leq 1$. And

$$\begin{aligned} \rho_{ij} = 0 \quad &<=> \quad s_i(t), s_j(t) \text{ are uncorrelated} \\ 0 < |\rho_{ij}| < 1 \quad &<=> \quad s_i(t), s_j(t) \text{ are partially correlated} \\ |\rho_{ij}| = 1 \quad &<=> \quad s_i(t), s_j(t) \text{ are coherent} \end{aligned}$$

Correspondingly, matrix **S** is diagonal when the incident waveforms represented by the elements of **S** are uncorrelated, and is singular when **S** contains coherent pairs. In more general cases, **S** is positive definite which reflects the arbitrary degrees of pair-wise correlations occurring between the incident waveforms. When the signal waveforms are non-coherent, the signal covariance matrix, **S**, has full rank. However, in some applications specular multipath is common and **S** may be ill-conditioned or even rank deficient. The methods to be studied are of particular interest when the rank of **S** is less than d. In general, let the rank of the $d \times d$ signal covariance matrix be d'.

With N observations $\mathbf{x}(1), \mathbf{x}(2), \cdots, \mathbf{x}(N)$ available, the sample covariance matrix of the array is formed and denoted by $\hat{\mathbf{R}}$

$$\hat{\mathbf{R}} = \frac{1}{N} \sum_{t=1}^{N} \mathbf{x}(t) \cdot \mathbf{x}^H(t) \tag{2.26}$$

A further assumption is that the following limit exists

$$\mathbf{S} = \lim_{N \to \infty} \frac{1}{N} \sum_{t=1}^{N} \mathbf{s}(t) \cdot \mathbf{s}^H(t) \tag{2.27}$$

then sample covariance matrix will converge to the array covariance matrix as the number of snapshots goes infinite

$$\mathbf{R} = \lim_{N \to \infty} \frac{1}{N} \sum_{t=1}^{N} \mathbf{x}(t) \cdot \mathbf{x}^H(t) = \mathbf{A}(\Theta) \cdot \mathbf{S} \cdot \mathbf{A}(\Theta) + \sigma^2 \mathbf{I} \tag{2.28}$$

2.5 Mathematical Preliminaries

Some mathematical concepts are quoted here in forms of definitions or theorems for a better understanding of the following discussion (*cf.* [GV83, LH73, Str80, etc]).

Definition 2.2 *A complete infinite unitary space is called a Hilbert space, denoted by H.*

Definition 2.3 *The eigenvalues of a matrix* $\mathbf{A} \in C^{n \times n}$ *are the n roots of its characteristic polynomial* $p(z) = det(z\mathbf{I} - \mathbf{A})$. *The set of these roots is called the spectrum and is denoted by* $\lambda(\mathbf{A})$. *If* $\lambda(\mathbf{A}) = \{\lambda_1, \lambda_2, \cdots, \lambda_n\}$, *then it follows that*

$$det(\mathbf{A}) = \lambda_1 \lambda_2 \cdots \lambda_n \tag{2.29}$$

Moreover, if we define the trace of $\mathbf{A}$ *by*

$$Tr(\mathbf{A}) = \sum_{i=1}^{n} a_{ii} \qquad \mathbf{A} \in C^{n \times n} \tag{2.30}$$

then $Tr(\mathbf{A}) = \sum_{i=1}^{n} \lambda_i$.

If $\lambda_i \in \lambda(\mathbf{A})$ *then the non-zero vectors* $\mathbf{e}_i \in C^{n \times 1}$ *that satisfy*

$$\mathbf{A}\mathbf{e}_i = \lambda_i \mathbf{e}_i \tag{2.31}$$

are referred to as eigenvectors. An eigenvector defines a one-dimensional subspace that is invariant with respect to pre-multiplication by $\mathbf{A}$. *Usually, the eigenvalues are arranged in descending order.*

Definition 2.4 *A vector space* $\mathbf{X}$ *is the direct sum of two subspaces* $\mathbf{Y}$ *and* $\mathbf{Z}$, *denoted* $\mathbf{X} = \mathbf{Y} \oplus \mathbf{Z}$, *if every* $\mathbf{x} \in \mathbf{X}$ *can be uniquely expressed as* $\mathbf{x} = \mathbf{y} + \mathbf{z}$ *for some* $\mathbf{y} \in \mathbf{Y}$ *and* $\mathbf{z} \in \mathbf{Z}$.

Definition 2.5 *Given a subset* $\mathbf{M}$ *of a Hilbert space* H, *the set of all vectors orthogonal to* $\mathbf{M}$ *is called the orthogonal complement of* $\mathbf{M}$ *and is denoted* $\mathbf{M}^{\perp}$.

Definition 2.6 *For a matrix* $\mathbf{A} \in C^{n \times n}$, *its range is defined by*

$$R(\mathbf{A}) = \{\mathbf{y} \in C^n \mid \mathbf{y} = \mathbf{A}\mathbf{x} \quad \textit{for some} \quad \mathbf{x} \in C^n\} \tag{2.32}$$

and the null space of $\mathbf{A}$ *by*

$$N(\mathbf{A}) = \{\mathbf{x} \in C^n \mid \mathbf{A}\mathbf{x} = \mathbf{0}\} \tag{2.33}$$

Theorem 2.1 ***Eigen-decomposition***

A Hermitian matrix $\mathbf{A} = \mathbf{A}^H$ *has an eigen-decomposition of the form*

$$\mathbf{A} = \mathbf{E}\Lambda\mathbf{E}^H = \sum_{i=1}^{n} \lambda_i \cdot \mathbf{e}_i \cdot \mathbf{e}_i^H \tag{2.34}$$

where Λ *is real and diagonal and* $\mathbf{E}$ *is orthogonal.*

The entries on the main diagonal of Λ are the eigenvalues of $\mathbf{A}$, and the columns of $\mathbf{E}$ are the corresponding eigenvectors.

Theorem 2.2 ***Singular Value Decomposition***

If $\mathbf{A} \in C^{m\times n}$ *then there exist unitary matrices*

$$\mathbf{U} = [\mathbf{u}_1, \mathbf{u}_2, \cdots, \mathbf{u}_m] \in C^{m\times m} \tag{2.35}$$

and

$$\mathbf{V} = [\mathbf{v}_1, \mathbf{v}_2, \cdots, \mathbf{v}_n] \in C^{n\times n} \tag{2.36}$$

such that

$$\mathbf{U}^H\mathbf{A}\mathbf{V} = diag(\sigma_1, \sigma_2, \cdots, \sigma_p) = \Sigma \in R^{m\times n}, \quad p = \min\{m, n\} \tag{2.37}$$

where

$$\sigma_1 \geq \sigma_2 \geq \cdots \geq \sigma_p \tag{2.38}$$

From Theorem 2.2, it is ready to have $\mathbf{A}$ decomposed as $\mathbf{A} = \mathbf{U}\Sigma\mathbf{V}^H$ by pre- and post-multiplying the two sides of equation (2.37) with $\mathbf{U}$ and $\mathbf{V}^H$, respectively.

Corollary 2.1 *If the SVD of* **A** *is given by Theorem 2.2 and*

$$\sigma_1 \geq \cdots \geq \sigma_r > \sigma_{r+1} = \cdots = \sigma_p = 0 \tag{2.39}$$

then

$$rank(\mathbf{A}) = r \tag{2.40}$$

$$N(\mathbf{A}) = span\{\mathbf{v}_{r+1}, \cdots, \mathbf{v}_n\} \tag{2.41}$$

$$R(\mathbf{A}) = span\{\mathbf{u}_1, \cdots, \mathbf{u}_r\} \tag{2.42}$$

2.6 Maximum Likelihood Estimators

The Maximum Likelihood (ML) method, as a general method of estimation, was first introduced by R. A. Fisher, and has been accepted as one of the most important methods of estimation and taken as a standard technique in statistical estimation theory. In this method, the likelihood function of the observed data is defined as the Conditional Probability Density Function (CPDF) of the data with unknown parameters, the objective is to choose the unknown parameters such that the likelihood function becomes as large as possible. Any solution to the likelihood equation associated with the likelihood function will be taken as an estimate of the unknown parameters.

When applied to the signal parameter estimation problem, the Maximum Likelihood (ML) method provides an optimal criterion. Under this criterion, optimal solutions can be defined and sorted out from optimal solutions under other criteria for the same problem.

2.6.1 Deterministic Maximum Likelihood Estimator [Wax85, OV88, SN89]

Recall the model formulated previously and assume that the number of signals, d, is known and smaller than the number of sensors, m. Since the N samples $\mathbf{x}(1), \mathbf{x}(2), \cdots, \mathbf{x}(N)$ are independent and identically distributed, the joint (conditional) probability density function of the sampled data is given by

$$f(\mathbf{x}_1, \cdots, \mathbf{x}_N) = \prod_{t=1}^{N} \frac{1}{\pi det[\sigma^2 \mathbf{I}]} e^{-\frac{1}{\sigma^2}|\mathbf{x}(t_i) - \mathbf{A}(\theta)\cdot\mathbf{s}(t_i)|^2} \tag{2.43}$$

Maximising equation (2.43) is equivalent to minimising its negative log likelihood function

$$-\log(f(\mathbf{x}_1,\cdots,\mathbf{x}_N)) = N\log\pi + mN\log\sigma^2 + \frac{1}{\sigma^2}\sum_{i=1}^{N}|\mathbf{x}(t_i) - \mathbf{A}(\theta)\cdot\mathbf{s}(t_i)|^2 \tag{2.44}$$

Ignoring the constant term,

$$L(\theta,\mathbf{s}(t_i),\sigma^2) = mN\log\sigma^2 + \frac{1}{\sigma^2}\sum_{i=1}^{N}|\mathbf{x}(t_i) - \mathbf{A}(\theta)\cdot\mathbf{s}(t_i)|^2 \tag{2.45}$$

is defined as the criterion function. Thus, the ML estimator is obtained by solving the following minimisation problem

$$[\hat{\theta},\hat{\mathbf{s}}(t_i),\hat{\sigma}^2] = arg\min_{\theta,\mathbf{s}(t_i),\sigma^2} L(\theta,\mathbf{s}(t_i),\sigma^2) \tag{2.46}$$

Fixing θ and $\mathbf{s}(t_i)$, and minimising with respect to σ^2, we obtain

$$\hat{\sigma}^2 = \frac{1}{mN}\sum_{i=1}^{N}|\mathbf{x}(t_i) - \mathbf{A}(\theta)\cdot\mathbf{s}(t_i)|^2 \tag{2.47}$$

Substituting this result back to the criterion function, and ignoring the constant terms, we have

$$L(\theta,\mathbf{s}(t_i)) = mN\log\left(\frac{1}{mN}\sum_{i=1}^{N}|\mathbf{x}(t_i) - \mathbf{A}(\theta)\cdot\mathbf{s}(t_i)|^2\right) \tag{2.48}$$

which functionally equals

$$L(\theta,\mathbf{s}(t_i)) = \sum_{i=1}^{N}|\mathbf{x}(t_i) - \mathbf{A}(\theta)\cdot\mathbf{s}(t_i)|^2 \tag{2.49}$$

in the maximisation problem in equation (2.46). To carry out the minimisation of $L(\theta,\mathbf{s}(t_i))$, we hold θ fixed and minimise with respect to $\mathbf{s}(t_i)$ yielding

$$\hat{\mathbf{s}}(t_i) = (\mathbf{A}^H \cdot \mathbf{A})^{-1} \cdot \mathbf{A}^H \cdot \mathbf{x}(t_i) \tag{2.50}$$

$(\mathbf{A}^H \cdot \mathbf{A})^{-1} \cdot \mathbf{A}^H$ is defined as the pseudo-inverse of $\mathbf{A}$ and denoted as

$$\mathbf{A}^+ = (\mathbf{A}^H \cdot \mathbf{A})^{-1} \cdot \mathbf{A}^H \tag{2.51}$$

Substituting equation (2.50) to (2.49) results in

$$L(\theta) = \sum_{i=1}^{N} |\mathbf{x}(t_i) - \mathbf{A}^+ \cdot \mathbf{A} \cdot \mathbf{x}(t_i)|^2 \tag{2.52}$$

This can be rewritten as

$$L(\theta) = \sum_{i=1}^{N} |\mathbf{x}(t_i) - \mathbf{P}_A \cdot \mathbf{x}(t_i)|^2 \tag{2.53}$$

$$= \sum_{i=1}^{N} |\mathbf{P}_A^{\perp} \cdot \mathbf{x}(t_i)|^2 \tag{2.54}$$

where two operators $\mathbf{P}_A$ and $\mathbf{P}_A^{\perp}$ are defined respectively as

$$\mathbf{P}_A = \mathbf{A}^+ \cdot \mathbf{A}, \qquad \mathbf{P}_A^{\perp} = \mathbf{I} - \mathbf{P}_A \tag{2.55}$$

$\mathbf{P}_A$ is the projection operator onto the space spanned by the columns of the matrix $\mathbf{A}$, and $\mathbf{P}_A^{\perp}$ is the orthogonal projection operator onto the null space of $\mathbf{A}$.

By properties of the trace operator, $Tr\{\cdot\}$, the likelihood function in equation (2.54) can be written in another form as

$$L(\theta) = Tr[\mathbf{P}_A^{\perp} \cdot \hat{\mathbf{R}}] \tag{2.56}$$

where $\hat{\mathbf{R}}$ is the sample covariance matrix given in (2.26). Thus, the ML estimator of θ is obtained as

$$\hat{\theta} = arg \min_{\theta} Tr[\mathbf{P}_{\tilde{A}} \cdot \hat{\mathbf{R}}] \tag{2.57}$$

2.6.2 Stochastic Maximum Likelihood Estimator [Sch81, Boh87]

Under the assumptions which have been made concerning the signal and noise, the joint probability density function of the N independent samples is given by

$$f(\mathbf{x}_1, \cdots, \mathbf{x}_N) = \prod_{t=1}^{N} \frac{1}{\pi^m det(\mathbf{R})} e^{-\mathbf{x}^*(t) \cdot \mathbf{R}^{-1} \cdot \mathbf{x}(t)} \tag{2.58}$$

and the normalised negative log likelihood function of $\{\mathbf{x}(1), \cdots, \mathbf{x}(N)\}$ has the following form,

$$L(\eta) = m \log \pi + \log det \mathbf{R}(\eta) + Tr\{\mathbf{R}^{-1}\{\eta) \cdot \hat{\mathbf{R}}\} \tag{2.59}$$

where η represents the unknown parameters $\theta, \mathbf{S}$, and σ^2 of the observation covariance. The ML estimate is the minimizing argument of $L(\eta)$. In this form, the Sto-ML method requires a non-linear, $(d^2 + d + 1)$-dimensional optimization. As noted in [Boh87], the log likelihood function (2.58) can be separated and thus, the dimension of the optimization can be reduced. For fixed θ, the minimisation of (2.59) with respect to (w.r.t.) $\mathbf{S}$ and σ^2 yields

$$\hat{\mathbf{S}}(\theta) = \mathbf{A}^{+}(\hat{\mathbf{R}} - \hat{\sigma}^2(\theta)\mathbf{I}) \cdot \mathbf{A}^{+^H} = \frac{1}{m-d} Tr\{\mathbf{P}_{\tilde{\mathbf{A}}} \cdot \hat{\mathbf{R}}\} \tag{2.60}$$

The following d-dimensional non-linear minimisation problem yields

$$\hat{\theta} = arg \min_{\theta} det\{\mathbf{A}\hat{\mathbf{S}}(\theta)\mathbf{A}^H + \hat{\sigma}^2(\theta)\mathbf{I}\} \tag{2.61}$$

CHAPTER 3

LITERATURE SURVEY OF DIRECTION-OF-ARRIVAL TECHNIQUES

In this chapter, some typical solutions to the array signal processing problem are reviewed. These solutions are mainly for the direction of arrival (DOA) estimation problem, which might require other knowledge such as the estimate of the number of signals, and may be extended to other applications such as the signal waveform estimation, etc.

The evolution of estimation techniques has experienced several stages. For clarity of presentation, the discussion will be divided into several parts which contain different classes of methods. To make the presentation self-contained, one section in this chapter is devoted to the detection problem at the end.

3.1 Conventional Techniques

The basic array processing structure is shown in figure 3.1, in which the array output is evaluated as a function of the angle. Conventional techniques aim to form a power spectrum at the array output and take its peaks as indications of the true directions of arrival of wavefronts present.

Under the narrowband signal assumption, a single complex coefficient in each channel (i.e., each sensor of the array) is sufficient to adjust the transfer function of the filter. Using $x_i(t)$ to denote the output at the ith sensor and $w_i(\theta)$ the corresponding weighting coefficient, the array output can be written as

$$y(t) = \sum_{i=1}^{m} w_i^*(\theta) \cdot x_i(t) = \sum_{i=1}^{m} w_i(\theta) \cdot x_i^*(t) \qquad (3.1)$$

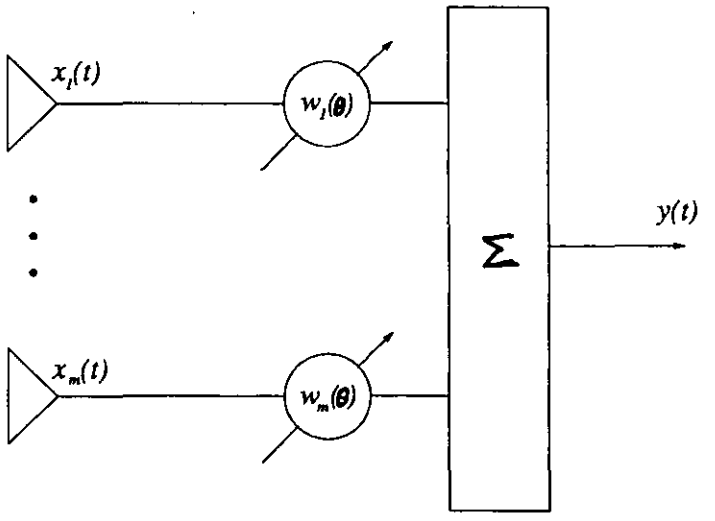

Figure 3.1 Basic Array Processing Scheme

where the superscript (*) denotes the complex conjugate operator.

Employing the vector notation

$$\mathbf{x}(t) = [x_1(t), \cdots, x_m(t)]^T \tag{3.2a}$$

and

$$\mathbf{w}(\theta) = [w_1(\theta), \cdots, w_m(\theta)]^T \tag{3.2b}$$

to represent the array measurements at time instant t and the weighting vector, where m is the number of sensors in the array, the ensemble average power output $P(\theta)$ is then given by

$$P(\theta) = \mathrm{E}[|y(t)|^2] = \mathbf{w}^H \cdot \mathrm{E}[\mathbf{x}(t) \cdot \mathbf{x}^H(t)] \cdot \mathbf{w} = \mathbf{w}^H \cdot \mathbf{R} \cdot \mathbf{w} \tag{3.3}$$

where $\mathbf{R}$ is defined as the array output covariance matrix

$$\mathbf{R} = \mathrm{E}[\mathbf{x}(t) \cdot \mathbf{x}^H(t)] \tag{3.4}$$

It will be shown that, by using the weighting vector in different ways, several methods can be developed from (3.3) which include the classical beamforming method, Capon's maximum

likelihood method, and Burg's maximum entropy method.

3.1.1 Classical Beamforming Method

The wave propagation phenomenon in physics stimulated the formulation of the conventional beamformer. It is well known therein that a coherent summation of all waveforms at sensor outputs produces a scalar output which includes a coherent sum of energy in signals and an incoherent sum of noise, and that incoherent summation exists for both signals and noise when signals arrive out-of-phase. The aim of the conventional beamformer is to choose a weighting vector $w(\theta)$ to compensate propagation delays at different sensors so as to steer a beam in the wanted direction.

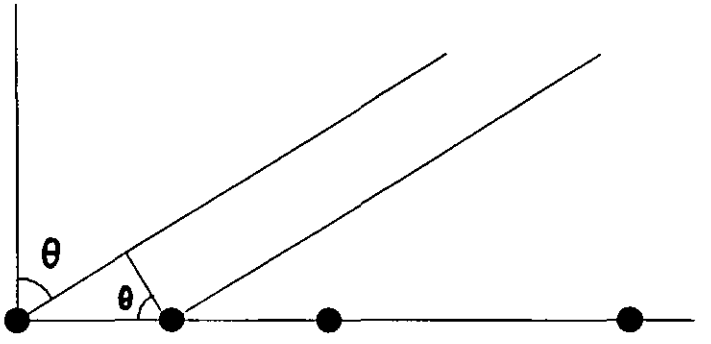

Figure 3.2 Uniform Linear Array with Δ Spacing

For the uniform linear array with inter-element spacing Δ in the metric of wavelength (ULA(Δ)) given in figure 3.2, the time delay between two adjacent sensors for the signal incident onto the array in direction θ to the normal of the array is given by

$$\tau_o = \frac{\Delta\lambda}{c}\mathrm{Sin}\,\theta = \frac{2\pi\Delta}{\omega}\mathrm{Sin}\,\theta \tag{3.5}$$

where c is the propagation speed of the waveform at radian frequency ω. Then, the delay between the ith sensor and the reference sensor is simply

$$\tau_i = (i-1)\tau_o \tag{3.6}$$

Therefore, the weighting vector for the conventional beamformer can be constructed as

$$\mathbf{w}(\theta) = \left[1, e^{-j\omega\tau_o}, \cdots, e^{-j\omega(m-1)\tau_o}\right]^T = \mathbf{a}(\theta) \tag{3.7}$$

which coincides to be equal to $\mathbf{a}(\theta)$, the steering vector defined in chapter 2. Thus the output power of the conventional beamformer is given by

$$P_{CBF}(\theta) = \mathbf{a}^H(\theta) \cdot \mathbf{R} \cdot \mathbf{a}(\theta) \tag{3.8}$$

In practice, only finite measurements are available and it is the estimated covariance matrix that can be used in the estimation of the power spectrum. Given N observations of the array output, the estimated power output is described by time averaging which can be given by the following alternative expression

$$\hat{P}_{CBF}(\theta) = \frac{1}{N}\sum_{t=1}^{N} |y(t)|^2 = \frac{1}{N}\sum_{t=1}^{N} \left| \sum_{i=1}^{m} e^{-j(i-1)\gamma} \cdot x_i(t) \right|^2 \tag{3.9}$$

where $\gamma = \omega\tau_o$ is defined as spatial frequency. This estimator takes the Discrete Fourier Transform (DFT) of the array aperture distribution (m-point DFT) as the spatial spectrum estimate and has very limited resolution, because the convolution of the unknown spectrum with the filter transform function destroys the details of the peak spectra [Gab80]. Poor resolution due to the finite array size and sidelobe leakage due to inter-element spacing are the main problems with the conventional beamformer which cannot be overcome by conventional techniques. However, because of its easy implementation and robustness it is still widely used in practical systems.

3.1.2 Burg's Maximum Entropy Method (MEM)

In the conventional beamformer, the weighting vector $\mathbf{w}(\theta)$ is chosen according to some desired criterion and is fixed in processing. In contrast, an adaptive system possesses the ability to adjust its weighting coefficients to meet the changing environment so as to achieve some particular requirements. Adaptive methods have been proven to have superior resolving capabilities compared to the conventional beamformer and provide optimum array gains.

The Maximum Entropy Method (MEM) of Burg [Bur67] is widely used in estimating the directions of arrival of wavefronts at a linear equispaced array, especially when the data records are short. The idea of the method is to keep the first coefficient of the weighting vector to be unity while allowing all other coefficients to take any value. The aim of this is to minimise the output subject to the first sensor constraint, and nulls will be placed at the positions of all the strong signals. The inversion of this response gives an estimate of the angular spectrum and the peaks are used to locate the source directions.

Defining the first unit vector as $\mathbf{u}_1 = [1, 0, \cdots, 0]^T$, the MEM angular spectrum is given by

$$P_{MEM}(\theta) = \frac{\mathbf{u}_1^H \mathbf{R}^{-1} \mathbf{u}_1}{|\mathbf{u}_1^H \mathbf{R}^{-1} \mathbf{a}(\theta)|^2} \tag{3.10}$$

The main advantages of MEM are that it shows much higher spatial resolution compared to the conventional beamforming technique even with short data records [Gab80], and that the unwanted "end effect" caused by the finite aperture sampling is also avoided. This method is useful in adaptive arrays for cases where the wanted signal itself is weaker that the background noise. The interferences are first removed and then the signal recovered from the noise by post-processing. Despite all these advantages, the so-called line-spliting problem exists, as does the lack of source power estimates. Another shortcoming inherent in the MEM is that it needs knowledge of the length of the prediction error filter, i.e., the order of the corresponding AR model [UB75]. This method was first claimed to be applicable to equispaced arrays only, but it is stated in [Nic88] that it can also be applied to irregular arrays.

3.1.3 Capon's Maximum Likelihood Method (MLM)

Capon's method, the Maximum Likelihood Method (MLM) [Cap69], is a modification of the conventional beamformer by using an adjustable weighting vector rather than a fixed one. This method is a mapping of the maximum likelihood filter used in time domain optimisation problems to the space domain with a wavenumber resolution superior to that obtained from the conventional method [Cap69, Gab80, KM81]. As has been stated, this maximum likelihood filter is designed to pass the power in a narrowband about the signal frequency of interest and minimise all other frequency components in an optimum manner.

In the direction of arrival estimation problem, the array output power in the wanted direction contains contributions from stimuli in that direction and, as well, in other unwanted directions. To minimize the responses to unwanted directions, a constrained optimal problem is formulated. The array output power is minimized while maintaining the gain along the wanted direction to be constant. This can be formulated as a zeroth-order main beam directional gain constraint optimization problem as follows :

$$\text{minimize :} \qquad P(\theta) = \mathrm{E}[|y(t)|^2] = \mathbf{w}^H(\theta) \cdot \mathbf{R} \cdot \mathbf{w}(\theta) \tag{3.11a}$$

$$\text{subject to :} \qquad |\mathbf{w}^H(\theta) \cdot \mathbf{a}(\theta_o)| = 1 \tag{3.11b}$$

where $\mathbf{a}(\theta_o)$ denotes the array response to the wanted direction θ_o. Solving the above problem is equivalent to constraining the weighting of the array to form a beam in the wanted direction while, at the same time, to minimise the mean square output from the array. Therefore, to distinguish it from true Maximum Likelihood (ML) techniques, Capon's method is also addressed as the Minimum Variance Method (MVM), which is a realisation of the ML technique in the real sense only when a single source is present.

The Lagrange method is usually used to solve the constrained optimisation problem stated in (3.11) and gives the optimal weighting vector as [Gri83]

$$\mathbf{w}_{opt}(\theta) = \frac{\mathbf{R}^{-1} \cdot \mathbf{a}^H(\theta)}{\mathbf{a}^H(\theta) \cdot \mathbf{R}^{-1} \cdot \mathbf{a}(\theta)} \tag{3.12}$$

and the angular spectrum estimate as

$$P_{MVM}(\theta) = \frac{1}{\mathbf{a}^H(\theta) \cdot \mathbf{R}^{-1} \cdot \mathbf{a}(\theta)} \tag{3.13}$$

So the angular spectrum can be estimated by sweeping the steering vector $\mathbf{a}(\theta)$ over the field-of-view with the inverse of a given covariance matrix.

Using the spectrum representation of the covariance matrix $\mathbf{R}$ given in (2.34) and the properties of matrix inversion, the MVM spectrum can be written as

$$P_{MVM}(\theta) = \frac{1}{\mathbf{a}^H(\theta) \cdot \left(\sum_{i=1}^{m} \frac{1}{\lambda_i} \mathbf{e}_i \cdot \mathbf{e}_i^H \right) \cdot \mathbf{a}(\theta)} \tag{3.14}$$

This implies that all eigenvalues and eigenvectors of the covariance matrix are used in the final evaluation of the output spectrum. The reciprocal of the eigenvalue is used to weight the corresponding eigenvector.

A better resolution is achievable by the MVM estimator than that by the conventional beamformer, and the angular spectrum is directly referenced to receiver noise power so that the peaks represent signal power estimates in those directions, which permits the measurement of relative source strength. The residual background ripple is low and relatively well behaved, and provided that the array manifold is known, it is not necessary for the array to be equally spaced; thus the array aperture can be widened and the resolution is substantially increased for a given number of sensors. Also, the MVM does not need knowledge of the number of signals present.

On the other hand, ill-conditioning may arise when calculating the inverse of the covariance matrix. This method fails to resolve coherent sources and its computation load is relatively high.

3.2 Signal Subspace Methods

The ML estimator for the deterministic sequences has been given in (2.57) and the likelihood function is rewritten here as

$$L(\theta) = Tr[\mathbf{P}_A(\theta) \cdot \mathbf{R}] \tag{3.15}$$

Substituting the spectral representation of the covariance matrix, which is the form of the covariance matrix denoted by its eigenvalues and eigenvectors, given in (2.34) into the likelihood function, and using the properties of the projection and trace operators, we have

$$L(\theta) = \sum_{i=1}^{m} \lambda_i |\mathbf{P}_A(\theta) \cdot \mathbf{e}_i|^2 \tag{3.16}$$

Maximising $L(\theta)$ yields the ML estimates of the directions of arrival. It is evident that all eigenvalues and eigenvectors of the covariance matrix **R** are used in the estimation. A non-linear, multidimensional maximising procedure is involved which means a heavy computational burden.

To reduce the computational complexity inherent in the ML estimator and to provide comparable performance at the same time, suboptimal procedures are needed. Work in the field of eigenstructure based methods was pioneered by Pisarenko [Pis73]. His work concentrated on extracting harmonics embedded in white noise in time series analysis. His method, however, has provided a fundamental basis for eigenstructure based methods which have dominated the field of DOA estimation since their emergence.

The common basis for all these suboptimal signal subspace methods is the eigendecomposition of the covariance matrix sampled at the array output. They differ from each other in the way in which they make use of the obtained eigenvalues and eigenvectors of the covariance matrix, with the aim being to find the direction estimates as exactly as possible. The orthogonality between the signal subspaces (spanned by the signal eigenvectors) and the noise subspace (spanned by the noise eigenvectors) and that between the signal steering vector and the noise subspace are the foundation of a number of high resolution DOA estimation techniques.

The MVM described in section 3.1.3 is one of such suboptimal method obtained by reducing the multidimensional optimisation problem involved in the ML estimator into a one-dimensional searching procedure. The MUSIC (MUltiple SIgnal Characterisation) algorithm of Schmidt [Sch79, Sch81] and Bienvenu and Kopp [BK80], and MNM of Reddi [Red79] and Kumaresan and Tufts [KT83], etc. provide a more appealing solution to the DOA estimation problem by reducing the computational load and providing better resolution performance.

3.2.1 The MUSIC Method

The MUSIC algorithm is based on a geometric interpretation of the signal parameter estimation problem. The main ideas behind this signal subspace approach are : 1) obtain the array manifold, 2) find the signal subspace, and 3) search for the intersections between the array manifold and the signal subspace. For d signals, the observed data vectors are constrained to the d-dimensional subspace of C^m, termed the signal subspace. The

intersections of these d-dimensional subspaces and the array manifold $\mathbf{A}(\theta)$ give d vectors $\mathbf{a}(\theta_i)$, $i = 1, \cdots, d$, which are the d columns of the array manifold $\mathbf{A}(\theta)$, termed as the signal steering vectors. That is, these vectors yield the set of vectors from the array manifold that span the observed signal subspace. Once these d independent vectors have been observed, the DOA estimates are immediately determined if no ambiguity exists in the array manifold. The signal subspace method separates the highly non-linear DOA estimation problem into two parts: the non-linear part which is the determination of the array manifold, and the linear part which is the observation of the signal and noise subspaces. Given the array manifold, either by analytical calculation or by calibration, the DOA estimation problem is equivalent to that of finding the intersections between the signal subspace and the array manifold and inferencing to the corresponding directions.

Intersections between the signal subspace and the array manifold are obtainable only in the ideal case when noise is absent. Estimates of these intersections have to be made, since with probability one (w.p.1) there will be no intersection between the estimated signal subspace and the array manifold. Procedure for seeking array manifold vectors that are closest to the estimated signal subspace must be provided. Schmidt's idea was to find a set of d vectors by minimising the squared distance from the array manifold vector to the estimated signal subspace.

From the orthogonality between the signal eigenvectors and the noise eigenvectors, assuming that the covariance matrix is precisely known, we have

$$\mathbf{e}_i^H \cdot \mathbf{e}_j = 0 \qquad i = 1, \cdots, d; \qquad j = d+1, \cdots, m \tag{3.17}$$

The squared Euclidean length from a steering vector $\mathbf{a}(\theta)$ to the signal subspace is

$$|l|^2 = \mathbf{a}^H(\theta) \cdot \mathbf{E}_N \cdot \mathbf{E}_N^H \cdot \mathbf{a}(\theta) \tag{3.18}$$

In the direction where $\mathbf{a}(\theta)$ is orthogonal to the noise subspace

$$|l|^2 = 0 \tag{3.19}$$

and the θ which makes the scalar function in (3.18) tend to zero is the estimate of the DOAs. The reciprocal of the function given in equation (3.18) yields the MUSIC spectrum estimate,

i.e.,

$$P_{MUSIC}(\theta) = \frac{1}{\mathbf{a}^H(\theta) \cdot \mathbf{E}_N \cdot \mathbf{E}_N^H \cdot \mathbf{a}(\theta)} \tag{3.20}$$

or

$$P_{MUSIC}(\theta) = \frac{1}{|\mathbf{a}^H(\theta) \cdot \mathbf{E}_N|^2} = \frac{1}{\sum_{j=d+1}^{m} |\mathbf{a}^H(\theta) \cdot \mathbf{e}_j|^2} \tag{3.21}$$

The MUSIC algorithm makes use of the noise eigenvectors only, and all the noise eigenvectors. In other words, it re-weights all eigenvectors by setting the noise eigenvalues to unity and signal eigenvalues to zero. The MUSIC algorithm provides an asymptotically unbiased estimate of many important parameters of the wavefronts arriving at a sensor array, such as the number of incident wavefronts, directions of arrival, strengths and cross-correlations among the incident wavefronts, and noise / interference strength, etc. [Sch81]. Spectra resulting from the MUSIC method are much smoother while, in the directions of signals, nulls appear with significant depth.

Equation (3.21) shows that an accurate estimate of the number of the incident signals is of great importance. Overestimate of the number of signals results in the introduction of spurious signal directions, and underestimate of it will effect the estimate of other directions of signals that are present. The effect of under-estimation of the number of signals is worse than that of over-estimation.

The maxima obtained by the MUSIC algorithm do not depict the signal strength because the spectrum given in equation (3.21) involves no information associated with signal eigenvalues, which are related to the signal powers. Theoretically the peaks in this spectrum appear to be infinitely high in the signal directions since the denominator tends to zero. This method does provide superior resolution compared with other non-eigenstructure based techniques although in a practical environment the peaks only have finite heights [MC85, JD82, SV84].

The MUSIC algorithm yields unbiased estimates of a general set of signal parameters whose variances match the Cramer-Rao lower bound asymptotically, i.e., when the number of snapshots becomes very large or Signal-to-Noise Ratio (SNR) is extremely high [Sch79, Sch81]. When only finite noisy data is available two types of estimate errors, local and global, exist [SPK86]. The former implies deviation of the shape of the observed peak from

that which should have resulted in the asymptotic case, and the latter describes the "false" peaks that are not within some small neighbourhood of the true directions. Since the directions of arrival are estimated from the intersections of signal subspace and the array manifold, i.e., the array geometry, the array geometry design is of particular importance in affecting the performance of MUSIC.

The main disadvantage of the MUSIC algorithm is that it is computationally expensive, because of the searching procedure and the use of all the noise eigenvectors. Kumarensan and Tufts' method eases the computational load by using a single vector in the final searching procedure.

3.2.2 Kumaresan and Tufts's Method (MNM)

The method suggested by Kumaresan and Tufts [KT83], usually referred to as Minimum Norm Method (MNM) or KT method in later literature, uses a single vector which is orthogonal to the signal subspace, generated either from the signal subspace or from the noise subspace, to calculate the angular spectra. This method estimates the arrival angles of multiple plane waves by forming a polynomial from the eigenvectors of the covariance matrix, and finding its zeros which give estimates of the angles of arrival. The polynomial may be formed from the signal or noise subspace eigenvectors, because they are complementary.

Recalling the definitions of signal subspace and noise subspace, they form two matrices with dimensions of $m \times d$ and $m \times (m-d)$, respectively. Partition these two matrices, $\mathbf{E}_S$ and $\mathbf{E}_N$, as follows

$$\mathbf{E}_S = \begin{bmatrix} \mathbf{g}^T \\ --- \\ \mathbf{E}_S' \end{bmatrix} \qquad \mathbf{E}_N = \begin{bmatrix} \mathbf{c}^T \\ --- \\ \mathbf{E}_N' \end{bmatrix} \tag{3.22}$$

where $\mathbf{g}$ and $\mathbf{c}$ are column vectors having the first elements of signal and noise subspace eigenvectors, respectively. $\mathbf{E}_S'$ and $\mathbf{E}_N'$ have the same elements of $\mathbf{E}_S$ and $\mathbf{E}_N$ with the first row deleted.

The vector $\mathbf{d}$ proposed by Kumaresan and Tufts to calculate the angular spectra is a constrained vector which spans the noise subspace, i.e., lies in the range of the noise subspace matrix $\mathbf{E}_N$.

$$\mathbf{d} = [d_1, d_2, \cdots, d_m]^T \tag{2.23}$$

Setting the first element of **d** to be one and minimizing its norm

$$\textit{minimise} \quad \sum_{i=1}^{m} |d_i|^2 \qquad \textit{subject to} \qquad d_1 = 1 \tag{3.24}$$

the rest of the elements of **d** are obtained by using the appropriate pseudo-inverse of $\mathbf{E}_S^H$ or of $\mathbf{E}_N'$

$$\mathbf{d} = \begin{bmatrix} 1 \\ \hline -\mathbf{E}_S' \cdot \mathbf{g}^* / (1 - \mathbf{g}^H \cdot \mathbf{g}) \end{bmatrix} \quad or \quad \mathbf{d} = \begin{bmatrix} 1 \\ \hline \mathbf{E}_N' \cdot \mathbf{c}^* / \mathbf{c}^H \cdot \mathbf{c} \end{bmatrix} \tag{3.25}$$

With the orthogonality between signal eigenvectors and noise eigenvectors, ideally,

$$\mathbf{E}_S^H \cdot \mathbf{d} = \mathbf{0} \tag{3.26}$$

The angular spectrum based on the vector **d** is suggested as

$$P_{MNM}(\theta) = \frac{1}{|\mathbf{a}^H(\theta) \cdot \mathbf{d}|^2} \tag{3.27}$$

Compared to the expression in equation (3.21) for MUSIC spectrum estimation, the KT method spends less time in the final searching procedure. The shortcoming of the KT method relies in the emerging of spurious peaks and merging of spectral peaks at lower SNR value.

Herein, the MUSIC technique and the MNM are described as examples of the so-called signal subspace methods. In the derivations of the methods it has been assumed that the additive noise is spatially white or the noise covariance matrix is known to within a scalar factor. Cases when the noise is completely unknown exist in practical situations. Significant performance degradation is expected if the noise is treated as white and the above cited algorithms are applied [Mar84]. Several methods have been suggested to tackle this problem [LeC89, PK86, Tew89].

3.3 Subspace Rotation Methods

3.3.1 ESPRIT

ESPRIT (Estimation of Signal Parameters via Rotational Invariance Techniques) is a relatively new approach to the general high resolution signal parameter estimation problem. Like the MUSIC algorithm, this is an eigenstructure based method and in many aspects, such as exploiting the underlying signal and noise models and generating asymptotically unbiased estimates of signal parameters, is similar to MUSIC. On the other hand, ESPRIT manifests significant performance and computational advantages over MUSIC by employing rotational invariance among signal subspaces induced by an array of sensors with translational invariance structure. The work in this algorithm was pioneered by Paulraj, Roy, and Kailath [PRK85, PRK86, RK89, etc].

ESPRIT is an attempt to retain most of the essential features of the arbitrary array of sensors while offering a significant reduction in computational complexity by imposing a constraint on the array. This is achieved at the price of less general applicability.

In order to exploit the translational invariance property of the array, it is convenient to describe the array used in the ESPRIT algorithm as being comprised of two subarrays, Z_X and Z_Y, which are identical in every respect except a physical displacement vector Δ. Denoting the outputs of all doublets in two subarrays in vector notation :

$$\mathbf{x}(t) = \mathbf{A} \cdot \mathbf{s}(t) + \mathbf{n}_x(t) \tag{3.28a}$$

$$\mathbf{y}(t) = \mathbf{A} \cdot \Phi \cdot \mathbf{s}(t) + \mathbf{n}_y(t) \tag{3.28b}$$

a matrix Φ is introduced here to represent the relation between the measurements from the two subarrays.

$$\Phi = diag\left(e^{j\phi_1}, \cdots, e^{j\phi_d}\right), \qquad \phi_k = \omega_o \Delta \operatorname{Sin}\theta_k / c \tag{3.29}$$

The auto-covariance matrix of the data received by subarray Z_X is given by

$$\mathbf{R}_{XX} = \mathrm{E}[\mathbf{x}(t)\mathbf{x}^H(t)] = \mathbf{A}\mathbf{S}\mathbf{A}^H + \sigma^2\mathbf{I} \tag{3.30}$$

and the cross-covariance matrix between the measurements from two subarrays, Z_X and X_Y, by

$$\mathbf{R}_{XY} = \mathrm{E}[\mathbf{x}(t)\mathbf{x}^H(t)] = \mathbf{A}\mathbf{S}\Phi^H\mathbf{A}^H \tag{3.31}$$

Here one theorem is formulated to provide the foundation for subsequent analysis and results.

Theorem 3.1 *Define* T *as the generalised eigenvalue matrix associated with the matrix pencil* $\{(\mathbf{R}_{XX} - \lambda_{\min}\mathbf{I}), \mathbf{R}_{XY}\}$ *where* $\lambda_{\min}$ *is the minimum (repeated) eigenvalue of* $\mathbf{R}_{XX}$. *Then, if* S *is non-singular, the matrices* Φ *and* T *are related by*

$$\mathrm{T} = \begin{bmatrix} \Phi & 0 \\ 0 & 0 \end{bmatrix} \tag{3.32}$$

to within a permutation of the elements of Φ.

A proof to this theorem can be found in [PRK85].

From the relation in equation (3.29) it is obvious that once Φ is known, the signal DOAs can easily estimated as

$$\hat{\theta}_k = arcsin\{c.\phi_k/\omega_o\Delta\} \tag{3.33}$$

In practical situations errors arise from the finite data measurements and the subsequent finite precision computations. For this reason, the smallest eigenvalues of $\hat{\mathbf{R}}_{XX}$ are clustered rather than having the same (repeated) value and the relation in equation (3.32) is not exactly satisfied. Two formulations of the ESPRIT algorithm have been suggested to obtain the desired DOA estimates and probably other parameters of the sources, the so-called Least Squares (LS) ESPRIT and Total Least Squares (TLS) ESPRIT.

The ESPRIT techniques fall in the class of the so-called Subspace Rotation (SR) methods , another representative of which is the less known Toeplitz Approximation Method (TAM). This method is based on the observation that the estimated covariance matrix is Toeplitz in

the case when sources are uncorrelated and statistically stationary. In coherent cases, the Toeplitz structure can be guaranteed by employing the smoothing techniques suggested either by T.J.Shan et al or by the authors of the TAM method [KLF86]. The TAM method was originally proposed for the harmonic retrieval problem in time series analysis [KAR83], and was then modified to be applicable to the DOA estimation problem in array processing [KLF86]. In the TAM approach, the data is modelled as the output of a self generating ARMA process and a state space representation is then formed from the Singular Value Decomposition (SVD) of the data matrix.

It is shown [SN91] that the asymptotic variance of the SR estimate is greater than the MUSIC asymptotic variance; furthermore, the difference between SR and MUSIC variances may be considerable for large m.

3.4 Deconvolution Methods

Apart from the ESPRIT method, most existing high resolution algorithms are "single stage" algorithms which generate spectral estimates and assume maxima or minima in the spectra as indications of directions of possible sources. Another class of methods to be described in the present section make multi-stage estimates of spatial spectra and compare some specific statistics associated with these estimates with a pre-defined threshold to give an estimate of source directions. These methods are often addressed as deconvolution methods which include the advanced CFAR (Constant False Alarm Rate) technique [BLP86, Wei82] as well as the Wagstaff and Berrou Broadband (WB^2) algorithm [WB84], Iterative Filtering Algorithm (IFA) of Kay [Kay84], CLEAN [Hog74, RLD87, Sch78, VL89] and IMP (Incremental Multi-stage Parameter) method [Cla87, Cla88, Cla89, Mat89a,b].

A common feature among deconvolution methods is the re-processing of data after the initial estimation of the output power distribution. Strictly speaking, deconvolution implies inverse linear filtering which means that the inverse of the system response is required and used to convolve with the measurement so as to give an estimate of the stimuli to the system. Deconvolution methods including CLEAN, IMP, WB^2 and IFA implement the deconvolution procedure iteratively. At each stage, an estimate of the stimuli is assumed according to the system output spectrum, and then convolved with the system response and compared with the observation (i.e. the system output spectrum). The correspondence between the convolved result and the original observation measures the fitness of the estimate and determines the termination of the procedure.

3.4.1 Iterative Filtering Algorithm

Kay's IFA (Iterative Filtering Algorithm) [Kay84] addresses the classical problem of estimating frequencies of sinusoids in white noise with the ability to provide accurate frequency estimates at low signal-to-noise ratios, provided that the number of sinusoids is known. It adjusts an all-pole filter which processes the data. At equilibrium, the frequencies of sinusoids can be deduced from the filter coefficients. It has been shown that IFA is related to Steiglitz-McBrides's algorithm for identification of linear systems.

3.4.2 Wagstaff and Berrou Broadband Technique

The technique developed by Wagstaff and Berrou [WB84] for high-resolution beamforming and spectral analysis is referred to as the WB^2 technique. The WB^2 algorithm derives its first estimate from the output power spectrum of a conventional beamformer, rather than from the array output, and performs the mathematical operations on the logarithm of the power rather than the power itself. These two departures from other commonly used high resolution methods make WB^2 a fast, simple, and nonlinear algorithm giving approximate solutions to a very complex problem.

The WB^2 algorithm is also an iterative algorithm. At the first stage, a "guess" of the environment comprising locations of point sources is found from the positions of the spectral peaks. The "guess" is convolved with the array beam pattern to give the estimated output spectrum. This spectrum is compared with the measured spectrum, and the decibel differences in the estimated and observed spectra are used to modify the "guessed" spectrum. This process is repeated until a suitable goodness of fit criterion is met.

The WB^2 algorithm utilises a very important principle : convolution in the time domain equals multiplication in the frequency domain; furthermore, multiplication in frequency domain equals addition of logarithms. These two transformations greatly simplify the mathematical operations, and thus speed up the processing.

Both IFA and WB^2 allow changes to any or all of the estimates from iteration to iteration, while only one estimate is allowed to change between iterations in the CLEAN method and the IMP algorithm which will be presented below.

3.4.3 CLEAN

The CLEAN technique was first introduced by Hogbom [Hog74] to radio astronomy and nowadays, with modifications and additions, is still widely used in aperture synthesis radio astronomy for image restoration. The basic assumptions made in the CLEAN method are that : 1) the brightness distribution contains only a few sources at well separated, small regions, i.e., the brightness distribution is essentially empty; 2) the maximum response in the dirty map is due to a single far-field point source at the location of the maximum, and only a minor part comes from the filter response from other sources placed further away; 3) complete knowledge of the array manifold $A(\theta)$ is available. The philosophy behind the CLEAN method is as follows :

> *Having found the maximum response in the dirty map, the energy contributions from a point source at this location to all other positions in the map can be determined and subtracted.*

In the CLEAN method, the observed map is called a "dirty" map (d) which is a convolution of the brightness distribution (t_o) with the instrumental response, called the "dirty" beam (b). The dirty map may have some unwanted secondary responses. The aim of the CLEAN method is to remove the effects of these responses. This is done in two steps : first a deconvolution step in which the dirty map is decomposed in a set of scaled δ-function, the component (t) which when convolved with the "dirty" beam would reproduce the original "dirty" map; second, the components are convolved with a hypothetical "clean" beam (h) which is free from the unwanted responses. This finally gives the "clean" map (c).

$d = b * t$ "dirty" map
$c = h * t$ "clean" map

A "true clean" map (c_o) can also be defined as the convolution of the "true" brightness distribution with the clean beam (h).

$c_o = h * t_o$ "true clean" map

The "clean" map (c) can be regarded as an estimate of the "true clean" map (c_o). The deconvolution need not be complete, i.e., leaving residuals (r) added to the "clean" map (c).

In practice, this method is implemented iteratively. A single peak is found at each iteration. Its contribution to the output is obtained by convolving a δ-function in the wavenumber with the system transfer function, and then is subtracted from the data. This procedure is repeated until some criterion is satisfied.

3.4.4 The IMP Algorithm

IMP (Incremental Multi-stage Parameter) of Clarke [Cla87, Cla88, Cla89] is an iterative algorithm. The IMP spatial spectrum starts from the output power distribution of a sensor array which implies that the conventional beamforming is used as the initial stage in the IMP algorithm. A single peak (the global maximum) is found in the output spectrum estimate and the contribution of stimuli in the corresponding direction of the peak is found by convolving a δ-function in wavenumber (or frequency in time series analysis) with the system transfer function. In order to remove the effect of the selected peak, the weighting (pre-conditioning, which is assumed to be uniform in the initial procedure) is modified and applied to the data. This is one feature that differs in IMP relative to CLEAN where the effect of the selected peak is subtracted from the input data directly.

The conventional spectrum estimate under the assumption that the noise correlation matrix is an identity matrix (i.e., the noise at sensors is assumed to be of equal power and uncorrelated from sensor to sensor) is given by

$$P(\theta) = \frac{\mathbf{a}^H(\theta) \cdot \mathbf{X} \cdot \mathbf{X}^H \cdot \mathbf{a}(\theta)}{\mathbf{a}^H(\theta) \cdot \mathbf{a}(\theta)} \tag{3.34}$$

In more general cases where a matrix filter is applied to the input, a suitable expression for the spectrum may be expressed as

$$P(\theta) = \frac{\mathbf{a}^H(\theta) \cdot \mathbf{C} \cdot \mathbf{X} \cdot \mathbf{X}^H \cdot \mathbf{C} \cdot \mathbf{a}(\theta)}{\mathbf{a}^H(\theta) \cdot \mathbf{C} \cdot \mathbf{a}(\theta)} \tag{3.35}$$

where C is the pre-conditioning matrix, which is the identity matrix in the initial iteration and modified afterwards according to the direction estimate in the previous iteration.

The statistic used in the IMP algorithm is the Signal plus Noise to Noise Ratio (SNNR), that

is

$$SNNR(\mathbf{a}) = \frac{\mathbf{a}^H(\theta) \cdot \mathbf{C} \cdot \mathbf{R} \cdot \mathbf{C} \cdot \mathbf{a}(\theta)}{\mathbf{a}^H(\theta) \cdot \mathbf{C} \cdot \mathbf{R}_N \cdot \mathbf{C} \cdot \mathbf{a}(\theta)} \tag{3.36}$$

In the conventional beamformer where uniform weighting is used or when noise pre-whitening is applied to the case when $\mathbf{R}_N = \mathbf{I}$, equation (3.36) is equivalent to equation (3.34) which is used in the initial stage of IMP.

When a dominant peak has been found in the output spectrum estimate, or a global maximum of the SNNR has been identified, the pre-conditioning is adjusted to eliminate, or null, the response in the corresponding direction. The contribution from this direction to the output spectrum is cancelled by a projection matrix which projects into the null space of the array manifold vector of the peak direction in SNNR. Such a projection matrix is as

$$\mathbf{Q} = \mathbf{I} - \frac{\mathbf{a}_{pk} \cdot \mathbf{a}_{pk}^H}{\mathbf{a}_{pk}^H \cdot \mathbf{C}_o \cdot \mathbf{a}_{pk}} \tag{3.37}$$

where $\mathbf{a}_{pk}$ is the array manifold vector in the peak direction, and $\mathbf{C}_o$ is a generalised pre-conditioning matrix in the initial stage which can be set to the identity matrix or the inverse of the noise correlation matrix, or possibly the inverse of the sampled data covariance matrix. The pre-conditioning is then updated

$$\mathbf{C}_1 = \mathbf{C}_o \cdot \mathbf{Q} \cdot \mathbf{C}_o = \mathbf{C}_o - \frac{\mathbf{C}_o \cdot \mathbf{a}_{pk} \cdot \mathbf{a}_{pk}^H \cdot \mathbf{C}_o}{\mathbf{a}_{pk}^H \cdot \mathbf{C}_o \cdot \mathbf{a}_{pk}} \tag{3.38}$$

It is evident from the fact that $\mathbf{a}_{pk}^H \cdot \mathbf{C}_1 \cdot \mathbf{a}_{pk} = 0$ that the output will not contain contributions from noise or signal components matching the array manifold vector $\mathbf{a}_{pk}$. Substituting (3.38) into (3.35), a modified spectrum results with a null in the direction of the global peak in the previous spectrum estimate. The power level of this spectrum is compared with some pre-defined threshold to decide whether to terminate the procedure. If the criterion is not satisfied, the maximum in this modified spectrum is found and the corresponding array manifold vector is used to form a projection matrix and then a new modified spectrum. This procedure is repeated until the termination criterion is met.

The cancellation philosophy employed by IMP has been implemented in the DICANNE (Digital Interference Cancelling Adaptive Null Network Equipment) sonar system [And69].

3.5 Subspace Fitting Methods

The concept of SubSpace Fitting (SSF) was proposed by Viberg and Ottersten [ORK89, OV88, VO91, VOK89, VOK91, etc] for sensor array processing, and so was a common framework to unify different high resolution methods into a so-called subspace fitting class. These methods include the deterministic ML (Det-ML), the Conventional BeamForming method (CBF), MUSIC, Multi-Dimensional MUSIC (MD-MUSIC), and ESPRIT et al. From this framework, algebraic relations between different methods are quite clear and a better understanding of the problem makes it possible to introduce the new algorithm. The optimal Weighted Subspace Fitting (WSF) method resulted.

The formation of the basic subspace fitting problem results from the fact that the Det-ML method tries to fit the subspace spanned by $\mathbf{A}(\theta)$ to the measurement $\mathbf{X}$, which can be defined as

$$[\hat{\mathbf{A}}, \hat{\mathbf{T}}] = arg \min_{\mathbf{A},\mathbf{T}} ||\mathbf{M} - \mathbf{AT}||_F^2 \tag{3.39}$$

where $\mathbf{M}$ is an $m \times q$ matrix representing the observed data, the $m \times p$ matrix $\mathbf{A}$ is parameterised by the directions of arrival, and $\mathbf{T}$ is any non-singular $p \times q$ matrix.

Since the subspace fitting problem is separable in $\mathbf{A}$ and $\mathbf{T}$ [GP73], substituting the pseudo-inverse solution, $\hat{\mathbf{T}} = \mathbf{A}^{+}\mathbf{M}$, into equation (3.39) yields the following equivalent problem

$$\hat{\mathbf{A}} = arg \min_{\mathbf{A}} Tr\{\mathbf{P}_{\bar{A}}(\theta) \cdot \mathbf{M} \cdot \mathbf{M}^{H}\} \tag{3.40}$$

Choosing $\mathbf{M}$ as a Hermitian square root of the covariance matrix $\mathbf{M}\mathbf{M}^{H} = \hat{\mathbf{R}}$ and searching simultaneously in the d-dimensional signal subspace, (3.39) yields the Det-ML method as given in (2.57). Setting $\mathbf{M} = \hat{\mathbf{E}}_S$ and forming a one-dimensional spectrum, the MUSIC algorithm is obtained. It is shown [Vib89] that for a large number of snapshots it is sufficient

to consider the case when $\mathbf{M} = \hat{\mathbf{E}}_S$ only if the signal subspace matrix is post-multiplied by a specific weighting matrix $\mathbf{W}$. Consequently, all methods within the subspace fitting framework minimise the following criterion function

$$V_N = Tr\{\mathbf{P}_A^{\perp}(\theta) \cdot \hat{\mathbf{E}}_S \cdot \mathbf{W} \cdot \hat{\mathbf{E}}_S^H\} \tag{3.41}$$

where $\mathbf{W}$ is a $d \times d$ weighting matrix. Equation (3.41) defines the weighting subspace fitting methods.

It is well known that the Det-ML method does not attain the Cramer-Rao Bound (CRB) as the number of snapshots tends to infinity, since the number of unknowns also increases without limit. This observation encouraged searching for an optimal weighting matrix that results in a method with better asymptotic performance. The covariance matrix of the estimate error for WSF is formed and then minimised with respect to the weighting matrix. It was found that there exists a weighting matrix such that WSF always outperforms Det-ML when the amount of data is large. Such a weighting matrix is

$$\mathbf{W}_{opt} = (\Lambda_S - \sigma^2\mathbf{I})^2\Lambda_S^{-1} \tag{3.42}$$

In practice, only finite measurements are available and the estimates rather than the true values are used to form the WSF criterion function as

$$V(\theta) = Tr\left\{\mathbf{P}_A^{\perp}(\theta) \cdot \hat{\mathbf{E}}_S(\hat{\Lambda}_S - \sigma^2\mathbf{I})^2 \cdot \hat{\Lambda}_S^{-1} \cdot \hat{\mathbf{E}}_S\right\} \tag{3.43}$$

3.6 Other DOA Estimation Techniques

The survey of the high resolution algorithms given above is by no means exhaustive. Only typical examples in each class of method have been included. Many other methods which also provide high resolution abilities have been proposed. In this section, some of the newly suggested methods are described. These include the Method Of Direction Method (MODE) of Stoica and Sharman [SS90a,b] and the CLOSEST estimator of Buckley and Xu et al [BX90b, XB90, HXB90, XBM90].

The MODE Technique

The MODE method is also an eigenstructure based approach with advantages of providing the comparable performance of the ML estimator at a computational load which is not much heavier than that inherent in the popular MUSIC algorithm. The performance advantage over the MUSIC method is that MODE behaves better in highly correlated situations.

The invention of the MODE method was stimulated by the thought of combining the computational simplicity of the MUSIC method and the resolving ability for highly correlated sources of the ML estimator. Eventually, the MODE estimator is a large sample realisation of the deterministic ML estimator under certain approximations, which simplifies the computational complexity while keeping the capability of resolving highly correlated sources.

The CLOSEST Estimator

A new approach to spatial spectrum estimation for arbitrary configured arrays was recently introduced by Buckley and Xu. This new approach is based on forming a spatial spectrum estimate by projecting onto a vector or vector set in the estimated noise-only subspace which is in some sense closest to the array manifold in a sector of source locations where high resolution is desired. Several measures have been used to derive different CLOSEST vector algorithms, such as the FINE (FIrst priNcipal vEctor) algorithm and the FINES (FIrst priNcipal vEctorS) algorithm. It was shown that in a location sector of interest the FINE algorithm provides higher spectral resolution than either MN or MUSIC, with location estimation variance comparable to MUSIC.

In the FINE algorithm, a single vector in the estimated noise subspace is defined which has a minimum angle to a subspace which essentially spans the $a(\theta)$ over Θ. Instead of finding a single vector, FINES finds a set of orthogonal vectors in the noise subspace, whose range has a minimum angle with the source representation subspace.

The selection of the sector width is of great importance in both FINE and FINES algorithms. Beam-width sectors are often recommended since they have both computational and resolution advantages.

3.7 Detection Techniques

Correct detection of signals is of great importance in most signal subspace methods and any parametric estimation method. The issue of estimating the number of signals has been addressed in many papers, e.g., [Sch81, WK83, WK85b, Wax85, WZ88, etc.]. For most situations, the correctness of the knowledge of the number of signals may be crucial for the following parameter estimation since it may lead to incorrect splitting between the signal subspace and the noise subspace. A lot of effort has been expended on this problem.

Anderson's hypothesis testing procedure [And63] might be the first attempt in estimating the number signals. This procedure was based on the confidence interval of the noise eigenvalues and a subjective threshold was required. To avoid the assignment of such a threshold, information theoretic criteria were developed by Akaike [Aka73, Aka74] and Rissanen [Ris78, Ris83], and the so-called AIC (Akaike Information Criterion) and MDL (Minimum Description Length) methods were formulated respectively.

Probably, Liggett [Lig73] was the first to address the problem of estimating the number of signals by exploiting the structure of the underlying model of the data. Under the assumption that the signals are Gaussian random processes, a so-called Likelihood Ratio (LR) statistic is formulated

$$LR(k) = \log\left\{ \frac{\prod_{i=k+1}^{m} \hat{\lambda}_i^{\frac{1}{m-k}}}{\frac{1}{m-k}\sum_{i=k+1}^{m} \hat{\lambda}_i} \right\}^{(m-k)N} \tag{3.44}$$

and tested for a sequence of hypotheses

$$H^{(k)}: \quad \lambda_{k+1} = \lambda_{k+2} = \cdots = \lambda_m$$

The value of k for which $H^{(k)}$ is first accepted is selected as the estimate of the number of signals. The LR test uses the ratio of the arithmetic mean of a set of eigenvalues to their geometric mean to measure their equality.

The two more commonly used criteria based on the information theoretic criteria are the eigenvalue forms of AIC and MDL derived by Wax and Kailath [WK83, WK85b]. They are widely applied in array signal processing since the eigenvalues are available in most high resolution techniques. It was shown that the AIC approach tends to overestimate the number of signals as the number of measurements tend to infinity whilst the MDL criterion yields an asymptotically consistent estimate of the number of signals. When N independent measurements at an array of m sensors are available, the AIC and MDL criteria are given as follows :

$$AIC(k) = -2LR(k) + 2k(2m-k) \qquad k = 0, \cdots, m-1 \tag{3.45}$$

$$MDL(k) = -LR(k) + \frac{1}{2}k(2m-k)\log N \qquad k = 0, \cdots, m-1 \tag{3.46}$$

where k is the number of free adjusted parameters in the parameter vector. The number of signals $\hat{d}$ is determined as the value of k for which either AIC or MDL is minimised.

Schmidt [Sch81] divided the space spanned by the covariance matrix of the array output into the signal subspace and its orthogonal complement, the noise subspace. Ideally, the number of signals can be estimated from the multiplicity of the smallest eigenvalues of the covariance matrix, i.e., the number of eigenvectors spanning the noise subspace. In practice, however, the covariance matrix is calculated as the time average from a finite set of observations, and w.p.1 eigenvalues which are supposed to be equal to the noise variance are all different, and even inseparable from the signal eigenvalues if the SNRs are not high enough or correlation between signals exists. Both AIC and MDL criteria provide more objective approaches to determine the number of signals incident upon a sensor array rather than making the judgement by observing the eigenvalues directly. Both the dimension of the signal subspace and the number of signals are determined simultaneously since they are equal in the case where signals are non-coherent. When signals in different directions are strongly correlated or even coherent (i.e., completely correlated) which is the case in specular multipath propagation, the resulting signal subspace estimate is of a dimension that is usually less than the number of signals. An incorrect division between the signal subspace and the noise subspace causes the failure of most subspace based techniques, including the famous MUSIC algorithm.

In [WZ88], Wax and Ziskind adapted the MDL criterion to the case when fully correlated (coherent) signals are present by using the knowledge of estimation of signal directions. The formulated estimator for the number of signals can be expressed as a minimisation problem as follows

$$\hat{k}_{MDLB} = arg \min_{k \in \{0,\cdots,m-1\}} MDLB(k) \tag{3.47}$$

where $MDLB(k)$ is a slightly different version of the MDL principle from that given in (3.46)

$$MDLB(k) = N(m-k) \cdot \log \frac{\frac{1}{m-k}\sum_{i=1}^{m-k} \lambda_i(\hat{\theta}^{(k)})}{\left(\prod_{i=1}^{m-k} \lambda_i(\hat{\theta}^{(k)})\right)^{\frac{1}{m-k}}} + \frac{1}{2}k(2m-k)\log N \tag{3.48}$$

where $\lambda_1(\theta^{(k)}) \geq \cdots \geq \lambda_{(m-k)}(\theta^{(k)})$ are the non-zero eigenvalues of the $m \times m$ matrix $\mathbf{P}_{\bar{A}}(\theta^{(k)}) \cdot \hat{\mathbf{R}} \cdot \mathbf{P}_{\bar{A}}(\theta^{(k)})$ which depends on $\theta^{(k)}$ that can be estimated by

$$\hat{\theta}^{(k)} = arg \min_{\theta^{(k)}} \left\{ \log \left(\frac{\frac{1}{m-k}\sum_{i=1}^{m-k} \lambda_i(\theta^{(k)})}{\left(\prod_{i=1}^{m-k} \lambda_i(\theta^{(k)})\right)^{\frac{1}{m-k}}} \right) \right\} \tag{3.49}$$

The recently proposed WSF approach requires knowledge of both the number of signals incident on the array and the dimension of the estimated signal subspace. Accompanied with the WSF estimation scheme, a new detection scheme was formulated [VOK91]. The basis of this new scheme is an observation noticed by several researchers [Sch81, Roy87, Cad88]. Given an estimate of the number of signals, the distance between the array manifold and the estimated signal subspace is measured, and the estimate will be accepted if this distance is small enough; otherwise coherent signals are indicated. This is expressed as the WSF cost function converging to zero as the amount of data increases.

CHAPTER 4

PERFORMANCE COMPARISON OF SPECTRAL AND ROOT VERSIONS OF MEM, MVM, MUSIC, AND MNM

MEM, MVM, MUSIC, and MNM have all shown superior angular resolution abilities compared to the conventional beamforming technique, although inevitably, at expense in some form. The estimated DOAs obtained by these methods are depicted by the dominant peak positions in the estimated output spectra, which involve a searching procedure over the field of interest. Intuitively, a heavy computational burden is unavoidable.

Based on the fact that the MUSIC algorithm utilises the orthogonality between the signal steering vectors and the eigenvectors in the noise subspace, a variation of MUSIC which makes use of the roots of the associated polynomial to estimate DOAs was first suggested by Barabell [Bar83], where it was stated that the polynomial rooting technique is also applicable to other methods such as MVM. This method of dealing with the roots of an all-pole direction finding spectrum is addressed as root MUSIC; more generally, it is called the root version of MUSIC and the original MUSIC as the spectral version of MUSIC. Although the uniform linear geometry constraint limits its popularity, it has also attracted public attention.

In this chapter, we would like to restate the root MUSIC and derive root versions of MEN, MVM, and MNM, while focusing our main attention on their asymptotic properties and numerical examples.

Another topic in this chapter is the description of the simulation programmes. Since a large number of simulations is going to be carried out in this and following chapters, the signal and noise models and some assumptions are necessary before the implementation of the

simulations and discussion of the results. The implementation of algorithms will be presented in relevant chapters and that of the four methods to be discussed in this chapter and their root versions will be given before presenting the simulation results.

4.1 Spectral and Root Representations

The output spectra for MEM, MVM, MUSIC, and MNM have been given in the previous chapter, they are rewritten here briefly for the convenience of deriving their root forms.

MEM :
$$P_{MEM}(\theta) = \frac{\mathbf{u}_1^H \cdot \mathbf{R}^{-1} \cdot \mathbf{u}_1}{|\mathbf{u}_1^H \cdot \mathbf{R}^{-1} \cdot \mathbf{a}(\theta)|^2} \tag{4.1}$$

MVM :
$$P_{MVM}(\theta) = \frac{1}{\mathbf{a}^H(\theta) \cdot \mathbf{R}^{-1} \cdot \mathbf{a}(\theta)} \tag{4.2}$$

MUSIC :
$$P_{MUSIC}(\theta) = \frac{1}{\mathbf{a}^H(\theta) \cdot \mathbf{E}_N \cdot \mathbf{E}_N^H \cdot \mathbf{a}(\theta)} \tag{4.3}$$

MNM :
$$P_{MNM}(\theta) = \frac{1}{|\mathbf{a}^H(\theta) \cdot \mathbf{d}|^2} \tag{4.4}$$

The averaging relationship between the ME method and the MV method has been observed soon after the invention of the ME estimator [Bur72], which can be mathematically expressed as

$$\frac{1}{P_{MVM}(\theta)} = \frac{1}{m} \sum_{i=1}^{m} \frac{1}{P_{MEM}(\theta, i)} \tag{4.5}$$

where $P_{MEM}(\theta, i)$ is the output power spectrum with ith order model. The averaging over the ME spectra from one point up to the m-point prediction error filter explains the lower resolution of the ML estimator.

A similar relationship between the MUSIC algorithm and the MN method was proved by Nickel [Nic88], with the exception that the harmonic averaging is weighted. Also, it was shown therein that the MUSIC spectrum and the MN spectrum are the extremes of the MV spectrum and the ME spectrum, respectively, as the signal-to-noise ratio tends to infinity.

This gives a good explanation to the better performance offered by the MUSIC and MN methods compared to that of the MV and ME methods, and also the smoother background in the MUSIC and MV spectra.

Root Versions

The polynomial rooting technique is applicable only to the uniform linear array where the array manifold consists of Vandermonde vectors. For such manifold vectors, the orthogonality to noise subspace eigenvectors occurs for roots of the noise eigenvector polynomials, which produce the peaks in the estimated output spectrum.

All of the four methods which will be included in this chapter can be written in a general "all-pole" direction finding form as follows :

$$P(\theta) = \frac{1}{\mathbf{a}^H(\theta) \cdot \mathbf{M} \cdot \mathbf{a}(\theta)} \tag{4.6}$$

where $\mathbf{M}$ is a Hermitian matrix taking different forms for different methods. We take the MUSIC algorithm as an example for our derivation where $\mathbf{M} = \mathbf{E}_N \cdot \mathbf{E}_N^H$.

In the MUSIC spectrum, peaks appear at positions where the array vectors are orthogonal to noise eigenvectors, i.e.,

$$\mathbf{a}^H(\theta) \cdot \mathbf{e}_k = 0, \qquad k = d+1, \cdots, m \tag{4.7}$$

which, for uniform linear arrays, is equivalent to

$$\sum_{i=1}^{m} e_{ik} \cdot e^{-j2\pi(i-1)\Delta \sin(\theta)/\lambda} = 0 \tag{4.8}$$

defined as the noise eigenvector polynomials. If we set $z = \exp(j2\pi\Delta \sin(\theta)/\lambda) \in C$, then the above expression can be rewritten as

$$D_k(z) = \sum_{i=1}^{m} e_{ik} \cdot z^{-(i-1)} = 0, \qquad k = d+1, \cdots, m \tag{4.9}$$

The signal zeros are defined as roots of each of these polynomials. A polynomial is therefore formulated to combine all these polynomials in the following way

$$D(z) = \sum_{k=d+1}^{m} D_k(z) \cdot [D_k(z)]^* \tag{4.10}$$

which can be simplified to (*cf.* [Bar83])

$$D(z) = \sum_{l=-m+1}^{m-1} b_l \cdot z^{-l} \tag{4.11}$$

where $b_l = \sum_{i-k=l} \mathbf{M}(i,k)$ is the sum of the entries of $\mathbf{M}$ along the lth diagonal.

For the MUSIC algorithm, equation (4.10) is equivalent to

$$\begin{aligned} D(z) &= \sum_{k=d+1}^{m} \left(\sum_{i=1}^{m} e_{ik} \cdot z^{-(i-1)} \right) \cdot \left(\sum_{i=1}^{m} e_{ik} \cdot z^{-(i-1)} \right)^* \\ &= \sum_{k=d+1}^{m} \mathbf{a}^H \cdot \mathbf{e}_k \cdot \mathbf{e}_k^H \cdot \mathbf{a} = \mathbf{a}^H \cdot \mathbf{E}_N \cdot \mathbf{E}_N^H \cdot \mathbf{a} \end{aligned} \tag{4.12}$$

Peaks in the MUSIC spectrum correspond to the zeros in the denominator of the expression in (4.3) which, in turn, are the roots of $D(z)$ lying close to the unit circle in the z-plane. Once these roots are available, the DOAs are ready to be estimated as

$$\theta_i = arcsin\left(\frac{\lambda}{2\pi\Delta}\right) arg(z_i), \qquad i = 1, \cdots, d \tag{4.13}$$

Similarly, the root forms for MEM, MVM, and MNM can be formulated, which are the same as that for the MUSIC algorithm except the form of matrix $\mathbf{M}$.

For MEM, it is seen that the numerator in equation (4.1), where $\mathbf{u}_1$ is the first unit vector, is a scalar which is the (1,1) element of $\mathbf{R}^{-1}$, the inverse of the covariance matrix, $\mathbf{R}$. It can be either included in the denominator or omitted without affecting the roots of eigenvector polynomial, $D(z)$. Matrix $\mathbf{M}$ is defined by the denominator and, for MEM, is given by

$$\mathbf{M} = \mathbf{R}^{-1^H} \cdot \mathbf{u}_1 \cdot \mathbf{u}_1^H \cdot \mathbf{R}^{-1} = \mathbf{r} \cdot \mathbf{r}^H \tag{4.14}$$

where $\mathbf{r} = \mathbf{R}^{-1^H} \cdot \mathbf{u}_1$ is the vector containing the first column of $\mathbf{R}^{-1}$.

Root versions for MVM and MNM are straightforward. The key is also the matrix **M** which, referred to equations (4.2) and (4.4), equals $\mathbf{R}^{-1}$ for MVM and $\mathbf{d} \cdot \mathbf{d}^H$ for MNM.

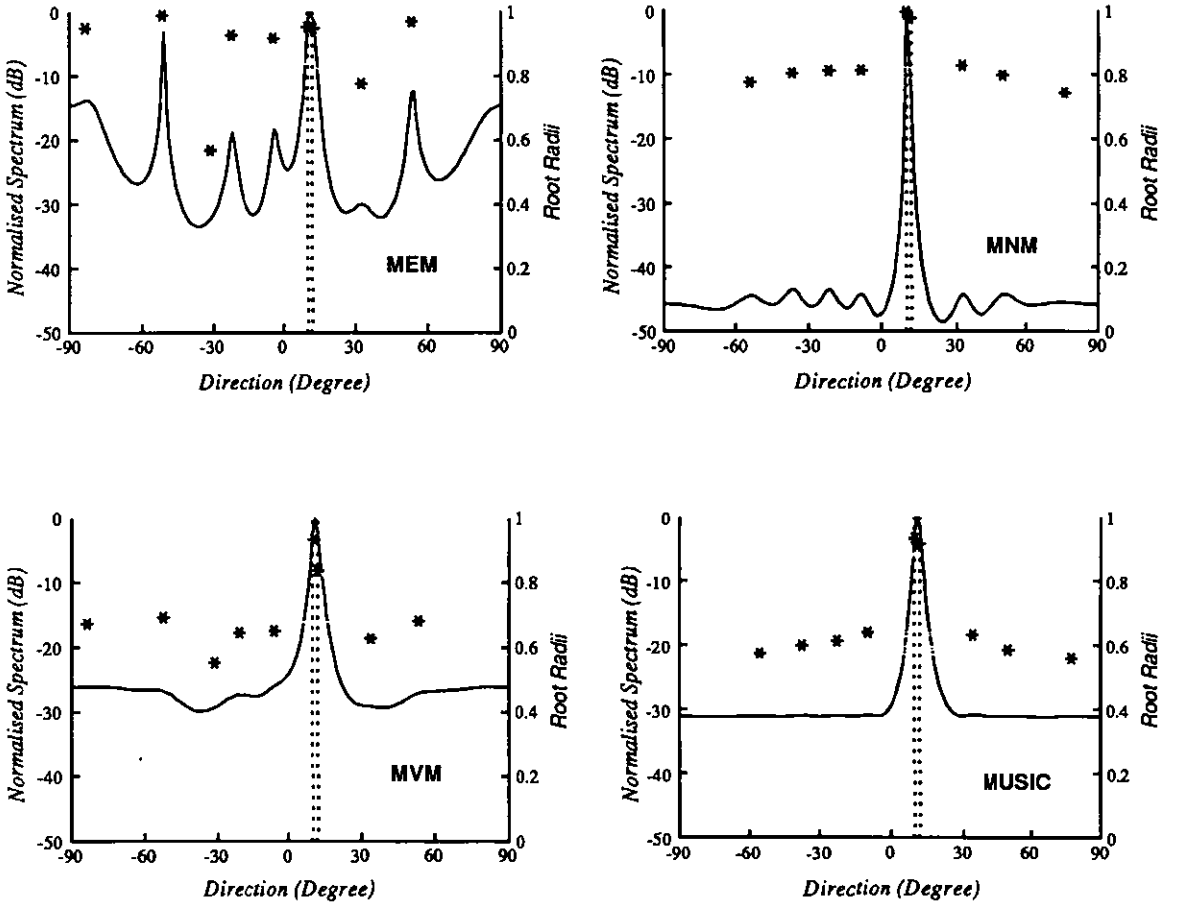

Figure 4.1 Spectra of MEM, MNM, MVM, and MUSIC and their associated polynomial roots for two equal-powered sources located at 10° and 12°. The vertical lines indicate the true locations of the sources. There is only one peak associated with the two closely placed emitters in each spectrum, while the roots show their proper locations. Two uncorrelated sources were used. The array was a uniform linear array with half wavelength spacing. 20 snapshots were taken to form the data matrix.

Figure 4.1 shows a simple but meaningful case where both the spectra and their associated roots for the above mentioned four methods are displayed. In this case, two closely spaced sources with equal powers are used. The spectral versions of the methods are shown to be unable to distinguish the two sources by giving a single peak somewhere in between the two given directions in each of the plots. However, the root versions demonstrate two separate roots near the true DOAs which are depicted by the dotted vertical lines.

4.2 Performance Comparison between Spectral and Root Versions

Figure 4.1 illustrates that root versions of the four methods under consideration can provide DOA estimates with reasonable accuracy while spectral versions fail to show two distinguished peaks in corresponding directions. This resolution degradation exists as long as an estimated covariance matrix is used in estimating the signal zeros and DOAs. It has been shown that spectral MUSIC and root MUSIC have the same asymptotic mean squared error while the derivation of the mean squared error for spectral MUSIC is under the assumption that distinct sources in space correspond to distinct peaks in the spectrum [PF88, RH89a]. However, since radial errors in signal zeros affect the angular spectrum as well as the angular errors in signal zeros, more loss in resolution in the spectral MUSIC is expected, which may cause showing one peak for two closely spaced sources especially when the signal-to-noise ratio is not high enough.

When an estimated covariance matrix is in use instead of the true covariance matrix, which is generally the case in practice, errors arise in the eigenvectors which in turn result in errors in the eigenvector polynomial $D(z)$. Consequently, the roots are perturbed, i.e., errors will appear in signal zeros as well. No matter whether spectral or root forms of eigenstructure based methods are used, errors in the DOA estimates are unavoidable which, in the case of root forms, are angular errors in signal zeros only; while, in the case of spectral forms, errors result from both angular and radial errors in signal zeros.

For a general root approach, equation (4.10) can be expressed in the factored form, given the zeros at $z = z_i, i = 1, \cdots, m-1$, in the following way

$$\begin{aligned} D(z) &= c \prod_{l=1}^{m-1} (1 - z_l \cdot z^{-1}) \cdot (1 - z_l^* \cdot z) \\ &= cH(z) \cdot H^*(1/z^*) \end{aligned} \tag{4.15}$$

where c is a constant resulting from the factorisation. Therefore $H(z) = \prod_{l=1}^{m-1}(1 - z_l \cdot z^{-1})$ can be expressed in the polynomial form as

$$H(z) = 1 - h_1 \cdot z^{-1} - \cdots - h_{m-1} \cdot z^{-(m-1)} \tag{4.16}$$

Define the perturbed zeros of $H(z)$ as $z_i + \Delta z_i, i = 1, \cdots, m-1$ when errors exist in the coefficients $h_i, i = 1, \cdots, m-1$. The error Δz_i can be expressed in terms of the errors in the coefficients as (*cf*, [OS75])

$$\Delta z_i = \sum_{k=1}^{m-1} \frac{\partial z_i}{\partial h_k} \cdot \Delta h_k, \qquad i = 1, 2, \cdots, m-1 \tag{4.17}$$

so we have, from (4.14) and the fact that $\left(\frac{\partial H(z)}{\partial z_i}\right)\Big|_{z=z_i} \cdot \frac{\partial z_i}{\partial h_k} = \left(\frac{\partial H(z)}{\partial h_k}\right)_{z=z_i}$

$$\frac{\partial z_i}{\partial h_k} = \frac{z_i^{-k}}{-z_i^{-1}\prod_{\substack{l=1 \\ l \neq i}}^{m-1}(1 - z_l \cdot z_i^{-1})} = \frac{z_i^{m-k}}{\prod_{\substack{l=1 \\ l \neq i}}^{m-1}(z_i - z_l)} \tag{4.18}$$

which is a measure of the sensitivity of the ith zero to an error in the kth coefficient of $H(z)$, and therefore

$$\Delta z_i = \sum_{k=1}^{m-1} \frac{z^{m-k}}{\prod_{\substack{l=1 \\ l \neq i}}^{m-1}(z_i - z_l)} \cdot \Delta h_k = \frac{z^m}{\prod_{\substack{l=1 \\ l \neq i}}^{m-1}(z_i - z_l)} \cdot \sum_{k=1}^{m-1} z^{-k} \cdot \Delta h_k \tag{4.19}$$

Correspondingly, the sensitivity of the zeros of $H(z)$ to perturbations in its coefficients can be defined as

$$s = \sum_{k=1}^{m-1} \left|\frac{\partial z_i}{\partial h_k}\right|^2 = \frac{m-1}{\prod_{\substack{l=1 \\ l \neq i}}^{m-1}|(1 - z_l \cdot z_i^{-1})|^2} \tag{4.20}$$

The estimated $D(z)$ due to errors in signal zeros is [RH89b]

$$\hat{D}(z) = \hat{c} \sum_{l=1}^{m-1} (1 - (z_l + \Delta z_l) \cdot z^{-1})(1 - (z_l + \Delta z_l)^* z) \tag{4.21}$$

where $\hat{c}$ is a constant. Substituting the "clean" signal zero $z = z_i, |z_i| = 1$, we have

$$\hat{D}\left(e^{j\omega_i}\right) \approx \hat{c} \cdot |\Delta z_i|^2 \prod_{\substack{l=1 \\ l \neq i}}^{m-1} |(1 - z_l z_i^{-1})|^2 \tag{4.22}$$

the approximation is $o(N^{-1})$, i.e., the terms dropped approach zero when multiplied by N and N tends to infinity. The mean squared error, $\overline{|\Delta z_i|^2}$, is obtained by taking expectations of both sides of the equation (4.19), i.e.,

$$\overline{|\Delta z_i|^2} = \frac{\overline{D}(e^{j\omega_i})}{\hat{c} \prod_{\substack{l=1 \\ l \neq i}}^{m-1} |(1 - z_l z_i^{-1})|^2} = S_{MU} \cdot \frac{\overline{D}(e^{j\omega_i})}{m} \tag{4.23}$$

where $S_{MU} = m / \left(\hat{c} \prod_{\substack{l=1 \\ l \neq i}}^{m-1} |(1 - z_l \cdot z_i^{-1})|^2 \right)$ is interpreted as the parameter sensitivity of the root

MUSIC method. A computationally more convenient expression for S_{MU} has been derived as

$$S_{MU} = \frac{m}{\mathbf{a}'^H(\theta) \cdot \mathbf{E}_N \cdot \mathbf{E}_N \cdot \mathbf{a}'(\theta)} \tag{4.24}$$

where $\mathbf{a}'(\theta)$ is the first derivation of the steering vector $\mathbf{a}(\theta)$. After the derivation of $\overline{D}(e^{j\omega_i})$ of equation (4.23) which is omitted here, $\overline{|\Delta z_i|^2}$ is given by

$$\overline{|\Delta z_i|^2} = \frac{S_{MU}}{m} \cdot \frac{(m-d)\sigma_n^2}{N} \cdot \left(\sum_{k=1}^{d} \frac{\lambda_k}{(\lambda_k^s)^2} \cdot |\mathbf{a}^H(\theta) \cdot \mathbf{e}_k|^2 \right) \tag{4.25}$$

where λ_k^s are "pure" signal eigenvalues while λ_k are those corrupted by noise covariance σ^2, i.e., $\lambda_k = \lambda_k^s + \sigma^2$.

Errors in signal zeros, Δz_i, distribute in both radian and angle. Denote $\Delta z_i = r_i \cdot e^{j\phi_i}$, then $\hat{z}_i = z_i + \Delta z_i = e^{j\omega_i} + r_i \cdot e^{j\phi_i} = |\hat{z}_i| \cdot e^{j\hat{\omega}_i}$. It was shown that [RH89b]

$$\overline{|\Delta\theta_i|^2} = \left(\frac{\lambda}{2\pi\Delta \operatorname{Cos}\theta_i}\right)^2 \cdot \overline{r^2 \cdot \operatorname{Sin}^2(\phi_i - \omega_i)} \tag{4.26}$$

which is deduced as

$$\overline{|\Delta\theta_i|^2} = \left(\frac{\lambda}{2\pi\Delta \operatorname{Cos}\theta_i}\right)^2 \cdot S_{MU} \cdot \frac{\sigma^2}{2mN} \cdot \left(\sum_{k=1}^{d} \frac{\lambda_k}{(\lambda_k^s)^2} \cdot |e_k^H \cdot a(\theta_i)|^2\right) \tag{4.27}$$

Compare $\overline{|\Delta z_i|^2}$ in (4.25) and $\overline{|\Delta\theta_i|^2}$ in (4.26), we can see that

$$\frac{\overline{|\Delta\theta_i|^2}}{\overline{|\Delta z_i|^2}} = \frac{2(m-d)}{\left(\frac{\lambda}{2\pi\Delta}\operatorname{Cos}\theta_i\right)^2} \geq \frac{2(m-d)}{\left(\frac{\lambda}{2\pi\Delta}\right)^2} \overset{\Delta=\lambda/2}{=} 2\pi^2(m-d) \tag{4.28}$$

Including the factor $(\lambda/(2\pi\Delta \operatorname{Cos}\theta_i))^2$, a parameter γ addressed as the spectral efficiency factor is defined as

$$\gamma = \left(\frac{2\pi\Delta \operatorname{Cos}\theta_i}{\lambda}\right)^2 \cdot \frac{\overline{|\Delta\theta_i|^2}}{\overline{|\Delta z_i|^2}} \tag{4.29}$$

which is a measure of the effectiveness of using a spectral approach. Evidently, spectral MUSIC is much less effective than root MUSIC. For any moderate Δ (not tending to zero), spectral MUSIC suffers a large degradation in resolution.

A similar relationship between spectral MNM and root MNM is proved to exist as well [RH89b]

$$\frac{\overline{|\Delta\theta_i|^2_{MN}}}{\overline{|\Delta z_i|^2_{MN}}} = \frac{1}{2} \cdot \left(\frac{\lambda}{2\pi\Delta \operatorname{Cos}\theta_i}\right)^2 \tag{4.30}$$

which is not related with the number of sources and that of sensors. The difference between spectral and root MNM is much smaller than that between spectral and root MUSIC.

4.3 Signal and Noise Models in the Computer Simulation

The computer simulations were carried out on an IBM PC using the package MATLAB (MATrix LABoratory). The array is assumed to be uniform linear array with half wavelength spacing. 10 elements are used and all the sensors are assumed to be omnidirectional.

Two uncorrelated signals are generated from sine waves at two different frequencies. The required correlation between the two signals is guaranteed by applying equation (2.25) if correlated signals are needed. The difference between the two signal frequencies is chosen so that non-correlation is guaranteed and so is the narrowband signal assumption. The noise is assumed to be Gaussian white noise with zero mean and unit variance.

Although fully correlated sources are expected when the correlation factor is assigned as 1, only very strongly correlated sources can be obtained in the finite sample case. In the following simulations, when the correlation factor is given as 1, it does not mean that completely coherent sources are applied.

4.4 Monte Carlo Results

Some Monte Carlo simulations have been carried out and are presented in this section, providing more insight into the performance of algorithms which have been analyzed in previous sections. Data was collected from a uniform linear array of 10 elements with half wavelength spacing receiving signals from two far field point sources which have been assumed uncorrelated, and correlated with a correlation factor being 0.5 and 0.95 respectively. Results, in terms of probability of resolution, bias and standard deviation of the estimated angles, were obtained for scenarios where the signal-to-noise ratio and angular separation of two sources were varied. In each of a number of discrete angular separations and signal to noise ratios, 500 trials were taken to form the statistics, and for each of these trials 100 independent samples were observed.

The observed field was $[\theta_1 - 5°, \theta_2 + 5°]$ for the spectral versions (where θ_1 and $\theta_2 (> \theta_1)$ are the two source directions), i.e., only the segment of spectra within this region was checked and the peaks were found. The angular increment was 0.1°. Once two estimates were observed, they were to be examined with respect to whether they could be regarded as estimates of the true directions of signals. Two criteria were deployed for the judgement : 1) the response at the mid-point of these direction estimates is smaller than both responses

at these two directions; 2) the estimates are within $\pm 3°$ from the true directions, which are known in simulations, i.e., $|\hat{\theta}_i - \theta_i| \leq 3°$. When only a single peak could be found in the resulting spectra, the methods are regarded as failing to resolve the two sources.

For the root versions, since 10 elements were assumed in the array, 9 roots were found in each trial and only two of them were the possible DOAs. To choose these two roots out of 9, criteria were set: the estimates nearest to the true directions were thought to be the wanted estimates if their moduli were greater than 0.7, and a separation of 0.5° between the two estimates were required.

Algorithms are grouped into A and B for convenience of discussion

A:	Spectral MEM	B:	Root MEM
	Spectral MVM		Root MVM
	Spectral MNM		Root MNM
	Spectral MUSIC		Root MUSIC

4.4.1 Results as Functions of Signal to Noise Ratio

To test the algorithm performance of Groups A and B as a function of signal to noise ratio (SNR), the angular separation is fixed at 2° with one source at 0° and the other at 2° from the normal of the array. The probability of resolution, biases and standard deviations of angular estimates of both sources were examined. The results are plotted as follows :

	Correlation Factor	**Group A**	**Group B**
Figure 4.2	$\rho = 0.0$	(a) - (e)	(f) - (j)
Figure 4.3	$\rho = 0.50$	(a) - (e)	(f) - (j)
Figure 4.4	$\rho = 0.95$	(a) - (e)	(f) - (j)

In each of these figures, (a) - (e) refer to the spectral versions (Group A) of the algorithms under examination and (f) - (j) to the root versions (Group B). More straightforwardly, the results in the left column are from the spectral versions and those in the right one from the

root versions. The samples are taken at 5 dB increments, and the results of different algorithms are depicted by different line styles as indicated in the plots of probability of resolution. The contents of each plot are listed as follows :

Plot	Version	Content
(a)	Spectral	Probability of Resolution
(b)	Spectral	Bias of Angular Estimates of Source at 0° (#1)
(c)	Spectral	Bias of Angular Estimates of Source at 2° (#2)
(d)	Spectral	Standard Deviation of Source #1
(e)	Spectral	Standard Deviation of Source #2
(f)	Root	Probability of Resolution
(g)	Root	Bias of Angular Estimates of Source #1
(h)	Root	Bias of Angular Estimates of Source #2
(i)	Root	Standard Deviation of Source #1
(j)	Root	Standard Deviation of Source #2

4.4.1.1 Probabilities of Resolution

The probabilities of resolution of all four of these methods and their root versions increase as the Signal-to-Noise Ratio (SNR) improves. The MNM starts to resolve the sources at the lowest threshold for both the spectral and root versions, and for all three cases when the correlation factors are assigned different values. For spectral versions, the MUSIC algorithm and the MEM possess similar resolving abilities; while, for the root versions, the MUSIC algorithm resolves the two sources at a lower SNR. Both versions of the MVM need the highest resolution threshold among these four methods at different correlation factors.

The SNRs at which the spectral versions begin to distinguish the two sources are the same for each method for the cases when the correlation factors are 0 and 0.50. The differences rely on the fact that for all methods the probabilities of resolution have smaller values in the 0.50 correlation case than in the uncorrelated case at the same SNRs.

The root versions demonstrate a bigger probability of resolving the two sources at lower SNRs when the correlation between the two sources is stronger. However, the trend of decreasing resolution abilities as the correlation increases is similar to that in the spectral cases. A bigger degradation is expected when the correlation factor is large.

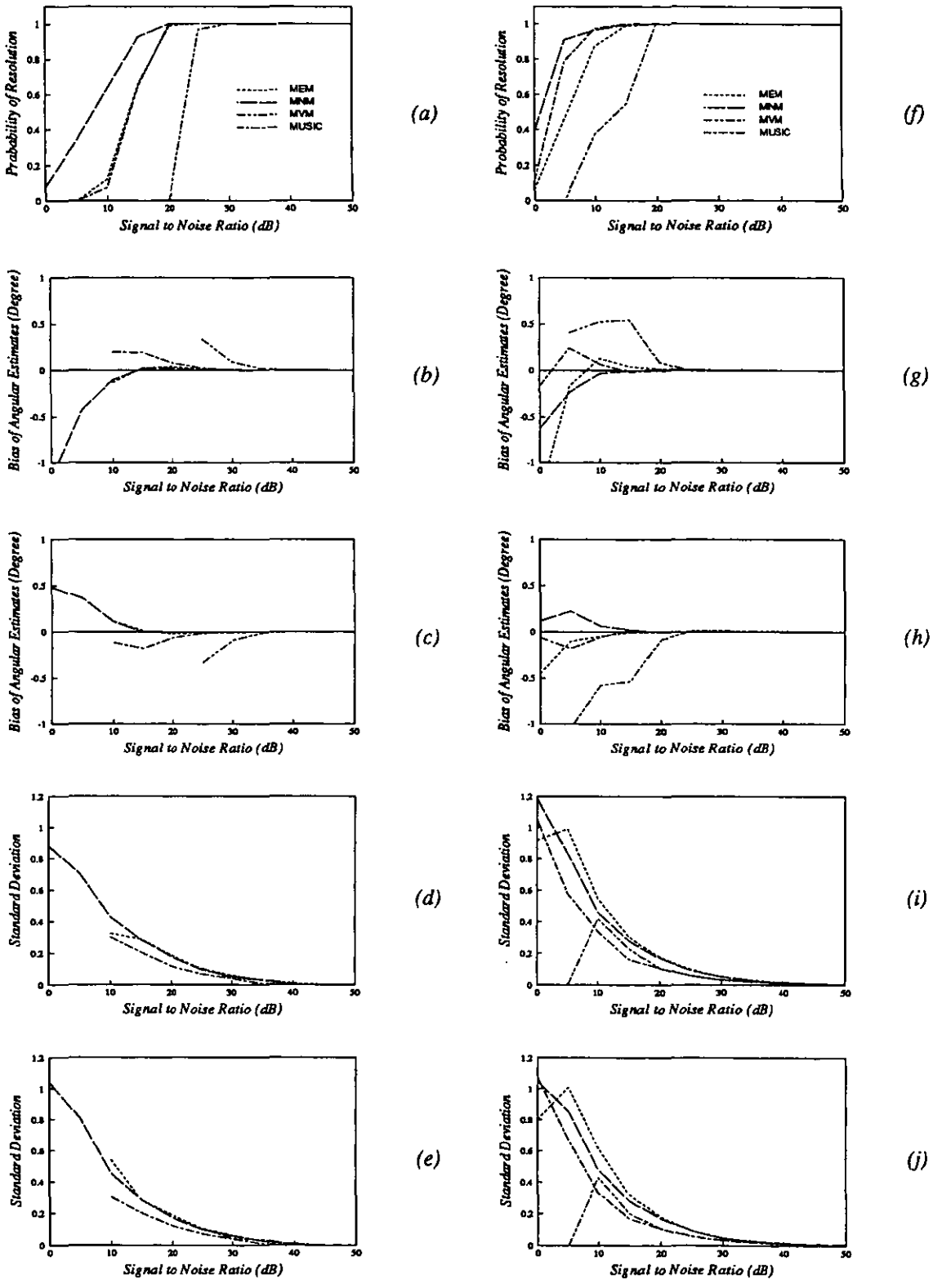

Figure 4.2 Statistics of spectral and root versions of MEM, MNM, MVM, and MUSIC

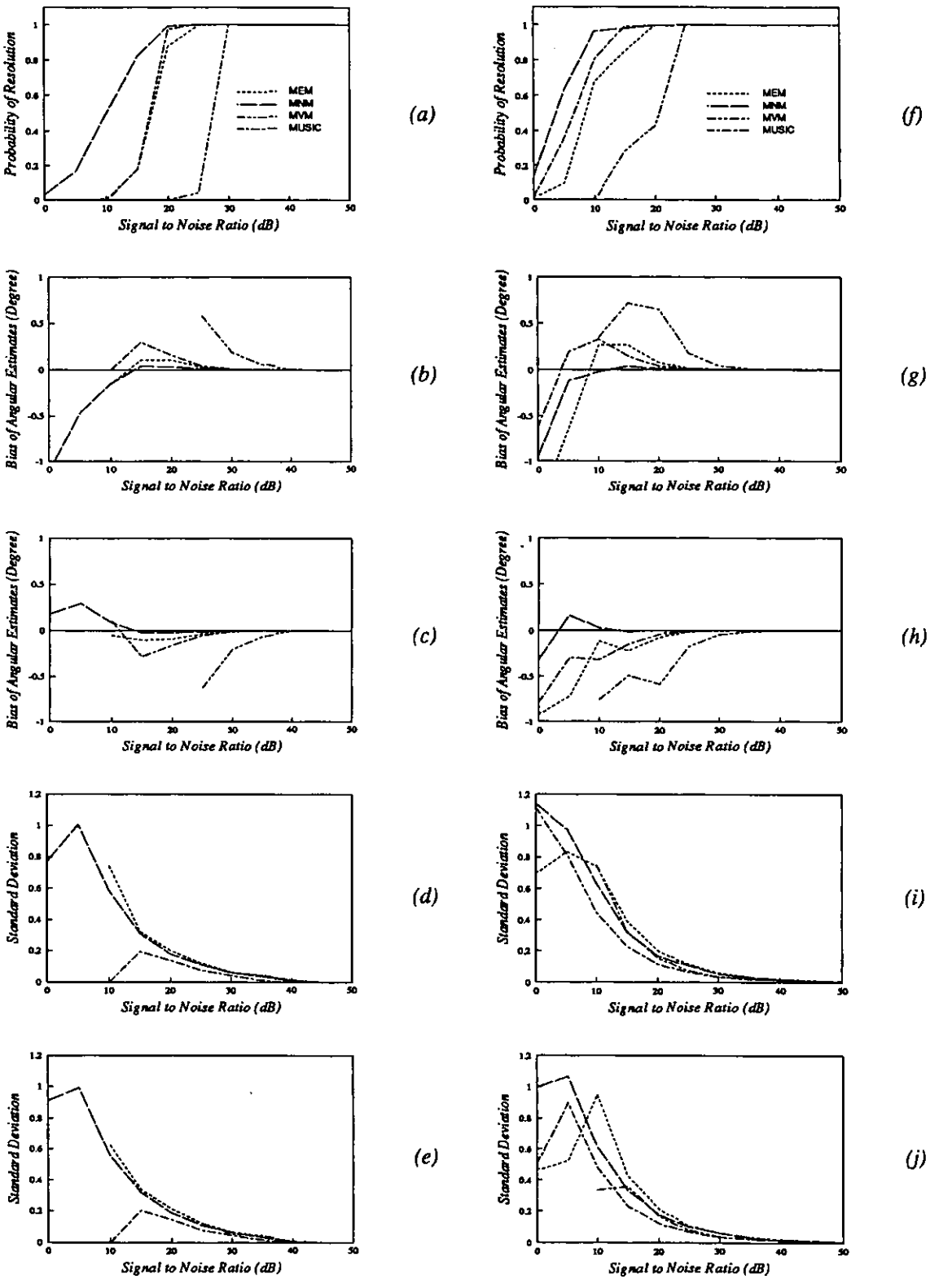

Figure 4.3 Statistics of spectral and root versions of MEM, MNM, MVM, and MUSIC

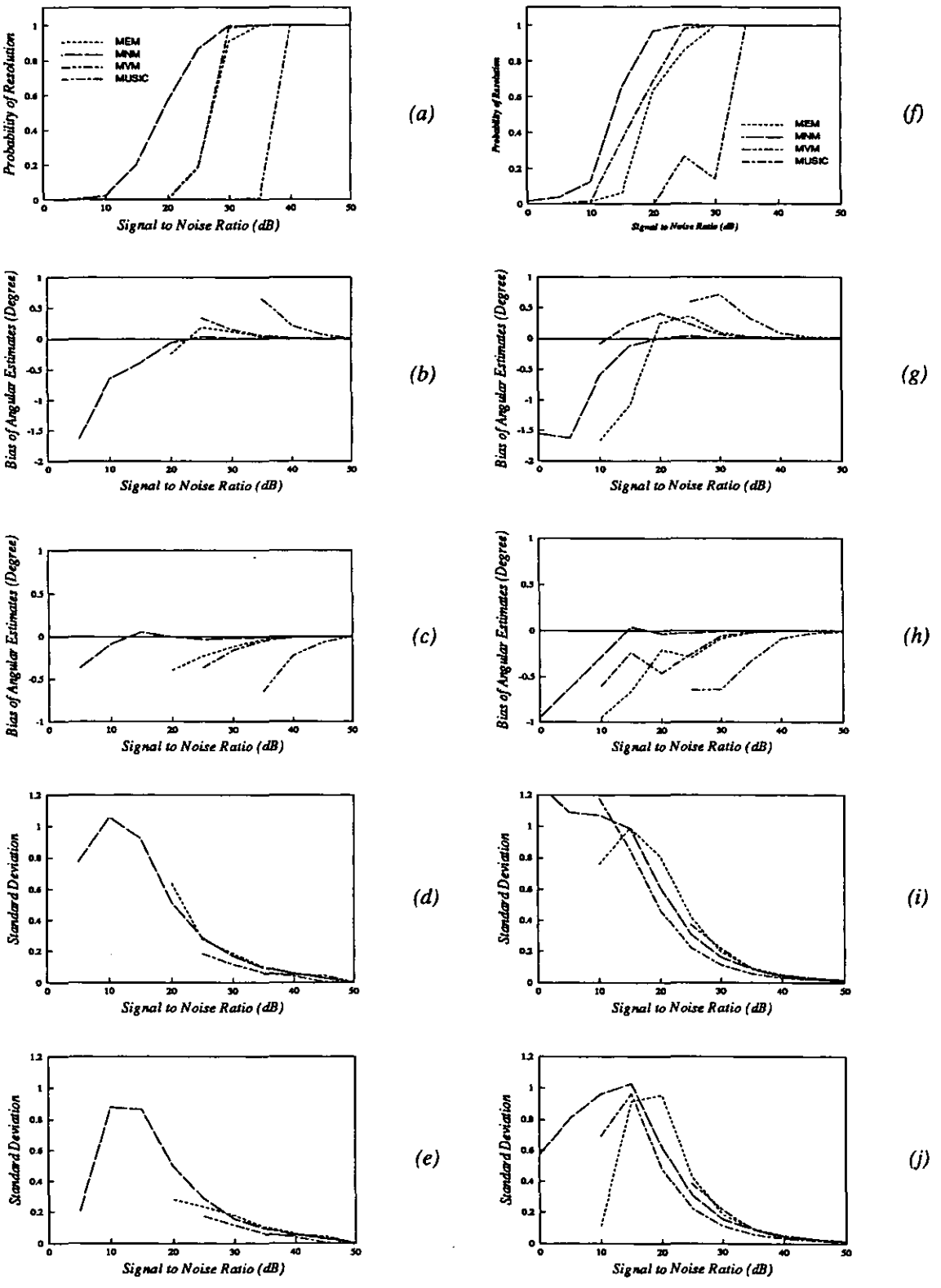

Figure 4.4 Statistics of spectral and root versions of MEM, MNM, MVM, and MUSIC

The resolvabilities degrade as the correlations between the two sources get bigger, i.e., higher SNR is needed to achieve the same probability of resolution at higher correlation. The right-bound shifts of the plots of the probabilities of resolution from the correlation factor from 0.50 to 0.95 are much bigger than those from correlation factor 0 to 0.50.

The case when the correlation factor is unity (fully correlated sources) was also examined. Both the spectral and root versions fail to resolve the two sources. In the spectral case, only a single peak was revealed. In the root case, among the 9 roots which were obtained from the 10 element array either only one root showed very big modulus or several of them were of the same order so that none of them could be reasonably regarded as the signal root. This is consistent with the theoretical prediction.

4.4.1.2 Biases of Angular Estimates

Biases of angular estimates for both sources were examined and plotted. For all situations considered in the simulations herein, biases tend to zero as the SNR goes very high. In the spectral cases, although the MNM starts to resolve the two sources at relatively lower SNR, it shows large biases over that region. The probabilities of resolution of spectral MUSIC and spectral MEM are similar while the MUSIC algorithm suffers slightly higher biases. MVM begins to separate the two sources at a higher SNR and also depicts higher biases. Positive biases in most of the plots of the first sources and negative in those of the second sources imply that the peaks (if there were two) declined to the middle point between the two source directions. This is especially the case when the correlation factors are getting bigger, while MNM seems to be an exception.

Comparatively, the biases resulting from the root versions show bigger fluctuations. Again, MVM gives the biggest biases in all three cases with different correlation factors even when the four methods are able to resolve the two sources, while the other three methods show comparative biases. When the probabilities of resolution are still small, the corresponding statistics are less meaningful in providing the comparable performance. As the probabilities get larger, MNM depicts the smallest biases while MUSIC shows smaller biases than MEM, which is opposed to that in the spectral cases. In the highly correlated case, the differences among the biases given by different methods are more noticeable. MUSIC and MEM perform similarly while MNM behaves better and MVM worse, concerning the biases of angular estimates.

4.4.1.3 Standard Deviations

Standard deviations of the direction estimates were also examined. They all tend to be near zero as the SNR goes very high, no matter whether the sources are uncorrelated or correlated and how strong the correlation is (but not fully correlated).

For the uncorrelated cases, both spectral and root versions show a smooth decrease in the standard deviations as the SNR goes higher. Although MNM demonstrates higher resolving abilities at lower SNRs and smaller biases than those from MUSIC and MVM, high standard deviations exist before other methods begin to resolve the two sources. At SNRs when all the four methods are able to resolve the two sources, the standard deviations are comparable to each other while those from the MUSIC method are lower in the spectral case; and those from MUSIC and MVM are both smaller than those from the other two methods in the root versions, mainly in the uncorrelated and weakly correlated cases.

All four methods demonstrate better resolving abilities at lower SNRs in the root forms than in the spectral forms. However, under the condition that the spectral versions give separate estimates, the standard deviations are roughly the same. This is consistent with the theoretical derivation in [PF88, RH89a].

In figure 4.3, where the case with 0.5 correlation is given, a few points in the plots need explanations. In figures (d) and (e), the standard deviations given by the MUSIC algorithm are on the horizontal axis when the SNR equals 10 dB. The probability of resolution at this point is 0.002 which implies that only one of the 500 trials gives two estimates that can be accepted as estimates. From the point of view of the statistics, this point should not be included since only a single sample is available. It is given here in the plot merely because the MUSIC method shows the possibility of separating two sources at this SNR. This is typical for this class of "false" points in the plots. 12 is usually taken as the minimum number of samples which can be used to calculate the statistical measures. Since 500 trials were used in the simulations for each set-up of parameters, the probability of resolution is required to be not less than 0.024 to give a meaningful statistical quantity. This helps to explain the sharp turnings in some of the plots shown in figure 4.4.

4.4.2 Results as Functions of Angular Separation

The performance of algorithms as functions of angular separation was studied when the signal to noise ratio was 10 dB for both sources (not the array signal to noise ratio which is conventionally defined as the SNR at each element of the array per snapshot + $10\log_{10}(m)$). The increment of angular separation was 1°. Again, the performance was tested for different correlation factors and results are shown in figures as follows:

	Correlation Factor	Group A	Group B
Figure 4.5	$\rho = 0.0$	(a) - (e)	(f) - (j)
Figure 4.6	$\rho = 0.50$	(a) - (e)	(f) - (j)
Figure 4.7	$\rho = 0.95$	(a) - (e)	(f) - (j)

Statistics which have been examined were the same as those in the previous sub-section and were arranged in each figure in the same way.

4.4.2.1 Probabilities of Resolution

The probabilities of resolution depicted in plots (a) and (f) from figure 4.5 through figure 4.7 show the same trends as those in figures 4.2 to 4.4 as functions of signal-to-noise ratios. For algorithms in Group A (the spectral versions), the MNM needs the lowest resolution threshold and the MVM the highest resolution threshold while the MUSIC method the MEM share roughly the same threshold and the same resolution possibility. This is similar to the situation in the previous sub-section. However, as the correlation between the two sources gets stronger the difference between the possibilities offered by the MUSIC method (which is obviously bigger) and the MEM emerges, although the thresholds are still the same which changed from 1° separation, to 2° and then to 4° separation. Meanwhile, the threshold for MVM is from 4°, to 5° and then to 6°, and that for MNM from 1° in both the uncorrelated case and the case with 0.5 correlation factor to 2° separation in the strongly correlated when the correlation factor is 0.95.

The root versions of all these methods also show degradation in the probabilities of resolution as the correlation gets stronger. Compared to the spectral case, a 2° equivalent advantage

SMART Plus UV/VIS Spectrophotometer

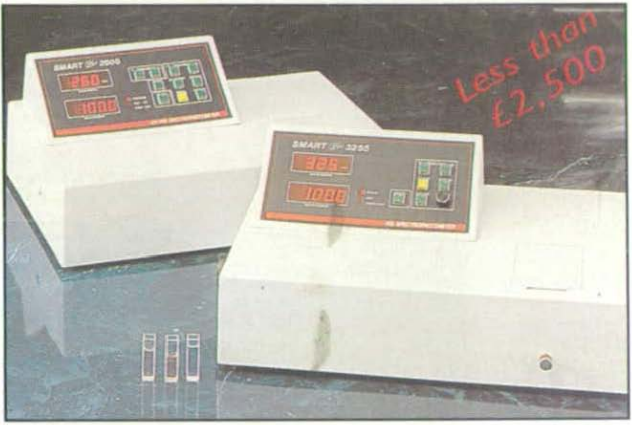

Measuring:

- Transmittance
- Absorbance
- Concentration

- Easy to operate
- Robust
- Reliable
- Low Cost

For more details please contact: –

Angela Davies

L.O.T.-ORIEL LTD

1 Mole Business Park, Leatherhead
Surrey KT22 7AY
Tel: 0372 378822 Fax: 0372 375353

LOT ORIEL LASERS • OPTICS TECHNOLOGY

BUSINESS REPLY SERVICE
Licence No. KT 4001

03/09

Name

Position

Company name

Company address

Postcode

Tel. No.

L.O.T.-ORIEL LTD
1 MOLE BUSINESS PARK
LEATHERHEAD
SURREY
KT22 7AY

exists in all three cases for all four methods. The order of four methods in resolving the two sources remain the same for different correlation factors and so does the diversion among them.

4.4.2.2 Biases of Angular Estimates

The biases shown in figure 4.5 tend to converge as the two sources are more widely placed. What is different from those as functions of SNRs is that the biases do not completely vanish as the angular separation becomes large. Especially, in the group of spectral versions, the biases obtained from MEM seem to be constant over a wide band of the angular separations. On the other hand, both MEM and MVM give visible biases even at the separation of 12° in the root versions.

In figure 4.6 where the sources with 0.5 correlation factor were examined, the spectral versions of MEM and MVM both suffer from biases at big angular separation; while in the root versions, the performance degradation of MVM is more severe than that of MEM. This performance degradation is more serious in the highly correlated source cases shown in figure 4.6. The MUSIC algorithm shows constant biases in both the spectral and root versions, and MVM gives about 0.5° bias. Although MEM shows very high bias at smaller angular separations, the biases tend to be at the same level as those in the uncorrelated and weakly correlated cases. Comparatively, MNM behaves much better in both versions.

4.4.2.3 Standard Deviations

Plots (d), (e), (i), and (j) in figures 4.5 through 4.7 give a clear picture of the behaviour of all four methods in both versions in the measure of standard deviation. Although the MN method shows lower bias in all three cases with different correlation factors, its standard deviations are higher than those given by MVM and MUSIC, at the same level as the ME method. At the 0.5 correlation factor, the difference between the standard deviations given by MNM and MEM, and that between MUSIC and MVM are still not significant. As the correlation increases to 0.95, these differences are shown in both the spectral and the root situations. MNM suffers from the highest deviations, which are higher than those given by MEM; the standard deviation given by the MUSIC method is beneath both those given by MNM and MEM, while MVM demonstrates the lowest deviations.

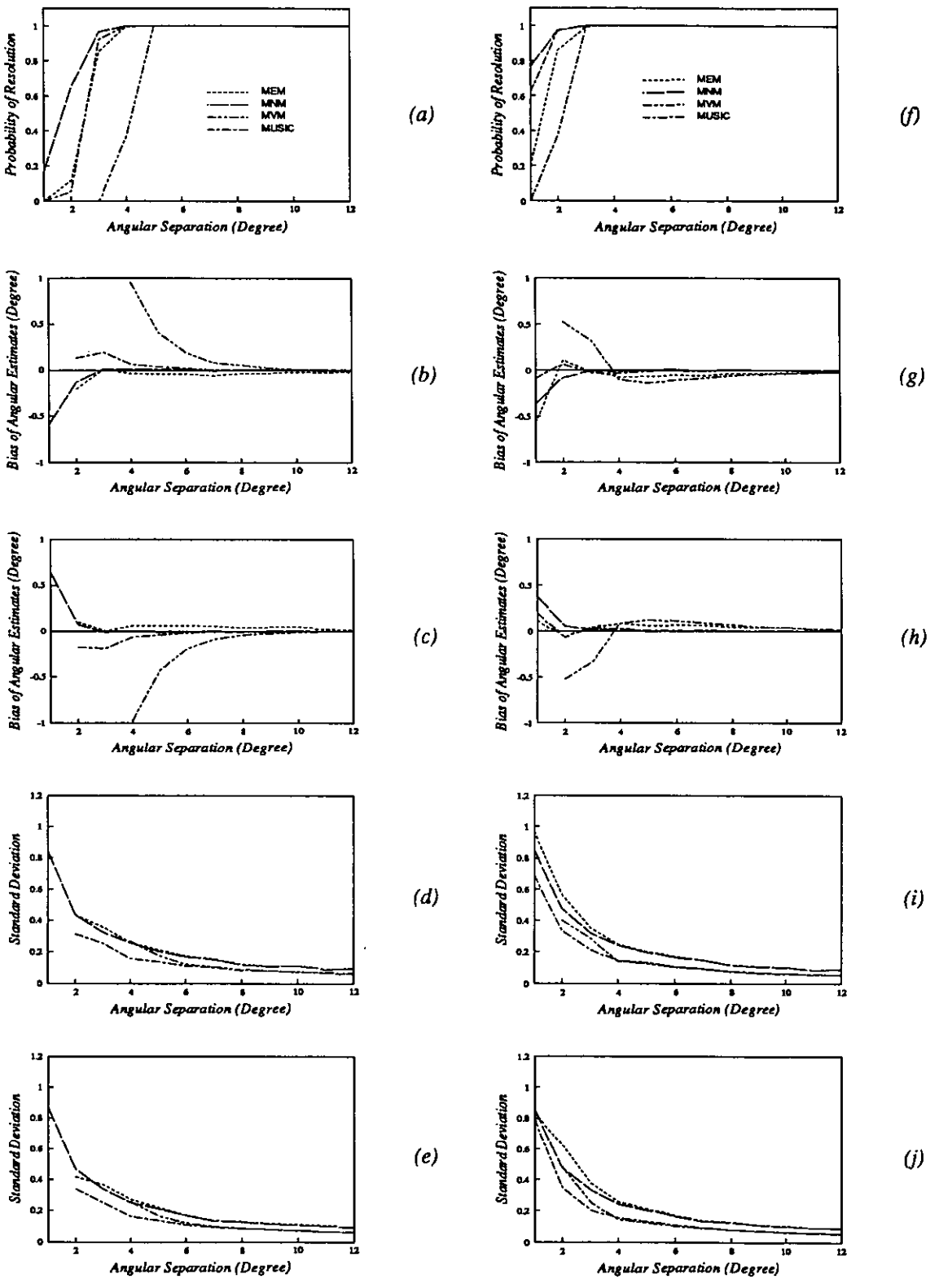

Figure 4.5 Statistics of spectral and root versions of MEM, MNM, MVM, and MUSIC

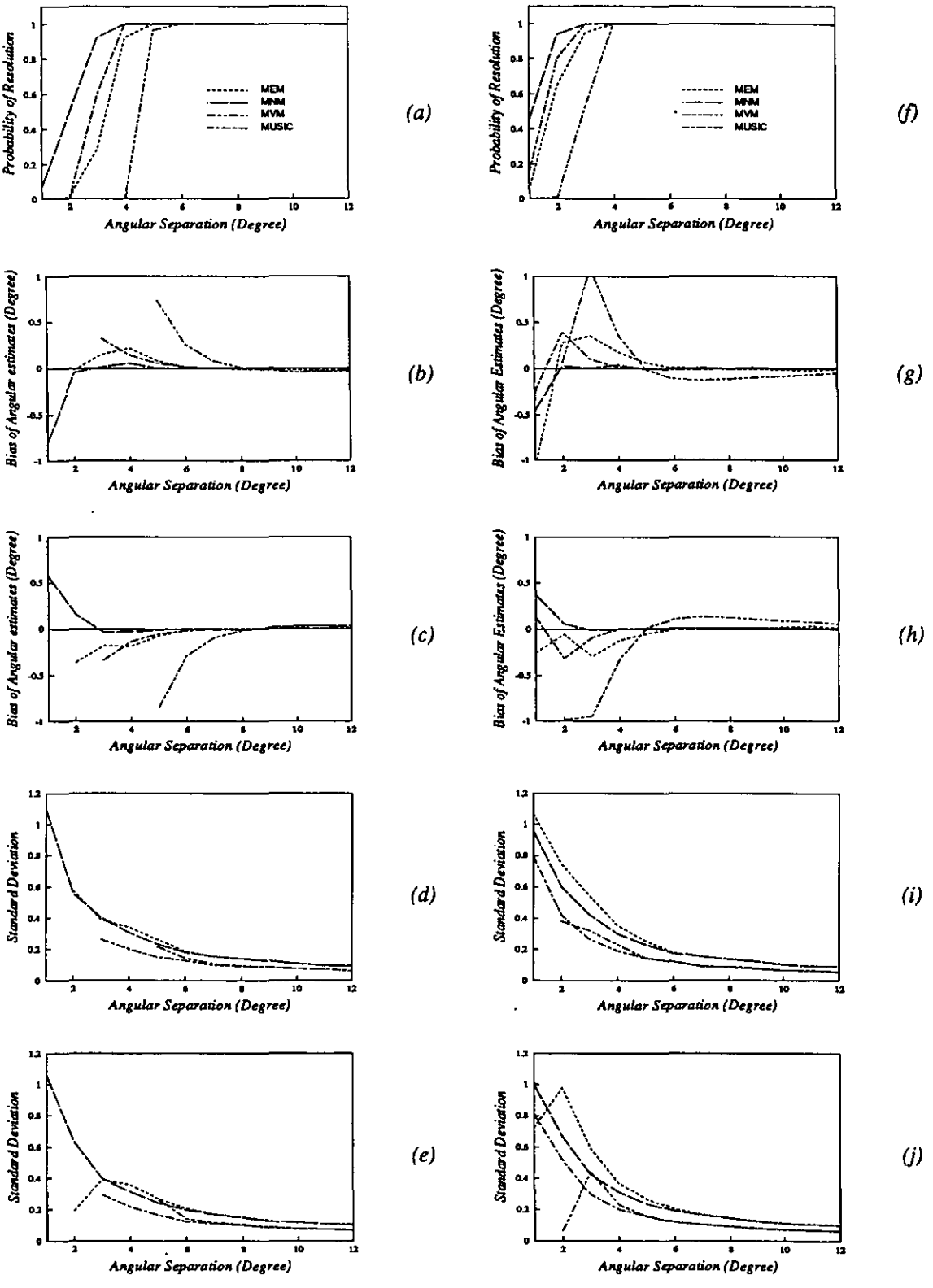

Figure 4.6 Statistics of spectral and root versions of MEM, MNM, MVM, and MUSIC

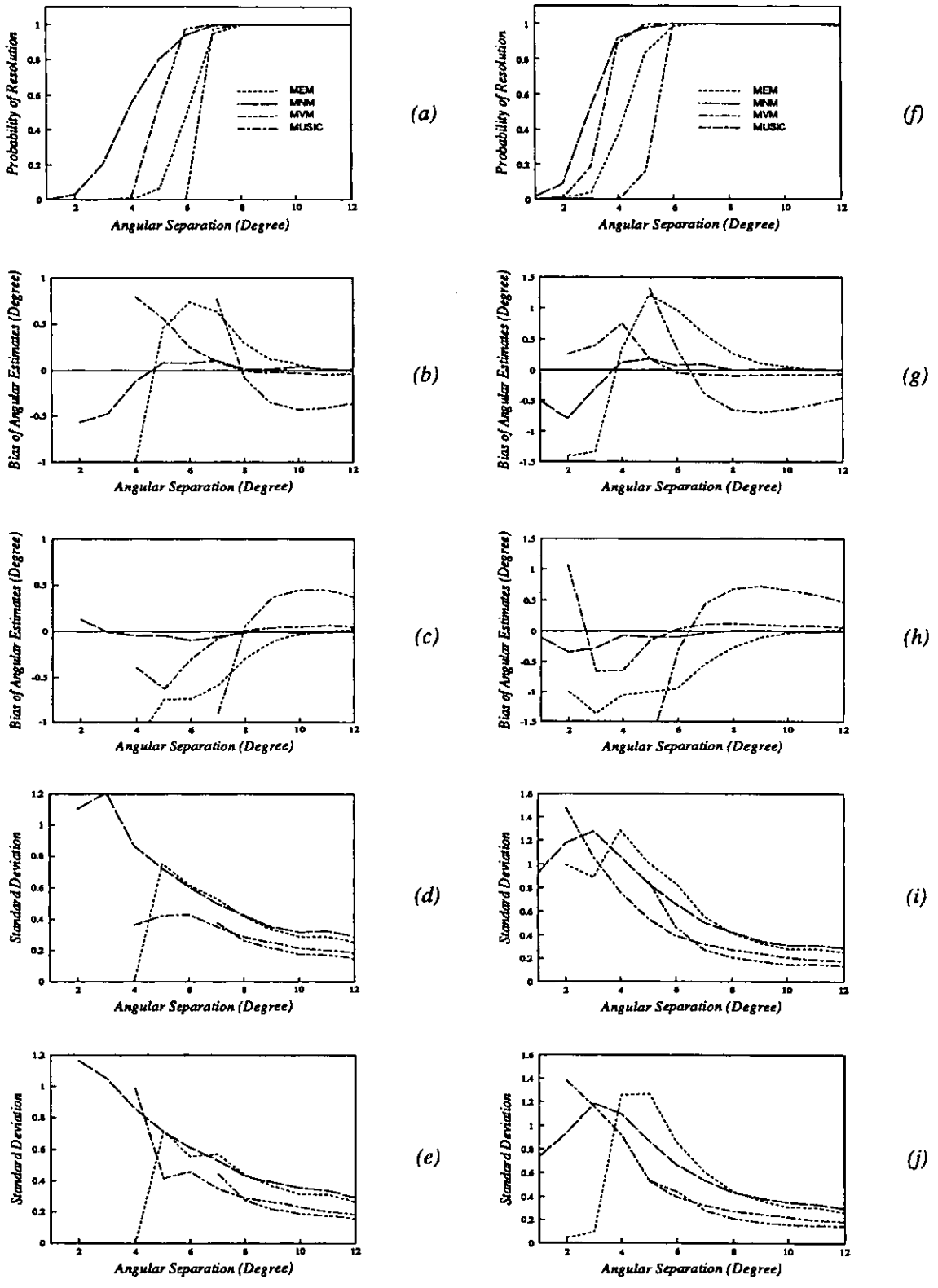

Figure 4.7 Statistics of spectral and root versions of MEM, MNM, MVM, and MUSIC

4.5 Discussion

Besides the representations of both spectral and root versions of MEM, MVM, MUSIC, and MNM, the asymptotic properties of the two versions were compared with MUSIC and MNM being two examples. The advantages of the root version were demonstrated. Computer simulations were also carried out and analysed. The results were presented as functions of signal to noise ratios and those of angular separations respectively. The calculation of statistics is greatly dependent upon the criteria which are set up in the processing. The results shown in this chapter are obtained from those criteria described in the relevant parts. Slightly different statistics are expected from the same simulation data if different criteria are applied.

CHAPTER 5

ESPRIT ALGORITHM

Although the MUSIC algorithm provides substantial performance advantages over many other high resolution methods, the searching procedure over the parameter space and the storage required for array calibration data limit its generality in practical implementation. A new member in the class of signal subspace methods has appeared which is superior to MUSIC in that it dramatically reduces the computation and storage requirements inherent in MUSIC. This new technique is termed ESPRIT (Estimation of Signal Parameters via Rotational Invariance Techniques) and is based on an eigen-decomposition of the sample covariance matrix and "second stage" processing to obtain the DOA estimates, or / and other parameters. This technique, like other eigenstructure based methods, has its origin in Pisarenko's method for harmonic retrieval and found applications in temporal signal processing [RPK86] as well as in sensor array processing [OV89, RGO89, RK87, RK89, RPK85, etc.].

So far two algorithms have been developed for the ESPRIT technique : LS-ESPRIT (Least Squares ESPRIT) and TLS-ESPRIT (Total Least Squares ESPRIT). The former was the original ESPRIT algorithm introduced in [PRK86, RK89] which has already been proven equivalent theoretically to TAM (Toeplitz Approximation Method) [May88, RH89c]. The latter algorithm is relatively new, formulated in an attempt to give consideration to errors in both signal subspace estimates resulting from noisy measurements. The difference between LS- and TLS-ESPRIT is not significant in most cases though LS-ESPRIT yields biased parameter estimates at low SNRs. The TLS solution of the ESPRIT algorithm is expected to yield better estimates, i.e., estimates with lower variances. Simulations have shown that TLS-ESPRIT is relatively insensitive to array errors, and that its use of the TLS minimisation criterion yields apparently unbiased parameter estimates even at low SNRs [SRK89].

Both LS- and TLS-ESPRIT algorithms have been analyzed in, e.g., [RH89d] and [OVK91] respectively. The TLS-ESPRIT was summarized in a more general class of subspace fitting

methods [OVK89, VO91]. An asymptotic equivalence between LS- and TLS-ESPRIT was suggested and proven [RH89d]. This chapter will describe the LS and TLS algorithms briefly, present their implementations in the computer simulations, and then focus on their performance comparisons with some well known methods, spectral MUSIC and root-MUSIC, which are chosen as representatives of the methods discussed in the previous chapter.

5.1 ESPRIT Algorithms

Beside the assumptions which have been made in chapter 2 concerning the sensor array and signal waveforms, the ESPRIT algorithm requires an essential constraint on the array; that is the array should be composed of two identical subarrays which are displaced by a known translational vector Δ. This special structure allows the parameter estimates to be obtained without the knowledge of the individual sensor responses (i.e., no calibration is required) and without computation or search of some spectral measure. Like the inter-element spacing, this vector is also specified in fractions of a wavelength. Because the array may possess arbitrary geometry, provided that the displacement is guaranteed, DOAs are specified relative to the normal of Δ instead of that of the array (in the linear array case, the two normals are the same). Let the array be composed of two identical arrays with a constant displacement vector and all measurements be referenced to a common reference point (sensor). Then, referring to equation (3.28), the outputs of two subarrays are related by phase shifts and expressed as follows :

$$\mathbf{x}(t) = [\mathbf{a}(\theta_1), \cdots, \mathbf{a}(\theta_d)] \cdot \mathbf{s}(t) + \mathbf{n}_x(t) = \mathbf{A} \cdot \mathbf{s}(t) + \mathbf{n}_x(t) \tag{5.1a}$$

$$\mathbf{y}(t) = \left[\mathbf{a}(\theta_1) \cdot e^{j\phi_1}, \cdots, \mathbf{a}(\theta_d) \cdot e^{j\phi_d}\right] \cdot \mathbf{s}(t) + \mathbf{n}_y(t) = \mathbf{A} \cdot \Phi \cdot \mathbf{s}(t) + \mathbf{n}_y(t) \tag{5.1b}$$

where

$$\Phi = diag\left[e^{j\phi_1}, \cdots, e^{j\phi_d}\right] \tag{5.2}$$

describes the propagation between the two subarrays and ϕ_k's are phase shifts relating outputs from the two subarrays and can be used to obtain the DOAs, θ_k's, by the following relation

$$\phi_k = 2\pi \cdot |\Delta| \cdot \mathrm{Sin}\,\theta_k \qquad k = 1, \cdots, d \tag{5.3}$$

Introducing a general array manifold G to describe array responses from the two subarrays

$$\mathbf{G} = \begin{bmatrix} \mathbf{A} \\ \mathbf{A} \cdot \Phi \end{bmatrix} \tag{5.4}$$

the overall output of the array can then be expressed in a compact form as

$$\mathbf{z}(t) = \begin{bmatrix} \mathbf{x}(t) \\ \mathbf{y}(t) \end{bmatrix} = \begin{bmatrix} \mathbf{A} \\ \mathbf{A} \cdot \Phi \end{bmatrix} \cdot \mathbf{s}(t) + \begin{bmatrix} \mathbf{n}_x(t) \\ \mathbf{n}_y(t) \end{bmatrix} = \mathbf{G} \cdot \mathbf{s}(t) + \mathbf{n}(t) \tag{5.5}$$

Under the assumptions that the noise sequence is a zero mean complex Gaussian process with variance σ^2 and uncorrelated with the signals, the asymptotic covariance matrix is given as follow :

$$\mathbf{R}_{ZZ} = \mathrm{E}[\mathbf{z}(t) \cdot \mathbf{z}^H(t)] = \mathbf{G} \cdot \mathbf{S} \cdot \mathbf{G}^H + \Sigma_N \tag{5.6}$$

Since $\mathbf{GSG}^H$ is of rank d, the generalised eigenvalues of the matrix pair $\{\mathbf{R}_{ZZ}, \Sigma_N\}$, i.e., the eigenvalues of $\mathbf{R}_{ZZ}$ in metric of Σ_N, can be represented as $\lambda_1 \geq \lambda_2 \geq \cdots \geq \lambda_d > \lambda_{d+1} = \cdots = \lambda_{2m} = \sigma^2$, and the associated eigenvectors $\mathbf{e}_i$ satisfy the identity

$$\mathbf{R}_{ZZ} \cdot \mathbf{e}_i = \lambda_i \cdot \Sigma_N \cdot \mathbf{e}_i \tag{5.7}$$

or

$$\mathbf{g}^H(\theta_k) \cdot \mathbf{e}_i = 0, \qquad k = 1, 2, \cdots, d, \qquad i = d+1, d+2, \cdots, 2m \tag{5.8}$$

where $\mathbf{g}(\theta_k), k = 1, \cdots, d$ are the d column vectors of $\mathbf{G}$. Equivalently, $\mathbf{e}_1, \mathbf{e}_2, \cdots, \mathbf{e}_d$ span the same subspace which is spanned by the column vectors of $\mathbf{G}$, i.e.

$$[\mathbf{e}_1, \mathbf{e}_2, \cdots, \mathbf{e}_d] = \mathbf{G} \cdot \mathbf{T} \tag{5.9}$$

where $\mathbf{T}$ is some non-singular $d \times d$ matrix. Define $\mathbf{E}_X$ and $\mathbf{E}_Y$ as partitioning $[\mathbf{e}_1, \mathbf{e}_2, \cdots, \mathbf{e}_d]$

$$[\mathbf{e}_1, \mathbf{e}_2, \cdots, \mathbf{e}_d] = \begin{bmatrix} \mathbf{E}_X \\ \mathbf{E}_Y \end{bmatrix} \tag{5.10}$$

then

$$\mathbf{E}_X = \mathbf{A} \cdot \mathbf{T}, \qquad \mathbf{E}_Y = \mathbf{A} \cdot \Phi \cdot \mathbf{T} \tag{5.11}$$

and

$$[\mathbf{E}_X \quad \mathbf{E}_Y] = \mathbf{A}[\mathbf{T} \quad \Phi\mathbf{T}] \tag{5.12}$$

which , denoting $\mathbf{E}_{XY} = [\mathbf{E}_X \quad \mathbf{E}_Y]$, gives

$$\mathbf{E} = \mathbf{E}_{XY}^H \cdot \mathbf{E}_{XY} = \begin{bmatrix} \mathbf{E}_X^H \\ \mathbf{E}_Y^H \end{bmatrix} [\mathbf{E}_X \quad \mathbf{E}_Y] = \begin{bmatrix} \mathbf{T}^H \\ \mathbf{T}^H\Phi^H \end{bmatrix} \mathbf{A}^H\mathbf{A}[\mathbf{T} \quad \Phi\mathbf{T}] \tag{5.13}$$

and $\mathbf{E}$ is non-negative definite Hermitian and is of rank d. Thus $\mathbf{E}$ has the representation of

$$\mathbf{E} = \mathbf{V} \cdot diag(l_1, l_2, \cdots, l_d, 0, \cdots, 0) \cdot \mathbf{V}^H \tag{5.14}$$

where $l_i > 0$, $i = 1, \cdots, d$ and $\mathbf{V}\mathbf{V}^H = \mathbf{I}_m$. Search for a $2d \times d$ full rank matrix $\mathbf{W}$ such that

$$[\mathbf{E}_X \quad \mathbf{E}_Y]\mathbf{W} = \mathbf{0} \tag{5.15}$$

i.e.

$$\mathbf{A}[\mathbf{T} \quad \Phi\mathbf{T}]\mathbf{W} = \mathbf{0} \tag{5.16}$$

Since $\mathbf{A}$ is of dimension $m \times d$ and of rank d, the above equation is equivalent to

$$[\mathbf{T} \quad \Phi\mathbf{T}]\mathbf{W} = \mathbf{0} \tag{5.17}$$

Once again, partition $\mathbf{W}$ as

$$\mathbf{W} = \begin{bmatrix} \mathbf{W}_1 \\ \mathbf{W}_2 \end{bmatrix} \tag{5.18}$$

where $\mathbf{W}_1$ and $\mathbf{W}_2$ are two $d \times d$ matrices. This, together with (5.17), yields

$$[\mathbf{T} \quad \Phi\mathbf{T}] \begin{bmatrix} \mathbf{W}_1 \\ \mathbf{W}_2 \end{bmatrix} = \mathbf{T}\mathbf{W}_1 + \Phi\mathbf{T}\mathbf{W}_2 = \mathbf{0} \tag{5.19}$$

or

$$-\mathbf{W}_1 \cdot \mathbf{W}_2^{-1} = \mathbf{T}^{-1}\Phi\mathbf{T} \tag{5.20}$$

Thus, any $\mathbf{W}$ satisfying (5.15) has the interesting property that the eigenvalues of the matrix $-\mathbf{W}_1 \cdot \mathbf{W}_2^{-1}$ generated from the partition in (5.18) are given by $e^{-j\phi_i}, i = 1, \cdots, d$. Therefore, the DOAs are obtained directly.

To complete this analysis, it is sufficient to exhibit such a $\mathbf{W}$ and toward this purpose, a re-examination of (5.14) shows that

$$\mathbf{E} \cdot \mathbf{v}_i = l_i \cdot \mathbf{v}_i = \mathbf{0} \qquad d < i \le 2d \tag{5.21}$$

where $\mathbf{v}_i$ represents the ith column vector of $\mathbf{V}$. Since $[\mathbf{E}_X \quad \mathbf{E}_Y]$ is also of rank d, from (5.13), (5.21) reduces to

$$[\mathbf{E}_X \quad \mathbf{E}_Y]\mathbf{v}_i = \mathbf{0} \qquad d < i \le 2d \tag{5.22}$$

Thus the desired $\mathbf{W}$ is given by

$$\mathbf{W} = [\mathbf{v}_{d+1}, \mathbf{v}_{d+2}, \cdots, \mathbf{v}_{2d}] = \begin{bmatrix} \mathbf{V}_{12} \\ \mathbf{V}_{22} \end{bmatrix} \tag{5.23}$$

where $\mathbf{V}_{12}$ and $\mathbf{V}_{22}$ are two $d \times d$ sub-matrices of

$$\mathbf{V} = \begin{bmatrix} \mathbf{V}_{11} & \mathbf{V}_{12} \\ \mathbf{V}_{21} & \mathbf{V}_{22} \end{bmatrix} \tag{5.24}$$

and eigenvalues of $-\mathbf{V}_{12} \cdot \mathbf{V}_{22}^{-1}$ gives the actual DOA estimates. These eventually are the TLS-ESPRIT estimates of the DOAs.

A spectrum representation of the covariance matrix of the whole array can be expressed as

$$\mathbf{R}_{ZZ} = \sum_{i=1}^{2m} \lambda_i \cdot \mathbf{e}_i \cdot \mathbf{e}_i^H = \mathbf{E}_S \cdot \Lambda_S \cdot \mathbf{E}_S^H + \mathbf{E}_N \cdot \Lambda_N \cdot \mathbf{E}_N^H \tag{5.25}$$

where $\mathbf{E}_S = [\mathbf{e}_1, \cdots, \mathbf{e}_d]$, $\mathbf{E}_N = [\mathbf{e}_{d+1}, \cdots, \mathbf{e}_{2m}]$, and $\lambda_1 \ge \lambda_2 \ge \cdots \ge \lambda_{2m}$. For non-coherent waveforms, the source covariance $\mathbf{S}$ is of full rank and $\mathbf{E}_S$ spans the same space as $\mathbf{G}$. Given finite data record, the sample covariance matrix must be estimated and so are $\mathbf{E}_S, \mathbf{E}_N$, and Λ

$$\hat{\mathbf{R}}_{ZZ} = \frac{1}{N}\sum_{i=1}^{N} \mathbf{x}(t_i)\cdot\mathbf{x}^H(t_i) = \hat{\mathbf{E}}_S\cdot\hat{\Lambda}_S\cdot\hat{\mathbf{E}}_S^H + \hat{\mathbf{E}}_N\cdot\hat{\Lambda}_N\cdot\hat{\mathbf{E}}_N^H \tag{5.26}$$

The TLS version of the ESPRIT algorithm has been shown [ROSK88, VO91] to minimise the following cost function

$$\min\left|\left|\begin{bmatrix}\hat{\mathbf{E}}_{S1}\\ \hat{\mathbf{E}}_{S2}\end{bmatrix} - \begin{bmatrix}\mathbf{A}\\ \mathbf{A}\cdot\Phi\end{bmatrix}\mathbf{T}\right|\right|_F^2 = \min\left|\left|\hat{\mathbf{E}}_S - \mathbf{G}\cdot\mathbf{T}\right|\right|_F^2 \tag{5.27}$$

where $\hat{\mathbf{E}}_{S1}$ and $\hat{\mathbf{E}}_{S2}$ are obtained by appropriately partitioning $\hat{\mathbf{E}}_S$ corresponding to the two subarrays. The original formulation of the ESPRIT algorithm is the LS-ESPRIT which assumes that there are no measurement errors in $\hat{\mathbf{E}}_{S1}$, i.e., letting $\hat{\mathbf{E}}_{S1} = \mathbf{A}\cdot\mathbf{T}$, and consequently the cost function reduces to

$$\min\left|\left|\hat{\mathbf{E}}_{S2} - \mathbf{A}\Phi\mathbf{T}\right|\right|_F^2 \tag{5.28}$$

Denoting $\Psi = \mathbf{T}^{-1}\cdot\Phi\cdot\mathbf{T}$, the cost function for LS-ESPRIT can be rewritten as

$$\min\left|\left|\hat{\mathbf{E}}_{S2} - \hat{\mathbf{E}}_{S1}\cdot\Psi\right|\right|_F^2 \quad \Rightarrow \quad \hat{\Psi}_{LS} = \hat{\mathbf{E}}_{S1}^{+}\cdot\hat{\mathbf{E}}_{S2} \tag{5.29}$$

or assume that no errors exist in $\hat{\mathbf{E}}_{S2}$ resulting in

$$\min\left|\left|\hat{\mathbf{E}}_{S1} - \mathbf{A}\mathbf{T}\right|\right|_F^2 = \min\left|\left|\hat{\mathbf{E}}_{S1} - \hat{\mathbf{E}}_{S2}\cdot\Psi^{-1}\right|\right|_F^2 \quad \Rightarrow \quad \hat{\Psi}_{LS}^{-1} = \hat{\mathbf{E}}_{S2}^{+}\cdot\hat{\mathbf{E}}_{S1} \tag{5.30}$$

where the symbol $(\cdot)^+$ denotes the Moore-Penrose pseudo inverse.

When only finite noisy measurements are available, the covariance matrix needs to be estimated from the given data. The estimated signal subspace is inevitably corrupted with noise which means that errors are present in both $\hat{\mathbf{E}}_{S1}$ and $\hat{\mathbf{E}}_{S2}$, in general. Assumption that either $\hat{\mathbf{E}}_{S1}$ or $\hat{\mathbf{E}}_{S2}$ is error free is inappropriate and the LS solution of the ESPRIT algorithm yields biased estimates, especially at low SNRs.

By applying a Total Least Squares (TLS) criterion to the preliminary version of the ESPRIT algorithm, the LS-ESPRIT algorithm, errors which might exist in both $\hat{\mathbf{E}}_{S1}$ and $\hat{\mathbf{E}}_{S2}$ are taken into account. Solving the minimisation problem expressed in (5.27), the intermediate variable

Ψ is given as (*cf.* [GV80, GV83])

$$\hat{\Psi}_{TLS} = -\mathbf{V}_{12} \cdot \mathbf{V}_{22}^{-1} \tag{5.31}$$

where $\mathbf{V}_{12}, \mathbf{V}_{22}$ are defined in equation (5.24). The eigenvalues of $\hat{\Psi}_{TLS}$ in (5.31) give the estimates of DOAs in the TLS sense.

Once $\hat{\Psi}_{TLS}$ is known, its eigenvalues can be calculated, which are also the eigenvalues of Φ by the relationship $\mathbf{T} \cdot \Psi \cdot \mathbf{T}^{-1} = \Phi$. That is, the signal parameters are obtained as nonlinear functions of the eigenvalues of Ψ which maps one set of vectors, $\hat{\mathbf{E}}_{S1}$, which span an m-dimensional signal subspace, into another set of vectors, $\hat{\mathbf{E}}_{S2}$.

$$\hat{\theta}_k = arcsin\{arg(\hat{\phi}_k)/(2\pi \cdot |\Delta|)\} \qquad \forall k = 1, \cdots, d \tag{5.32}$$

An SVD variant of ESPRIT was also suggested which may be preferred in cases where there is large amount of data and numerical issues are important. The SVD versions of ESPRIT, both LS and TLS, are easily obtained by replacing all the eigendecompositions in the covariance versions with SVD's except for the final eigen-decomposition of Ψ where phase information is required [RK89].

5.2 Array Geometry for ESPRIT

Although applicable to arbitrary geometry, the ESPRIT algorithm is not as general as the MUSIC algorithm due to the fact that the array is assumed to be translationally invariant. The original version of ESPRIT assumes a single displacement invariance in time or space which results in that only a single parameter per signal may be uniquely estimated. There are arrays that possess multiple invariances. Two important examples are rectangular phased arrays and uniform linear arrays (ULAs). The most frequently employed arrays in practice, ULAs, are considered herein.

From (5.3), it is easily seen that the range of DOAs in which there are no ambiguities is determined by the following relationship

$$-\pi \le 2\pi|\Delta| \, \mathrm{Sin}\,\theta_k \le \pi \quad \Rightarrow \quad |\theta_k| \le arcsin\left(\frac{1}{2|\Delta|}\right) \tag{5.33}$$

If the front half space is to be observed, the subarray displacement is restricted to be no bigger than half the wavelength. The estimation error variance is expected to decrease when the displacement $|\Delta|$ is increased. A procedure was suggested to compromise these two aspects by first using a small $|\Delta|$ to determine in which sector the sources are and then within this sector reducing the estimation error variance with a large $|\Delta|$. However, this procedure is applicable only when sources are clustered. Problems arise when sources are present in a large parameter range [OVK91].

Obviously only simultaneous exploiting all possible invariances in the array gives an optimal ESPRIT estimation.

5.3 Implementation of the ESPRIT Algorithm

Before going to describe the implementation of the ESPRIT technique, both LS-ESPRIT and TLS-ESPRIT algorithms are summarised. Based on this summary the implementation of the two algorithms is straightforward.

Summary of LS-ESPRIT Algorithm:

1) *Calculate an estimate of the covariance matrix,* $\hat{\mathbf{R}}_{ZZ}$, *from the obtained measurements,* $\mathbf{Z}$
2) *Compute the generalised eigen-decomposition of* $\{\hat{\mathbf{R}}_{ZZ}, \Sigma_N\}$

$$\hat{\mathbf{R}}_{ZZ}\mathbf{E} = \Sigma_N \mathbf{E}\Lambda$$

3) *Estimate the number of sources,* d, *if necessary*
4) *Obtain the signal subspace estimate* $\hat{S}_Z = span\{\mathbf{E}_Z\}$ *where*

$$\mathbf{E}_Z = \Sigma_N[\mathbf{e}_1 \mid \cdots \mid \mathbf{e}_{\hat{d}}] = \begin{bmatrix} \mathbf{E}_X \\ \mathbf{E}_Y \end{bmatrix}$$

5) *Compute the eigenvalues of* $[\mathbf{E}_X^H \cdot \mathbf{E}_Y]^{-1} \cdot \mathbf{E}_X^H \cdot \mathbf{E}_X$

$$\hat{\phi}_i = \lambda_i\left([\mathbf{E}_X^H \cdot \mathbf{E}_Y]^{-1} \cdot \mathbf{E}_X^H \cdot \mathbf{E}_X\right), \qquad \forall i = 1, \cdots, \hat{d}$$

6) *Estimate the signal parameters using* $\hat{\theta}_i = f^{-1}(\hat{\phi}_i)$

Summary of TLS-ESPRIT Algorithm:

1)-4) *the same as LS-ESPRIT*

5) *Compute the eigen-decomposition of* $\mathbf{E}_{XY}^H \cdot \mathbf{E}_{XY}$ *where* $\mathbf{E}_{XY} = [\mathbf{E}_X \quad \mathbf{E}_Y]$

$$\mathbf{E}_{XY}^H \cdot \mathbf{E}_{XY} = \mathbf{E}\Lambda\mathbf{E}^H$$

and partition $\mathbf{E}$ *into* $\hat{d} \times \hat{d}$ *sub-matrices*

$$\mathbf{E} = \begin{bmatrix} \mathbf{E}_{11} & \mathbf{E}_{12} \\ \mathbf{E}_{21} & \mathbf{E}_{22} \end{bmatrix}$$

6) *Calculate the eigenvalues of* $-\mathbf{E}_{12} \cdot \mathbf{E}_{22}^{-1}$

$$\hat{\phi}_i = \lambda_i(-\mathbf{E}_{12} \cdot \mathbf{E}_{22}^{-1}), \qquad \forall i = 1, \cdots, \hat{d}$$

7) *the same as step (6) in LS-ESPRIT*

Using the package, MATLAB, the matrix computations involved in the ESPRIT algorithms can be implemented without much difficulty. Table 5.1 gives the simulation results from LS-ESPRIT from 10 trials, and the simulation results from the root MUSIC method are given in table 5.2 and those from the spectral MUSIC method are illustrated in figure 5.1.

Table 5.1 LS-ESPRIT

$\hat{\theta}_1$	$\hat{\theta}_2$
-0.82	*1.42*
-0.10	*1.58*
-0.15	*1.60*
0.49	*1.84*
-0.45	*2.35*
-0.57	*2.26*
-0.38	*1.93*
0.25	*1.77*
0.13	*2.21*
0.22	*1.92*

Table 5.2 Root MUSIC

$\hat{\theta}_1$	ρ_1	$\hat{\theta}_2$	ρ_2
0.34	*0.89*	*1.25*	*0.95*
-0.24	*0.92*	*1.62*	*0.96*
-0.06	*0.91*	*1.65*	*0.95*
0.48	*0.93*	*1.96*	*0.94*
-0.20	*0.90*	*1.85*	*0.95*
-0.28	*0.95*	*2.26*	*0.93*
0.06	*0.91*	*1.60*	*0.94*
0.26	*0.91*	*1.45*	*0.94*
-0.01	*0.96*	*2.49*	*0.94*
0.27	*0.93*	*1.95*	*0.95*

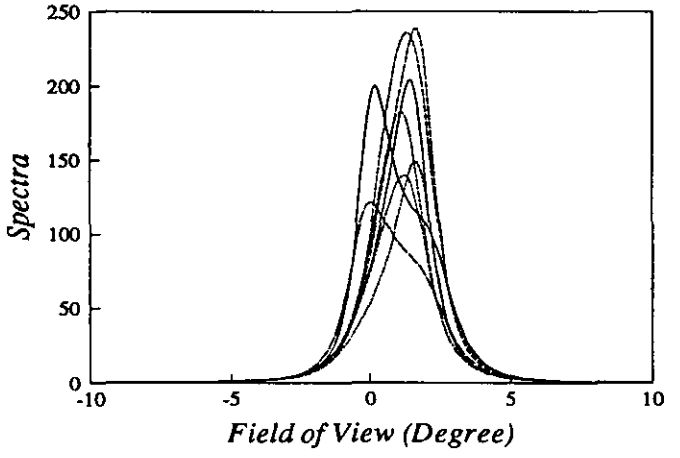

Figure 5.1 Spectral MUSIC

The signal parameters for the above simulations are given as follows : $d = 2, m = 10, N = 100$, the two sources are assumed to have equal power of 10 dB relative to the unit noise variance and are placed at 0° and 2° to the normal of the array. The element spacing in the uniform linear array is half a wavelength so the beam-width is about 11.5°. The conventional beamforming method fails completely in this closely spaced source case, as does the spectral MUSIC method shown in figure 5.1. The number of sources is assumed known in all three methods. The 2 estimates which are closest to the true directions in the 9 estimated in the root MUSIC method are chosen and so are their corresponding radial estimates. For the ESPRIT algorithm, only two estimates are brought out and they are re-ordered because of the permutation in the processing.

The performance advantages of the ESPRIT technique over the spectral MUSIC method is noticeable from the example shown above. To compare the performance of the two techniques, more results are necessary. To investigate their behaviour under different parameter set-ups, a large amount of simulation work has been carried out and will be presented in the following section.

Only the LS-ESPRIT was implemented to compare the ESPRIT technique with the MUSIC technique. As was stated in the description of the algorithms, the advantages of TLS-ESPRIT over the LS-ESPRIT are mainly at low SNRs and are based on the explicit examination of the noise components present in both estimated subspaces. Because the noise is assumed as ideally white Gaussian noise and uncorrelated with signals, the structure of the noise covariance is neglected. Under the same assumption, the noise distributed in both subspace

estimates will not receive the treatment which makes the TLS-ESPRIT superior to the LS-ESPRIT. Therefore, only the LS-ESPRIT was examined for the performance comparison of the two different techniques, ESPRIT and MUSIC.

5.4 Computer Simulations

The same statistics as those which have been examined in the previous chapter will be investigated herein to check the performance of the ESPRIT method under different circumstances. Three statistics are explored as functions of signal to noise ratio and angular separation, separately. The signal to noise ratio range is 0 dB to 50 dB with 5 dB increments when the angular separation is fixed at 2° in the former case, while, in the latter one, the angular separation is allowed to change from 1° to 12° which is just above the conventional resolution of the array in use. In this case, source one is placed at 0° to the normal of the array, while source two is moved along the array and the signal to noise ratio is set as 10 dB. The number of sources is given in all three methods under examination. The spectrum of spectral MUSIC is formed on a 0.1° grid. The 2 estimates of DOAs which are nearest to the true directions are chosen out of 9 in the root MUSIC method. The only two estimates from the ESPRIT method are recorded first and then, together with the results from the other two methods, are processed to compute the probabilities of resolution, biases and angular estimates and their standard deviations. The same criteria for root MUSIC as specified in the previous chapter are applied to the ESPRIT method.

5.4.1 Results as Functions of Signal to Noise Ratio

Signals with different correlations were checked when the signal to noise ratio was changed. The correlation factor between the two sources was assigned as 0.0, 0.5, and 0.95, respectively, and the correspondent results are shown in figures 5.2, 5.3, and 5.4. The inability of the MUSIC technique for coherent sources has been shown in chapter 4, and the ESPRIT technique is also unable to resolve the fully correlated sources due to the philosophy behind it. So the case of fully correlated sources has not been included in the discussion.

Again, 100 independent snapshots were taken in each trial to form the data matrix and 500 trials were used to calculate the statistics.

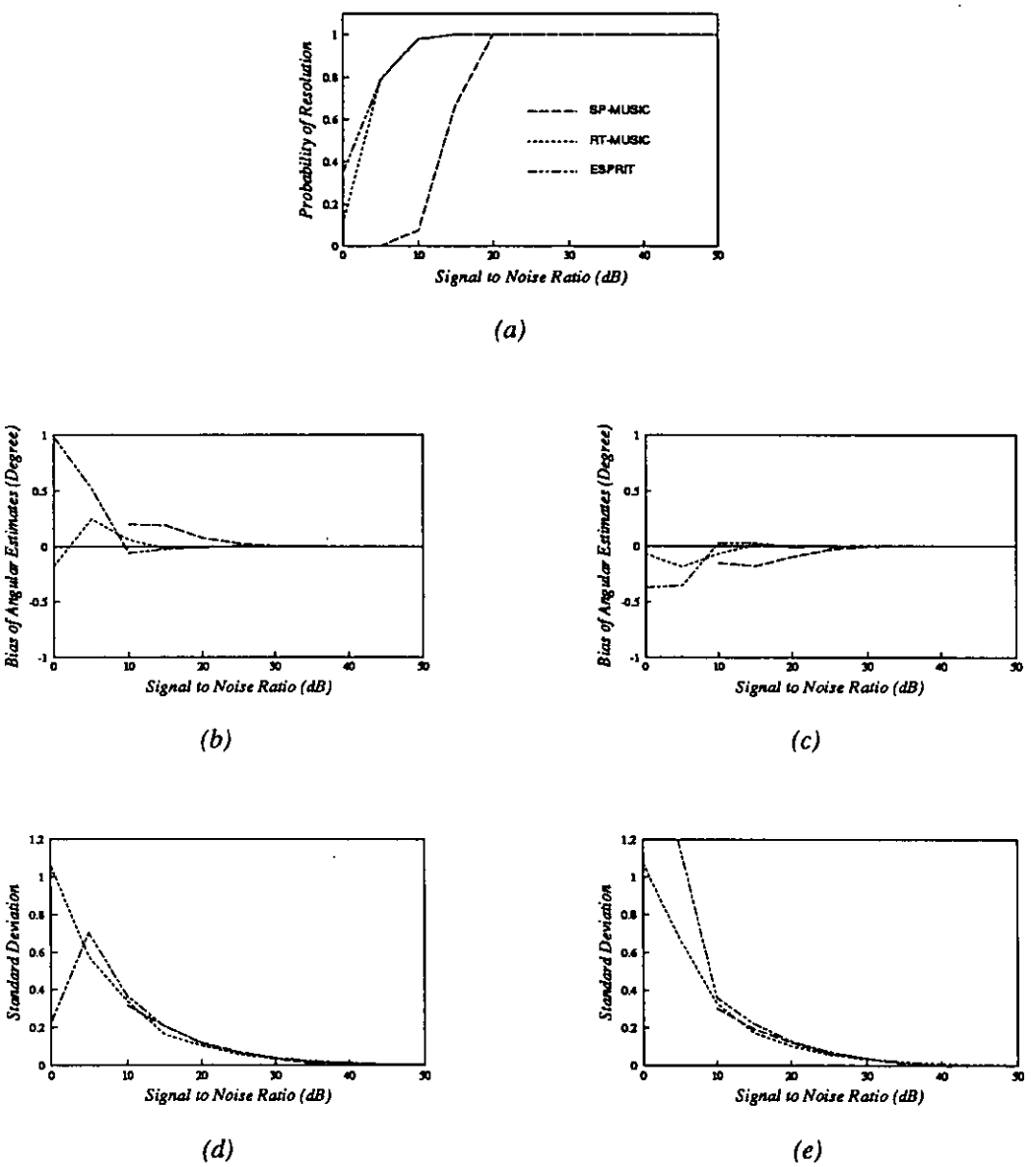

Figure 5.2 *Statistics of spectral MUSIC, root MUSIC, and ESPRIT as functions of signal to noise ratio when* $\rho = 0.0$

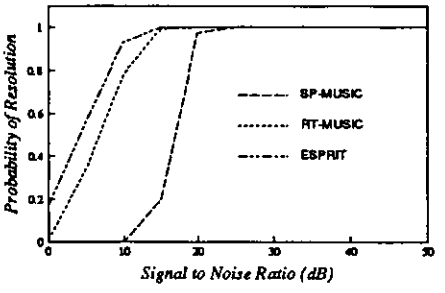

(a)

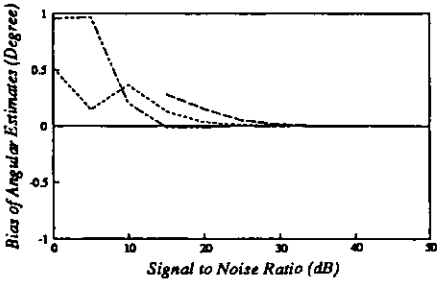

(b)

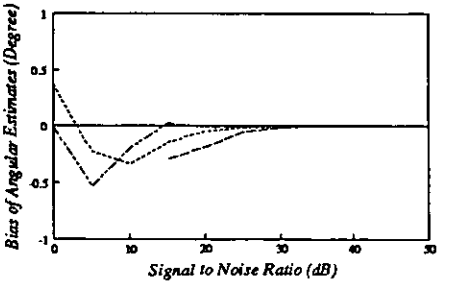

(c)

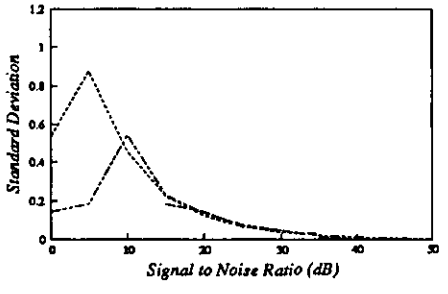

(d)

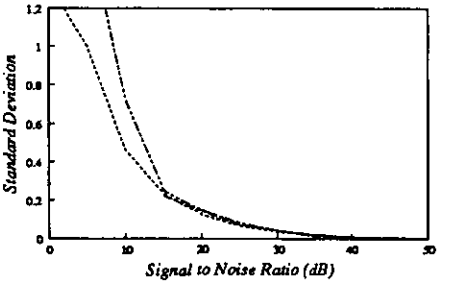

(e)

Figure 5.3 *Statistics of spectral MUSIC, root MUSIC, and ESPRIT as functions of signal to noise ratio when* $\rho = 0.5$

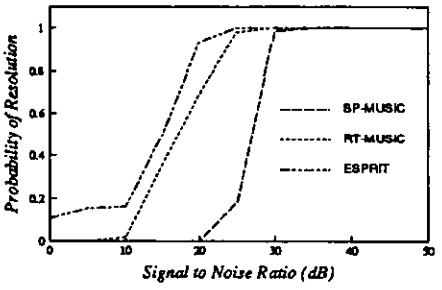

(a)

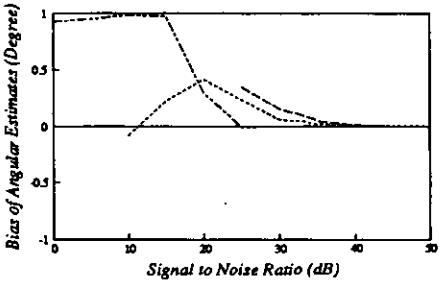

(b)

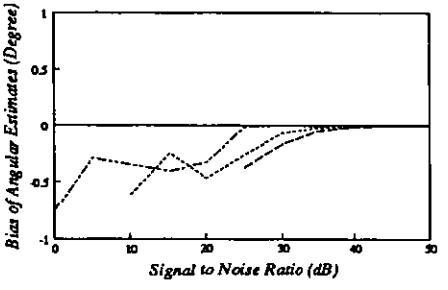

(c)

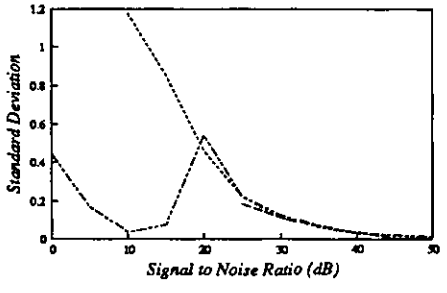

(d)

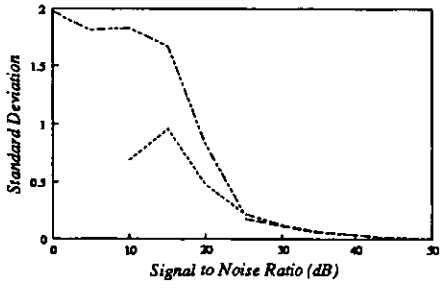

(e)

Figure 5.4 *Statistics of spectral MUSIC, root MUSIC, and ESPRIT as functions of signal to noise ratio when* $\rho = 0.95$

5.4.1.1 Uncorrelated Case

Figure 5.2(a) shows the probabilities for the three methods in the uncorrelated case, denoted by different line styles as specified in the plot. Similar resolution thresholds are demonstrated by root MUSIC and LS-ESPRIT, while the spectral MUSIC has a threshold about 10 dB higher. However high biases are shown in the estimates of the ESPRIT method at lower SNRs although the corresponding probability of resolution is slightly higher than that of root MUSIC. Biases of the ESPRIT estimates decrease quickly at 10 dB to be the lowest. As signal to noise ratio continues to increase, the root MUSIC and LS-ESPRIT give roughly the same biases while spectral MUSIC shows higher biases until around 30 dB and above when the difference among the biases merges.

As far as the standard deviation is concerned, asymptotically similar properties are proved by all three methods. Although root MUSIC and LS-ESPRIT begin to resolve the two sources at lower SNRs, high standard deviations also resulted.

5.4.1.2 Correlated Sources with Correlation Factor 0.5

As the correlation between the two sources gets stronger, the performance of the methods is expected to degrade. Figure 5.3 illustrates the properties in the sense of probability of resolution, bias, and standard deviation. Compared to those in figure 5.2, the performance degradation can be seen in all three aspects under examination.

The degradation in the probability of resolution is more significant than in the other two statistics. All three plots in figure 5.3(a) shift right-wards about 5 dB. The plots given by root MUSIC and LS-ESPRIT begin to separate showing a larger probability for LS-ESPRIT to distinguish the two sources in the correlated case.

The biases degrade mainly at lower signal to noise ratios, below 30 dB, which is generally the case in practical situations. Since the value of the probability of resolution of root MUSIC is too small at 0 dB, the corresponding statistics are meaningless. Those given by LS-ESPRIT are uneven for the two sources, very high in one and very low in the other. At 5 dB, the biases from LS-ESPRIT are still very high. Only when the SNRs are higher, are smaller biases depicted.

The unevenness of the root MUSIC and LS-ESPRIT is also shown in the standard deviations in the low SNR region. In contrast to the biases, smaller values are given in source one and bigger values are in source two. Starting from 10 dB both standard deviations decrease smoothly as the signal to noise ratio increases. Larger standard deviations are given by LS-ESPRIT. The spectral MUSIC, however, starts to resolve the two sources at relatively higher SNRs, but possesses similar standard deviations as root MUSIC and LS-ESPRIT.

5.4.1.3 Highly Correlated Sources with Correlation Factor 0.95

A correlation factor of 0.95 was given to test the performance of the three methods in the highly correlated case. Comparing the plots in figure 5.4 to those in figure 5.3, a 10 dB equivalent degradation can be observed in all three statistics which are inspected. The probability pattern is similar to that in figure 5.3(a) and the LS-ESPRIT does not show improvement over the root MUSIC method as it did from the uncorrelated case to the case with correlation factor 0.5. Again, the threshold of resolution of spectral MUSIC is the highest one.

Although the LS-ESPRIT method shows the ability to resolve the two sources at low SNRs in the highly correlated case, high biases of angular estimates are also shown. Especially, source one depicts a constant positive bias of about 1.0° over 15 dB. This widens the range in the previous case (figure 5.3(b)) with a 10 dB extension. Comparatively, the bias for source two is nearer to those from the MUSIC methods. And the biases from LS-ESPRIT drop to zero about 15 dB earlier.

The standard deviations of the ESPRIT estimates are less even than before at lower SNRs. Only when the signal to noise ratio is high (at and above 20 dB), they show a more noticeable tendency to converge. Root MUSIC also shows larger standard deviations at low SNRs. On the other hand, spectral MUSIC, although starting to resolve the two sources at higher SNRs, similar standard deviations are shown as those from the other two methods.

5.4.2 Results as Functions of Angular Separation

Statistics were also examined as functions of angular separation when the signal to noise ratio was fixed at 10 dB. 12 separations were checked from 1° to 12° with 1° increment. Statistics were calculated from 500 trials which were based on data matrices formed by 100 independent snapshots. The same correlation factors were assigned as those in last subsection.

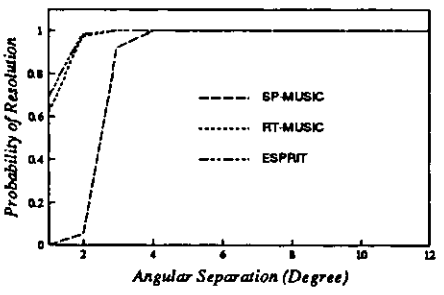

(a)

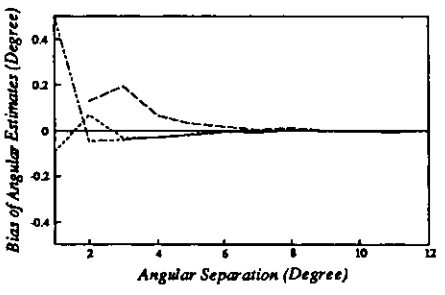

(b)

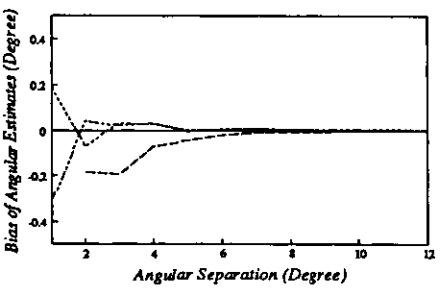

(c)

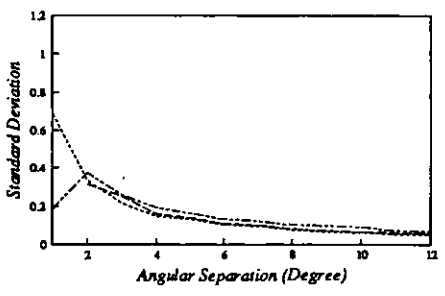

(d)

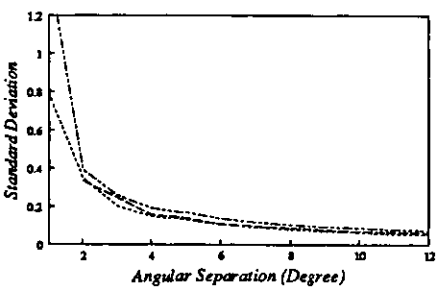

(e)

Figure 5.5 *Statistics of spectral MUSIC, root MUSIC, and ESPRIT as functions of angular separation when* $\rho = 0.0$

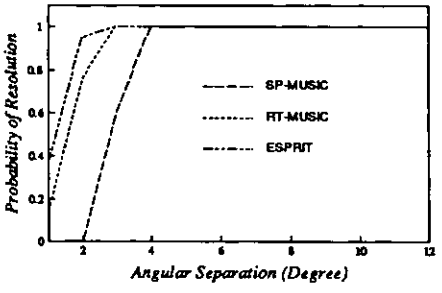

(a)

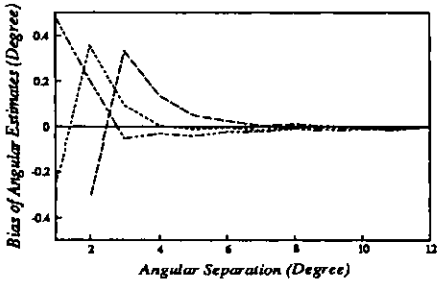

(b)

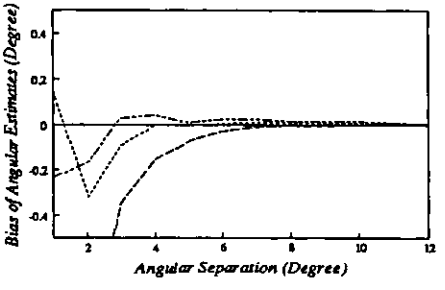

(c)

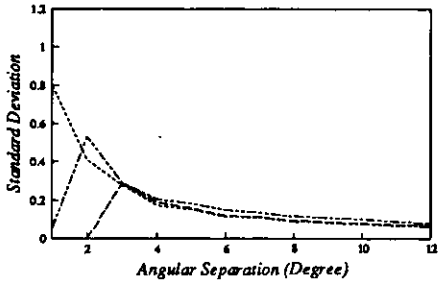

(d)

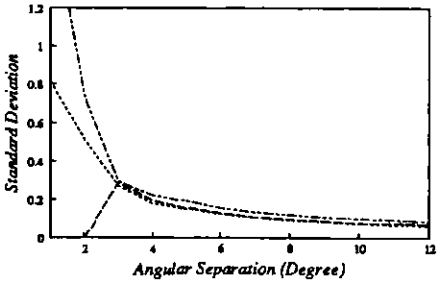

(e)

Figure 5.6 *Statistics of spectral MUSIC, root MUSIC, and ESPRIT as functions of angular separation when* $\rho = 0.5$

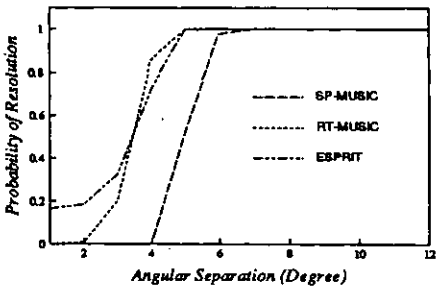

(a)

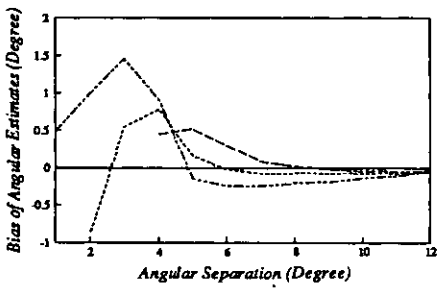

(b)

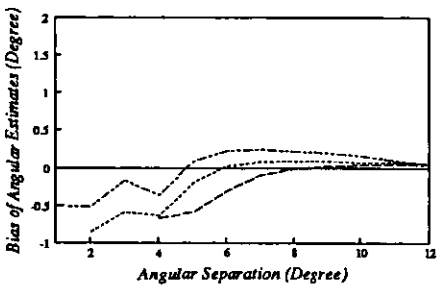

(c)

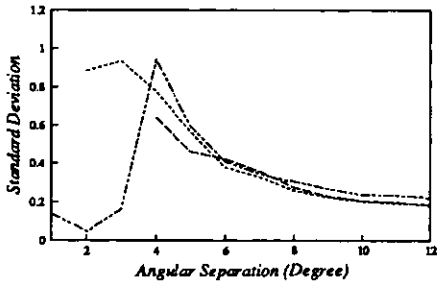

(d)

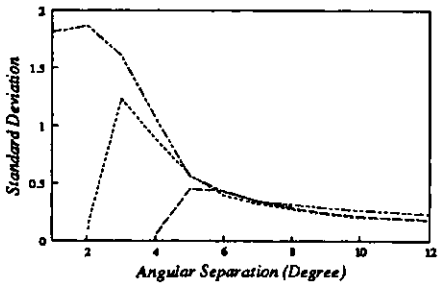

(e)

Figure 5.7 *Statistics of spectral MUSIC, root MUSIC, and ESPRIT as functions of angular separation when* $\rho = 0.95$

5.4.2.1 Uncorrelated Case

The non-correlation case is illustrated in figure 5.5. As shown in figure 5.5(a), the two methods which give the direction estimates directly rather than locating them in the spectral estimate demonstrate similar abilities to distinguish the two sources; the spectral MUSIC starts to resolve them at a bigger separation, 2° in the 10 dB signal to noise case.

Comparatively, the biases are smoother than those as functions of signal to noise ratios. The spectral MUSIC gives bigger biases when the separation is relatively small. Positive bias in source one and negative bias in source two given by spectral MUSIC imply that the two peaks in the spectral estimate tend to each other, shifting from their true directions.

Despite that estimates from all three methods are unbiased as the angular separation is big, the standard deviations always exist. From figures 5.5(d) and 5.5(e), the standard deviations from the LS-ESPRIT are slightly higher than those from the two MUSIC methods. The standard deviation does not tend to merge as the angular separation is very large, even larger than the conventional resolution beam-width, when the signal to noise ratio is unchanged.

5.4.2.2 Correlation Sources with Correlation Factor 0.5

For sources with correlation, larger angular separations are required to achieve the same probabilities of resolution as those in the uncorrelated case. LS-ESPRIT shows a little higher ability than the root MUSIC method while spectral MUSIC remains the last one to be able to resolve the two sources.

The biases are also higher even after the probability of 1 has been shown. What is different from the results as functions of signal to noise ratio is that LS-ESPRIT gives higher biases than the root MUSIC method does. The highest biases are from the spectral MUSIC technique, and the tendency of giving two peaks within the true directions is depicted by positive bias for source one and negative bias for source two.

Where the standard deviations are concerned, the LS-ESPRIT technique gives larger values when all three methods are able to resolve the two sources, whilst the two versions of MUSIC have asymptotically equivalent performance. At the smallest separation of 1°, the standard deviations are less meaningful in the sense of statistics. The zero standard deviations of spectral MUSIC at 2° separation resulted from the fact that only a single trial out of the 500

gave acceptable estimates of the true source directions. The standard deviations from all three methods stay at the same level as those in the uncorrelated case when the separation between the two sources is very large.

5.4.2.3 Highly Correlated Sources with Correlation Factor 0.95

The properties of both ESPRIT and MUSIC techniques are worse in the highly correlated case than in the two previous cases. The resolution thresholds are 2° higher than those in the correlated case with 0.5 correlation factor. Besides the general movement towards the right in figure 5.7(a), the two plots from LS-ESPRIT and root MUSIC are mixed, differing from the picture of two distinct lines in figure 5.6(a) at small separations.

Big biases exist in the three plots for each source over the whole range under examination. Comparatively, those from the spectral MUSIC method are smaller and those from LS-ESPRIT are the largest. As the separation is 12°, this small difference in the biases vanishes.

Standard deviations are at a higher level than in the two previous cases. Asymptotically LS-ESPRIT gives bigger values than the two MUSIC methods.

5.5 Discussion

The computational advantage of the ESPRIT technique is claimed as the key advantage over the popular MUSIC methods. Unfortunately the computation time is not calculated in the simulations here. However, the high speed of the LS-ESPRIT method was noticed in the simulation procedure. Although the TLS-ESPRIT provides better performance at low SNRs at the cost of more complex computations, it is still much quicker to obtain direction of arrival estimates from the ESPRIT method rather than from the peak position estimates of a spectrum in the spectral MUSIC. No searching procedure is involved in the root MUSIC method, but it needs the rooting of a polynomial, whose order may be very high in the large number of sensors case, besides the eigen-decomposition of the covariance matrix.

CHAPTER 6

IMP ALGORITHM

Apart from those high resolution algorithms discussed in previous chapters, most of which are based upon eigen-analysis of the sample covariance matrix, another class of method, the so-called deconvolution algorithms, has also been proposed to improve spectral estimates. The IFA algorithm, the WB^2 method, the CLEAN technique, and the IMP approach, all of which fall into this type of method, have been described briefly in Chapter 3. To explore the performance of this class of method, the IMP algorithm, which has been mainly applied in the field of the direction estimation problem in array processing so far, is examined in detail in this chapter as a representative.

6.1 Introduction

Most of the modern high resolution algorithms, such as MNM, MUSIC, and ESPRIT described earlier in this thesis, involve eigen-analysis of the sample covariance matrix, and in the ESPRIT algorithm, an intermediate matrix formed as well. In contrast, the IMP (Incremental Multi-Parameter) algorithm proposed by I.J.Clarke [Cla87, Cla88, Cla89] makes use of the information preserved in the conventional beamformer as its basic processing component, and defines a scheme for re-processing the data after the initial beamforming in order to determine the number of sources and their bearings. This algorithm borrows the concept used in CFAR (Constant False Alarm Rate) methods [BLP86, Wei82] for detection and uses the difference between global maximum and minimum values of the output signal plus noise to noise ratio (SNNR) as its detection statistic. A single peak is found at each iteration, and the angular information depicted by this peak is used to modify a so-called pre-conditioning matrix. This pre-conditioning matrix is used as a weighting to the sampled

data, giving the effect of removing the peak on which the pre-conditioning is based. This procedure continues until no significant peak appears in the resulting signal plus noise to noise ratio spectrum and then the algorithm terminates.

In the DOA estimation problem, the aim is to extract details of source directions from the data received from sensors. This includes two aspects in which effort is needed : 1) an estimator which will give more detail of source directions, i.e., how to extract more information about the source directions from the available data; 2) how to make full use of the information contained in the sampled data, i.e., not to discard any information which might be useful in the processing.

The conventional beamformer does not discard information contained in the data, but provides very poor resolution because of the mechanism used in the beamformer. High resolution estimators, such as MUSIC, frequently throw information away by using different weights to emphasise or discard components of the data. The resolution is improved by the complicated computations on the received data. The IMP algorithm which will be described in this chapter preserves all the information contained in the received data and, at the same time, provides much higher resolution than the MUSIC algorithm.

The advanced Constant False Alarm Rate (CFAR) technique provides an automatic detection accomplished by setting an adaptive threshold relative to the local estimate of the noise mean. The detection control is applied to both IMP and CLEAN. No matter whether manual or automatic detection is used, when the local noise mean is corrupted by other targets or sidelobe leakage, the probability of detection is degraded. This raises the detection threshold and may result in a target being missed. Therefore, a strong target may mask a weaker signal, or it may be masked by a multiplicity of nearby targets. It is this masking effect that motivates the study on these decomposition methods.

In most passive systems, the statistic commonly used for detection is the power in the field of view of interest. By contrast, the CLEAN algorithm uses relative brightness of a spot to the background, while the IMP algorithm uses the difference between the global maximum and minimum values of the Signal plus Noise to Noise Ratio (SNNR).

6.2 Data Model

As before, a sample of the array output can be represented in the form

$$\mathbf{x}(t) = \mathbf{A} \cdot \mathbf{s}(t) + \mathbf{n}(t) \tag{6.1}$$

which is a snapshot sampled at the array outputs at time instant t. After the data processing, the information concerning the source to be detected and estimated is contained in

$$\mathbf{y}(t) = \mathbf{A}^H \cdot \mathbf{C} \cdot \mathbf{x}(t) \tag{6.2}$$

where $\mathbf{C}$ is a pre-conditioning matrix, which involves the applications of a matrix filter to the input, and $\mathbf{A}$, as before, is the array manifold containing array responses in all possible directions. For passive sensor arrays, it is the output power that is preserved for further processing. The averaged power output over N snapshots of the array outputs is given by

$$P = \frac{1}{N}\sum_{t=1}^{N} |y(t)|^2 = \frac{1}{N}\mathbf{A}^H \cdot \mathbf{C} \cdot \mathbf{X} \cdot \mathbf{X}^H \cdot \mathbf{C} \cdot \mathbf{A} = \mathbf{A}^H \cdot \mathbf{C} \cdot \mathbf{R} \cdot \mathbf{C} \cdot \mathbf{A} \tag{6.3}$$

Under the assumption that noise and signals are not correlated, the estimate of the covariance matrix can be calculated as the time average from snapshot to snapshot as

$$\mathbf{R} = \frac{1}{N}\sum_{t=1}^{N} \mathbf{x}(t) \cdot \mathbf{x}(t)^H = \mathbf{R}_S + \mathbf{R}_N \tag{6.4}$$

where $\mathbf{R}_S = \mathbf{A} \cdot \mathbf{S} \cdot \mathbf{A}^H$ with $\mathbf{S}$ defined as the source covariance matrix in (2.24) and $\mathbf{R}_N = 1/N \sum_{t=1}^{N} \mathbf{n}(t) \cdot \mathbf{n}(t)^H$. Denoting the noise covariance matrix $\mathbf{R}_N$ by a normalised noise covariance matrix Σ_N, we have $\mathbf{R}_N = \sigma_n^2 \Sigma_N$ where σ_n^2 is the noise power. Thus,

$$\mathbf{R} = \mathbf{A} \cdot \mathbf{S} \cdot \mathbf{A}^H + \sigma_n^2 \Sigma_N \tag{6.5}$$

The pre-conditioning matrix $\mathbf{C}$ is assumed to be Hermitian. Determining whether a target is present involves comparing a statistic with a pre-defined threshold, where such a statistic comprises the output power in the direction to be detected and information available in the rest of the data.

6.3 The IMP Algorithm

Based on the model given in section 6.2, the IMP algorithm will be discussed in detail in this section with the objective of giving a better understanding of the IMP technique.

IMP (Incremental Multi-stage Parameter) is an iterative algorithm. The IMP spatial spectrum starts with the output power distribution of a sensor array which implies that conventional beamforming is used as the initial stage in the IMP algorithm. A single peak is found in the output spectrum estimate and the contribution of stimuli in the corresponding direction of the peak is found by convolving a δ-function in wavenumber (or frequency in time series analysis) with the system transfer function. In order to remove the effect of the selected peak, the weighting (pre-conditioning) is modified and applied to the data.

The statistic used in the IMP algorithm is the signal plus noise to noise ratio (SNNR) which has been given in equation (3.36) and is rewritten here for convenience of referencing

$$SNNR(\mathbf{a}) = \frac{\mathbf{a}^H(\theta) \cdot \mathbf{C} \cdot \mathbf{R} \cdot \mathbf{C} \cdot \mathbf{a}(\theta)}{\mathbf{a}^H(\theta) \cdot \mathbf{C} \cdot \mathbf{R}_N \cdot \mathbf{C} \cdot \mathbf{a}(\theta)} \tag{6.6}$$

Under the general assumption that the noise field is spatial white and the noise measurement is uncorrelated from sensor to sensor, equation (6.6) is simplified to

$$SNNR(\mathbf{a}) = \frac{\mathbf{a}^H(\theta) \cdot \mathbf{C} \cdot \mathbf{R} \cdot \mathbf{C} \cdot \mathbf{a}(\theta)}{\mathbf{a}^H(\theta) \cdot \mathbf{C} \cdot \mathbf{a}(\theta)} \tag{6.7}$$

This is the conventional beamforming spectrum when the pre-conditioning matrix $\mathbf{C} = \mathbf{I}$. When only a single source is present, in the presumed isotropic noise background, the IMP estimator performs like the conventional beamformer giving the best estimate of the source direction at its first stage. The corresponding source steering vector, denoted by $\mathbf{a}_{max}$, is used to form a projection matrix to project the received data into the null space of this direction vector

$$\mathbf{Q} = \mathbf{I} - \frac{\mathbf{a}_{max} \cdot \mathbf{a}_{max}^H}{\mathbf{a}_{max}^H \cdot \mathbf{a}_{max}} \tag{6.8}$$

Replacing the pre-conditioning matrix $\mathbf{C}$ in equation (6.6) with the above projection matrix, a modified spectrum is formed as

$$P(\theta) = \frac{\mathbf{a}^H(\theta) \cdot \mathbf{Q} \cdot \mathbf{R} \cdot \mathbf{Q} \cdot \mathbf{a}(\theta)}{\mathbf{a}^H(\theta) \cdot \mathbf{Q} \cdot \mathbf{a}(\theta)} \tag{6.9}$$

It should be remembered that any projection matrix is both idempotent and symmetric (Hermitian in the complex case), i.e., $\mathbf{Q} = \mathbf{Q}^2$, and $\mathbf{Q} = \mathbf{Q}^H$. No signal component will fall into the nullspace of $\{\mathbf{a}_{max}\}$ if $\mathbf{a}_{max}$ exactly presents the signal direction, and thus no significant peak will appear in the output power spectrum $P(\theta)$ in equation (6.9). The algorithm terminates.

Example 1 (One Source Case)

Figure 6.1 illustrates the simplest case when only a single source is present. A 10 element uniform linear array with half wavelength spacing is used. A single source of 10 dB source power (the noise variance is assumed as unity) is located at 2.4° from broadside. 100 independent snapshots are taken to form the data matrix. The threshold is calculated as 9.95 dB. Plot 6.1(a) shows the initial stage of the algorithm which is the conventional spectrum of the array output. A global maximum of this spectrum is found at 2.4° to the normal of the array. A projection matrix is then formed and applied to equation (6.9) for the modified spectrum.

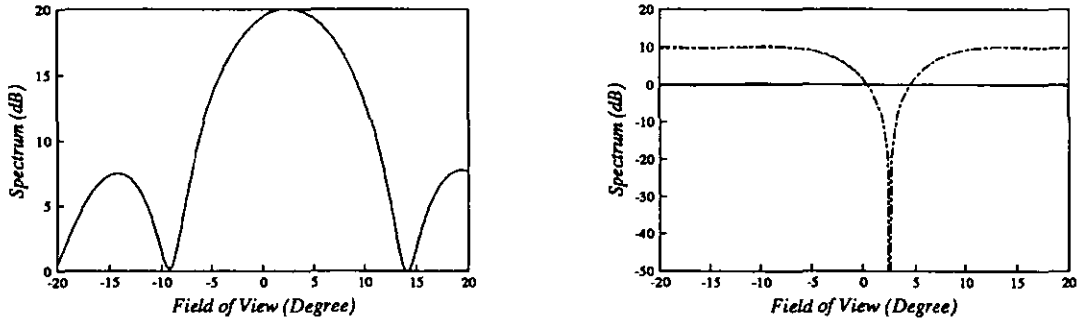

Figure 6.1 IMP algorithm in the single source case

Both numerator and denominator as well as the modified spectrum are plotted in plot 6.1(b), denoted by the dotted, long chained, and solid lines respectively. (The numerator and the denominator give the same curve since the numerator drops to the noise level when no signal

components exist.) Deep nulls are formed in both the numerator and the denominator corresponding to the peak position in plot 6.1(a), while a flat spectrum results with respect to the spatial angle, dropping to the noise level.

End

By using the conventional beamformer, when two signals are present a double hump structure exists in the output power spectrum if the separation of the sources is sufficient (otherwise a single broad peak results), but the two peaks tend to the mid-point and estimation biases are obvious. Usually two peaks are not of the same height even though two equal strength signals might be used. In the IMP algorithm, the globally highest peak, denoted by $\mathbf{a}_1$, or the only one when a single exists, is taken for the formation of the projection matrix which will be used in the second iteration of the algorithm. Applying this projection matrix to the received data, the resulting power spectrum eliminates the components of both signals in the nullspace of the column vector $\mathbf{a}_1$. Since there is a second signal, the residual output power of this modified beamformer shows a principal peak with respect to θ, and this is taken as the initial angular estimate of the second source, denoted by $\mathbf{a}_2$.

So far we have obtained two estimates of the signal directions, corresponding to source steering vectors $\mathbf{a}_1$ and $\mathbf{a}_2$, respectively. Since bias exists at least in the estimate of the first signal direction, refinement is necessary for more accurate estimates of the signal directions. To refine the first signal direction estimate, a projection matrix is formed on $\mathbf{a}_2$. Since many signal components concerning the second signal, contained in the received data, are eliminated when the latest projection matrix is applied to the received data, the resulting power spectrum is much purer and gives a better angular estimate of the first signal. Alternatively, this procedure is applied to re-estimate the direction of the second signal. This continues until the angular estimates for both signals are stable and then the algorithm terminates.

To verify the accuracy of the estimates, a projection matrix $\mathbf{Q}$ can be formed on $[\mathbf{a}_1, \mathbf{a}_2]$ when both of them are stable. Defining $\mathbf{A}_S = [\mathbf{a}_1, \mathbf{a}_2]$, we have

$$\mathbf{Q} = \mathbf{I} - \frac{\mathbf{A}_S \cdot \mathbf{A}_S^H}{\mathbf{A}_S^H \cdot \mathbf{A}_S} \tag{6.10}$$

Substituting this projection matrix into equation (6.9), the power spectrum having eliminated the components of both signals is available. No significant peak will appear and the power

will drop to the noise power level.

Example 2 (Two Source Case)

Figure 6.2 gives the details of the convergence of a two source case. The two sources are given equal power of 10 dB (relative to the unit noise variance) and placed at -1.2° and 3.4°. The same array as that in the previous example is used and again 100 snapshots are taken to form the data matrix. The threshold for this case is 9.90 dB. A lot of 13 iterations were executed before termination of the procedure. The first 5 of them are shown in plots 6.2(a) through 6.2(e) and the iteration is depicted in plot 6.2(f). The situation of iterations in between is omitted and the history of the convergence is given in plot 6.2(g). The peak positions at each iteration are listed beside plot 6.2(g). The re-processing stops at the stable estimates of $\hat{\theta}_1 = -1.0°$ and $\hat{\theta}_2 = 3.4°$. The dotted lines in plot 6.2(g) depict the true directions of sources. It is easily seen from the plot, and also the list of peak positions at each iteration, that the adjustment is applied to only one peak position at each iteration. In the last iteration, a projection matrix based on the two direction estimates is formed and applied to the observed data so as to eliminate the signal components in these two directions. The residual spectrum contains mainly the noise component and some possible signal leakage, and drops to the noise level.

End

When more than two signals are present, the algorithm will continue after finding the stable angular estimates of the first two signals. In this case, $P(\theta)$ in equation (6.9) depicts a significant peak even though the projection matrix $\mathbf{Q}$ is based on $[\mathbf{a}_1, \mathbf{a}_2]$, which indicates the existence of the third source. This peak is assumed as the initial estimate of the third source, with source steering vector denoted by $\mathbf{a}_3$. Because of the existence of the third signal, the estimates of the first two signal directions in stage 2 are stable but not accurate. Refinement is necessary for the angular estimates of all three signals.

To refine the first angular estimate, the projection matrix $\mathbf{Q}$ is based on $[\mathbf{a}_2, \mathbf{a}_3]$. Then using the latest estimates of $\mathbf{a}_1$ and $\mathbf{a}_3$, the second one is re-estimated by applying the projection matrix based on $[\mathbf{a}_1, \mathbf{a}_3]$. For the third one, the projection matrix is formed on $[\mathbf{a}_1, \mathbf{a}_2]$. These three steps are repeated to re-estimate all three signal directions alternatively. The criterion for judging whether to terminate the algorithm is the same as that in stage 2 for the two signal case.

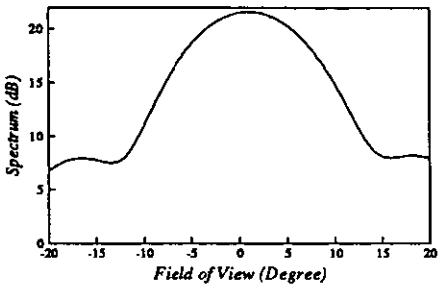

(a)

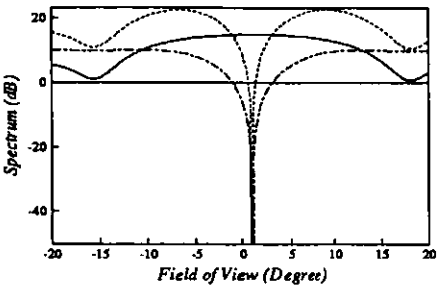

(b)

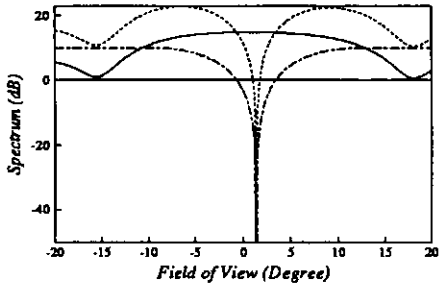

(c)

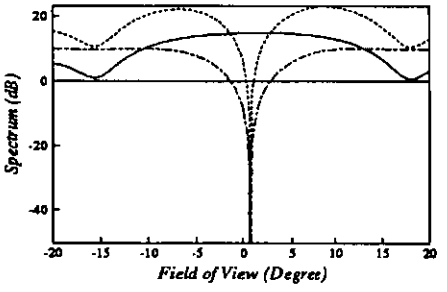

(d)

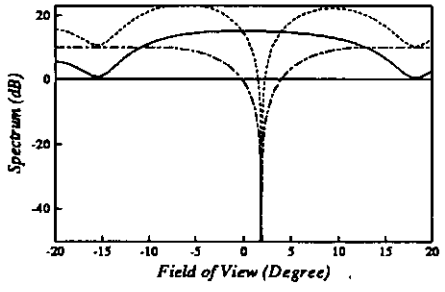

(e)

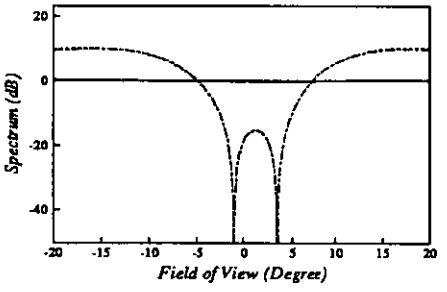

(f)

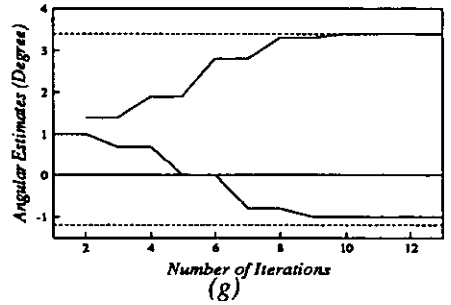

(g)

Figure 6.2 convergence details and history in the two source case

$\hat{\theta}_1$	$\hat{\theta}_2$
1.0	
1.0	*1.4*
0.7	*1.4*
0.7	*1.9*
0.0	*1.9*
0.0	*2.8*
-0.8	*2.8*
-0.8	*3.3*
-1.0	*3.3*
-1.0	*3.4*
-1.0	*3.4*
-1.0	*3.4*
-1.0	*3.4*

Example 3 (Three Source Case)

This example shows the processing of the three source case by means of the IMP algorithm. The same array is assumed. Three sources with equal power of 20 dB are placed at -3.2°, 1.5°, and 4.1°, and the threshold is calculated as 10.08 dB. 21 iterations are completed to give the stable estimates of all three source directions and the procedure terminates successfully. Four plots are drawn in figure 6.3 to show the modified spectra in 4 iterations chosen from the total 21 iterations. Plot 6.3(a) is the conventional spectrum which fails to resolve the three sources placed within one beamwidth of the array. The global maximum of this spectrum is used to null the received data in that direction and the resulting spectrum is shown in plot 6.3(b) by the solid line. The dotted and long chained lines represent the numerator and denominator of the equation (6.9) respectively. Expressed in decibels, the difference of these two spectra results in the modified power spectrum given by the solid line. Plot 6.3(c) shows the situation when the first two direction estimates are stable and are nulled from the spectrum, the 11th iteration. Since the residual power level is still above the threshold, the existence of the third source is indicated and the peak position in the residual power spectrum is assigned as its initial estimate. The refinement is applied to the three direction estimates alternatively until stable estimates are obtained. The residual power is compared with the threshold and termination of the procedure is decided.

End

This procedure can be extended to higher order models without difficulty.

Defining a generalised matrix $\mathbf{A}_S$ to contain the array manifold vector(s) which has been calculated at each iteration according to the peak direction(s) in the previous iteration. At stages when only one peak has been found, $\mathbf{A}_S$ will be a column vector containing the corresponding array manifold vector as $\mathbf{A}_S = [\mathbf{a}_{max}]$; when more than one peak is going to be cancelled, the matrix $\mathbf{A}_S$ will be composed of multiple of array manifold vectors, which correspond to these peak directions, as $\mathbf{A}_S = [\mathbf{a}_1, \mathbf{a}_2]$ in the two peak case, and $\mathbf{A}_S = [\mathbf{a}_1, \mathbf{a}_2, \mathbf{a}_3]$ when three peaks are to be eliminated. When k peaks are to be cancelled, the projection matrix is as

$$\mathbf{Q} = \mathbf{I} - \frac{\mathbf{A}_s^{(k)} \cdot \mathbf{A}_s^{(k)H}}{\mathbf{A}_s^{(k)H} \cdot \mathbf{C}_o \cdot \mathbf{A}_s^{(k)}} \tag{6.11}$$

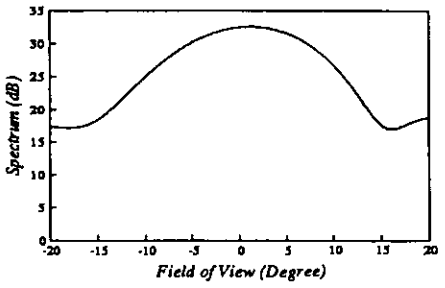

(a)

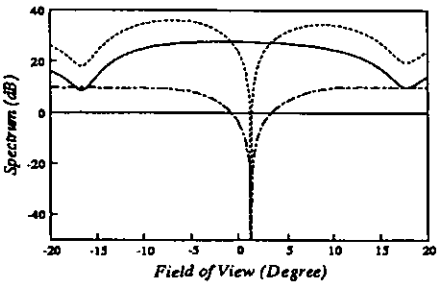

(b)

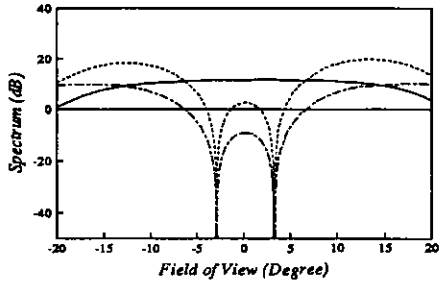

(c)

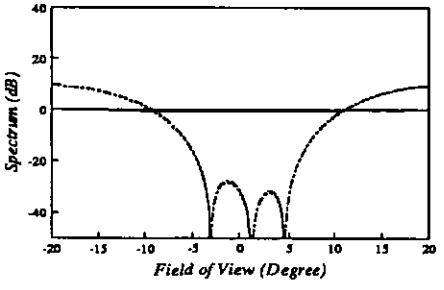

(d)

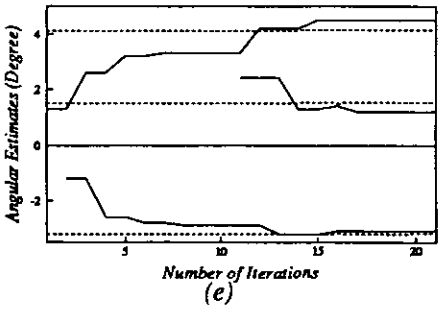

(e)

Figure 6.3 convergence details and history in the three source case

$\hat{\theta}_1$	$\hat{\theta}_2$	$\hat{\theta}_3$
1.3		
1.3	-1.2	
2.6	-1.2	
2.6	-2.6	
3.2	-2.6	
3.2	-2.8	
3.3	-2.8	
3.3	-2.9	
3.3	-2.9	
3.3	-2.9	
3.3	-2.9	2.4
4.2	-2.9	2.4
4.2	-3.2	2.4
4.2	-3.2	1.3
4.5	-3.2	1.3
4.5	-3.1	1.3
4.5	-3.1	1.2
4.5	-3.1	1.2
4.5	-3.1	1.2
4.5	-3.1	1.2
4.5	-3.1	1.2

where the superscript (k) denotes the number of peaks to be cancelled, and $\mathbf{C}_o$ is the pre-conditioning matrix in the initial stage which has been assumed as identity matrix in the above three examples. Therefore, the corresponding pre-conditioning matrix is shown to be

$$\mathbf{C}_k = \mathbf{C}_o - \mathbf{C}_o \cdot \mathbf{A}_S^{(k)} \cdot \left(\mathbf{A}_S^{(k)H} \cdot \mathbf{C}_o \cdot \mathbf{A}_S^{(k)}\right)^{-1} \cdot \mathbf{A}_s^{(k)H} \cdot \mathbf{C}_o \tag{6.12}$$

The IMP algorithm can be summarised as follows :

1) *Initialise the procedure :* $k = 0, \quad \mathbf{C}_o = \mathbf{I}$

2) *Evaluate the Signal plus Noise to Noise Ratio (SNNR) :*

$$SNNR(\theta) = \frac{\mathbf{a}^H \cdot \mathbf{C}_k \cdot \mathbf{R} \cdot \mathbf{C}_k \cdot \mathbf{a}}{\mathbf{a}^H \cdot \mathbf{C}_k \cdot \mathbf{R}_N \cdot \mathbf{C}_k \cdot \mathbf{a}} \tag{6.13}$$

and find the global maximum

3) *Adjust the weighting* $\mathbf{C}_k$ *according to the latest estimates of the peak positions by using equation (6.12)*

4) *Compare the maximum and the pre-defined threshold. If the maximum is bigger than the threshold, return to Step 2; otherwise, terminate the process.*

Substituting $\mathbf{R}$ given in equation (6.5) into the numerator of (6.13), the following relationship results

$$SNNR(\theta) = \frac{\mathbf{a}^H \cdot \mathbf{C}_k \cdot \mathbf{A} \cdot \mathbf{S} \cdot \mathbf{A}^H \cdot \mathbf{C}_k \cdot \mathbf{a}}{\mathbf{a}^H \cdot \mathbf{C}_k \cdot \mathbf{R}_N \cdot \mathbf{C}_k \cdot \mathbf{a}} + 1 \tag{6.14}$$

where it is assumed that $\mathbf{R}_N = \sigma_n^2 \cdot \Sigma_N$. From the above expression it follows that the projection matrix into the nullspace of the all signals will cancel all the signal components in the data because of the orthogonality between the $\mathbf{C}_k$ and the signal array manifold vectors. This results in the *SNNR* reaching the level of unity asymptotically.

6.4 Computer Simulations

Computer simulations have been carried out to compare the performance of the IMP algorithm to that of the popular MUSIC method and its root version. Two groups of simulations are going to be presented in this section to show statistics as functions of signal to noise ratio and those of angular separation, respectively. The correlation factor between the two sources is assumed to be 0, 0.95, and 1. Two highly correlated situations are considered to show the superior performance of the IMP algorithm over the MUSIC method which is claimed in the highly correlated cases.

The simulation programs were written using MATLAB. In all cases the number of sources was assumed to be known, and the *m-d* smallest eigenvalues of the estimated covariance matrix were used in estimating the noise variance and in defining the threshold. To reduce computations involved in the search procedures, the angular range was restricted to $[\theta_1 - 4°, \theta_2 + 4°]$. The search grid was set to 0.1°.

The conventional spectrum output of the array is first checked for the existence of any source. If the peak level in the spectrum is below the pre-defined threshold, no source is indicated and the program terminates; otherwise at least one source is present and its angular position is estimated and used in forming the projection matrix to check the existence of more sources.

In the procedure for finding more sources, two criteria are set for the termination of the program :

1) The difference of the latest estimates of the directions and those of the previous ones is smaller than a given tolerance, which is given as 1E-05 in the simulation. Since the grid of angular estimates is given as 0.1°, this criterion means that the latest estimates should be the same as the previous ones when the program terminates successfully.

2) The given maximum number of iterations is exceeded. In the simulations to be presented in this chapter, 10 iterations are allowed for each source, i.e., in total 20 iterations can be performed at the stage when two sources are refined and 30 iterations in the three source case, and so on.

When calculating the modified spectrum, the numerator and denominator of equation (6.9) are computed separately and then used to form the power spectrum. This is to avoid possible

division by 0 so as to keep the continuum of the resulting spectrum. When the denominator of (6.9) is less than 1E-06, the spectrum value at this direction is assigned the value of the previously searched direction; otherwise the spectrum is calculated as the division of the current numerator by the current denominator.

The correctness of the angular estimates given by the IMP algorithm is judged by two criteria: one is that the estimates fall in the neighbourhood of the true directions, and the other one is that the separation between the two estimates is bigger than a given angle. For the processing of the simulated data, the neighbourhood of the true directions is defined as ±3°, and sufficient separation between the two estimates in each trial is given as 0.5°. The judgement of the fitness of the estimates given by MUSIC is the same as that in previous chapters. Again, only the successful estimates for each parameter set-up are included in the calculation of the statistics.

6.4.1 Results as Functions of Signal to Noise Ratio

Probabilities of resolution, biases of angular estimates, and their standard deviations are calculated over 500 trials and shown in figures 6.4 to 6.6. The two sources are located at 0° and 2° to the normal of the 10 element array with half wavelength spacing, that is about 0.17 beamwidth. The initial signal to noise ratio for the simulations is given as 0 dB and is then increased at 5 dB increments to 50 dB.

The resolving threshold of the IMP algorithm is similar to that of the spectral MUSIC but higher than that of the root MUSIC. This is the case for both uncorrelated sources and the sources with correlation factor $\rho = 0.95$, but IMP seems to suffer from lower probability of resolution over a range of the signal to noise ratio after all three methods are able to solve the two sources in the uncorrelated case. From the uncorrelated case in figure 6.4 to the highly correlated case in figure 6.5, the resolution threshold of all three methods increases about 10 dB equivalent in signal to noise ratio, while the resolution degradation of the IMP algorithm is relatively less than that of both spectral and root versions of the MUSIC method. As the correlation gets stronger (fully correlated), as shown in figure 6.6, only the IMP algorithm shows the ability to resolve the two sources. Two other methods, spectral and root MUSIC, fail completely, as predicted theoretically.

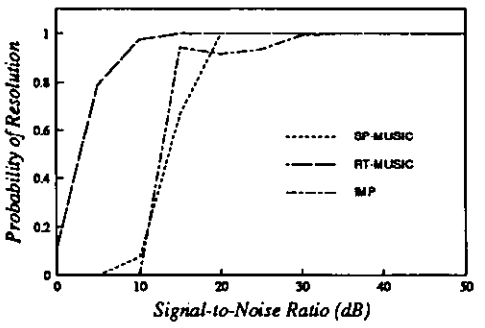

(a)

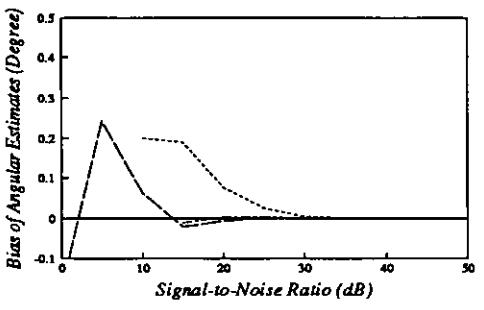

(b)

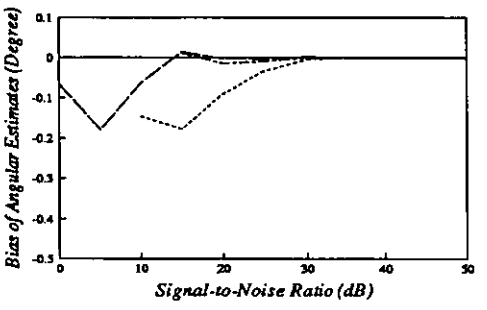

(c)

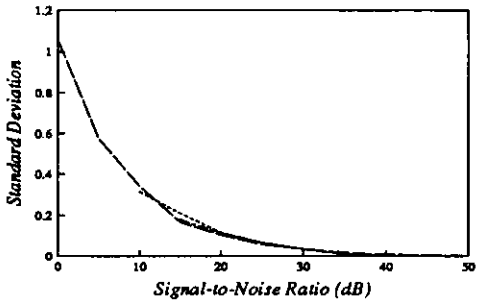

(d)

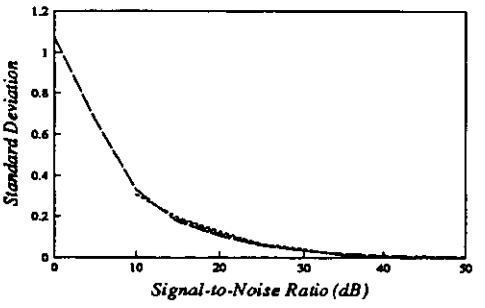

(e)

Figure 6.4 *Performance comparison of spectral MUSIC, root MUSIC, and IMP as functions of signal to noise ratio when two sources are uncorrelated*

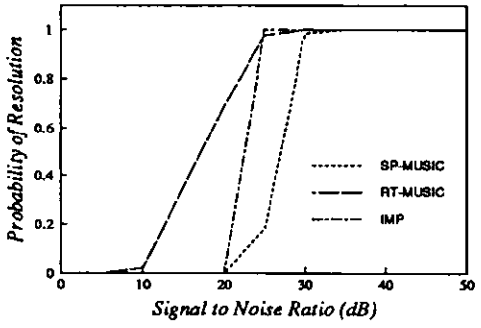

(a)

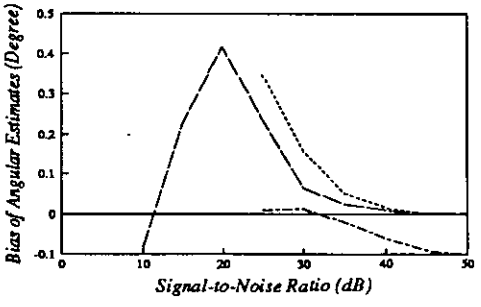

(b)

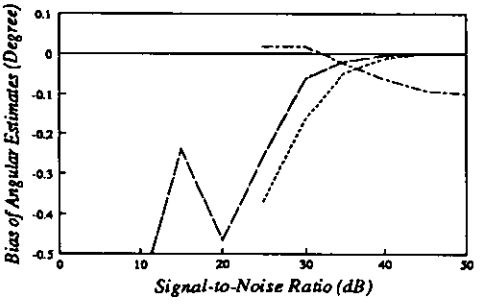

(c)

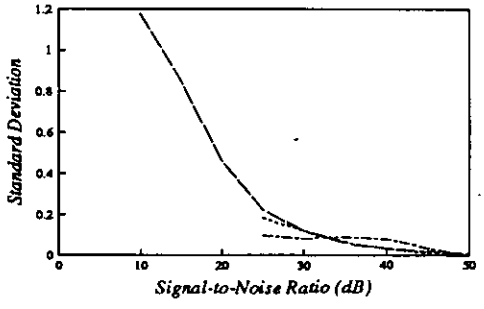

(d)

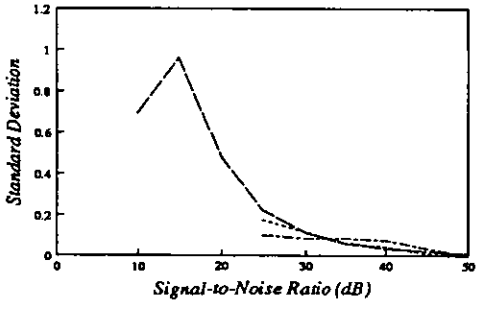

(e)

Figure 6.5 *Performance comparison of spectral MUSIC, root MUSIC, and IMP as functions of signal to noise ratio when two sources are correlated with* $\rho = 0.95$

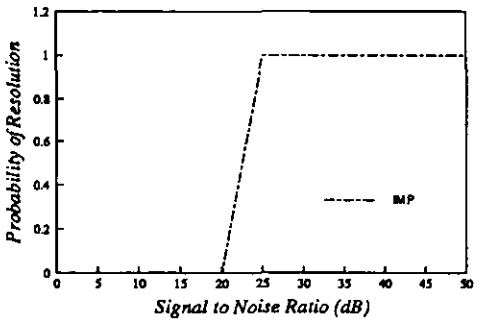

(a)

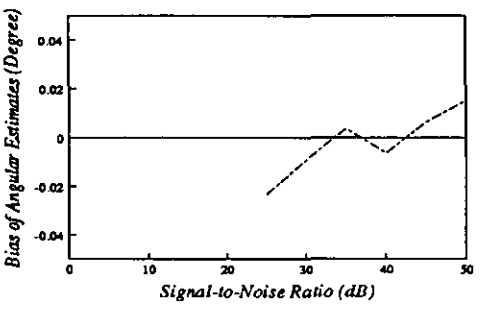

(b)

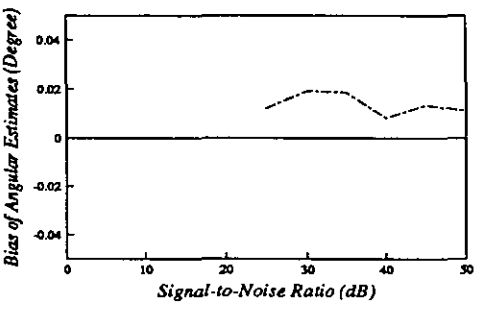

(c)

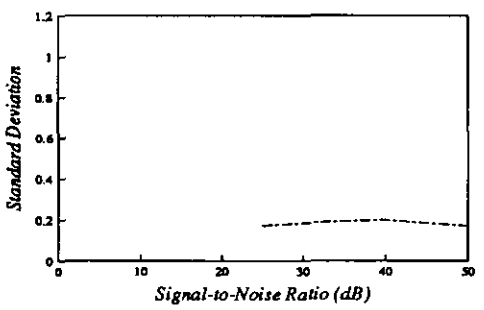

(d)

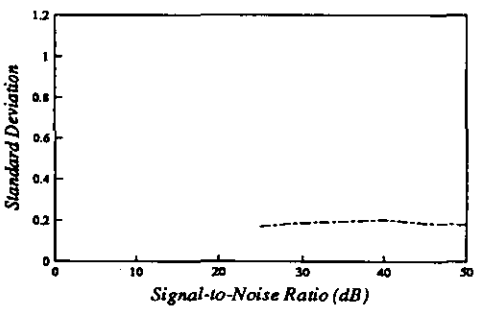

(e)

Figure 6.6 *Performance comparison of spectral MUSIC, root MUSIC, and IMP as functions of signal to noise ratio when two sources are correlated with* $\rho = 1.0$

The reason for the loss of resovability of the IMP algorithm between 15 dB to 25 dB is thought to be the criterion defined for testing the probability of resolution. Since the grid for searching the directions is set to 0.1°, so all the estimates which are only 0.1° apart are taken as unresolved estimates. This reduces the probability of resolution and the biases and the standard deviations at the same time.

Concerning the biases of the estimated source directions in the uncorrelated case, the root MUSIC method shows larger values at lower signal to noise ratios where the other two methods are still unable to resolve the two sources. As the signal to noise ratio goes higher, the IMP method and the spectral MUSIC technique start to separate the two sources but give biases in the angular estimates. The biases given by the spectral MUSIC method are relatively higher, while those given by the IMP algorithm are similar to that of the root MUSIC technique. When the signal to noise ratio is even higher, at or above 30 dB, all three methods tend to estimate the directions without bias.

Meanwhile, the standard deviations resulting from all three methods are nearly the same, and go to zero as the signal to noise ratio increases.

In the highly correlated case in figure 6.5, all three methods give approximately the same performance in the sense of the standard deviation. However, significant differences are evident in the biases. Two versions of the MUSIC technique give asymptotically unbiased angular estimates, whilst the estimates from the IMP algorithm are off the true directions even when the signal to noise ratio is very high.

The simulated data were checked for the reason of the high biases in estimated source directions from the IMP method. It was found that IMP gives very good estimates of the source directions when it starts to resolve the two sources at 25 dB with the estimates almost evenly being -0.1°, 0°, or 0.1° for source 1 and 1.9°, 2.0°, or 2.1° for source 2. This results in smaller biases and relatively larger standard deviations. As the signal to noise ratio goes higher, the estimates of the two sources tend to possess the smaller values of the three in the 25 dB case, i.e., more estimates remain at -0.1° and 1.9° for two sources, until at 50 dB all 500 trials give the same estimates of [-0.1°, 1.9°]. A -0.1° bias exists for both source directions while the standard deviations are zero.

Figure 6.6 shows the coherent case where only the IMP algorithm is still able to distinguish between the two sources. The possibility of resolution remains the same as that in the highly

correlated case, while the relative values of biases and standard deviations are opposite to those in the previous case. The scale for the plot in figure 6.6(b) and 6.6(c) is changed to show the very small values of the biases for all the signal to noise ratio cases when the two sources are resolvable. On the other hand, the standard deviations are stable at about 0.2°. The estimates do not converge at all.

6.4.2 Results as Functions of Angular Separation

The simulated data carried out as functions of angular separation were analysed in the same way as that in the previous sub-section, and the same statistics were tested and plotted. The signal to noise ratio was given as 10 dB throughout the computer simulations. The correlation factor given to the three cases was 0, 0.95, and 1.0, and the results are shown in figures 6.7 to 6.9.

In the uncorrelated case, all three statistics are similar to those as functions of signal to noise ratio. The root MUSIC technique has the smallest resolution threshold, while the thresholds for the other two methods are 5 dB higher and the IMP algorithm suffers from some loss of probability of resolution at the middle part of the plot. The biases converge as the angular separation increases with higher biases resulting from the spectral MUSIC algorithm at relatively smaller separations. Despite the differences in the biases, standard deviations are very similar but do not tend to zero as the angular separations increase.

The degradation in the probabilities of resolution is also similar to that in the case of functions of signal to noise ratio when the correlation between the two sources is stronger. As shown in figure 6.8, the degradation in IMP algorithm is the smallest, shifting from the spectral MUSIC method towards the root MUSIC technique. Biases given by the MUSIC techniques are much higher at smaller separations but decrease as the separation becomes bigger while, at the same time, the IMP algorithm possesses a small bias at smaller separations and a large one at larger separations. Concerning the standard deviation, the two MUSIC based methods have similar but larger values while those given for the IMP method are almost constant over the whole range of angular separation where it is able to resolve the two sources.

The MUSIC techniques fail completely when the correlation between the two sources is extremely high or the two sources are coherent, as was stated in chapter 4. In the three aspects under examination, the behaviour of the IMP algorithm remains the same as that in the previous case.

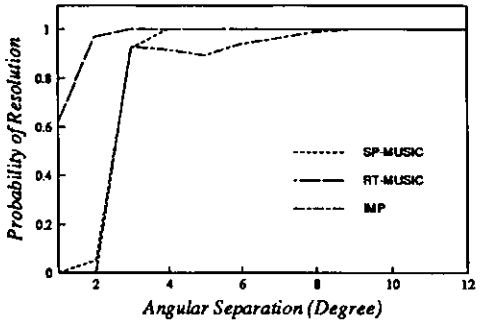

(a)

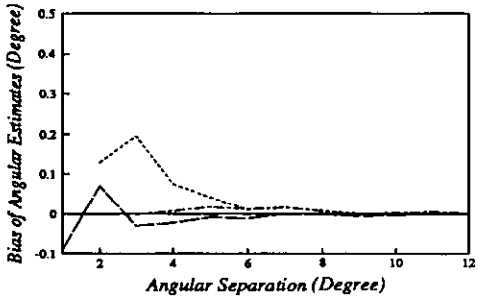

(b)

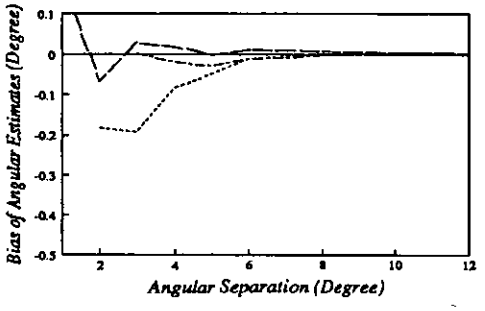

(c)

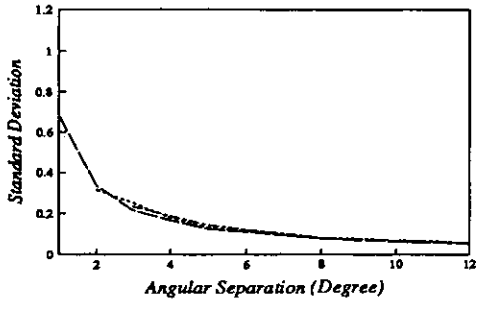

(d)

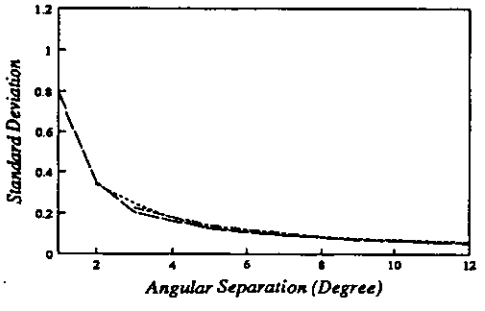

(e)

Figure 6.7 *Performance comparison of spectral MUSIC, root MUSIC, and IMP as functions of angular separation when two sources are uncorrelated*

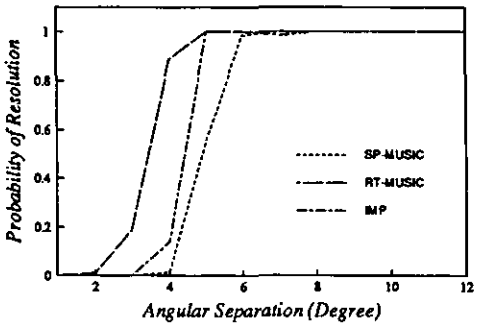

(a)

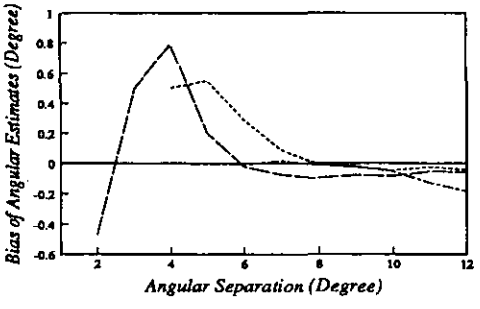

(b)

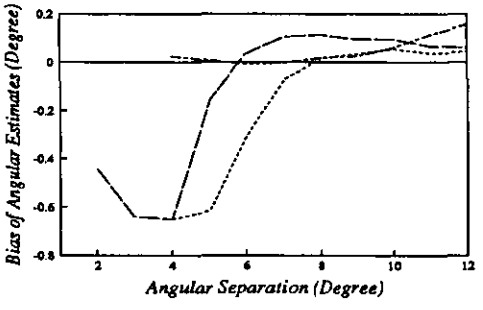

(c)

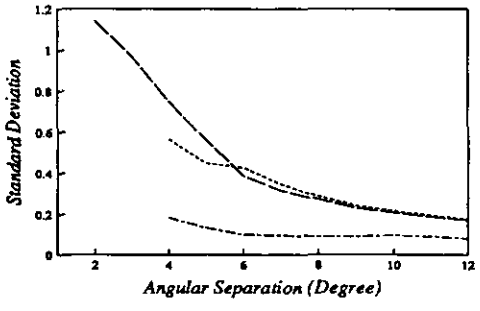

(d)

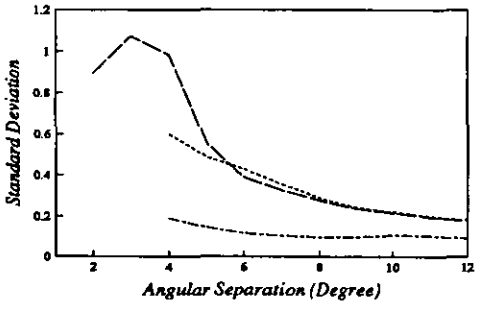

(e)

Figure 6.8 *Performance comparison of spectral MUSIC, root MUSIC, and IMP as functions of angular separation when two sources are correlated with* $\rho = 0.95$

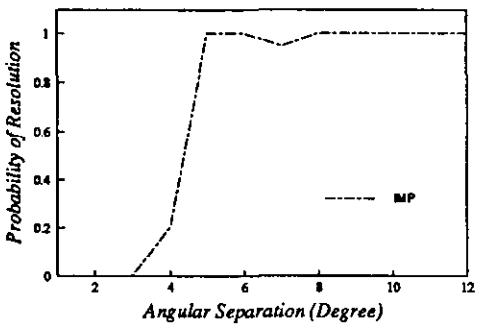

(a)

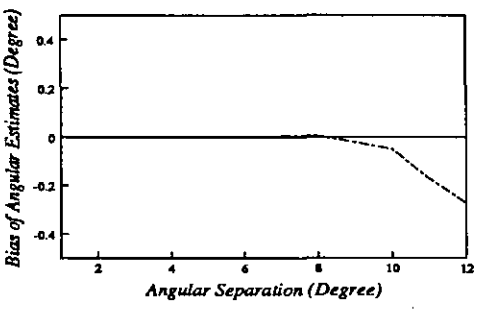

(b)

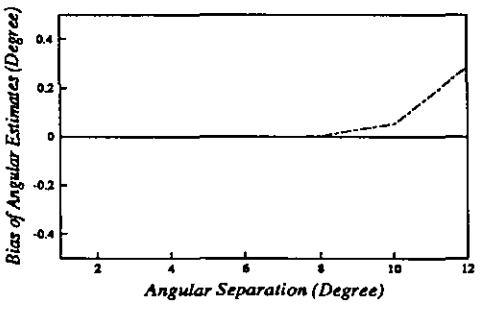

(c)

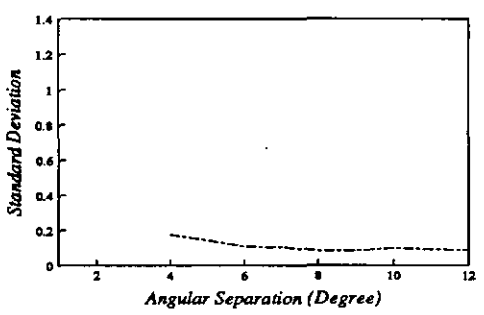

(d)

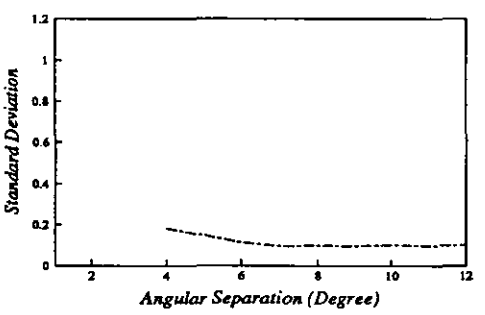

(e)

Figure 6.9 *Performance comparison of spectral MUSIC, root MUSIC, and IMP as functions of angular separation when two sources are correlated with* $\rho = 1.0$

6.5 Conclusion

6.5 Conclusion

The simulation results presented in this chapter provide a means for a better understanding of the IMP algorithm. The performance advantages of the IMP algorithm over the most popular MUSIC techniques, especially in the highly correlated source case are demonstrated in the computer simulations. In the uncorrelated case, the performance of the IMP method is similar to that of the root MUSIC method and superior to the spectral version of MUSIC. As the correlation between the sources is stronger, the performance advantages of the IMP algorithm are significant.

CHAPTER 7

WEIGHTED SUBSPACE FITTING METHODS

Multidimensional methods in array signal processing possess advantages, such as the ability to handle coherent signals, over conventional one-dimensional techniques at the cost of expensive computations. Although, the Maximum Likelihood (ML) approaches have been systematic approaches to many parameter estimation problems for several decades, only in the past ten years or so have the appropriate methods for maximising the cost function been proposed, see e.g. [BM86, Sha88, SN88, ZW88] for deterministic ML (Det-ML) and [Sch81, Boh87] for stochastic ML (Sto-ML). To avoid the heavy computational burden inherent in the multidimensional approaches, many suboptimal methods were suggested for the DOA estimation problem among them the so-called eigenstructure or signal subspace techniques have received much attention because of their high resolution properties (*cf.* [Sch81, BK80]). A one-dimensional search over the parameter space is employed in these methods instead of the multidimensional search in the optimal ML methods resulting in that they are unable to resolve highly correlated or coherent signals. Recently some multidimensional subspace methods have been proposed to deal with the coherency problem and, at the same time, have high resolution abilities [Cad88, ZW88].

More recently, a Weighting Subspace Fitting (WSF) scheme was introduced by Viberg and Ottersten in, e.g. [OV89, VO91], which include a wide range of direction estimation algorithms. Based on an investigation of the variance of the estimation errors, a new multidimensional estimation procedure was proposed which is applicable to arbitrary array geometries and signal correlation. This so-called optimal WSF method belongs to the same class of subspace fitting based algorithms as the deterministic ML method, but attains the stochastic Cramer-Rao Bound (CRB) while the optimization is of similar structure as that required by deterministic ML. It was demonstrated in [VOK89] that the WSF method is not only statistically efficient, but also offers other advantages over deterministic ML.

A brief description of the optimal WSF method has been given in the literature survey in chapter 3. This chapter will restate the problem under consideration briefly and concentrate on the implementation of the algorithm and its performance analysis by means of computer simulations.

7.1 The Basic Subspace Fitting Problem and Subspace Fitting Methods

The problem under consideration here is also extracting information from the array output measurements. The output of the m element sensor array is assumed to be a weighted super-position of d wavefronts corrupted by sensor noise which is assumed to be a white Gaussian process and uncorrelated with the emitter signals

$$\mathbf{x}(t) = \mathbf{A}(\theta) \cdot \mathbf{s}(t) + \mathbf{n}(t) \tag{7.1}$$

The output of the array is sampled at N time instants and these snapshots are collected to form an $m \times N$ data matrix $\mathbf{X}_N$. Given measurements $\mathbf{X}_N$, the basic subspace fitting problem is defined by the deterministic ML criterion as trying to fit the subspace spanned by $\mathbf{A}(\theta)$ to the measurement $\mathbf{X}_N$. Described mathematically, this problem is expressed as

$$[\hat{\mathbf{A}}, \hat{\mathbf{T}}] = arg \min_{\mathbf{A},\mathbf{T}} ||\mathbf{M} - \mathbf{A}(\theta) \cdot \mathbf{T}||_F^2 \tag{7.2}$$

where $\mathbf{M}$ is an $m \times q$ matrix representing the measurement data, $\mathbf{A}(\theta)$ is an $m \times p$ matrix parameterised by the DOAs, and $\mathbf{T}$ is any $p \times q$ matrix. According to Golub and Pereyra [GP73], the subspace fitting problem defined in (7.2) can be separated in $\mathbf{A}$ and $\mathbf{T}$. By substituting the pseudo-inverse solution $\hat{\mathbf{T}} = \mathbf{A}^+ \cdot \mathbf{M}$ into (7.2), the following equivalent problem results

$$\hat{\mathbf{A}}(\theta) = arg \max_{A} Tr\{\mathbf{P}_A \mathbf{M}\mathbf{M}^H\} \tag{7.3}$$

or equivalently

$$\hat{\mathbf{A}}(\theta) = arg \min_{A} Tr\{\mathbf{P}_A^{\perp} \mathbf{M}\mathbf{M}^H\} \tag{7.4}$$

where $\mathbf{P}_A = \mathbf{A}(\mathbf{A}^H\mathbf{A})^{-1}\mathbf{A}^H$ is the projection matrix that projects into the range of $\mathbf{A}$ and $\mathbf{P}_{\bar{A}} = \mathbf{I} - \mathbf{P}_A$ is that which projects in to the nullspcae of $\mathbf{A}$. The parameter vector Θ is estimated from $\hat{\mathbf{A}}$.

The deterministic ML method given by equation (2.57) is a straightforward member of this set of subspace fitting methods by taking $\hat{\mathbf{R}} = \mathbf{M}\mathbf{M}^H$ and employing a d-dimensional search over the subspace spanned by the columns of $\mathbf{A}(\theta)$.

Finding maxima in the MUSIC spectrum in (3.21) equals maximizing $1 - 1/P_{MUSIC}(\theta) = \mathbf{a}^H(\theta) \cdot \mathbf{E}_S \cdot \mathbf{E}_S^H \cdot \mathbf{a}(\theta)$, which results in the DOA estimates as

$$\hat{\theta} = arg\ \max Tr\{\mathbf{P}_A \cdot \hat{\mathbf{E}}_S \cdot \hat{\mathbf{E}}_S^H\} \tag{7.5}$$

This is a case of the subspace fitting method when $\mathbf{M} = \hat{\mathbf{E}}_S$ and $\mathbf{A} \in A$.

To overcome the problem of coherency, a multidimensional version of the MUSIC algorithm was suggested in [Cad88] which can be formulated in the subspace fitting framework as

$$\hat{\theta} = arg \max_{\mathbf{A} \in A^d} Tr\{\mathbf{P}_A \cdot \hat{\mathbf{E}}_S \cdot \hat{\mathbf{E}}_S^H\} \tag{7.6}$$

This, again, is a computationally expensive multidimensional optimization problem. A special case of the multidimensional method is achieved when it is applied to arrays with special constraints. This is the so-called ESPRIT method applicable only to arrays of identical translationally displaced subarrays, by which the computation is reduced with the price of an inability to handle coherent sources.

From the expressions for the Det-ML and MUSIC techniques given above, the representation of the data can be chosen in two ways, either as the Hermitian square root of the estimated covariance matrix or the estimated signal subspace matrix. The relation between these two choices for a large number of snapshots is described by the following theorem which motivates the optimal weighting subspace method.

Theorem 7.1 *The deterministic ML (Det-ML) method has the same asymptotic distribution as the following estimator*

$$\hat{\theta} = arg \min_{\mathbf{A} \in A^d, \mathbf{T}} \| \hat{\mathbf{E}}_S \tilde{\Lambda}^{1/2} - \mathbf{A}\mathbf{T} \|_F^2 = arg \min_{\mathbf{A} \in A} Tr\{\mathbf{P}_A^{\perp} \hat{\mathbf{E}}_S \tilde{\Lambda} \hat{\mathbf{E}}_S^H\} \qquad (7.7)$$

where $\tilde{\Lambda} = \Lambda_S - \sigma^2 \mathbf{I} = \tilde{\Lambda}^{1/2} \tilde{\Lambda}^{H/2}$

A proof to this theorem can be found in [Vib89].

Applying Theorem 7.1 to equation (7.2), the subspace fitting problem may be restated as

$$[\hat{\mathbf{A}}, \hat{\mathbf{T}}] = arg \min_{\mathbf{A},\mathbf{T}} \| \hat{\mathbf{E}}_S \mathbf{W}^{1/2} - \mathbf{A}(\theta)\mathbf{T} \|_F^2 \qquad (7.8)$$

where $\mathbf{W}$ is a positive definite weighting matrix. Referring to equation (7.3), the directions of arrival can consequently be estimated as

$$\hat{\theta} = arg \min_{\theta} Tr\{\mathbf{P}_A^{\perp}(\theta) \hat{\mathbf{E}}_S \mathbf{W} \hat{\mathbf{E}}_S^H\} \qquad (7.9)$$

Forming the variance of the estimation error in terms of the weighting matrix and finding the derivative with respect to the weighting matrix, an optimal weighting can then be found which gives the lowest possible variance of the estimation errors. Such a weighting matrix was derived in [OV91] and given as

$$\mathbf{W}_{opt} = \tilde{\Lambda}^2 \cdot \hat{\Lambda}_S^{-1} = (\hat{\Lambda}_S - \hat{\sigma}^2 \mathbf{I})^2 \cdot \hat{\Lambda}_S^{-1} \qquad (7.10)$$

7.2 Asymptotic Analysis of Subspace Fitting Methods

<u>Cramer-Rao Bound</u>

The Cramer-Rao Bound (CRB) provides a lower bound for the covariance matrix of the estimation error of any unbiased estimate. CRBs were developed in [SN89] for deterministic

signals when either m or N is infinite or both are infinite and summarised into several theorems. Two theorems for the cases when m is finite while N is finite and infinite, respectively, are restated here.

Theorem 7.2 *Let $\hat{\theta}$ be an asymptotically unbiased estimate of the true parameter vector θ_o, the CRB for θ_o is given by*

$$CRB(m,N) = \frac{\sigma^2}{2}\left\{\sum_{t=1}^{N} Re[\mathbf{s}^H(t)\cdot\mathbf{D}^H\cdot\mathbf{P}_A^{\perp}\cdot\mathbf{D}\cdot\mathbf{s}(t)]\right\}^{-1} \tag{7.11}$$

where

$$\mathbf{s}(t) = diag\{\mathbf{s}_1(t),\cdots,\mathbf{s}_d(t)\}$$

$$D = \left[\frac{d}{d\theta_1}\mathbf{a}(\theta_1),\cdots,\frac{d}{d\theta_d}\mathbf{a}(\theta_d)\right] \tag{7.12}$$

Theorem 7.3 *For sufficiently large N, the CRB is given by*

$$CRB(m,\infty) = \frac{\sigma^2}{2N}\{Re[\{\mathbf{D}^H\cdot\mathbf{P}_A^{\perp}\cdot\mathbf{D}\}\odot\mathbf{S}^T]\}^{-1} \tag{7.13}$$

where $\mathbf{S}$ is the source covariance matrix as defined in (2.24).

For the deterministic signals under consideration here, $1+d(N+1)$ parameters are to be estimated from mN data. The ratio of the amount of data to the number of the estimated parameters remains bounded if $m<\infty$, even if $N\rightarrow\infty$; only if m, as well as N, tends to infinity does this ratio increase without bound. This observation suggests that the CRB cannot be achieved by increasing N; the essential requirement for attaining the CRB should be to increase m. This point was discussed more precisely in, e.g. [SN89, SN90].

It is proved in [VO91], however, that the covariance of the asymptotic distribution of the optimal WSF estimates is the same as the asymptotic Cramer-Rao bound for Gaussian source signals. That is, the optimal WSF solution gives the lowest possible estimation error variance of any unbiased estimator.

To investigate the asymptotic properties of the subspace fitting methods, a single criterion function for all methods provides a more convenient means. As shown in [Ott89], the methods choosing **M** as the Hermitian square root of the covariance matrix can be put in a unified fashion as those using the signal subspace matrix as **M** by post-multiplying the signal subspace matrix with a specific weighting matrix. The unified criterion function for all methods within the subspace fitting framework is in the following asymptotic form

$$V(\theta) = Tr\{\mathbf{P}_A(\theta) \cdot \hat{\mathbf{E}}_S \cdot \mathbf{W} \cdot \hat{\mathbf{E}}_S^H\} \tag{7.14}$$

where $\mathbf{W}$ is a $d' \times d'$ weighting matrix. The choice of $\mathbf{W}$ affects the asymptotic properties of the estimate error. The weighted subspace fitting estimate $\hat{\theta}_N$ is given by

$$\hat{\theta} = arg \max_{\theta} V(\theta) \tag{7.15}$$

The weighting matrix $\mathbf{W}$ in (7.14) is restricted to be Hermitian and positive definite. It is shown that the criterion function, $V_N(\theta)$, converges with probability one (w.p.1), uniformly in θ to the limit function $\overline{V}(\theta)$

$$\overline{V}(\theta) = Tr\{\mathbf{P}_A(\theta) \cdot \mathbf{E}_S \cdot \mathbf{W} \cdot \mathbf{E}_S^H\} \tag{7.16}$$

as N tends to infinity.

7.3 Implementation of Subspace Fitting Methods

The subspace fitting methods involve multidimensional searching procedures which require efficient algorithms for implementation. The algorithm to be used for this purpose is the Modified Variable Projection (MVP) method of Kaufman [Kau75], which is a slightly modified version of the Gauss-Newton method of Golub and Pereyra [GP73].

The non-linear least squares problem involved in the subspace fitting methods can be described as follows

$$\hat{\theta} = arg \min_{\theta} V(\theta) \tag{7.17}$$

$$V(\theta) = Tr\{\mathbf{P}_A^{\perp}(\theta) \cdot \mathbf{M} \cdot \mathbf{M}^H\} = ||\mathbf{P}_A^{\perp}(\theta) \cdot \mathbf{M}||_F^2 \tag{7.18}$$

where $\mathbf{M} = \hat{\mathbf{E}}_S \cdot \mathbf{W}^{1/2}$ is used as a general matrix to represent the observation so as to simplify the notations. By using the damped Newton method [GMW81, DS83], which is thought as the most efficient and globally convergent optimisation method for unconstrained smooth criteria, the searching procedures are formulated iteratively and the estimate is calculated as

$$\theta_{k+1} = \theta_k + \mu_k \cdot \mathbf{H}^{-1} \cdot V' \tag{7.19}$$

where μ_k is a step length, $\mathbf{H}$ and V' represent the Hessian matrix and the gradient of the criterion function, respectively. The Hessian and the gradient need to be evaluated at each iteration and are given as

$$\mathbf{H} = 2Re\left\{(\mathbf{D}^H\mathbf{P}_A^{\perp}\mathbf{D}) \odot (\mathbf{A}^{+}\mathbf{M}\mathbf{M}^H\mathbf{A}^{+H})^T\right\} \tag{7.20}$$

$$V' = -2Re\{diag(\mathbf{A}^{+}\mathbf{M}\mathbf{M}^H\mathbf{P}_A^{\perp}\mathbf{D})\} \tag{7.21}$$

To start the iterations given in equation (7.19), an initial value of the direction estimate is required. In the following two subsections, the initialisation of the iterations and the iteration itself will be discussed, respectively.

7.3.1 Initialisation

The initial estimates of the directions of arrival are crucial to the global convergence of the final estimates. Although several direction estimation algorithms can be employed to give the initial estimates, such as the ESPRIT technique or even the IMP algorithm in the previous chapter, a reliable initialisation procedure is still needed to provide good enough initial estimates especially at low signal to noise ratios. Examining the convergence of different initialisation methods is outside the scope of this thesis. Herein, the Alternating Maximisation (AM) technique suggested by Ziskind and Wax [ZW88] for obtaining the initial estimates in their realisation of the ML estimator, the Alternating Projection (AP) algorithm, was applied.

By applying the AM technique, the initial estimates of the DOAs are also given iteratively. The multidimensional maximisation is accomplished in a sequence of procedures maximising a single parameter at each iteration.

The first source direction estimate is assigned the global peak position found in the generalised spectrum given as

$$P(\theta) = \frac{\mathbf{a}^H(\theta) \cdot \mathbf{M} \cdot \mathbf{M}^H \cdot \mathbf{a}(\theta)}{\mathbf{a}^H(\theta) \cdot \mathbf{a}(\theta)} \tag{7.22}$$

which is

$$\hat{\theta}_1 = arg \max_{\theta} P(\theta) \tag{7.23}$$

Given this estimate, the spectrum given in (7.22) is modified by applying a projection matrix, $\mathbf{Q}$, onto the nullspace of the first direction vector, $\mathbf{a}(\hat{\theta}_1)$. And the second source direction estimate is found as

$$\hat{\theta}_2 = arg \max_{\theta} \frac{\mathbf{a}^H(\theta) \cdot \mathbf{Q} \cdot \mathbf{M} \cdot \mathbf{M}^H \cdot \mathbf{Q} \cdot \mathbf{a}(\theta)}{\mathbf{a}^H(\theta) \cdot \mathbf{Q} \cdot \mathbf{a}(\theta)} \tag{7.24}$$

When more sources are present and the initial estimates are required, the projection matrix needs to be modified to be based on all the initial direction estimates and then applied to equation (7.24). The maximum in the modified spectrum is regarded as the initial value of the direction to be estimated.

In the estimation of the initial directions of arrival, the number of sources is necessary, either as prior information or estimated. The philosophy behind the initialisation is rather like that employed in the IMP algorithm, but the refinement of each estimates is not included.

The one-dimensional Newton method is then used to refine these initial estimates which are usually given over a coarse grid.

7.3.2 Iterations

After obtaining the initial estimates, the modified variable projection method is employed to accomplish the iterative searching procedures. To simplify the computations involved in the calculation of the Hessian matrix and the gradient of the criterion function, which needs to be evaluated at each iteration, some mathematical work will be necessary.

By applying the QR-decomposition using the Householder transformation [GV83], the direction vectors (signal array manifold vectors) can be written in multiplicative form of an orthogonal matrix **Q** and a upper triangular matrix **R**

$$\mathbf{A} = \mathbf{Q}_{m\times m} \cdot \mathbf{R}_{m\times d} = [\mathbf{Q}_1, \mathbf{Q}_2]\begin{bmatrix}\mathbf{R}_1 \\ \mathbf{0}\end{bmatrix} \tag{7.25}$$

and **Q** and **R** are partitioned into respective sub-matrices with appropriate dimensions. Therefore, the Moore-Penrose pseudo-inverse of the direction vectors $A(\theta)$, $\mathbf{A}^+$, and its projection matrix, $\mathbf{P}_{\bar{A}}$, are described as

$$\mathbf{A}^+ = \mathbf{R}_1^{-1}\mathbf{Q}_1^H, \qquad \mathbf{P}_{\bar{A}} = \mathbf{Q}_2\mathbf{Q}_2^H \tag{7.26}$$

Introducing several intermediate variables as follows :

$$\Phi = \mathbf{Q}_2^H\mathbf{D}, \qquad \Psi = \mathbf{M}^H\mathbf{Q}_2, \qquad \mathbf{T} = \mathbf{R}_1^{-1}\mathbf{Q}_1^H\mathbf{M} \tag{7.27}$$

the criterion function, its Hessian matrix and gradient, referring to (7.18), (7.20), and (7.21), are derived as

$$V = Tr\{\Psi\Psi^H\} \tag{7.28}$$

$$V' = Re\{diag(\mathbf{T}\Psi\Phi)\} \tag{7.29}$$

$$\mathbf{H} = Re\{(\Phi^H\Phi) \odot (\mathbf{T}\mathbf{T}^H)^T\} \tag{7.30}$$

These three expressions rather than the original ones are substituted back into (7.19) for the iterative calculation of the direction estimates.

The termination of the iteration is determined by three criteria :

1) if the given maximum number of iterations is exceeded,
2) if no more improvement along the searching direction is possible,
3) if local minima are found.

In the computer simulations to be shown in following sections, the maximum number of iterations is assigned as 10; the iteration number is initialised as 0 and incremented at each iteration. When the iteration number equals the maximum number of iterations, the procedure terminates and also brings out a flag to show the status of the termination.

At each iteration, the criterion function is evaluated to check the improvement of the search. The current value of this function is compared with the minimum value of the function retained as a variable and a decision is made whether to refresh this variable. If the current value is smaller, then it is assigned to the variable and the current estimates of the source directions are taken as the latest direction estimates; otherwise previous values for the criterion function and the direction estimates are kept.

One important parameter in the iterations is the step length, μ, in equation (7.19). This controls the convergence speed and also determines the possibility of convergence. A bigger value of μ gives a quick search but allows the missing of possible local minima; on the other hand, a smaller value slows down the searching speed dramatically. In the simulations, μ is assigned as unity at the beginning of each iteration and then half of the previous value is taken to accomplish the search along the searching direction. This procedure is continued until the value of μ is less than 0.0001 when it is accepted as that no improvement (or no "sufficient decrease") is possible for the current search direction. This also leads to an unsuccessful termination of the procedure and the status of the termination is again brought out for later processing of the simulation results.

The norm of the multiplication of the inverse of the Hessian matrix and the gradient of the criterion function is evaluated at each iteration and compared to a pre-defined tolerance. If it is smaller than this tolerance, the estimates of the source directions are considered as successful direction estimates. Only these estimates will be used in later processing for the statistics.

7.4 Computer Simulations

Based on the algorithm implementation proposal given in the previous section, computer simulations have been carried out for the ML and WSF approaches. The simulation set-up is similar to that in simulations in previous chapters. Also, the statistics used to show the performance are the same as those given before, i.e., the probability of resolution, biases of angular estimates and their standard deviations. Simulations to be presented in this section are in two categories : 1) signal to noise ratio of the sources is varied in the simulations, and 2) angular separation between the two sources is changed. 500 trials were run for the statistics with 100 snapshots taken in each trial. A 10 element uniform linear array was used with half wavelength spacing. The conventional resolution of such an array was about 11.5°.

7.4.1 Results as Functions of Signal to Noise Ratio

To evaluate the performance of ML and WSF under different signal to noise ratios, the angular separation is fixed at 2°. Results are shown in figures 7.1 to 7.3 for three cases when the correlation factor between the two sources is assigned as 0 (uncorrelated), 0.95, and 1 (coherent) respectively.

The uncorrelated case is the case when all the high resolution methods give good direction estimates at reasonable signal to noise ratio and angular separation. Both the ML estimator and the optimal WSF estimator show excellent performance, as depicted in figure 7.1, including higher resolving abilities at low signal to noise ratio and low and smooth biases and standard deviations. The statistics from ML and WSF are extremely close except at 0 dB signal to noise ratio where the ML methods performs a little better.

In highly correlated source case, the optimal WSF method outperforms the ML method in the sense of separating the two sources at low signal to noise ratios. Large differences exist between the biases and standard deviations given for ML and WSF at signal to noise ratios less than 10 dB. The biases resulting from the WSF method tend to be even outside the true source directions, but those from the ML method are both smaller than the true values of source directions. For signal to noise ratios at or above 10 dB, the two methods give very similar performance in every statistic shown in the figures.

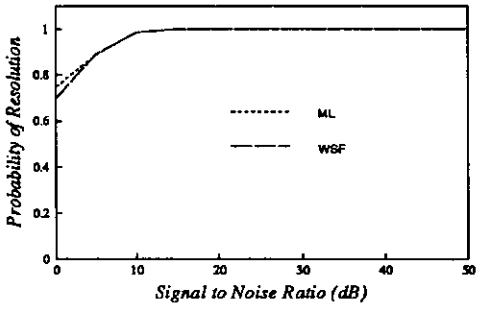

(a)

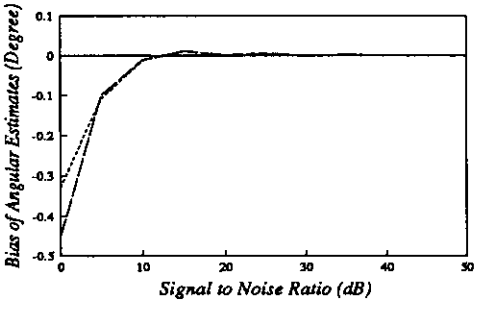

(b)

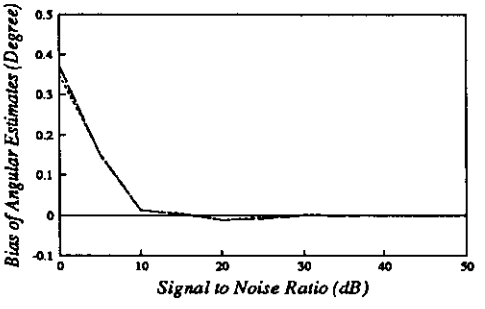

(c)

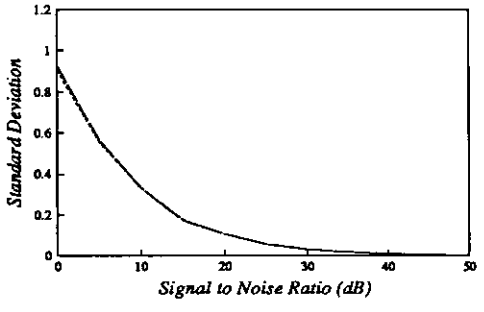

(d)

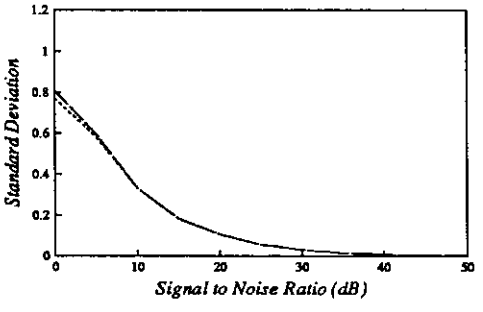

(e)

Figure 7.1 *Statistics of ML and WSF as functions of signal to noise ratio when the angular separation is 2° and the correlation factor is* $\rho = 0.0$

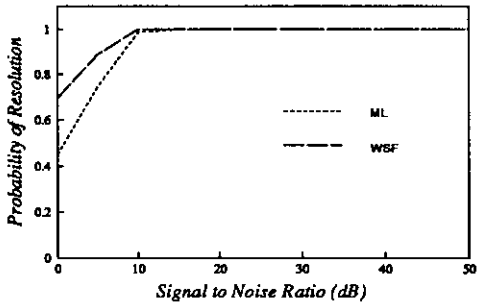

(a)

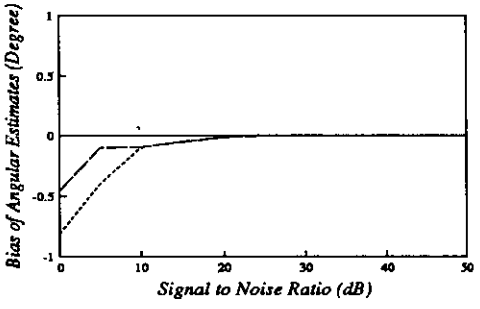

(b)

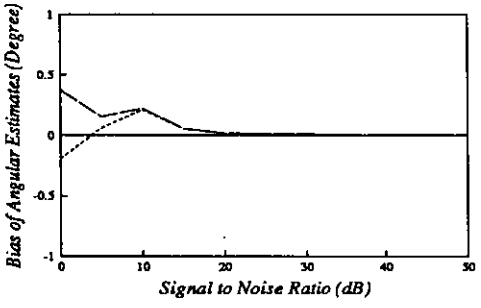

(c)

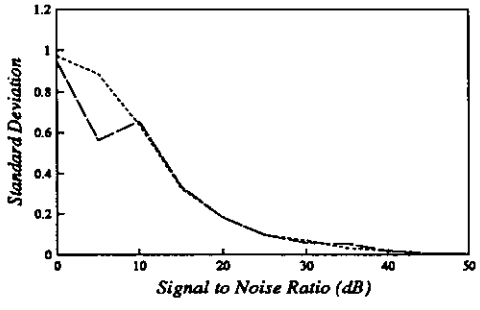

(d)

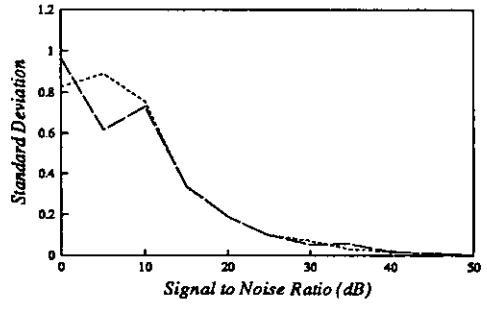

(e)

Figure 7.2 *Statistics of ML and WSF as functions of signal to noise ratio when the angular separation is 2° and the correlation factor* $\rho = 0.95$

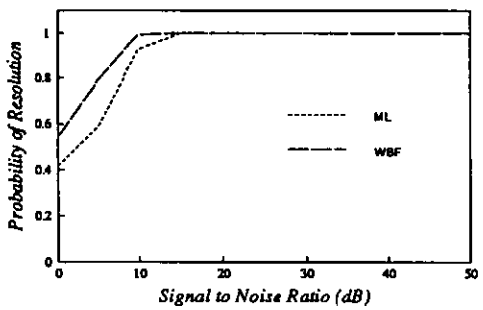

(a)

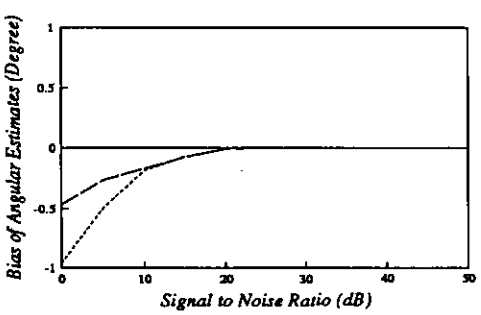

(b)

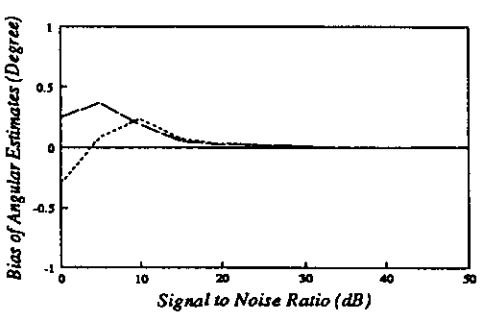

(c)

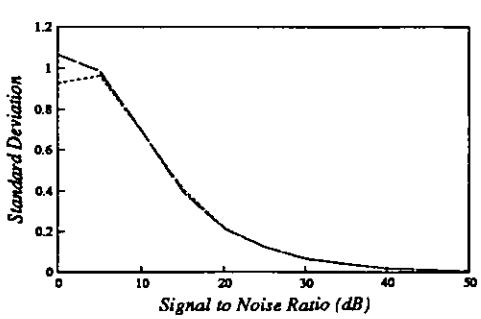

(d)

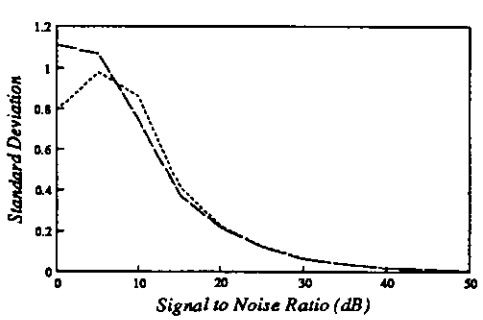

(e)

Figure 7.3 *Statistics of ML and WSF as functions of signal to noise ratio when the angular separation is 2° and the correlation factor is* $\rho = 1.0$

Figure 7.3 shows the coherent case. The possibility of resolving the two sources at lower signal to noise ratios is less than that in the highly correlated case. The performance degradation in the biases is not significant while that in the standard deviation is more noticeable.

7.4.2 Results as Functions of Angular Separation

Varying the angular separation between the two sources, the source correlation was changed. Uncorrelated signals, signals with 0.95 correlation factor, and fully correlated (coherent) signals were used respectively, and correspondingly, the results are illustrated in figure 7.4 through figure 7.6.

In figure 7.4, where the results for uncorrelated signals are shown, both approaches depict high resolution abilities even at the angular separation as small as 1°. What is noticeable for this case is that ML and WSF give almost equivalent performance. The biases of both sources are very small as are the standard deviations which, however, do not tend to approach the minimum level (zero) as the angular separation increases.

When the correlation between the two sources gets stronger, the probabilities of resolution of both ML and WSF are expected to degrade. Statistics of these two approaches are demonstrated in figure 7.5 for the case of a correlation factor of 0.95. It can be seen that both methods lose resolving ability at small angular separations, mainly at the separation of 1°. Biases of angular estimates of both sources get bigger than those in the uncorrelated case, while the bias for source 1 (the one assumed at the normal direction of the array) is slightly larger than that for source 2 (the source whose position is moved in the simulations). At the separation of 1°, although the bias given by ML is a bit larger for source 1, the correspondent standard deviation is relatively lower than that given by WSF; for source 2, a big difference in biases is shown between ML and WSF while a pattern is given in the standard deviation similar to that for source 1. The standard deviations remain stable at about 0.1° no matter how big the angular separation gets.

Figure 7.6 shows the coherent case. Compared to that given in figure 7.5(a), the ability to resolve two closely spaced sources degrades again, but only slightly. The possibility of higher resolution is demonstrated by WSF at angular separation 1° and 2°. Biases given by WSF

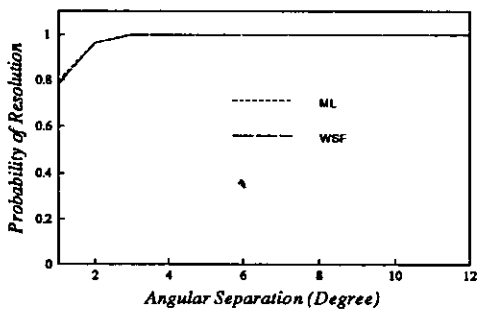

(a)

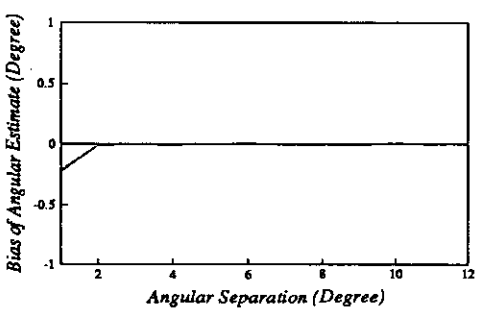

(b)

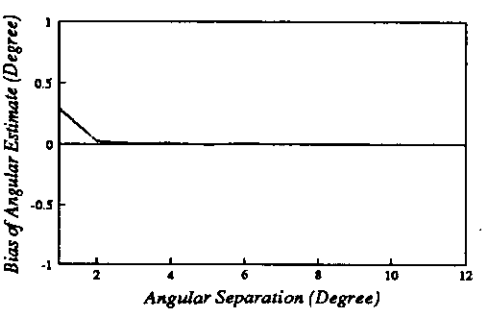

(c)

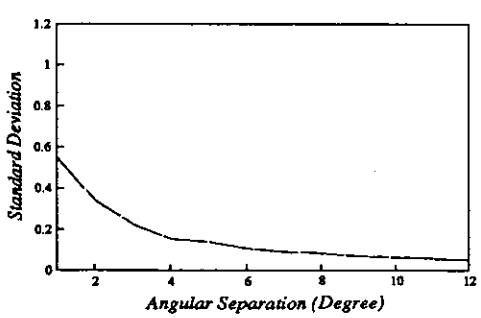

(d)

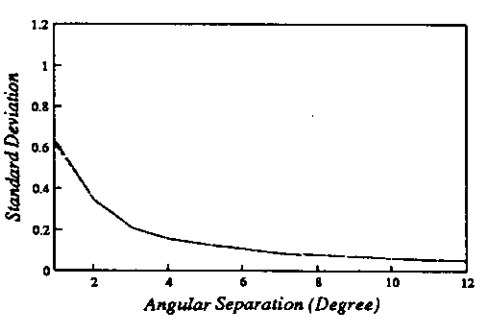

(e)

Figure 7.4 *Statistics of ML and WSF as functions of angular separation when the signal to noise ratio is 10 dB and the correlation factor is* $\rho = 0.0$

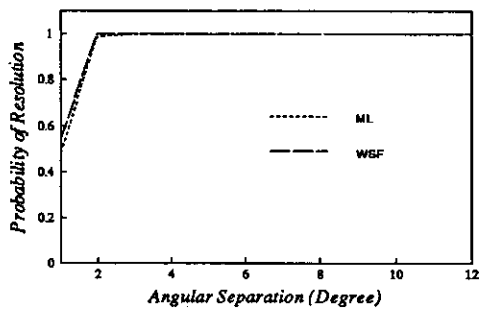

(a)

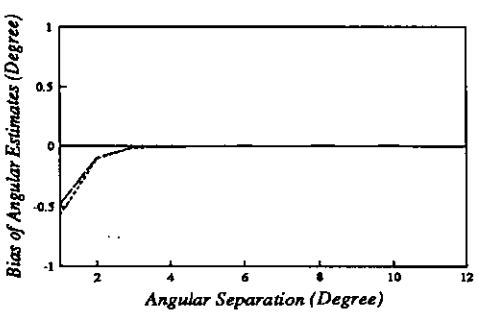

(b)

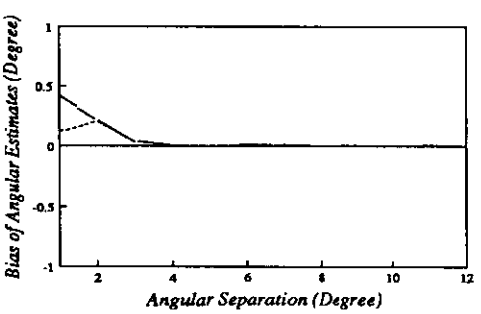

(c)

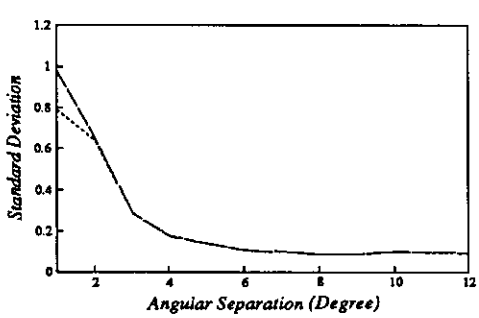

(d)

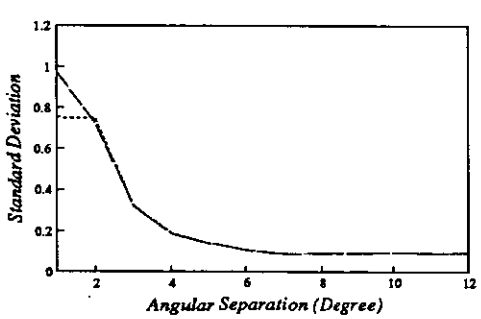

(e)

Figure 7.5 *Statistics of ML and WSF as functions of angular separation when the signal to noise ratio is 10 dB and the correlation factor* $\rho = 0.95$

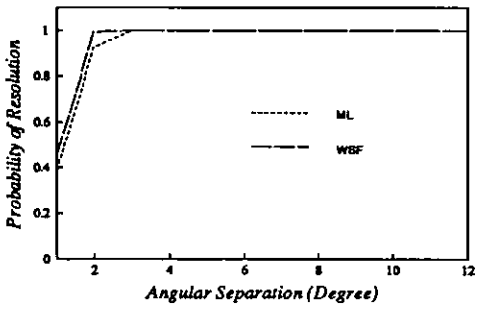

(a)

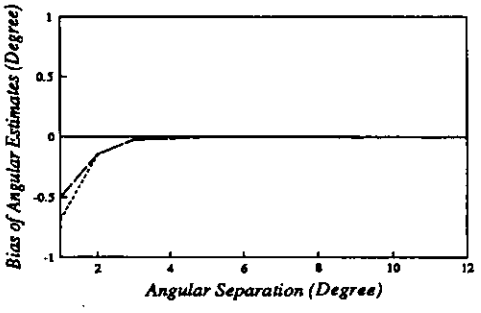

(b)

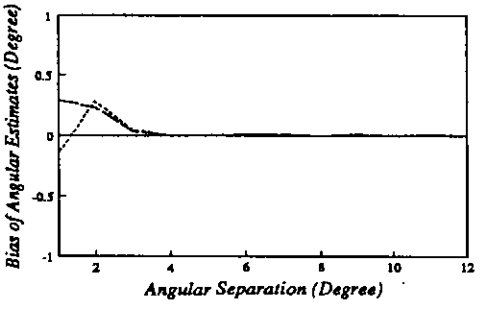

(c)

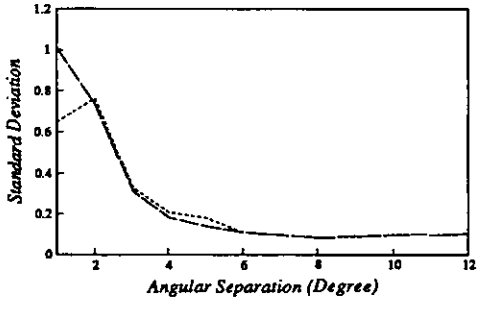

(d)

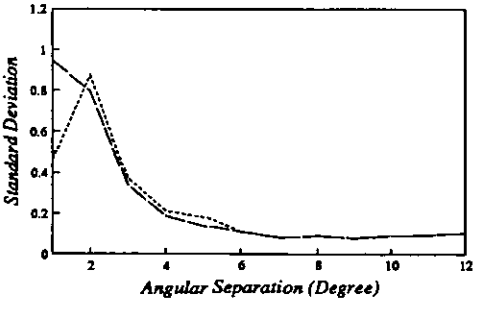

(e)

Figure 7.6 *Statistics of ML and WSF of functions of angular separation when the signal to noise ratio is 10 dB and the correlation factor* $\rho = 1.0$

are narrowly smaller than those given by ML at small angular separations except for the second source which shows lower bias for ML at separation 1°. Concerning the standard deviation, ML demonstrates lower standard deviation at the smallest angular separation whilst at other separations smaller than 6°, WSF performs better. For all other separations, both methods give almost identical results. Like the two previous cases, standard deviations do not approach zero although the angular estimates tend to be unbiased at bigger angular separations.

7.4.3 More Results of Functions of Signal to Noise Ratio

Since the performance given by ML and WSF is superior to those algorithms which have been discussed and analysed in previous chapters, under the same set-up of parameters these two methods do not show much change in the given statistics and the predicted performance advantages over other high resolution methods have not been shown significantly. Since it is interesting to investigate the behaviour of these two methods under "bad" conditions, more computer simulations have been carried out and the processing results will be presented in this and the following subsections.

To observe the performance of ML and WSF when the signal to noise ratio changes, the angular separation between the two sources is reduced to 1°, while all other parameters are given as the same as those in section 7.4.1. Results are shown in figure 7.7 to figure 7.9 with correlation factor being 0, 0.95, and 1.0 respectively. Comparing the plots in these three figures with those in figures 7.1 to 7.3, the performance degradation can be easily seen. What is unchanged is that the performances of ML and WSF are still very similar in the correlated case and differences exist in both biases and standard deviations for highly and fully correlated cases.

The performance degradation mainly lies in the low signal to noise ratio region. The performance difference is around 10 db equivalent in the signal to noise ratio for all the three cases. And relative performance of ML and WSF is similar to that in the 2° case. In the highly and fully correlated source cases, source 1 gives smooth statistics while source 2 shows more fluctuations at low signal to noise ratios. At the signal to noise ratios where the probability of resolution is unity, both ML and WSF demonstrate the tendency to give unbiased estimates and minimum standard deviations as the signal to noise ratio tends to infinity.

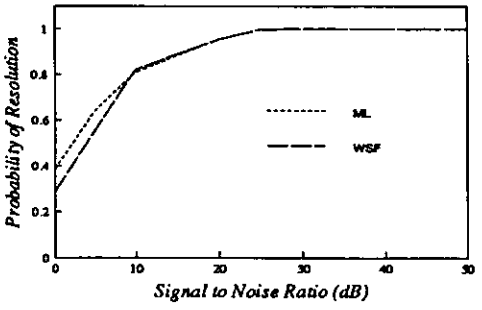

(a)

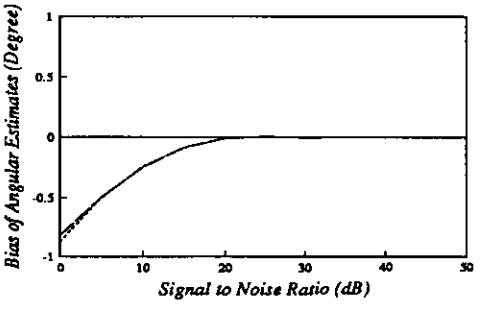

(b)

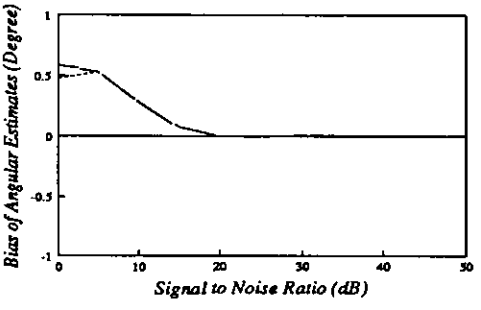

(c)

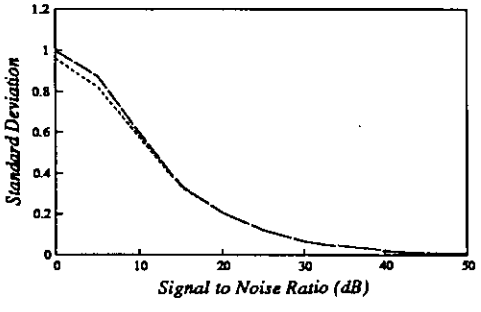

(d)

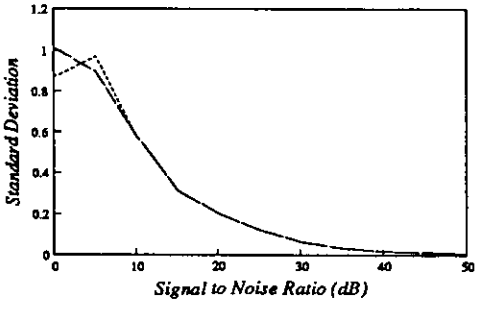

(e)

Figure 7.7 *Statistics of ML and WSF as functions of signal to noise ratio when the angular separation is 1° and two sources are uncorrelated* ($\rho = 0.0$)

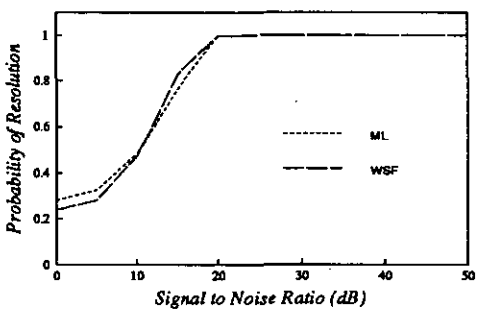

(a)

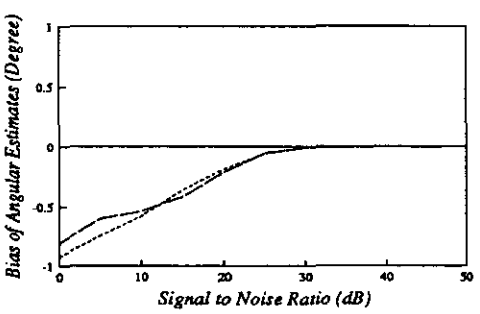

(b)

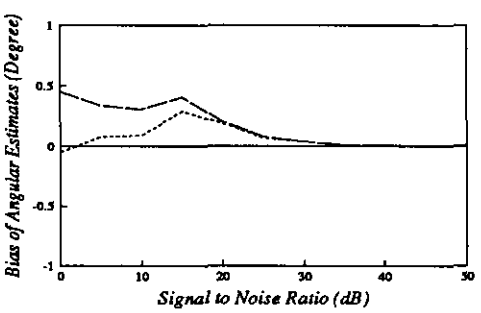

(c)

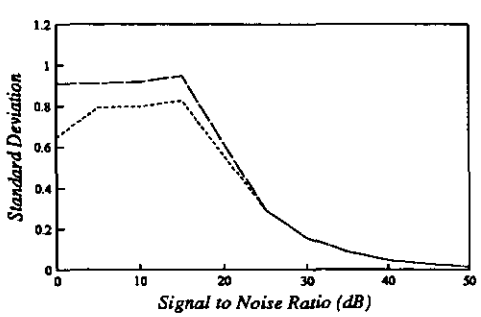

(d)

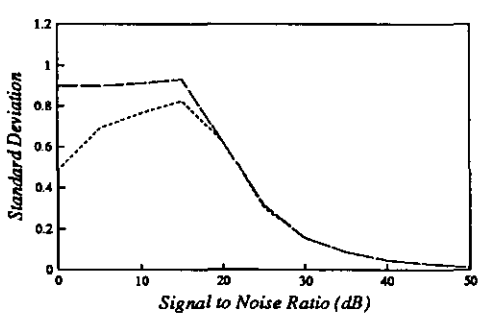

(e)

Figure 7.8 *Statistics of ML and WSF as functions of signal to noise ratio when the angular separation is 1° and the correlation factor is* $\rho = 0.95$

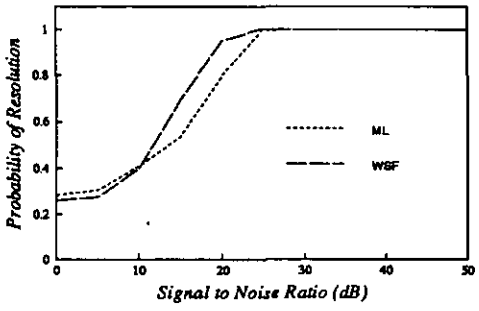

(a)

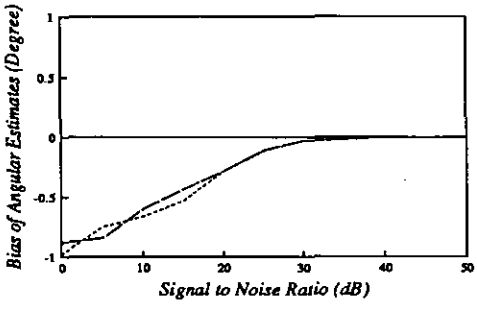

(b)

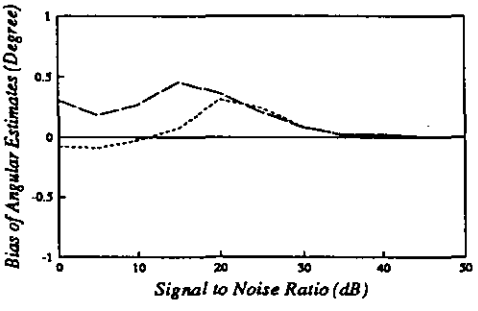

(c)

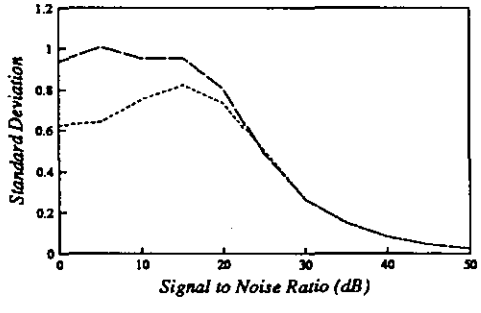

(d)

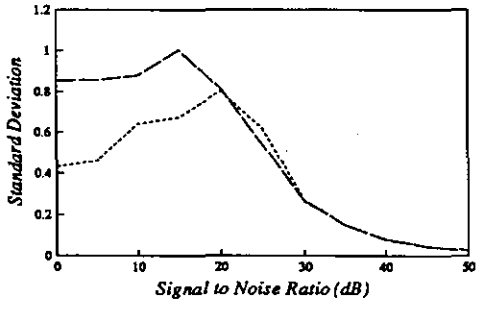

(e)

Figure 7.9 *Statistics of ML and WSF as function of signal to noise ratio when the angular separation is 1° and two are fully correlated* $\rho = 1$

7.4.4 More Results as Functions of Angular Separation

The results to be shown in this subsection are obtained as functions of angular separation when the fixed signal to noise ratio is assigned as 5 dB and 0 dB, respectively. The same statistics are tested and presented in figures 7.10 to 7.15.

Figure 7.10 gives the statistics of ML and WSF when the signal to noise ratio is 5 dB and the two sources are uncorrelated. Compared with the corresponding plots in figure 7.4, the performance degradation which is mainly in the standard deviation can be seen. The thresholds of resolution remain the same while the possibility of resolving the two targets is lower in the small angular separation region. Biases for both sources are large in the situations when the angular separation is small, but tend to be comparative with those in figure 7.4 at and above 3°. In contrast, the standard deviations are higher than those in figure 7.4 within the whole DOA range which has been examined.

The results for highly correlated sources are shown in figure 7.11. The degradation of performance caused by the correlation between the two sources is similar to that in the 10 dB signal to noise ratio case. More fluctuations in the biases are revealed in the large angular separation case, and in the segment of small separations source 1 depicts larger biases for both ML and WSF while source 2 shows smaller but non-smooth statistics. These two different types of biases at the smaller separation result, however, in similar standard deviations. For the larger separation part, the standard deviations are smooth and tend to increase slightly as the angular separation becomes large.

Although the correlation factor for the results shown in figure 7.12 is given as one, i.e., fully correlated signals, the actual generated signals are extremely highly correlated rather then fully correlated in the finite sample cases in the strict sense. The performance degradation resulting from this increase in the correlation is visible in all three statistics given in figure 7.12. Compared to the plots in figure 7.11, no severe degradation of performance is observed. The abilities to solve highly correlated signals for both the ML and WSF methods are evidenced in these simulation results.

To investigate the performance of these two methods in low signal to noise situations, the simulations have been repeated when the signal to noise ratio is 0 dB while other conditions remain the same. Again, three cases were considered when the correlation between the two sources is changed.

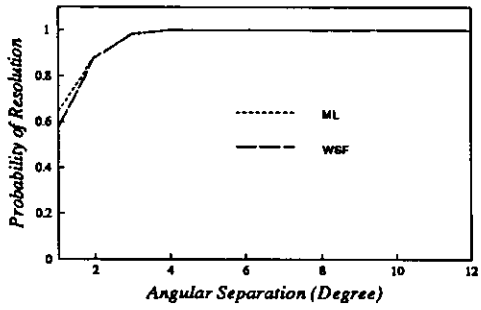

(a)

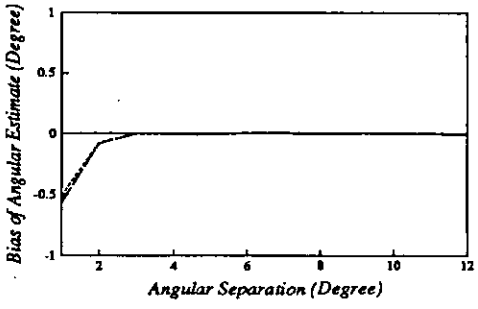

(b)

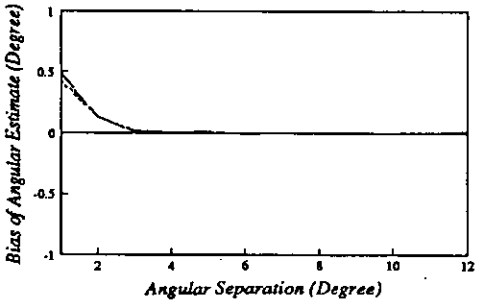

(c)

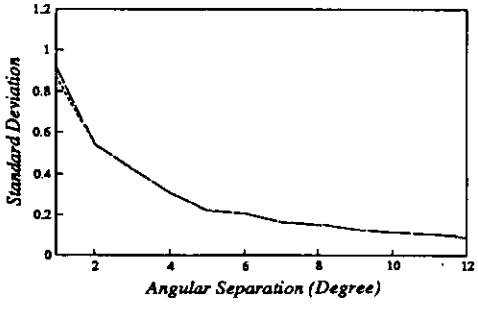

(d)

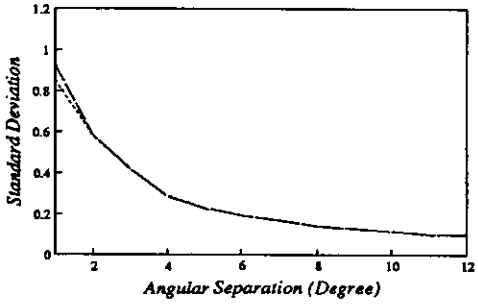

(e)

Figure 7.10 *Statistics of ML and WSF as functions of angular separation when the signal to noise ratio is 5 dB and the correlation factor is* $\rho = 0.0$

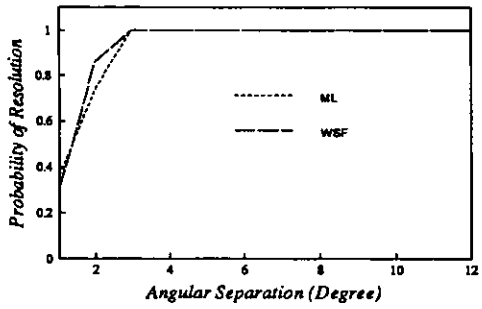

(a)

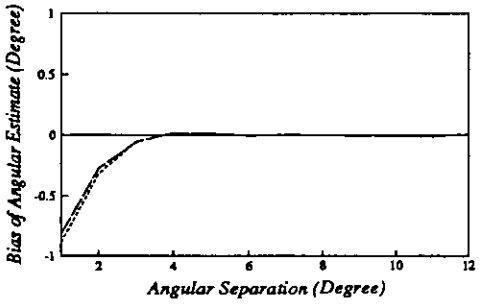

(b)

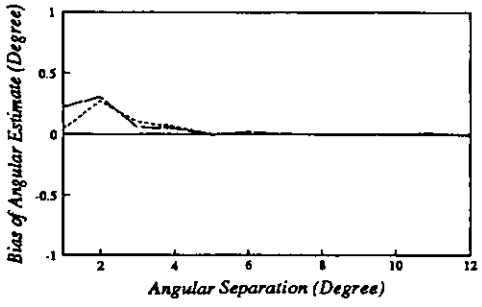

(c)

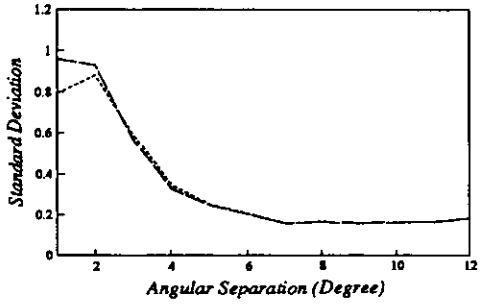

(d)

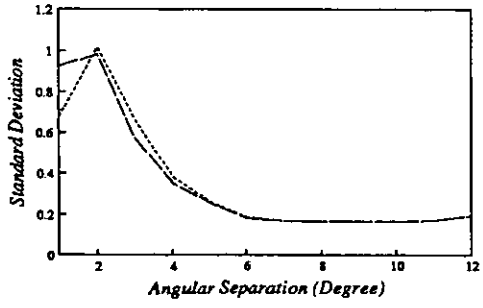

(e)

Figure 7.11 *Statistics of ML and WSF as functions of angular separation when the signal to noise ratio is 5 dB and the correlation factor is* $\rho = 0.95$

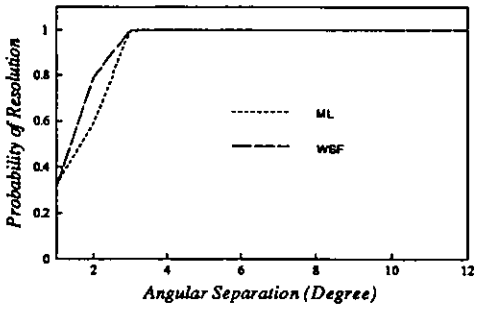

(a)

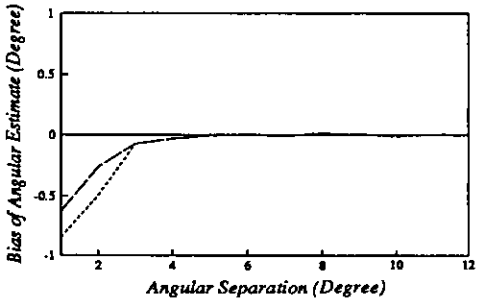

(b)

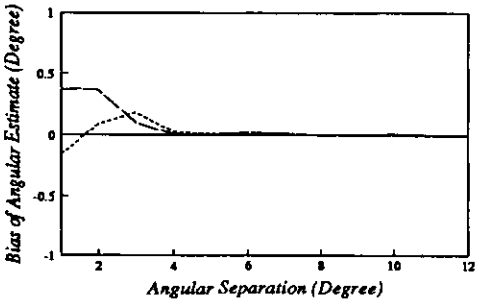

(c)

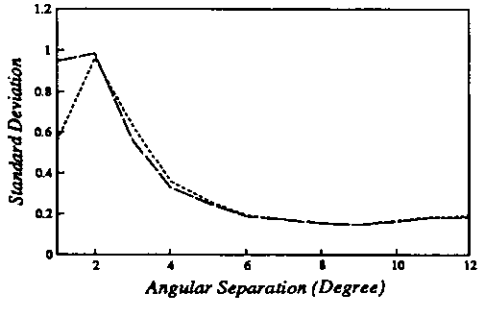

(d)

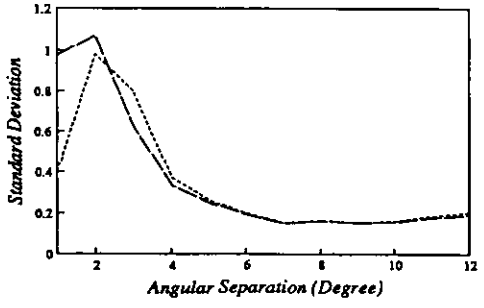

(e)

Figure 7.12 *Statistics of ML and WSF as functions of angular separation when the signal to noise ratio is 5 dB and the correlation factor is* $\rho = 1.0$

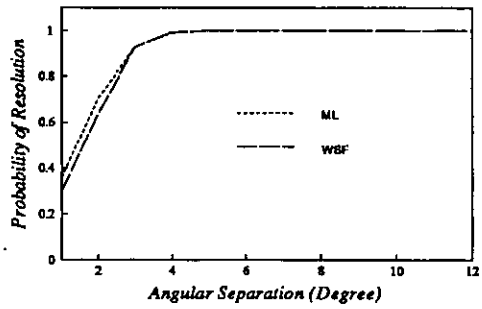

(a)

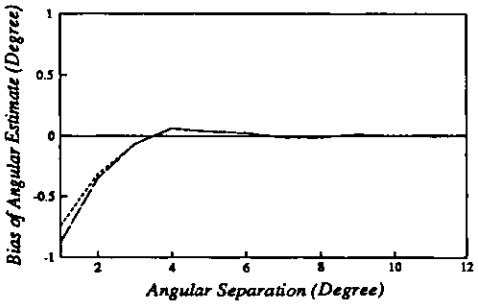

(b)

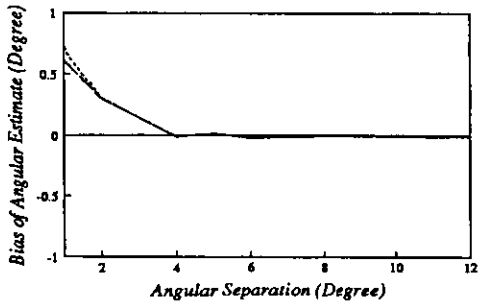

(c)

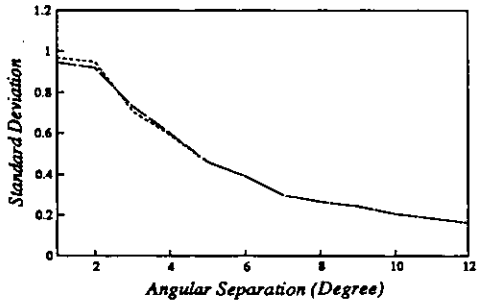

(d)

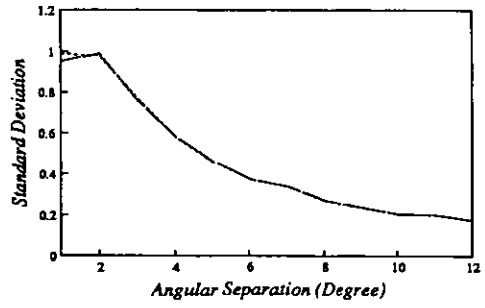

(e)

Figure 7.13 *Statistics of ML and WSF as functions of angular separation when the signal to noise ratio is 0 dB and the correlation factor is* $\rho = 0.0$

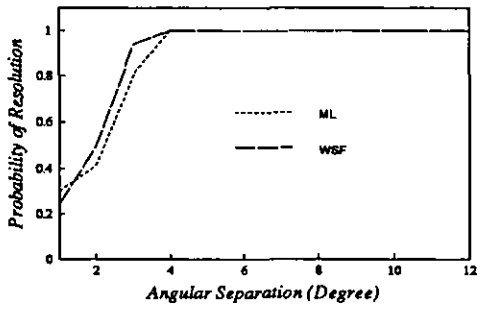

(a)

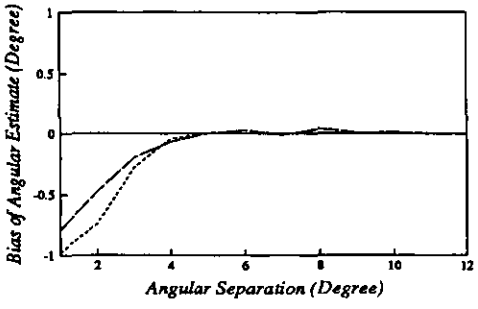

(b)

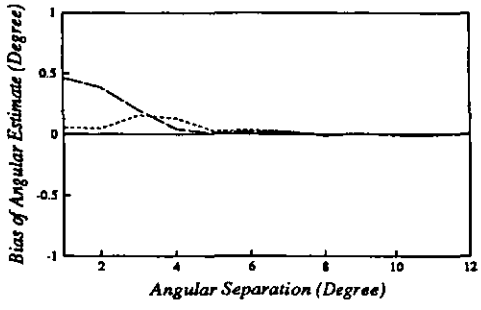

(c)

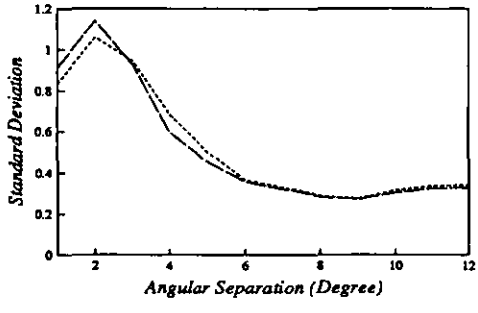

(d)

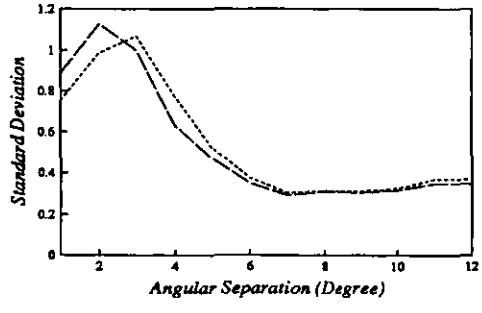

(e)

Figure 7.14 *Statistics of ML and WSF as functions of angular separation when the signal to noise ratio is 0 dB and the correlation factor is* $\rho = 0.95$

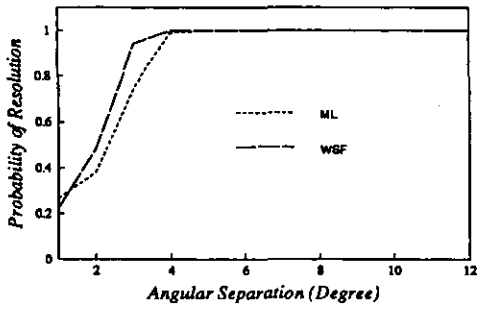

(a)

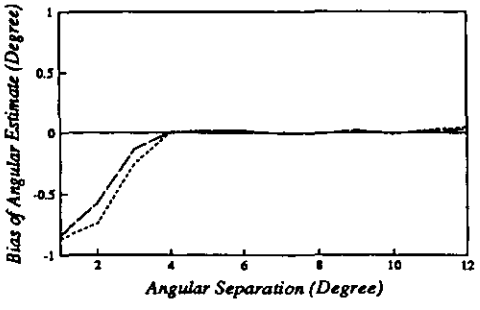

(b)

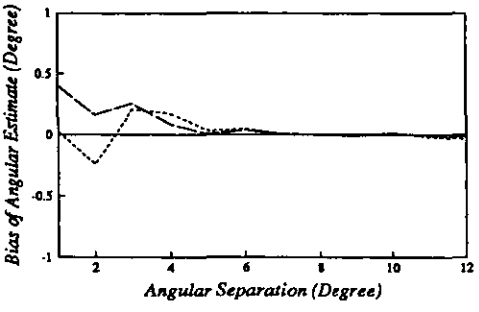

(c)

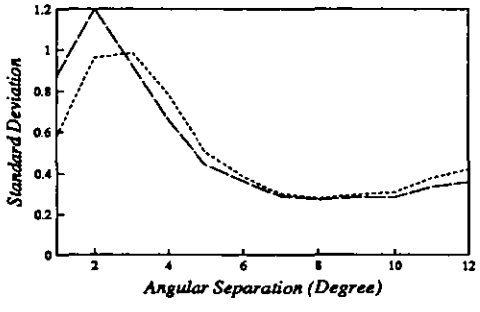

(d)

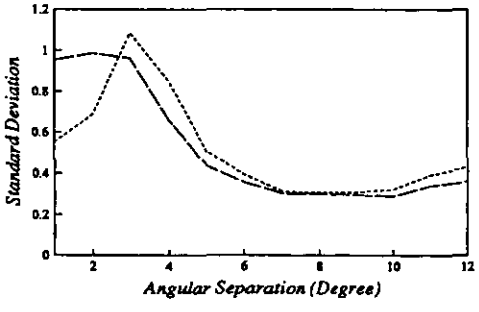

(e)

Figure 7.15 *Statistics of ML and WSF as functions of angular separation when the signal to noise ratio is 0 dB and the correlation factor is* $\rho = 1.0$

The effects of the reduction in the signal to noise ratio can be seen in all three statistics illustrated. Probabilities of resolution decrease in the smaller angular separation region but show full abilities to resolve the two sources when they are placed at a larger distance from each other. However, biases exist even when the source separation is very large. Unlike the beamforming methods which usually tend to give estimates of directions between the true directions, the biases given by ML and WSF show that these two methods are more likely to give estimates outside the true directions, especially in the uncorrelated cases, no matter what the signal to noise ratio is. The standard deviations shown in figure 7.13(d) and figure 7.13(e) are much higher that those in figure 7.4 and figure 7.10 although they decrease as the angular separation increases.

Figures 7.14 and 7.15 show the behaviours of ML and WSF at the low signal to noise ratio and high correlation cases. Performance degradation is obvious.

7.5 Discussion

The performance of the Maximum Likelihood (ML) estimator and the optimal Weighted Subspace Fitting (WSF) estimator in the application of direction estimation has been analysed in this chapter, mainly by means of computer simulations. The large number of results presented herein demonstrate the behaviour of the two methods in different scenarios, as functions of signal to noise ratio and angular separation between the two sources, respectively. And under each circumstance, more results than those in previous chapters were obtained for the examination of these methods under "bad" conditions. The abilities of these two methods to resolve two closely positioned sources with low signal to noise ratios are evident from the results presented. And also the estimates have good statistics in the sense of biases and standard deviations of the direction estimates. Although it is claimed by the original authors that the optimal WSF outperforms the ML method asymptotically, the difference in the statistics shown here is not significant, sometimes even better results were obtained from the ML estimator. Whether this is because the "asymptotic" conditions are not met or any other reason, these two methods give roughly identical performance in most situations.

CHAPTER 8

DISCUSSION OF COMPUTER SIMULATION RESULTS

Through chapter 4 to chapter 7, simulation results have been presented for several high resolution direction estimation algorithms. These algorithms represent different philosophies in dealing with the direction estimation problem and also demonstrate the evolution of direction estimation algorithms. The methods which have been simulated and discussed in the previous four chapters include

* the Maximum Entropy Method (MEM) of Burg and the Minimum Variance Method (MVM) of Capon (or Capon's Maximum Likelihood Method) in the class of adaptive techniques

* MUltiple SIgnal Characteristics (MUSIC) of Schmidt and Bienvenu and Kopp, and Minimum Norm Method (MNM) of Reddi and Kumaresan and Tuft, representing the signal subspace methods

* root versions of the above four methods, promoted by Barabell, which explore the roots of associated polynomials rather than searching the peak positions in the resulting spectra

* Estimation of Signal Parameters via Rotation Invariance Techniques (ESPRIT) of Roy, Paulraj, and Kailath et al, which reduces the computation load of the MUSIC algorithm by constraining the array in use and, at the same time, retains most of the features of MUSIC

* Incremenatal Multiple Parameter (IMP) estimation method, in the class of decomposition methods, of Clarke, which re-processes the received data by applying projections and provides high resolution ability even for fully correlated sources

* deterministic Maximum Likelihood (ML) method which is able to solve for coherent sources at the cost of heavy computation due to the multidimensional searching involved

* optimal Weighted Subspace Fitting (WSF) method of Viberg and Ottersten which is deduced to give the lowest possible variance of estimation errors with reduced computations due to the low rank representation of the observed data

In the simulations, two scenarios were mainly considered : the performance of the algorithms at different signal to noise ratios when the angular separation between the two sources was fixed, and that under different angular separations when the signal to noise ratio was unchanged. For each scenario, various correlation factors were applied to test the algorithm abilities to resolve sources with different correlations. The inability of the signal subspace methods and the ESPRIT techniques to handle coherent sources was known, so the simulations concentrated on the uncorrelated and the weakly correlated source cases while sources with correlation factor 0.95 were also examined to show the algorithm performance in the highly correlated situation. In order to demonstrate the performance advantage of the IMP algorithm in the highly correlated case, besides the correlated case, two large correlation factors were assigned to the sources in chapter 6. In chapter 7 where the ML and optimal WSF were simulated, the correlation factor between the two sources was given the same values as that in chapter 6 but more values were assigned to the signal to noise ratios and the angular separations to study the performance of these two "superior" resolution algorithms.

In chapter 4, the four methods which fall in the signal subspace methods and their root versions were examined. It was shown there that the MUSIC technique gives the lowest standard deviations in both versions as functions of signal to noise ratio and shows the lowest standard deviations together with the MVM as functions of angular separations. The MUSIC methods, both spectral and root versions, were chosen as "models" to be compared with the ESPRIT algorithm in chapter 5 and the IMP technique in chapter 6.

For the ESPRIT algorithm, multiple choices of subarray displacement vector are possible in the uniform linear array case. However, only the one with the maximum over lapping

subarrays was tested in the simulations here. Bigger displacement between the two subarrays are in favour when the sources are known to cluster, by giving smaller direction estimation errors.

The asymptotic properties of the ESPRIT method are very similar to those of the MUSIC methods. The probability of resolution provided by the ESPRIT method is near to that of the root MUSIC method, both being higher than that of the spectral MUSIC method, although the correspondent biases and standard deviations are also higher before the spectral MUSIC begins to resolve the two sources. The computation time of the simulation for these three methods was not compared quantitatively, but it has been noticed that the ESPRIT technique consumed much less time due to the lack of the searching procedure inherent in the spectral MUSIC method. If the output spectrum of the array is not needed, which is generally the case in the direction estimation problem, ESPRIT is a good substitute for the MUSIC method by providing similar performance with less computation time.

The IMP algorithm provides a different philosophy to the direction estimation problem. The re-processing of the observed data does provide high resolution and the ability to handle coherent sources, but the computation burden involved in the processing makes it prohibitive. Remedies have been suggested, such as searching spectrum on a coarse grid and then narrowing the field of search and refining the estimates, or applying the quadratic fitting of the rough estimates of three points at and around the peak position to give a more accurate estimate. This, however, does not help much especially in the high order case (more sources are present). Probably this method will find applications in some areas where the processing speed is not a important factor. But it is not promising to meet the need in most cases because high processing speed is generally required and this technique has less chance of real-time implementation.

Comparatively, the optimal WSF method is more appealing although the multidimensional search procedure involved makes it look less so. The low-rank representation of the data in the optimisation saves much computation, compared to the ML method. Also the development in computers and electronics allows the complicated computations in the multidimensional processing to be accomplished at very high speed. By means of "modern" parallel processing techniques and special-purpose chips, the complexity of the computations can be more easily realised than the search procedure in estimating the spectra which seems much easier in appearance.

The excellent performance of the optimal WSF algorithm shown in chapter 7 is worth the effort in implementing the inherent complicated computations. Under the same parameter set-ups as those in chapter 4 to chapter 6, the performance advantages are readily seen from the plots shown figures 7.7 to 7.6. To verify these merits, the optimal WSF method and the ML method have gone through tests under bad conditions. The two sources were placed only 1° apart to repeat the simulations as functions of signal to noise ratios and the signal to noise ratios were set to 5 dB and 0 dB respectively to undergo the performance analysis as functions of angular separations. Performance degraded in the worse situations but still gave reasonably good results.

Besides the comparison of performance of various algorithms, the simulation results shown in the previous chapters draw clear pictures of each of these algorithms under the conditions given in the simulations. Although the factors taken into account in the simulations are very limited, the results provide a good guide for the analysis of the practical measurements which will be presented in the following chapter.

CHAPTER 9

PRACTICAL MEASUREMENTS WITH DIFFERENT ALGORITHMS

In previous chapters, computer simulations of algorithms and methods in several different classes have been carried out and discussed. Results strongly supported the theoretical analyses and provided insight into understanding of algorithm performance. However, the behaviour of these algorithms or methods in practical environments is still unknown. Although they are expected to depict similar results as anticipated from the theoretical discussion, it is necessary to apply these algorithms to practical measurements when their performance in practical situations is considered. This chapter will present some off-line processing results of data collected from a sonar system which was available within the research group.

The measurement system used for experiments in this chapter was an air acoustic sonar system which had been built by the Sonar Research Group at Loughborough University of Technology (LUT). This system consists of a passive receiving array and a transputer-board based signal acquisition and analysis system. Either emitters or targets were employed to transmit or reflect signals at a distance. The array responses to these signals were captured and sent to the signal acquisition and analysis system. The received signals were saved in 12 bit digital form on the memory board. These data were then accessed by a transputer board which could process data in the OCCAM language or save data on floppy disks via an IBM-286 host computer for off-line processing. The results presented in this chapter were obtained by using the software package MATLAB (Matrix Laboratory).

Two scenarios were examined : first, the acoustic array worked in the passive mode and two emitters were placed at a distance in front of the array. Two categories of signals were applied in this working mode, one was the case when two emitters worked at different frequencies

and the other at the same frequency. Secondly, two targets were placed in front of the array to reflect signals transmitted from a separate sensor which was placed on the top of the receiving array.

9.1 Description of the Measurement System

9.1.1 Array

The array used for experiments was an echelon array of two layers with eight transducers on the top and seven on the bottom, as shown in figure 9.1. Parameters of the transducers and the array are also depicted in figure 9.1.

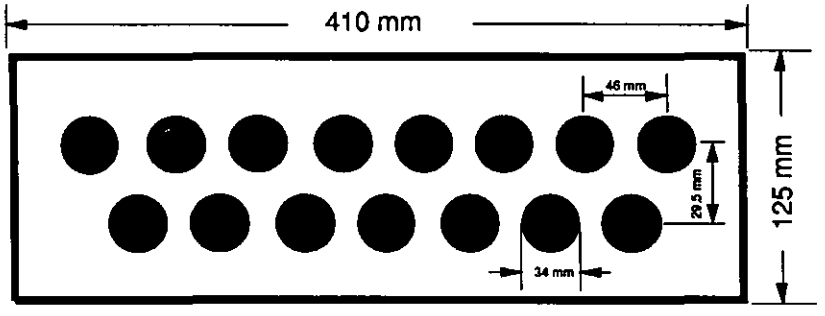

Figure 9.1 The Diagram of the Echelon Air Array

The transducers used in the array were made by the Polaroid Company and have good acoustic characteristics. The relative sensitivities of these fifteen transducers were measured and are listed in table 9.1. The conditions for these measurements are given underneath. From table 9.1, it can be seen that the standard deviation was only about 10% of the mean value.

Since the transducers are circular plane transducers, the beam pattern of a single transducer, if the circular aperture is uniformly excited, can be calculated as

$$S(\phi) = \frac{J_1(\phi)}{\phi} \tag{9.1}$$

where $J_1(\phi)$ is the first-order Bessel function of $\phi = 2\pi r \sin(\theta)/\lambda$, r is the radius of the circular plane [Ell81]. The radius of transducers used in the array is 17 *mm*, and the calculated beam

Table 9.1 Relative Sensitivities of Individual Transducers

No. of Elements	Output (V)
1	0.95
2	0.88
3	0.92
4	0.94
5	0.91
6	0.97
7	1.04
8	1.03
9	1.12
10	1.12
11	1.11
12	1.17
13	1.20
14	1.13
15	1.06
Mean Value	1.04
Standard Deviation	0.10

Measurement Conditions :

Transmitting frequency : 40 *kHz*

Pre-amplifier used : channel 5 *

Distance between Tx and Rx : 3 *m*

* *When measuring individual sensitivities the same pre-amplifier, the one in channel five, was used.*

pattern using equation (9.1) is shown in figure 9.2 and compared to the measured result. By calculation, the beam width of one transducer is about 15° at 40 *kHz*, which is measured as about 14°.

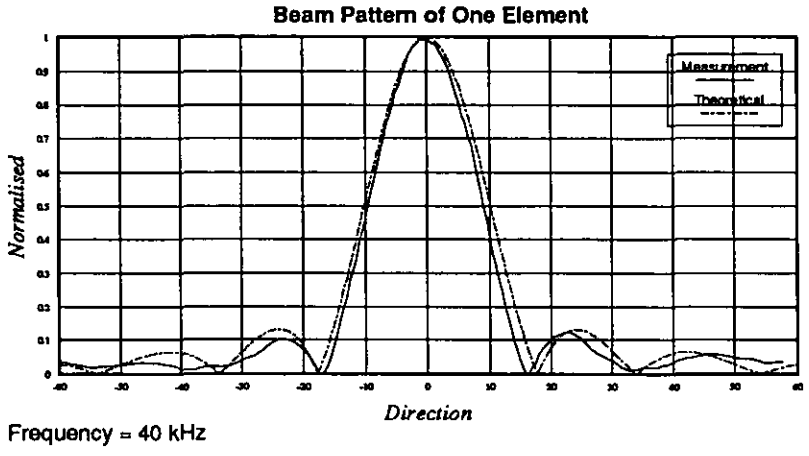

Figure 9.2 The Theoretical and Measured Beam Patterns of One Element

Although the array is composed of two layers, it can be approximated by a linear array if the sources are in the far-field and are in the horizontal plane containing the normal to the centre of the array. The equivalent linear array has fifteen sensors in the same line with inter-element spacing half of that in the original echelon array, i.e., 23 *mm*. The wavelength of signals at the transmitting frequency of 40 *kHz* is 8.5 *mm*, thus the inter-element spacing in the metric of the signal wavelength is $\Delta/\lambda = 2.7$.

The beam pattern of a linear array with omnidirectional sensors is well known and given by the following equation

$$D(\theta) = \frac{\mathrm{Sin}(m \cdot \pi \cdot \Delta \cdot \mathrm{Sin}\,\theta/\lambda)}{m \cdot \mathrm{Sin}(\pi \cdot \Delta \cdot \mathrm{Sin}\,\theta/\lambda)} \tag{9.2}$$

According to the product theorem [Uri75], the beam pattern of the array with directional elements will be the product of the beam pattern of an identical array of non-directional elements and the beam pattern of each element alone. Thus, the beam pattern of the employed array will be given by

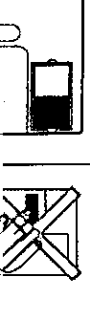

- Protected position
- Schreiben nicht möglich
- Position protégée
- Protezione inserita
- Posición de protección
- Posição protegida

- Write position
- Schreiben möglich
- Position écriture
- Protezione non inserita
- Posición de grabación
- Posição para escrita

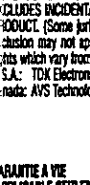

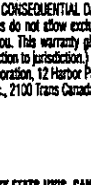

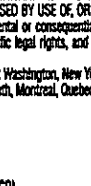

- 4-53°C
(39-127°F)

ULL LIFETIME WARRANTY–(EFFECTIVE ONLY IN U.S.A., CANADA AND MEXICO)

is product, if defective in materials or workmanship and returned postage prepaid with proof of purchase to e appropriate address below, will be replaced free of charge.

EPLACEMENT IS THE SOLE OBLIGATION UNDER THIS WARRANTY. THIS WARRANTY EXPRESSLY XCLUDES INCIDENTAL AND CONSEQUENTIAL DAMAGES CAUSED BY USE OF, OR INABILITY TO USE, THIS RODUCT. (Some jurisdictions do not allow exclusion of incidental or consequential damages, so the above clusion may not apply to you. This warranty gives you specific legal rights, and you may also have other ghts which vary from jurisdiction to jurisdiction.)

S.A.: TDK Electronics Corporation, 12 Harbor Park Drive, Port Washington, New York 11050
nada: AVS Technologies Inc., 2100 Trans Canada Highway South, Montreal, Quebec H9P 2N4, Canada

ARANTIE A VIE

PPLICABLE SEULEMENT AUX ETATS-UNIS, CANADA ET MEXICO)

ce produit s'avère défectueux dû à un vice de matériau ou de main-d'oeuvre, et qu'il est retourné port payé, compagné d'une preuve d'achat, il sera remplacé gratuitement.

E PRÉSENTE GARANTIE NE COUVRE QUE LE REMPLACEMENT DU PRODUIT, ET EXCLUT SPECIFIQUEMENT S DOMMAGES DIRECTS OU INDIRECTS QUE POURRAIT ENTRAINER L'UTILISATION (OU L'INCAPACITÉ UTILISER) CE PRODUIT. (Certaines juridictions interdisent l'exclusion de dommages directs ou indirects de te que cette exclusion pourrait ne pas s'appliquer à vous. La présente garantie vous confère des droits aux spécifiques, vous pourriez également jouir d'autres droits, lesquels varient d'une juridiction à l'autre.)

ARANTIA DE POR VIDA

FECTIVA SOLAMENTE EN LOS ESTADOS UNIDOS, CANADA Y MEXICO)

esta producto tuviera algún defecto en materiales o manufactura, debe ser devuelto por correo acompañado r una prueba de compra a la dirección que aparece abajo, y será reemplazado sin ningún cargo.

REEMPLAZO ES LA UNICA OBLIGACION BAJO ESTA GARANTIA. ESTA GARANTIA EXPRESAMENTE CLUYE DAÑOS INCIDENTALES O CONSECUENCIALES CAUSADOS POR EL USO O LA IMPOSIBILIDAD DE SO DE ESTE PRODUCTO.

lgunas jurisdicciones no permiten la exclusión de daños incidentales o consecuenciales, de modo que la clusión anterior puede no aplicarse a usted. Esta garantía le otorga derechos legales específicos, y usted ede tener otros derechos que varían de jurisdicción en jurisdicción.)

ARRANTY–(EFFECTIVE ONLY IN U.K. AND AUSTRALIA)

y TDK product failing through defects in original materials or workmanship will be replaced. Consumer's tutory rights excepted, TDK accepts no liability for consequential loss, howsoever caused.

DK ELECTRONICS CORP.

: Harbor Park Drive, Port Washington, N.Y. 11050 U.S.A.

DK RECORDING MEDIA EUROPE S.A.

l. Bommelscheuer L-4901 BASCHARAGE, Grand Duchy of Luxembourg

DK (AUSTRALIA) PTY. LIMITED

.N. 001 708 336, 22 Lambs Road, Artarmon, NSW2064, AUSTRALIA

GARANTIE A VIE
(APPLICABLE SEULEMENT AUX ETATS-UNIS, CANADA ET MEXICO)
Si ce produit s'avère défectueux dû à un vice de matériau ou de main-d'oeuvre, et qu'il est retourné port accompagné d'une preuve d'achat, il sera remplacé gratuitement.
LA PRÉSENTE GARANTIE NE COUVRE QUE LE REMPLACEMENT DU PRODUIT, ET EXCLUT SPECIFIQUE LES DOMMAGES DIRECTS OU INDIRECTS QUE POURRAIT ENTRAINER L'UTILISATION (OU L'INCAP D'UTILISER) CE PRODUIT. (Certaines juridictions interdisent l'exclusion de dommages directs ou indire sorte que cette exclusion pourrait ne pas s'appliquer à vous. La présente garantie vous confère des légaux spécifiques, vous pouvez également jouir d'autres droits, lesquels varient d'une juridiction à l'autr

GARANTIA DE POR VIDA
(EFECTIVA SOLAMENTE EN LOS ESTADOS UNIDOS, CANADA Y MEXICO)
Si este producto tuviera algún defecto en materiales o manufactura, debe ser devuelto por correo acomp por una prueba de compra a la dirección que aparece abajo, y será reemplazado sin ningún cargo.
EL REEMPLAZO ES LA UNICA OBLIGACIÓN BAJO ESTA GARANTÍA. ESTA GARANTIA EXPRESAM EXCLUYE DAÑOS INCIDENTALES O CONSECUENCIALES CAUSADOS POR EL USO O LA IMPOSIBILIDA USO DE ESTE PRODUCTO.
(Algunas jurisdicciones no permiten la exclusión de daños incidentales o consecuenciales, de modo q exclusión anterior puede no aplicarse a usted. Esta garantía le otorga derechos legales específicos, y puede tener otros derechos que varían de jurisdicción en jurisdicción.)

WARRANTY–(EFFECTIVE ONLY IN U.K. AND AUSTRALIA)
Any TDK product failing through defects in original materials or workmanship will be replaced. Consu statutory rights excepted, TDK accepts no liability for consequential loss, howsoever caused.

TDK ELECTRONICS CORP.
12 Harbor Park Drive, Port Washington, N.Y. 11050 U.S.A.

TDK RECORDING MEDIA EUROPE S.A.
Z. I. Bommelscheuer L-4901 BASCHARAGE, Grand Duchy of Luxembourg

TDK (AUSTRALIA) PTY. LIMITED
A.C.N. 001 708 336, 22 Lambs Road, Artarmon, NSW2064, AUSTRALIA

FULL LIFETIME WARRANTY–(EFFECTIVE ONLY IN U.S.A., CANADA AND MEXICO)
This product, if defective in materials or workmanship and returned postage prepaid with proof of purch the appropriate address below, will be replaced free of charge.
REPLACEMENT IS THE SOLE OBLIGATION UNDER THIS WARRANTY. THIS WARRANTY EXPRE EXCLUDES INCIDENTAL AND CONSEQUENTIAL DAMAGES CAUSED BY USE OF, OR INABILITY TO USE, PRODUCT. (Some jurisdictions do not allow exclusion of incidental or consequential damages, so the exclusion may not apply to you. This warranty gives you specific legal rights, and you may also have rights which vary from jurisdiction to jurisdiction.)
U.S.A.: TDK Electronics Corporation, 12 Harbor Park Drive, Port Washington, New York 11050
Canada: AVS Technologies Inc., 2100 Trans Canada Highway South, Montreal, Quebec H9P 2N4, Canada

- Protected position
- Schreiben nicht möglich
- Position protégé
- Protezione inserita
- Posición de protección
- Posição protegida

- Write position
- Schreiben mögl
- Position ecriture
- Protezione non inserita
- Posición de grabación
- Posição para es

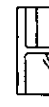

- 4-53°C (39-127°F)

$$P(\theta) = D(\theta) \times S(\theta) \tag{9.3}$$

The beam pattern of the array obtained by using equations (9.1) - (9.3) is compared with those measured by using electrical steering and mechanical steering of the array in figure 9.3 and figure 9.4. In figure 9.3, by using electronic steering the array was stationary and the measured beam pattern was obtained by scanning the space with the steering vector assigned a unity modulus, that is, the directivity of individual transducer was not taken into account. Correspondingly, the theoretical beam pattern was given by equation (9.2) without multiplication with the beam pattern of each element. Substituting the parameters of the array into (9.2), the beam pattern will have maximum values (grating lobes) at $\theta = 0°$, $\pm 21.8°$, $\pm 47.8°$, etc., as shown in figure 9.3. The measured beam pattern in figure 9.4 was obtained using mechanical steering of the array when the array was driven by a beam plotter [WZG+90]. Since each single element in the array had a sharp directivity, grating lobes in figure 9.3 were greatly suppressed, and the resulting beam pattern shows much lower responses in the corresponding directions. The measured results were very consistent with the theoretical calculation by using equation (9.1) - (9.3), and the beam width of the whole array is about 1.4° at 40 *kHz*.

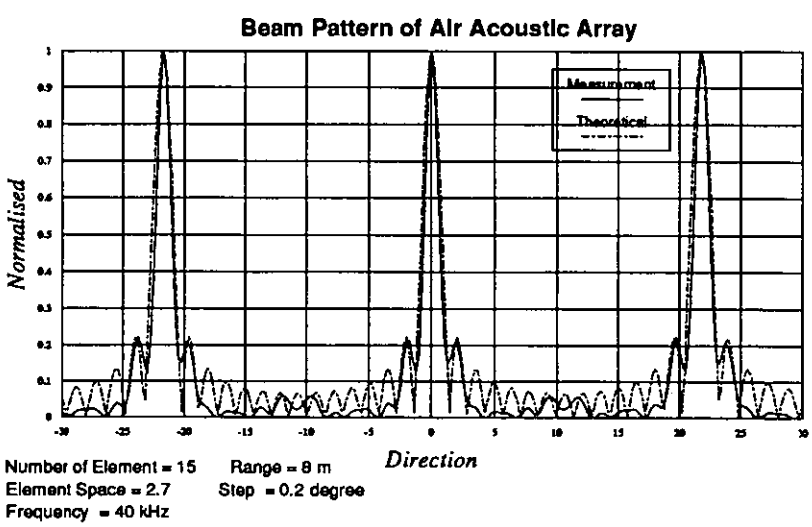

Figure 9.3 *The Theoretical and Measured Beam Patterns of the Air Acoustic Array Using Electronic Steering*

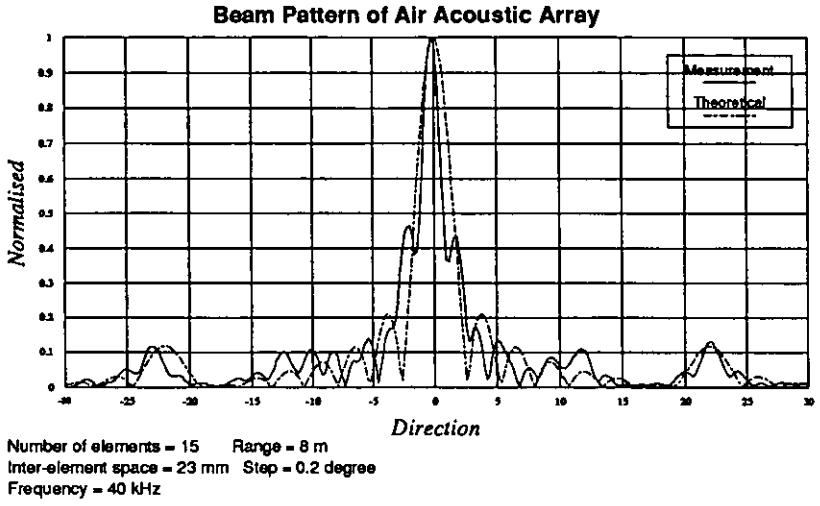

Figure 9.4 *The Theoretical and Measured Beam Patterns of the Air Acoustic Array Using Mechanical Steering*

9.1.2 The Measurement System

Figure 9.5 shows the layout of the measurement system used for carrying out experiments in this thesis. The original system was designed and built for both signal acquisition and analysis. Since programs written for processing data, either simulated on computers or measured in practice, had not been translated into the OCCAM language which was required by the transputer, the system was used for signal acquisition only and off-line processing was carried out.

The data acquisition part of this system, as shown in figure 9.5, is composed of pre-amplifiers, analogue multipliers, low pass filters, analogue to digital convertors (ADCs), a memory board, and the signal generator and control board.

Each of the fifteen transducers in the array is linked to one of the fifteen channels in the acquisition system. In each channel, a pre-amplifier is employed to raise the output level to the desired value, which is required by the dynamic range of 72 dB for 12 bit digital data. The output signal from the pre-amplifier is then passed to an analogue multiplier , where the In-phase and Quadrature (I&Q) components of the received signal are extracted by multiplying with Sine and Cosine reference signals. Because the sonar signals are generally narrowband signals, the I&Q sampling technique shifts the received signals to baseband,

illustrated in figure 9.6, and consequently reduces the required sampling frequency at the A/D convertors. To remove the sum-frequency components of the shifted signals from the I&Q sampling, a low pass filter is used with 5 *kHz* cutoff frequency. The filtered signals then pass to the Sample / Hold (S&H) amplifiers which hold constant signal amplitudes before analogue to digital conversion.

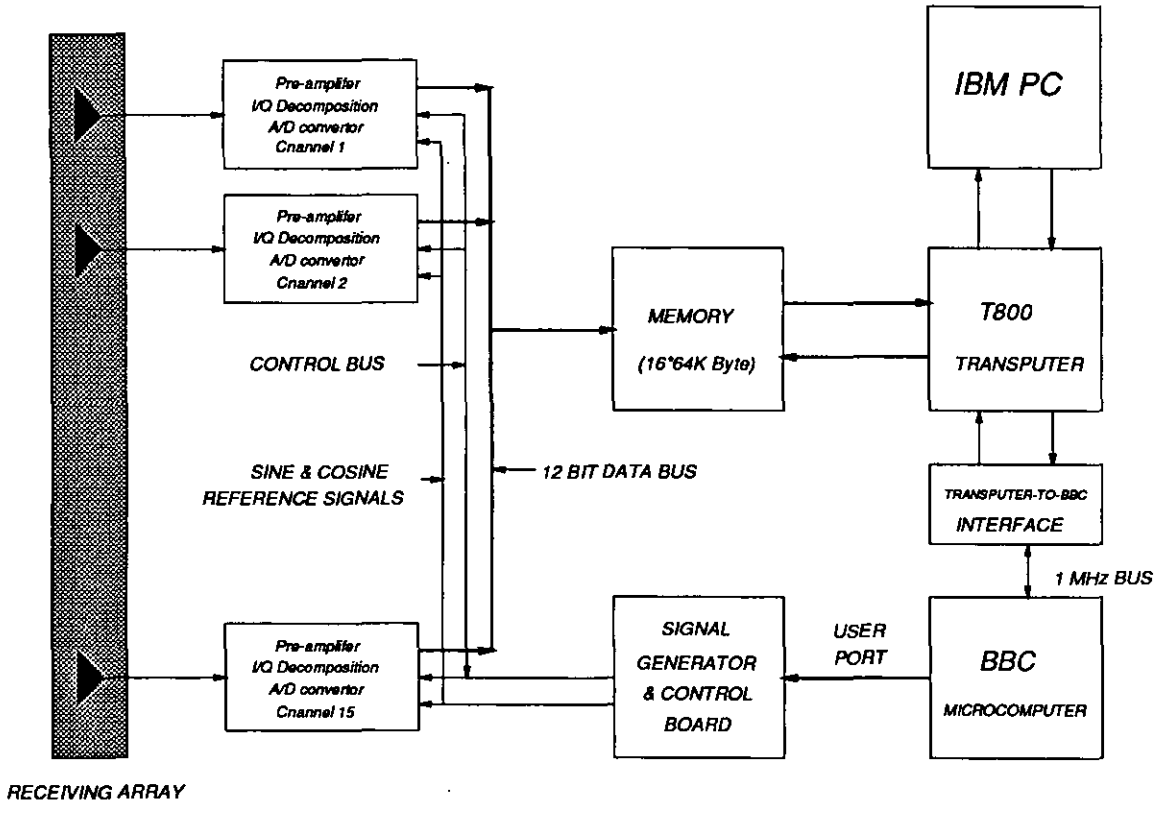

Figure 9.5 The Layout of the Measurement System

The outputs from the A/D convertors are in 12 bit digital form and are conveyed over a 12 bit bus to a memory buffer which is accessible by the transputer T800. The sampled data can be either processed on the transputer board in the system or saved on floppy disks via the IBM PC for off-line processing.

A BBC microcomputer serves as the main controller in this system. The Signal Generator and Control board generates the transmitted pulses and other reference signals such as the Sine and Cosine reference signals for the I&Q decomposition. The 1 MHz bus of the BBC is used for the transputer and BBC interface.

An IBM PC is used as the host of the transputer. Since the data is to be processed off-line, programs have been developed to transfer the data saved on the memory board to floppy disks via the IBM PC.

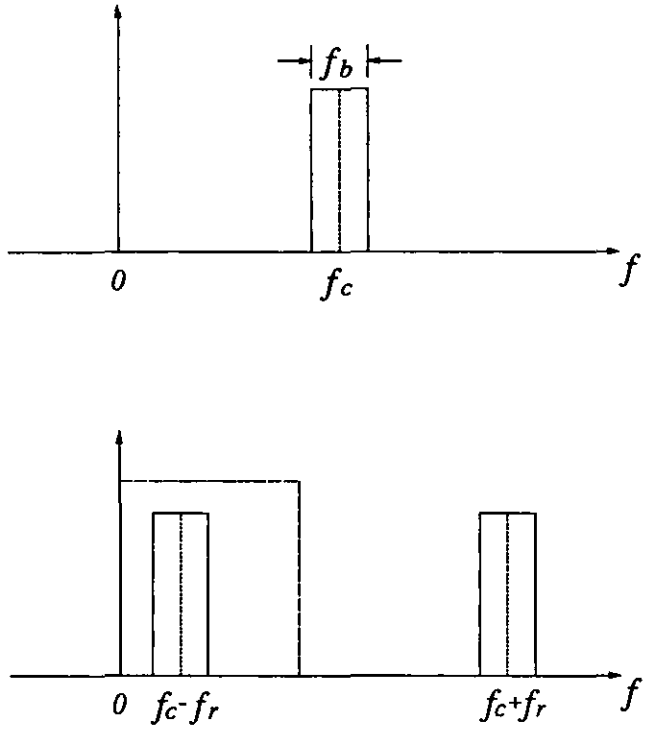

Figure 9.6 Frequency Shifting by IQ Technique

This system was originally designed and developed for the implementation of high resolution direction finding (DF) algorithms to resolve closely placed underwater targets / sources. The choice of the main system parameters was made according to practical measurement conditions such as the limited physical size of the water tank available in the Department, working frequency range of the available transducers, the tradeoff between the cost and resolution and speed of an A/D convertor, and so on.

The rest of this chapter is organised as follows : the design of experiments is proposed in section 9.2 where two cases (when the system works in passive mode and active mode respectively) are supposed with different scenarios for each case; section 9.3 presents experimental results in accordance with the different situations in section 9.2; the last section, section 9.4, presents a discussion and a conclusion of the practical work carried out so far.

9.2 Design of Experiments

The array used in experiments for this thesis was an air acoustic sonar array which could work in active mode when a single sensor was used as an emitter and the whole array received reflections from target(s), and also in passive mode when the array simply received signals radiated from emitter(s). For both modes, the measurement environment was the same as that shown in figure 9.7. Targets / Sources were placed at a distance in front of the array. The distance between targets / sources varied in experiments and will be specified later with individual experiment designs.

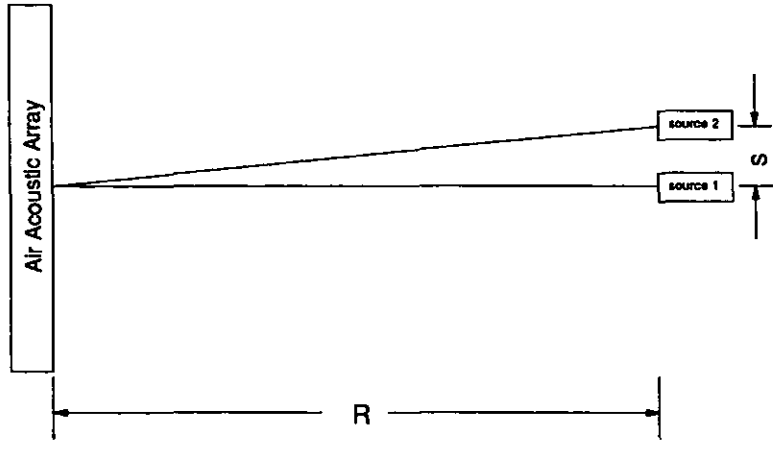

Figure 9.7 Geometry of the Measurement Environment

9.2.1 Passive Case

Working in this mode, the array "passively" received signals radiated from sources which are detectable at the array sensors.

One advantage of starting the experiments with the passive working mode of the array was that uncorrelated signal could be guaranteed by choosing different working frequencies for two sources. Since sub-optimal high resolution algorithms including the most popular MUSIC method were applied only to non-coherent sources with performance degradation when the correlation factor is high, uncorrelated sources were required to assess these algorithms for practical experiments.

The case when a signal source was present was considered as a preliminary of the two source case. Unlike computer simulation or theoretical analysis, knowledge of the source positions relative to the array and the relative position was unavailable, or at least inaccurate. Measurements with a single source present helped to align the sources.

When two sources were present, one was fixed around the normal position to the array while the other one was moved, in parallel with the array, from a distance toward the fixed source. The angle between the sources to the array was approximately calculated, and also measured by switching off one source and measuring the direction of the other source and the other way round. This procedure was repeated for each angular separation and, of course, data when both sources were switched on was also recorded.

The case for two emitters working at the same frequency was then considered. Measurements were for different separations between the two emitters and also for each of the two emitters when the other one was switched off, for alignment of the emitter positions.

9.2.2 Active Case

In the active mode of the array, one individual transducer was placed near the array. (In this sense, the array is not really working in the active mode). Two targets were placed in front of the array at an appropriate distance, in the experiments to be described herein chosen as 5.6 *m*, so that the reflections from them are detectable while the far-field approximation could still be met roughly. Again, cases when one single target was in use and when two targets were used were considered. And the position(s) of the target(s) was defined in the same way as that in the passive mode.

The targets were made of metal, the material which is known to have strong reflectivity. Two targets were of the same circular shape and of the same size of 85 *mm* in diameter, which was 10 times of the signal wavelength. Two factors were taken into account when choosing the size of the targets, these were the reflected energy and the directivity of the targets. If the target size was too small, the targets would have to be placed nearer the receiving array so that the reflections were detectable. On the other hand, a sharper directivity was expected from a larger target which, in turn, would cause difficulty in receiving target reflections.

9.3 Experiment Implementations and Results

According to the experiment designs in section 9.2, a large number of practical measurements have been carried out and analyzed by using the different algorithms, which have been discussed previously. These algorithms include the conventional beamforming technique, the MUSIC technique and its root version, the LS-ESPRIT method, the IMP method, and two multidimensional approaches, ML and WSF. Results of the experiments by means of applying the above-mentioned algorithms to the experimental measurements will be presented in this section.

9.3.1 Experiments, Group 1

In this group of experiments, the array worked in the passive mode. Two sources were placed in front of the array at a distance of 7.56 meters. The measurement environment was shown in figure 9.7. Source #2 was fixed at a position while source #1 was moved along the direction of the array (in parallel with the array). The position of source #2 was given by the peak in the spectrum obtained when source #1 was switched off. Holding source #2 at this position, measurements were taken when source #2 was turned off to give a location estimate of source #1 which was moved [illegible] when both sources were on. The distance between these two sources was initially 600 *mm* and decreased with decrements of 50 *mm* to 100 *mm*. For each set-up of these parameters, measurements were repeated twice. Results are tabulated in table 9.3 and the conventional beamforming spectra and MUSIC spectra are given in figure 9.9 and figure 9.10 respectively

For this group of experiments, the two sources worked at different frequencies : 39.52 *kHz* and 40.00 *kHz*. 30 snapshots were taken for each experiment. The illustration for the calculation of the angles is given in figure 9.8, where $R = 7560$ *mm* is the distance between the source and the receiving array. The position of the fixed source, source #2, was measured. The moving source, source #1, was placed at different positions in parallel with the array. Distances between these two sources were measured and used to calculate the angular separations so as to compare with the estimated results obtained from algorithms.

The position of source #2 was measured when source #1 was switched off. The corresponding angle was about 1.6° from the normal of the array and the distance from the normal was

calculated as 211 *mm*. This distance added with the source separation was used to compute the position of source #1 and compare with the estimated angular directions given by different algorithms.

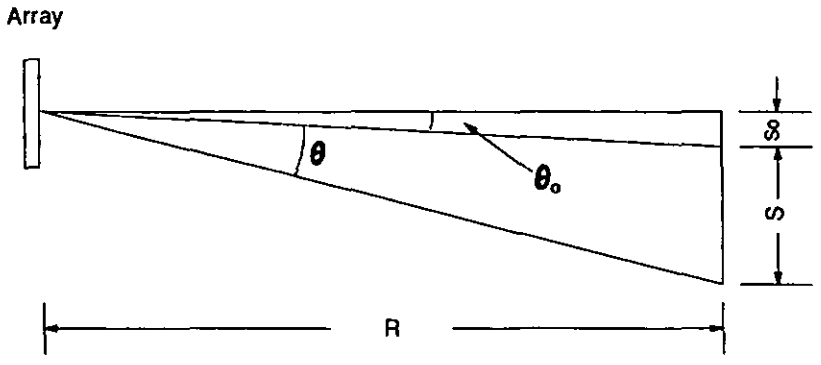

Figure 9.8 Illustration of the Calculation of Angles

The calculation of the corresponding source #1 positions, when it was moved, followed the equations given below and the results are listed in table 9.2.

$$\tan\theta = (s + s_o)/R \tag{9.4}$$

where $s_o = R \cdot \tan\theta_o = 211\ mm$ with θ_o being estimated by switching off source #1.

Table 9.2 Emitter Directions Obtained by Calculation

$s(mm)$	$s + s_o(mm)$	$\tan\theta$	$\theta + \theta_o(°)$
600	811	0.1072	6.1
550	761	0.1007	5.7
500	711	0.0940	5.4
450	661	0.0874	5.0
400	611	0.0808	4.6
350	561	0.0742	4.2
300	511	0.0676	3.9
250	461	0.0610	3.5
200	411	0.0544	3.1
150	361	0.0478	2.7
100	311	0.0411	2.4

Table 9.3 shows the results of this set of experiments by applying different algorithms. Inside the column of the source separation, the calculated directions of source #1 at different positions are also given for comparison. These are the directions to the normal of the array rather than the separation between the two sources.

The angular estimates shown in table 9.3 and those in following subsections were obtained according to the following criteria :

CBF:	peak positions in the estimated spectrum
SP-MUSIC:	peak positions in the estimated spectrum
RT-MUSIC:	angle estimates with the biggest modulus estimates, which usually are > 0.8 but sometime $0.8 > \rho > 0.7$
ESPRIT:	angles given from the algorithm with assigned number of sources
IMP:	angles given from the algorithm with assigned number of sources
ML:	angles given from the algorithm with assigned number of sources
WSF:	angles given from the algorithm with assigned number of sources

The plots in figures 9.9 and 9.10 give the spectra obtained by the conventional beamforming method and the MUSIC technique. In each plot in these two figures, solid lines denote the cases when a single source was on and the dashed lines represent the cases when two sources were on. Figure 9.9.1 and figure 9.10.1 show the four measurements when the fixed source #2 was on. The other 11 figures give the situations when source #1 was moved from a distance towards source #2.

From table 9.3, it can be seen that the estimates given from different algorithms are strongly consistent when a single source was on, except those given by ESPRIT which tend to be biased. The estimates given by the ESPRIT algorithm are smaller than the calculated angles and the estimates from other methods. The biases existing in the ESPRIT estimates are more noticeable at the larger emitter separations and, in the cases with 150 *mm* and 100 *mm* separations are much less significant.

For the cases where both sources were on, when the source separation is big enough ($\geq$ 200 *mm*), the results from all algorithm except the ESPRIT method show excellent indications of the true positions of the sources, while the ESPRIT algorithm inclines to give biased

estimates when the source separation is not less than 400 *mm*. As the source separation decreases, the performance of ESPRIT begins to degrade by giving estimates which are apparently different from estimates given by other methods.

When the source separation gets small, at 150 *mm* or 100 *mm*, the conventional beamforming method fails to give two separate peaks. The results shown in relevant columns are the unique peak positions in the corresponding spectra, as depicted in figure 9.9.11 and 9.9.12. They lie in directions somewhere between the two sources.

Although two estimates were given in table 9.3 for spectral MUSIC (SP-MUSIC) when the separation is 150 *mm*, from the corresponding figure 9.10.11, it is seen that the estimate at 2.7° does not show a clear peak. At 100 *mm* source separation, one of the two estimates gives two separate values which, from figure 9.10.12, are estimates from two distinguishable peaks.

It can easily seen from the plots in figures 9.9 and 9.10 that the resolution abilities of both the conventional and the MUSIC methods degrade as the source separation decreases. Although the MUSIC method is proved to possess higher resolution, it is not fully shown in this group of experiments although figure 9.10.11 and figure 9.10.12 provide some evidence. The advantages of the MUSIC method over the conventional beamforming method are shown in that the spectra from the MUSIC method give sharper peaks and smoother backgrounds. The array deployed in these experiments has very sharp directivities so that even the conventional beamforming method can resolve very closely placed sources and the resolution abilities of both methods might be limited by other practical factors, such as environment noise, etc..

The root MUSIC (RT-MUSIC) method shows similar results as the spectral MUSIC method at all the source separations and in both cases when a single source and two sources are on. For source separations of 150 *mm* and 100 *mm*, only one estimate is given in one of the two experiments. This is because only one angular estimate has a modulus which is big enough to be recognized as an estimate.

Results obtained from IMP, ML, and WSF demonstrate very good consistency in most of the cases except the last separation of 100 *mm* where the IMP algorithm gives only one source direction estimate although the number of sources is two. The program terminated after giving the estimate of the first source since the residual power level was lower than the threshold. The estimates are the same as those from the conventional method (which

Table 9.3 Results when two sources working at differnet frequencies (39.52 kHz, 40.00 kHz)

Emitter State	Emitter Separation	CBF	SP-MUSIC	RT-MUSIC	ESPRIT	IMP	ML	WSF
#1 OFF #2 ON		1.7 1.6 1.6 1.6	1.7 1.6 1.6 1.6	1.7 1.6 1.6 1.6	1.7 1.4 1.4 1.5	1.7 1.6 1.6 1.6	1.7 1.6 1.6 1.6	1.7 1.6 1.6 1.6
#1 ON #2 OFF	600 mm (6.1°)	6.2 6.2	6.2 6.2	6.2 6.2	5.7 5.8	6.2 6.2	6.2 6.2	6.2 6.2
#1 ON #2 ON		1.5 6.0 1.6 6.1	1.5 6.0 1.6 6.1	1.5 6.1 1.6 6.1	1.3 5.7 1.6 5.9	1.5 6.0 1.6 6.1	1.5 6.0 1.6 6.1	1.5 6.0 1.6 6.1
#1 ON #2 OFF	550 mm (5.7°)	5.7 5.8	5.7 5.8	5.7 5.8	5.3 5.5	5.7 5.8	5.7 5.8	5.7 5.8
#1 ON #2 ON		1.6 5.8 1.5 5.8	1.6 5.8 1.5 5.7	1.6 5.9 1.6 5.8	1.5 5.9 1.5 5.7	1.7 5.7 1.7 5.6	1.7 5.7 1.8 5.6	1.7 5.7 1.7 5.6
#1 ON #2 OFF	500 mm (5.4°)	5.3 5.3	5.3 5.4	5.3 5.4	5.0 5.1	5.3 5.4	5.3 5.4	5.3 5.4
#1 ON #2 ON		1.6 5.5 1.5 5.4	1.6 5.5 1.6 5.4	1.6 5.5 1.6 5.4	1.5 5.3 1.4 4.3	1.6 5.5 1.6 5.4	1.6 5.5 1.6 5.4	1.6 5.5 1.6 5.4
#1 ON #2 OFF	450 mm (5.0°)	5.0 5.0	5.0 5.0	5.0 5.0	4.7 4.5	5.0 5.0	5.0 5.0	5.0 5.0
#1 ON #2 ON		1.6 5.0 1.6 5.0	1.6 5.0 1.6 5.0	1.6 5.0 1.6 5.0	1.5 4.7 1.5 4.7	1.6 5.0 1.6 5.0	1.6 5.0 1.6 5.0	1.6 5.0 1.6 5.0
#1 ON #2 OFF	400 mm (4.6°)	4.6 4.6	4.6 4.6	4.6 4.6	4.0 4.1	4.6 4.6	4.6 4.6	4.6 4.6
#1 ON #2 ON		1.5 4.2 1.5 4.3	1.4 4.3 1.5 4.3	1.4 4.1 1.4 4.4	1.2 4.3 1.3 4.4	1.5 4.3 1.5 4.3	1.5 4.3 1.5 4.4	1.5 4.3 1.5 4.4

(to be continued)

(continued)

Emitter State	Emitter Separation	CBF	SP-MUSIC	RT-MUSIC	ESPRIT	IMP	ML	WSF
#1 ON #2 OFF	350 mm (4.2°)	4.3 4.3	4.3 4.3	4.3 4.3	3.9 4.0	4.3 4.3	4.3 4.3	4.3 4.3
#1 ON #2 ON		1.4 4.0 1.9 4.2	1.4 4.0 1.8 4.3	1.4 4.0 1.8 4.3	0.8 3.8 2.4 5.5	1.4 4.0 1.7 4.5	1.4 4.0 1.7 4.5	1.4 4.0 1.7 4.5
#1 ON #2 OFF	300 mm (3.9°)	3.9 3.9	3.9 3.9	3.9 3.9	3.6 3.6	3.9 3.9	3.9 3.9	3.9 3.9
#1 ON #2 ON		1.9 4.1 1.7 3.9	1.8 4.2 1.6 4.1	1.8 4.2 1.6 4.1	-4.3 2.7 1.1 3.2	1.9 4.1 1.5 4.2	1.9 4.1 1.5 4.2	1.9 4.1 1.5 4.2
#1 ON #2 OFF	250 mm (3.5°)	3.5 3.6	3.5 3.6	3.5 3.6	3.2 3.3	3.5 3.6	3.5 3.6	3.5 3.6
#1 ON #2 ON		1.4 3.5 1.4 3.5	1.4 3.7 1.4 3.7	1.5 3.6 1.4 3.6	1.9 3.0 1.8 4.0	1.4 3.5 1.4 3.6	1.3 3.6 1.4 3.6	1.4 3.5 1.4 3.6
#1 ON #2 OFF	200 mm (3.1°)	3.1 3.2	3.1 3.2	3.1 3.2	2.9 2.8	3.1 3.2	3.1 3.2	3.1 3.2
#1 ON #2 ON		1.3 3.4 1.3 3.3	1.3 3.5 1.4 3.4	1.3 3.4 1.4 3.3	1.8 4.7 1.9 4.1	1.3 3.4 1.4 3.2	1.3 3.4 1.4 3.2	1.3 3.4 1.4 3.2
#1 ON #2 OFF	150 mm (2.7°)	2.8 2.9	2.8 2.9	2.9 2.9	2.6 2.7	2.8 2.9	2.8 2.9	2.8 2.9
#1 ON #2 ON		2.2 2.6	2.2 1.8 2.7	1.9 1.6 2.9	-4.8 2.5 2.6 4.0	1.8 3.2 1.7 3.1	1.8 3.2 1.7 3.1	1.8 3.2 1.7 3.1
#1 ON #2 OFF	100 mm (2.4°)	2.4 2.4	2.4 2.4	2.4 2.5	2.2 2.4	2.4 2.4	2.4 2.5	2.4 2.5
#1 ON #2 ON		1.9 1.8	1.9 1.5 2.7	1.8 1.4 2.8	-1.3 1.8 1.1 2.9	1.9 1.8	1.0 2.1 1.6 2.9	0.9 2.1 1.6 2.9

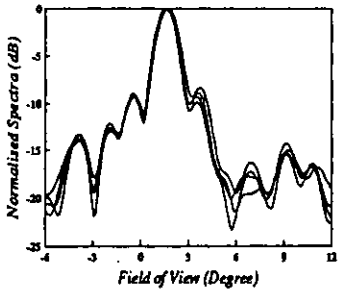

Figure 9.9.1

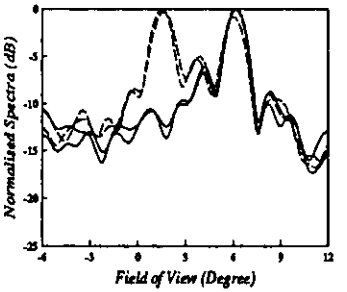

Figure 9.9.2

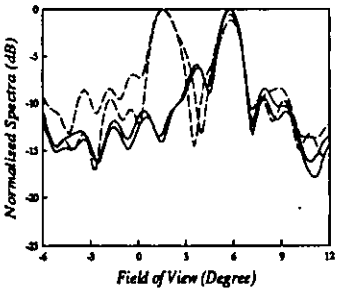

Figure 9.9.3

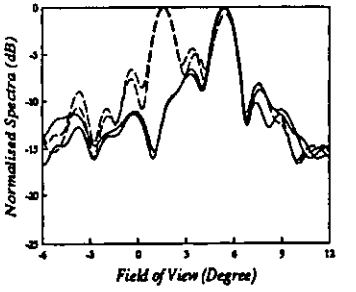

Figure 9.9.4

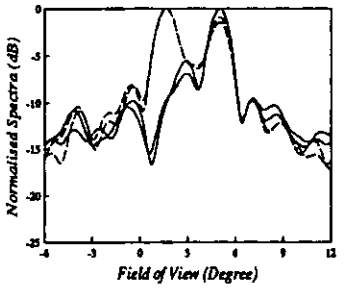

Figure 9.9.5

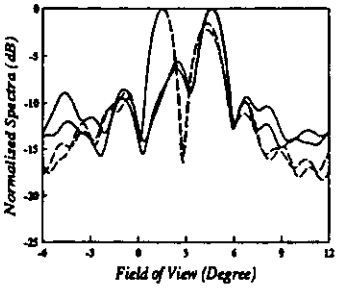

Figure 9.9.6

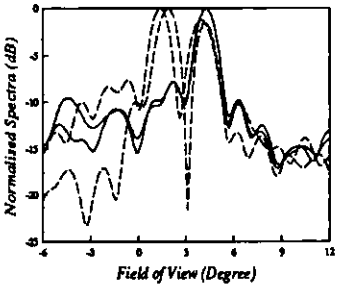

Figure 9.9.7

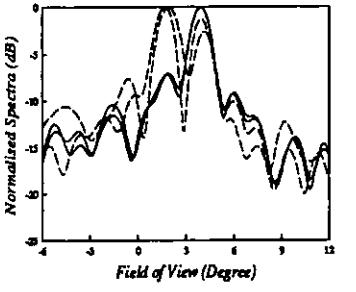

Figure 9.9.8

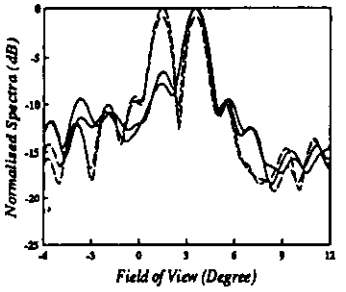

Figure 9.9.9

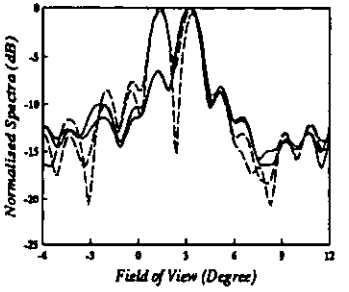

Figure 9.9.10

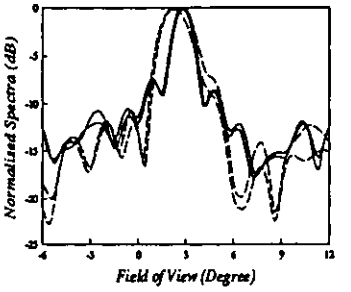

Figure 9.9.11

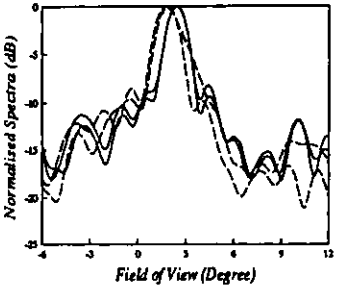

Figure 9.9.12

Figure 9.9 Spectra obtained by the conventional beamforming method

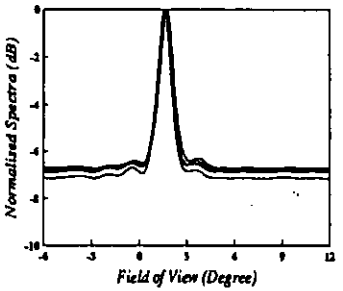

Figure 9.10.1

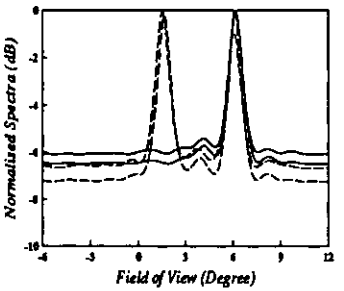

Figure 9.10.2

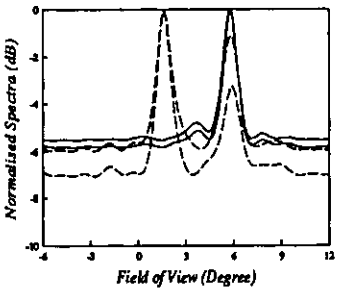

Figure 9.10.3

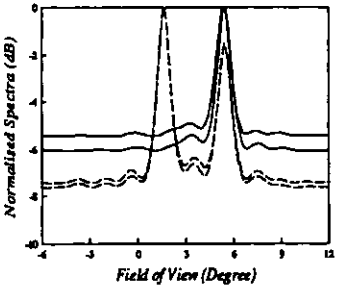

Figure 9.10.4

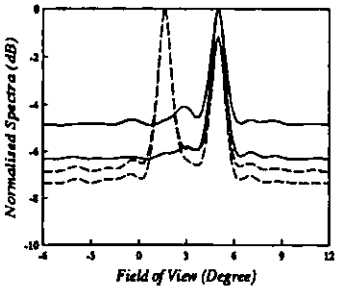

Figure 9.10.5

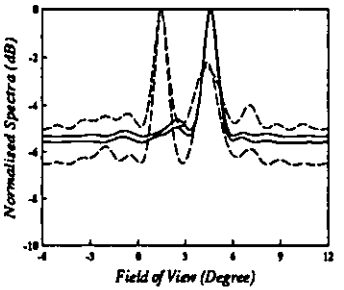

Figure 9.10.6

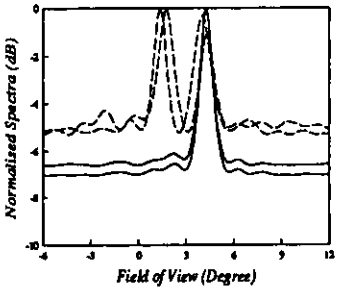

Figure 9.10.7

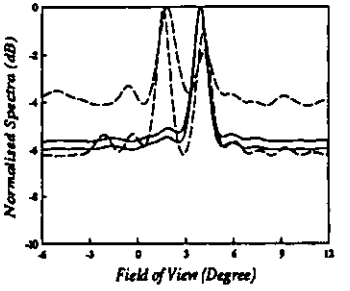

Figure 9.10.8

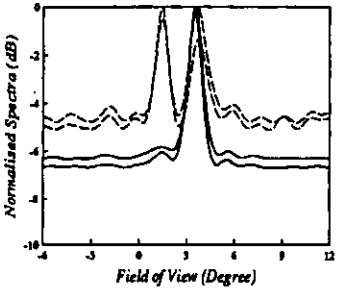

Figure 9.10.9

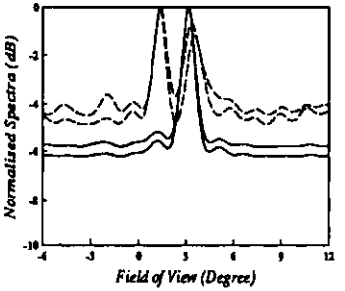

Figure 9.10.10

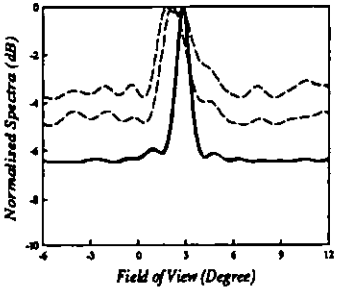

Figure 9.10.11

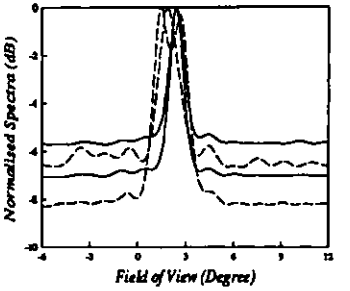

Figure 9.10.12

Figure 9.10 Spectra obtained by the MUSIC technique

constitutes the first stage of the IMP algorithm). Probably changing the definition of the threshold or using a more flexible threshold would allow the processing to carry on till the second source was found.

From table 9.3, the position estimate of source #2 at each separation, the fixed source, does not hold the estimate given by the switching off source #1 in the first row of the table. This is thought to be the result of switching on / off the sources manually.

9.3.2 Experiments, Group 2

For this group of experiments, the two sources worked at the same frequency, 40.00 *kHz*, while other parameters were the same as that in the previous group of experiments. For source #2 which was unmoved in the experiments, four measurements were taken to align its position at the beginning of the measurements. Afterwards, two measurements were taken when only source #1 was on to determine the source positions which were changed in the experiments. When both sources were on, four measurements were taken to provide more information for the following processing and for the observation of the algorithm abilities to resolve the two sources.

The source separation was reduced from 600 *mm* to 100 *mm* with a decrement of 50 *mm*, i.e., 11 separations were considered. The calculated angles of the source directions were the same as those in the previous group of experiments, as listed in table 9.2. The results obtained by using different algorithms are tabulated in table 9.4.

The position of the fixed source, source #2, was consistently determined by all the methods. Like in the Experiment Group 1, the ESPRIT method gave estimates which were smaller than the average of estimates from all other methods. But the "bias" herein was smaller than in the previous case.

For all the separations through the experiments, the positions of source #1 were well determined. Although the ESPRIT method tended to give smaller angular estimates, the differences were getting less noticeable and, at the separation of 150 *mm* and 100 *mm*, the same estimates resulted as those from other methods.

When both sources were on, the results required more attention. For separations which were larger than 300 *mm*, all methods depicted good indication of source positions. Especially for the separations of 600 *mm*, 550 *mm*, and 500 *mm*, all methods showed excellent results with great consistency, except the ESPRIT estimates at 500 *mm* separation which show biases. For the separation of 450 *mm*, IMP, ML, and WSF still performed extremely well in the sense of giving consistent estimates. Other methods also gave good estimates but did not behave as consistently with the other methods as before. The conventional beamforming method showed a tendency to give estimates which were in the true directions. The other spectral method, SP-MUSIC, did not show this trend by giving estimates which were much nearer those from the IMP, ML, and WSF. Comparatively, the estimates from RT-MUSIC seemed to be better than those for ESPRIT.

The three optimal methods, again, gave very consistent estimates at separations of 400 *mm* and 350 *mm*. The CBF method, however, showed quite good results, similar to those from the optimal methods, while estimates from both MUSIC methods were biased. The results from ESPRIT were more "arbitrary".

It can be seen that when the source separations are large, the performance of all algorithms is similar to that in the case when two sources worked at different frequencies. But as the separation decreases, the performance degrades. This performance degradation can be seen from the results when the source separations are 300 *mm* or smaller.

In the row where the source separation was 300 *mm* and two sources were on, none of the four measurements gave two distinct peaks in the conventional beamforming spectra while three of them found both estimates in the MUSIC spectra. Only one of the two estimates given by the ESPRIT algorithm seemed reasonable and seemed to be lying at a direction somewhere between the two source directions rather than near either of them. Two of the RT-MUSIC estimates among the four gave similar results as the SP-MUSIC and the other two were less convinced. All the roots were checked and it was found that the estimates at -0.6° possessed larger moduli than the ones at 2.8°. Although the largest moduli in this case were more clustered and less distinguishable from the rest, the two angular estimates with the largest moduli were picked out and listed in the table.

Despite the performance degradation in the above-mentioned methods, both multidimensional approaches, ML and WSF, provided very good angular estimates. The IMP method also performed well except in the last measurement where only one estimate was given (the

searching procedure terminated after finding the first source).

The same measurements were then processed under the assumption that only one source was present. Conventional beamforming did not depend on this knowledge and the assumption would not affect its performance and the correspondent estimates were not repeated in the table. However, the SP-MUSIC was greatly affected and gave only one estimate in each measurement which was the same as the correspondent estimate from CBF. RT-MUSIC, on the other hand, gave similar results to the ESPRIT method except in the first measurement. The roots were again checked for the reason and it was the same as under the assumption of two sources present. An angular estimate existed at 2.8° but the corresponding modulus was smaller than the one at 4.1°, which was listed in the table.

The results from the IMP algorithm were somehow surprising. This algorithm failed to find any peak in three of these four measurements. The reason for this was thought probably to be that one of the two signals was taken as the noise component and the wrong classification raised the threshold which was dependent on the noise power estimate. The other measurement, however, gave two estimates although the number of sources was given as 1 and the two estimates were the same as those in the above row.

The multidimensional approaches, ML and WSF, gave only one estimate for each measurement and the estimate was similar to that from CBF.

For all the cases when the source separations were less than 300 *mm*, the data were analysed under both assumptions when the number of sources was 2 or 1. The conventional beamforming, the SP-MUSIC method, and the RT-MUSIC method gave only one estimate in all these measurements. Only a single peak was found in each of the spectra obtained from the conventional beamforming method or from the SP-MUSIC technique, and, for the RT-MUSIC technique, only one estimate could be found with a modulus which was larger than all the clustered moduli.

The number of estimates obtained from ESPRIT, ML, and WSF depended on the given estimate of the number of sources. The estimates from ML and WSF seemed to be acceptable estimates of the true source directions while only one of the two given by ESPRIT was likely to be an estimate of the source direction.

Table 9.4 Results when two sources working at the same frequency (40.00 kHz)

Emitter State	Emitter Separation	CBF	SP-MUSIC	RT-MUSIC	ESPRIT	IMP	ML	WSF
#1 OFF #2 ON		1.6 1.6 1.6 1.6	1.6 1.6 1.6 1.6	1.7 1.6 1.6 1.6	1.5 1.6 1.5 1.6	1.6 1.6 1.6 1.6	1.6 1.6 1.6 1.6	1.6 1.6 1.6 1.6
#1 ON #2 OFF	600 mm (6.1°)	6.1 6.1	6.1 6.1	6.1 6.1	5.9 5.8	6.1 6.1	6.1 6.1	6.1 6.1
#1 ON #2 ON		1.7 6.0 1.6 5.9 1.7 5.9 1.6 5.9	1.7 6.1 1.5 6.0 1.6 5.9 1.6 6.0	1.7 6.1 1.5 6.0 1.6 6.0 1.6 6.0	1.7 6.2 1.4 6.0 1.4 5.9 1.6 5.9	1.7 6.1 1.5 6.0 1.6 6.0 1.6 6.0	1.7 6.1 1.5 6.0 1.6 6.0 1.5 6.0	1.7 6.1 1.5 6.0 1.6 6.0 1.5 6.0
#1 ON #2 OFF	550 mm (5.7°)	5.8 5.8	5.8 5.8	5.8 5.8	5.6 5.5	5.8 5.8	5.8 5.7	5.8 5.8
#1 ON #2 ON		1.8 5.8 1.8 5.8 1.8 5.8 1.8 5.8	1.7 5.9 1.7 5.8 1.7 5.8 1.7 5.8	1.7 5.9 1.7 5.8 1.7 5.8 1.7 5.8	1.8 6.0 1.8 5.8 1.6 5.7 1.9 6.0	1.7 5.9 1.8 5.8 1.7 5.8 1.7 5.8	1.7 5.9 1.8 5.9 1.7 5.8 1.7 5.8	1.7 5.9 1.8 5.8 1.7 5.8 1.7 5.8
#1 ON #2 OFF	500 mm (5.4°)	5.5 5.3	5.5 5.3	5.5 5.3	5.3 5.2	5.5 5.3	5.5 5.3	5.5 5.3
#1 ON #2 ON		1.8 5.3 1.7 5.3 1.5 5.3 1.8 5.3	1.7 5.3 1.7 5.2 1.6 5.3 1.7 5.2	1.7 5.3 1.6 5.3 1.6 5.4 1.7 5.4	1.4 5.5 1.3 5.3 1.5 5.4 1.8 4.9	1.8 5.3 1.7 5.2 1.7 5.2 1.8 5.3	1.8 5.2 1.8 5.3 1.7 5.3 1.8 5.3	1.8 5.2 1.8 5.2 1.7 5.3 1.8 5.3
#1 ON #2 OFF	450 mm (5.0°)	5.0 5.0	5.0 5.0	5.0 5.0	4.8 4.8	5.0 5.0	5.0 5.0	5.0 5.0
#1 ON #2 ON		1.9 4.8 2.0 4.7 1.9 4.7 1.9 4.8	1.6 4.9 1.8 4.7 1.7 4.8 1.7 4.8	1.5 4.8 1.8 4.7 1.7 4.8 1.7 4.8	1.3 4.6 1.3 4.8 1.6 4.6 1.5 4.9	1.7 4.9 1.8 4.9 1.7 4.9 1.7 4.9	1.7 4.9 1.8 4.9 1.7 4.9 1.7 4.9	1.7 4.9 1.8 4.9 1.7 4.9 1.7 4.9

(to be continued)

(continued)

Emitter State	Emitter Separation	CBF	SP-MUSIC	RT-MUSIC	ESPRIT	IMP	ML	WSF
#1 ON #2 OFF	400 mm (4.6°)	4.7 4.6	4.7 4.6	4.7 4.6	4.6 4.5	4.7 4.6	4.7 4.6	4.7 4.6
#1 ON #2 ON		1.7 4.8 1.7 4.8 2.1 4.7 2.1 4.7	1.6 4.9 1.5 4.9 1.6 4.8 1.8 4.7	1.6 4.8 1.4 4.8 1.6 4.8 1.7 4.7	2.0 5.4 1.8 5.0 1.6 4.8 1.7 4.4	1.7 4.8 1.7 4.8 1.9 4.7 2.0 4.7	1.7 4.8 1.7 4.8 1.9 4.7 2.0 4.7	1.7 4.8 1.7 4.9 1.9 4.7 2.0 4.7
#1 ON #2 OFF	350 mm (4.2°)	4.3 4.3	4.3 4.2	4.3 4.2	4.2 4.1	4.3 4.3	4.3 4.2	4.3 4.2
#1 ON #2 ON		1.9 4.5 2.1 4.5 1.9 4.5 1.8 4.5	1.7 4.6 1.9 4.5 1.6 4.6 1.5 4.7	1.6 4.6 1.5 4.5 1.5 4.6 1.4 4.6	1.9 4.6 2.8 4.1 2.0 5.2 1.8 4.9	2.0 4.4 2.1 4.4 2.0 4.4 2.0 4.4	2.0 4.4 2.1 4.4 2.0 4.4 2.1 4.4	2.0 4.4 2.1 4.4 2.0 4.4 2.1 4.4
#1 ON #2 OFF	300 mm (3.9°)	3.9 3.9	3.9 3.9	3.9 3.9	3.8 3.8	3.9 3.9	3.9 3.9	3.9 3.9
#1 ON #2 ON $\hat{d}=2$		3.1 3.0 2.9 2.7	1.3 3.0 1.5 2.8 1.4 2.8 2.8	-0.6 1.2 1.3 3.8 1.2 3.8 -0.6 1.2	2.8 -2.6 2.8 2.0 2.7 6.9 2.7 -6.7	1.4 3.4 1.6 3.6 1.6 3.5 2.7	1.5 3.5 1.7 3.6 1.6 3.6 1.9 3.8	1.6 3.5 1.6 3.6 1.5 3.5 2.0 3.9
#1 ON #2 ON $\hat{d}=1$			3.1 3.0 2.9 2.7	4.1 2.8 2.8 2.7	2.9 2.8 2.8 2.7	□ □ 1.6 3.5 □	3.2 2.9 2.9 2.7	3.2 3.0 2.9 2.7
#1 ON #2 OFF	250 mm (3.5°)	3.4 3.5	3.4 3.5	3.4 3.5	3.2 3.4	3.4 3.5	3.4 3.5	3.4 3.5
#1 ON #2 ON $\hat{d}=2$		2.9 2.8 2.8 2.8	2.9 2.9 2.8 2.7	2.9 2.9 2.8 2.8	2.6 -6.0 2.6 6.5 2.6 -6.8 2.6 -7.6	1.6 3.3 1.6 3.3 1.5 3.2 1.5 3.2	1.5 3.3 1.6 3.3 1.5 3.2 1.6 3.3	1.5 3.3 1.6 3.3 1.6 3.3 1.6 3.3
#1 ON #2 ON $\hat{d}=1$			2.9 2.8 2.8 2.8	2.9 2.9 2.9 2.8	2.7 2.7 2.7 2.7	1.6 3.3 1.6 3.3 1.5 3.2 2.8	2.9 2.8 2.8 2.8	2.9 2.8 2.8 2.8

(to be continued)

(continued)

Emitter State	Emitter Separation	CBF	SP-MUSIC	RT-MUSIC	ESPRIT	IMP	ML	WSF
#1 ON #2 OFF	200 mm (3.1°)	3.1 3.1	3.1 3.1	3.1 3.1	3.0 2.9	3.1 3.1	3.1 3.1	3.1 3.1
#1 ON #2 ON $\hat{d}=2$		2.6 2.6 2.6 2.5	2.6 2.6 2.5 2.4	2.7 2.6 2.5 2.4	2.6 -8.4 2.5 -7.3 2.6 -7.5 2.5 -8.5	1.6 3.1 1.6 3.1 2.6 2.5	1.7 3.2 1.7 3.2 1.7 3.2 1.6 3.1	1.7 3.2 1.7 3.2 1.7 3.2 1.6 3.1
#1 ON #2 ON $\hat{d}=1$			2.6 2.6 2.6 2.5	2.6 2.6 2.6 2.5	2.6 2.5 2.6 2.5	2.6 1.6 3.1 2.6 2.5	2.7 2.6 2.6 2.5	2.6 2.6 2.6 2.5
#1 ON #2 OFF	150 mm (2.7°)	2.8 2.7	2.8 2.7	2.8 2.7	2.8 2.7	2.8 2.7	2.8 2.7	2.8 2.7
#1 ON #2 ON $\hat{d}=2$		2.2 2.3 2.3 2.3	2.1 2.3 2.3 2.3	2.0 2.3 2.3 2.3	2.2 1.0 2.3 -5.8 2.3 -8.0 2.3 -2.6	2.0 3.5 2.3 1.0 2.5 2.3	1.9 3.3 2.0 3.5 1.6 3.0 1.8 3.2	1.8 3.2 2.0 3.5 1.4 2.8 1.5 2.9
#1 ON #2 ON $\hat{d}=1$			2.2 2.3 2.3 2.3	2.2 2.3 2.3 2.3	2.3 2.3 2.3 2.3	2.2 2.3 2.3 2.3	2.2 2.3 2.2 2.2	2.2 2.3 2.2 2.3
#1 ON #2 OFF	100 mm (2.4°)	2.4 2.4	2.4 2.4	2.4 2.4	2.4 2.4	2.4 2.4	2.4 2.5	2.4 2.5
#1 ON #2 ON $\hat{d}=2$		2.0 1.9 1.9 2.0	2.1 1.9 1.9 1.9	2.1 1.9 1.9 1.8	2.0 9.8 1.9 -9.3 1.9 -9.4 2.0 8.8	0.8 2.2 1.9 3.6 1.9 1.9 3.6	0.8 2.2 1.8 3.5 1.8 3.5 1.9 3.5	0.8 2.2 0.8 2.1 0.9 2.2 1.9 3.5
#1 ON #2 ON $\hat{d}=1$			2.0 1.9 2.0 2.0	2.0 1.9 2.0 2.0	2.0 1.9 1.9 2.0	2.0 1.9 1.9 2.0	2.0 2.0 2.0 2.0	2.0 2.0 2.0 2.0

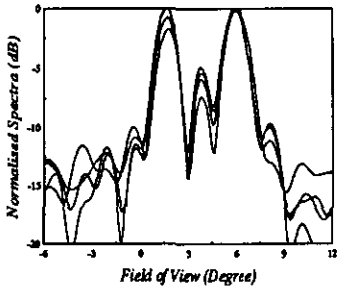

Figure 9.11.1

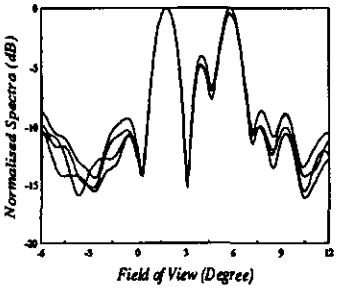

Figure 9.11.2

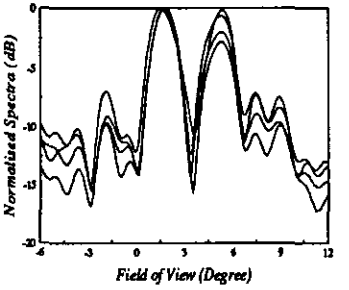

Figure 9.11.3

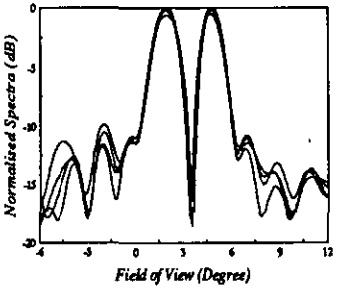

Figure 9.11.4

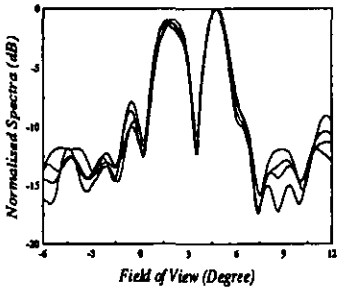

Figure 9.11.5

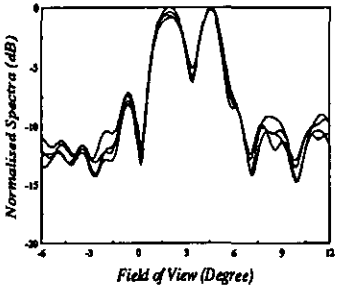

Figure 9.11.6

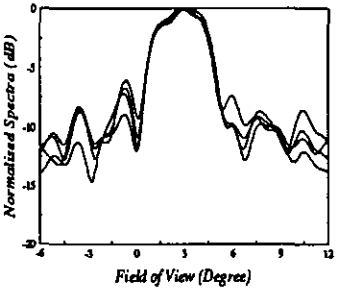

Figure 9.11.7

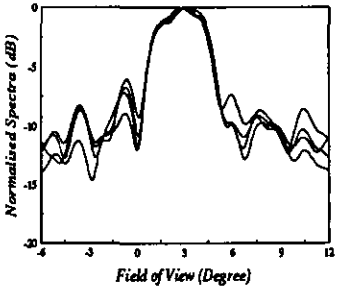

Figure 9.11.8

Figure 9.11 Spectra obtained by the conventional beamforming method

(to be continued)

(continued)

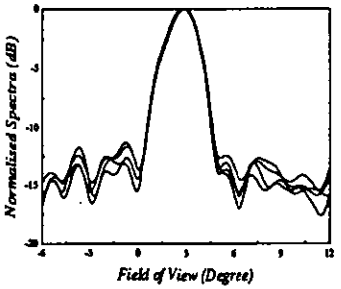

Figure 9.11.9

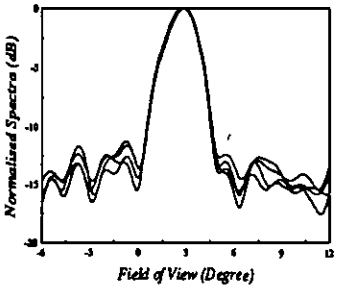

Figure 9.11.10

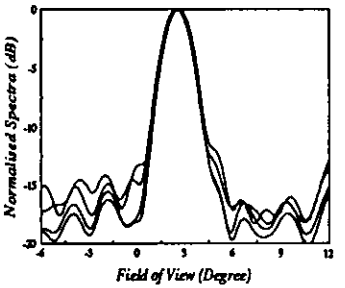

Figure 9.11.11

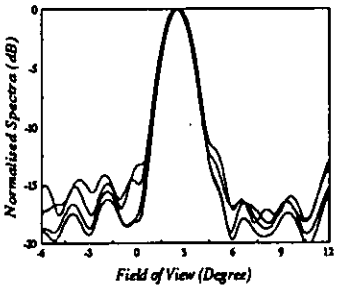

Figure 9.11.12

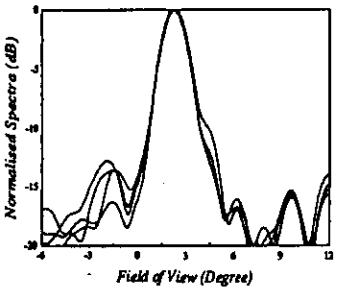

Figure 9.11.13

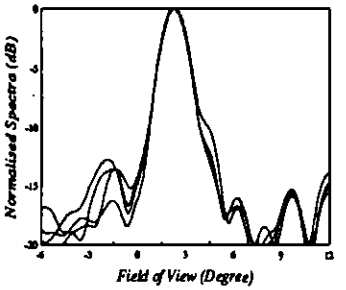

Figure 9.11.14

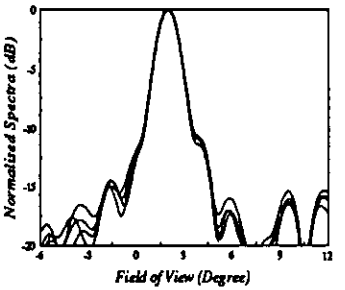

Figure 9.11.15

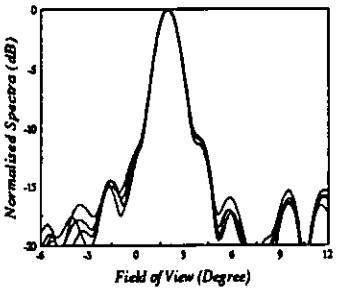

Figure 9.11.16

Figure 9.11 Spectra obtained by the conventional beamforming method

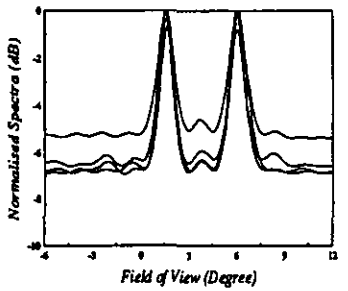

Figure 9.12.1

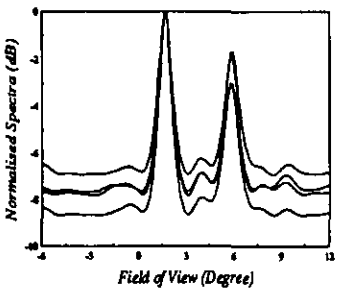

Figure 9.12.2

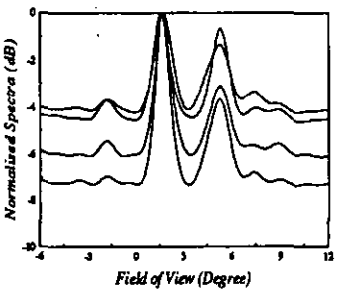

Figure 9.12.3

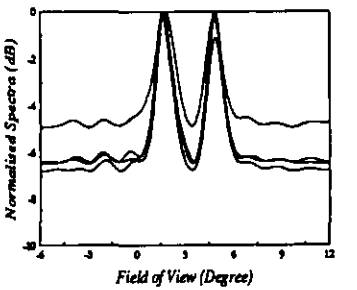

Figure 9.12.4

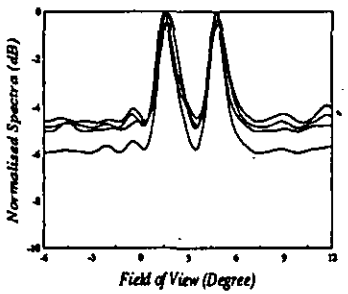

Figure 9.12.5

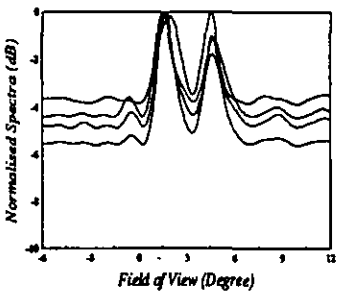

Figure 9.12.6

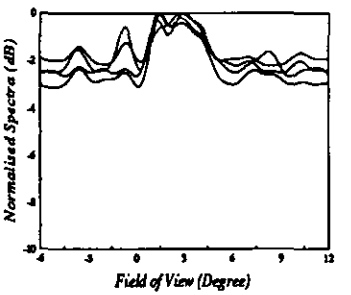

Figure 9.12.7

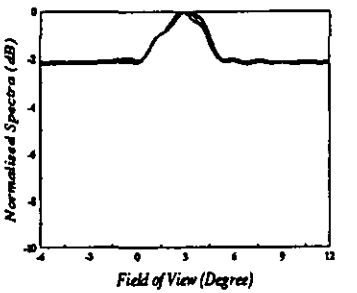

Figure 9.12.8

Figure 9.12 Spectra obtained by the specrtal MUSIC method

(to be continued)

(continued)

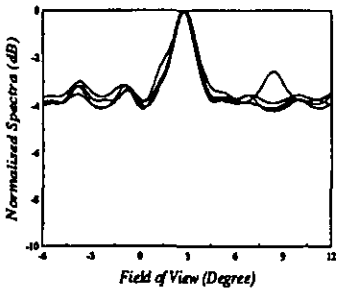

Figure 9.12.9

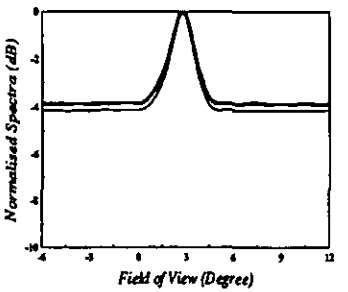

Figure 9.12.10

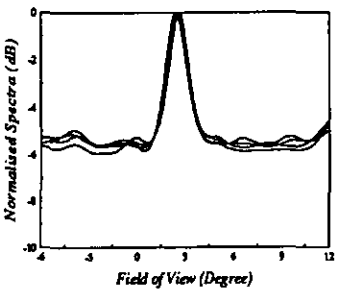

Figure 9.12.11

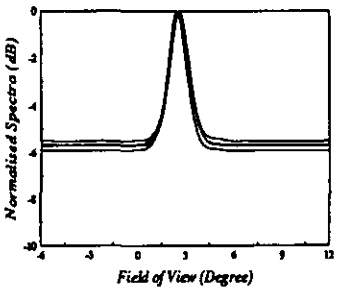

Figure 9.12.12

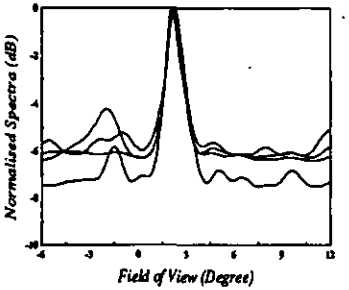

Figure 9.12.13

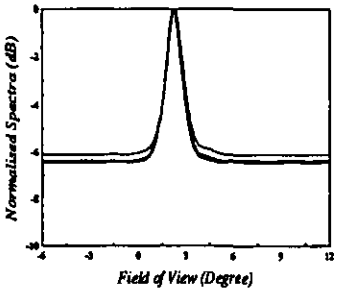

Figure 9.12.14

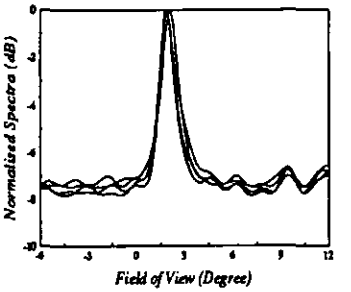

Figure 9.12.15

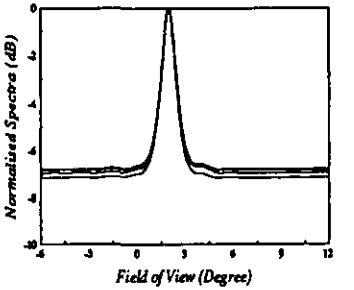

Figure 9.12.16

Figure 9.12 Spectra obtained by the spectral MUSIC method

The number of estimates obtained from the IMP algorithm varied from measurement to measurement, which was believed to be related with the threshold pre-defined in the processing program. And also this indicated that the IMP algorithm was probably unrelated with the number of sources assumed, provided that a more flexible threshold was defined. But this was not the case in the results shown here.

The conventional spectra and the MUSIC spectra of the measurements presented in this section are plotted in figure 9.11 and figure 9.12. The case when a single source was on is not included because good spectra are expected as in the previous section. The first 6 plots in each figure are for the 6 biggest angular separations, from 600 *mm* to 350 *mm*. The other 8 plots are for cases when the angular separations are less that 350 *mm* and the number of sources are alternatively assumed as 2 and 1 (i.e, plots with odd numbers are for the cases when the number of sources is given as 2, and those with even numbers are for those when the number of sources is 1). The CBF spectra did not depend on the number of sources assumed, but the plots were repeated to keep the figure complete.

The two sources working at the same frequency were supposed to be coherent, and the SP-MUSIC, the RT-MUSIC technique, and the ESPRIT methods were expected to be unable to distinguish the two sources even though the source separation was large enough. However, these three methods still showed good results in the experiments presented here. Nevertheless, compared with those results listed in the table 9.3, the performance degradation could be easily seen because of the larger correlation between the two sources.

9.3.3 Experiments, Group 3

This group of experiments is an extension of those in the previous group. The number of source separations was reduced from 11 in last section to 4, which were 400 *mm*, 300 *mm*, 200 *mm*, and 100 *mm*, while more measurements were taken to inspect the algorithm performance in the correlated source cases. For each of 4 separations, 12 measurements were taken. Estimates of the angular locations for all these 12 observations are listed in table 9.5.1 through table 9.5.10, while the first 8 of the spectra obtained from the conventional beamforming method and the SP-MUSIC are plotted in figure 9.13.1 through figure 9.13.10.

Table 9.5.1 Position of Source #2 (the Fixed Source)

No.	CBF	SP-MUSIC	RT-MUSIC	ESPRIT	IMP	ML	WSF
1	1.6	1.6	1.6	1.6	1.6	1.6	1.6
2	1.6	1.6	1.6	1.5	1.6	1.6	1.6
3	1.6	1.6	1.6	1.6	1.6	1.6	1.6
4	1.6	1.6	1.6	1.6	1.6	1.6	1.6
5	1.6	1.6	1.6	1.6	1.6	1.6	1.6
6	1.6	1.6	1.6	1.6	1.6	1.6	1.6
7	1.6	1.6	1.6	1.6	1.6	1.6	1.6
8	1.6	1.6	1.6	1.5	1.6	1.6	1.6
9	1.6	1.6	1.6	1.6	1.6	1.6	1.6
10	1.6	1.6	1.6	1.5	1.6	1.6	1.6
11	1.6	1.6	1.6	1.6	1.6	1.6	1.6
12	1.6	1.6	1.6	1.6	1.6	1.6	1.6

Figure 9.13.1 Spectra Obtained from CBF (on left) and MUSIC (on right)

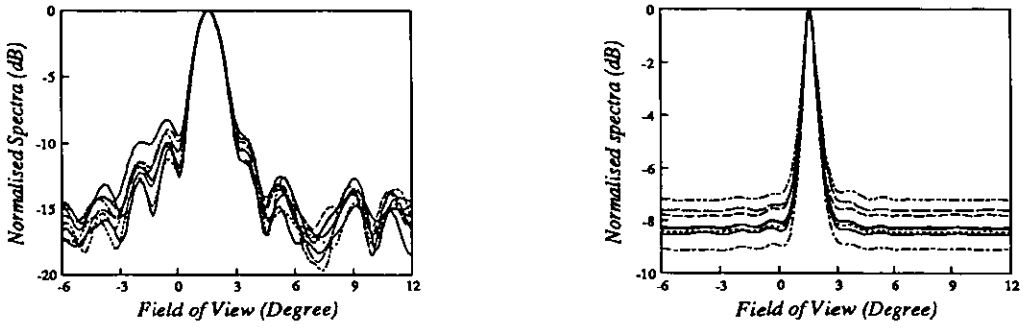

As before, the position of the fixed source was first measured. The results are listed and drawn in table 9.5.1 and figure 9.13.1. The estimates for the source directions were very consistent, as were the estimated spectra. As can be seen from the two plots in figure 9.13.1, the MUSIC spectra were much smoother than the CBF spectra.

Table 9.5.2 represents the estimates of the positions of source #1 when the source separation was given as 400 *mm*, and the corresponding CBF and MUSIC spectra are shown in figure 9.13.2. Good estimates of the position were revealed both from the table and the plots. The situation when both sources were switched at this separation is described in table 9.5.3 and figure 9.13.3. ML and WSF performed well again, and so did IMP which gave very similar estimates except for measurement no.7 where only one source was found by the IMP algorithm. Both CBF and SP-MUSIC behaved very well which can be seen both from the table and the figures. But RT-MUSIC gave some confusion in selecting the estimates. Measurement no.3 resulted in only one estimate with a reasonable modulus, and 4 of other 11 measurements showed two acceptable angular estimates with moduli not being the two biggest ones (denoted by a superscript * in table 9.5.3). ESPRIT did give good estimates in most but not every measurement.

Table 9.5.2 Position of Source 1

No.	CBF	SP-MUSIC	RT-MUSIC	ESPRIT	IMP	ML	WSF
1	4.6	4.6	4.6	4.4	4.6	4.6	4.6
2	4.6	4.6	4.6	4.4	4.6	4.6	4.6
3	4.6	4.6	4.6	4.3	4.6	4.6	4.6
4	4.6	4.6	4.6	4.3	4.6	4.6	4.6
5	4.6	4.6	4.6	4.4	4.6	4.6	4.6
6	4.6	4.6	4.6	4.5	4.6	4.6	4.6
7	4.6	4.6	4.6	4.4	4.6	4.6	4.6
8	4.6	4.6	4.6	4.4	4.6	4.6	4.6
9	4.6	4.6	4.6	4.4	4.6	4.6	4.6
10	4.6	4.6	4.6	4.4	4.6	4.6	4.6
11	4.6	4.6	4.6	4.5	4.6	4.6	4.6
12	4.6	4.6	4.6	4.4	4.6	4.6	4.6

Figure 9.13.2 Spectra Obtained from CBF (on left) and MUSIC (on right)

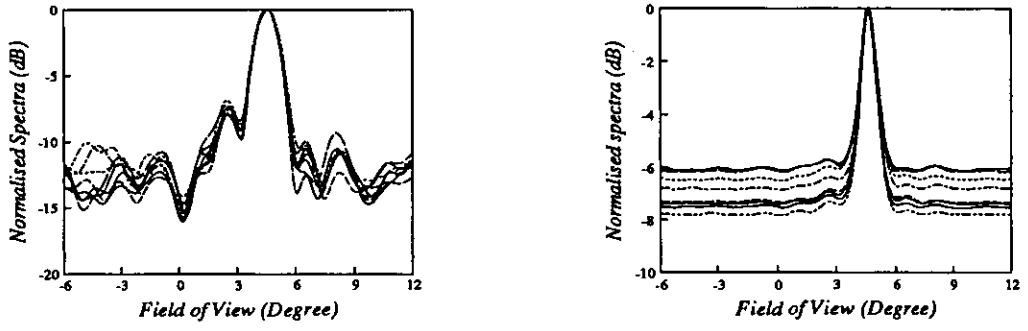

Table 9.5.3 Positions of Both Sources with Separation of 400 mm

No.	CBF	SP-MUSIC	RT-MUSIC	ESPRIT	IMP	ML	WSF
1	1.4 4.5	1.4 4.6	1.4 4.7	2.5 4.2	1.5 4.4	1.5 4.4	1.5 4.3
2	1.4 4.5	1.5 4.5	1.5 4.6	-6.1 2.9	1.5 4.4	1.5 4.4	1.5 4.3
3	1.5 4.5	1.5 4.5	1.4	2.4 3.6	1.5 4.3	1.5 4.3	1.5 4.2
4	1.5 4.5	1.4 4.7	1.4 5.0	2.4 4.2	1.5 4.3	1.5 4.3	1.5 4.3
5	1.4 4.5	1.3 4.6	1.3 4.5*	2.5 5.0	1.4 4.3	1.4 4.3	1.4 4.3
6	1.4 4.6	1.4 4.7	1.4 4.8	-6.2 2.8	1.4 4.4	1.5 4.4	1.4 4.4
7	1.4 4.6	1.4 4.8	1.4 4.9	1.8 4.4	1.4	1.5 4.5	1.5 4.4
8	1.3 4.6	1.3 4.9	1.3 5.0*	1.5 4.6	1.4 4.3	1.4 4.3	1.4 4.3
9	1.4 4.6	1.4 4.8	1.4 4.8*	1.8 4.5	1.5 4.4	1.5 4.4	1.5 4.4
10	1.4 4.5	1.4 4.7	1.4 4.9*	1.4 4.5	1.5 4.3	1.5 4.2	1.5 4.2
11	1.4 4.4	1.4 4.5	1.4 4.5	-1.0 3.0	1.5 4.3	1.4 4.3	1.4 4.3
12	1.4 4.5	1.4 4.8	1.4 5.0	2.0 5.8	1.5 4.2	1.5 4.2	1.5 4.2

Figure 9.13.3 Spectra Obtained from CBF (on left) and MUSIC (on right)

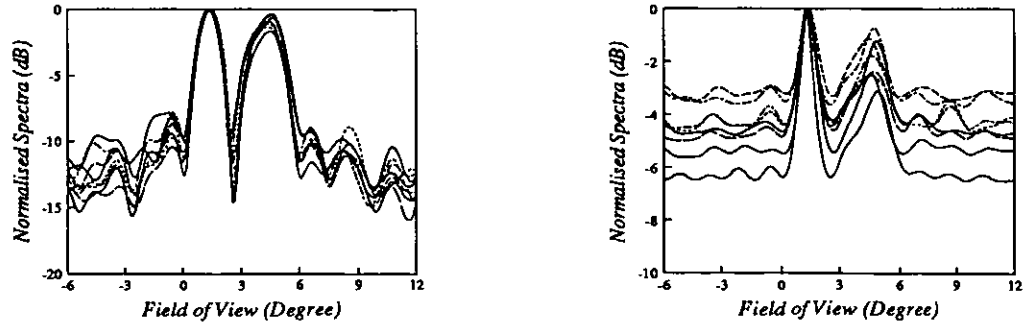

Table 9.5.4 Position of Source 1

No.	CBF	SP-MUSIC	RT-MUSIC	ESPRIT	IMP	ML	WSF
1	4.0	4.0	4.0	3.9	4.0	4.0	4.0
2	3.8	3.8	3.8	3.7	3.8	3.9	3.8
3	4.0	4.0	4.0	3.7	4.0	4.0	4.0
4	3.8	3.8	3.8	3.7	3.8	3.8	3.8
5	3.9	3.9	3.9	3.8	3.9	3.9	3.9
6	3.8	3.8	3.8	3.7	3.8	3.8	3.8
7	3.9	3.9	3.9	3.7	3.9	3.9	3.9
8	3.9	3.9	3.9	3.7	3.9	3.9	3.9
9	3.8	3.8	3.8	3.7	3.8	3.9	3.8
10	3.8	3.8	3.8	3.5	3.8	3.8	3.8
11	3.9	3.9	3.9	3.8	3.9	3.9	3.9
12	3.8	3.8	3.8	3.7	3.8	3.8	3.8

Figure 9.13.4 Spectra Obtained from CBF (on left) and MUSIC (on right)

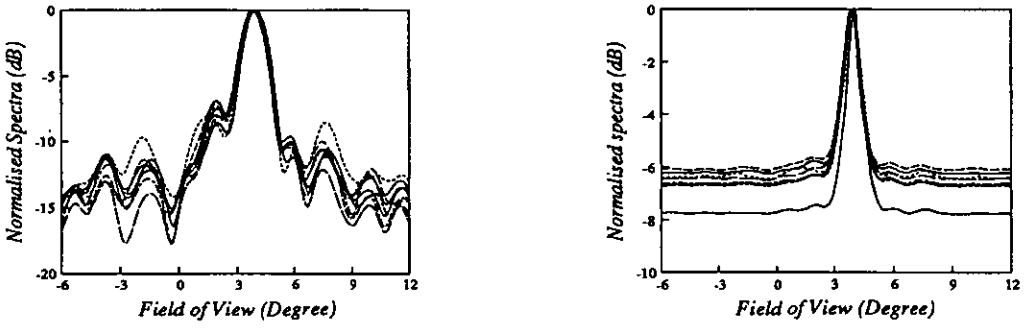

Table 9.5.5 Positions of Both Sources with Separation of 300 mm

No.	CBF	SP-MUSIC	RT-MUSIC	ESPRIT	IMP	ML	WSF
1	1.5 3.8	1.5 4.0	1.5 4.0	2.1 4.7	1.3 3.9	1.3 3.9	1.3 3.9
2	1.5 3.8	1.4 4.0	1.4 4.0	1.0 3.9	1.3 3.9	1.3 3.9	1.3 3.9
3	1.4 3.7	1.4 3.8	1.4 3.8	1.7 4.1	1.3 3.8	1.3 3.8	1.3 3.8
4	1.5 3.8	1.6 3.9	1.6 3.8	2.0 2.6	1.4 3.9	1.4 3.9	1.4 3.9
5	1.5 3.7	1.5 3.7	1.6 3.7	1.2 3.2	1.4 3.8	1.4 3.8	1.4 3.8
6	1.5 3.8	1.4 3.9	1.4 3.9	1.3 3.3	1.4 3.9	1.4 3.9	1.3 3.9
7	1.5 3.8	1.4 3.8	1.4 3.8	0.6 2.8	1.3 3.8	1.3 3.8	1.3 3.8
8	1.5 3.7	1.4 3.8	1.4 3.8	1.7 3.7	1.4 3.8	1.4 3.8	1.4 3.8
9	1.5 3.8	1.4 3.9	1.4 3.9	0.8 3.4	1.4 3.8	1.4 3.8	1.4 3.8
10	1.4 3.7	1.5 3.8	1.5 3.8	2.2 4.0	1.4 3.8	1.4 3.8	1.4 3.8
11	1.4 3.7	1.4 3.9	1.5 3.8	1.6 3.8	1.3 3.8	1.3 3.8	1.3 3.8
12	1.4 3.7	1.4 3.9	1.4 3.9	1.3 3.8	1.3 3.8	1.3 3.8	1.3 3.8

Figure 9.13.5 Spectra Obtained from CBF (on left) and MUSIC (on right)

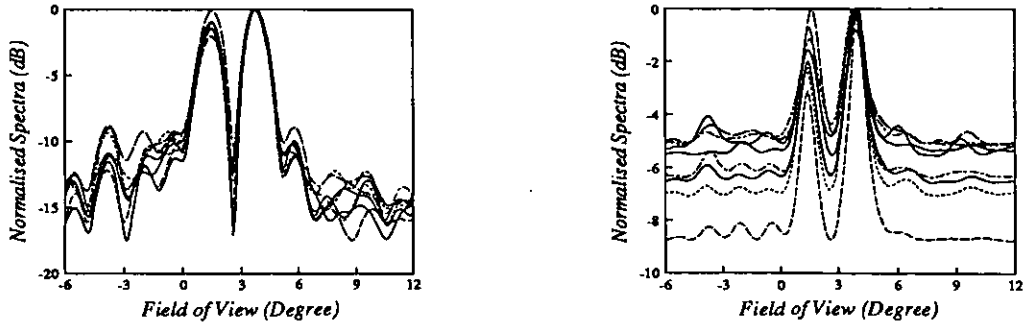

Table 9.5.6 Position of Source 1

No.	CBF	SP-MUSIC	RT-MUSIC	ESPRIT	IMP	ML	WSF
1	3.2	3.2	3.2	3.0	3.2	3.2	3.2
2	3.1	3.1	3.1	2.9	3.1	3.1	3.1
3	3.1	3.1	3.1	3.0	3.1	3.1	3.1
4	3.1	3.1	3.1	3.0	3.1	3.1	3.1
5	3.1	3.1	3.2	3.0	3.1	3.2	3.2
6	3.2	3.2	3.2	3.1	3.2	3.2	3.2
7	3.1	3.1	3.1	3.0	3.1	3.1	3.1
8	3.1	3.1	3.1	3.0	3.1	3.2	3.2
9	3.1	3.1	3.1	3.0	3.1	3.1	3.1
10	3.1	3.1	3.1	2.9	3.1	3.1	3.1
11	3.1	3.1	3.1	3.0	3.1	3.1	3.1
12	3.1	3.1	3.1	2.9	3.1	3.1	3.1

Figure 9.13.6 Spectra Obtained from CBF (on left) and MUSIC (on right)

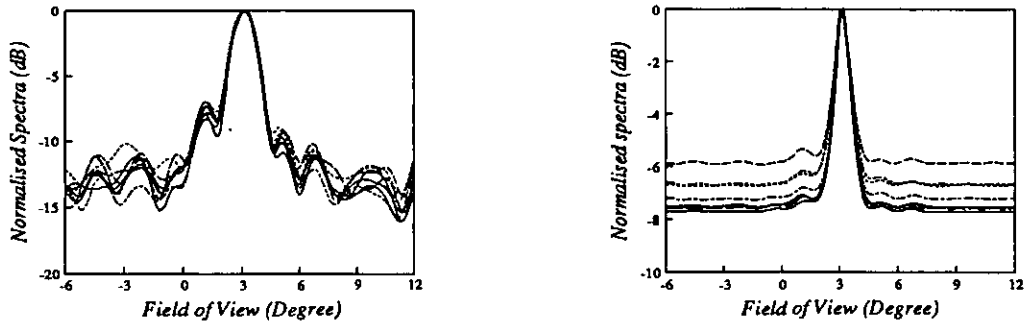

Table 9.5.7 Positions of Both Sources with Separation of 200 mm

No.	CBF	SP-MUSIC	RT-MUSIC	ESPRIT	IMP	ML	WSF
1	1.4 3.2	1.4 3.3	1.4 3.2	2.4 2.8	1.4 3.2	1.4 3.2	1.5 3.2
2	1.4 3.3	1.3 3.4	1.3 3.3	2.3 4.2	1.4 3.3	1.4 3.3	1.4 3.3
3	1.4 3.3	1.4 3.3	1.4 3.4	1.7 3.4	1.4 3.3	1.4 3.3	1.4 3.3
4	1.3 3.1	1.3 3.1	1.3 3.1	0.8 2.4	1.4 3.0	1.4 3.0	1.4 3.0
5	1.3 3.2	1.2 3.1	1.2 3.1	0.4 3.1	1.4 3.1	1.4 3.1	1.4 3.1
6	1.4 3.2	1.4 3.2	1.4 3.2	2.4 4.4	3.2	1.4 3.2	1.4 3.2
7	1.4 3.1	1.4 3.2	1.3 3.2	2.0 3.5	1.3 3.1	1.3 3.1	1.4 3.1
8	1.4 3.1	1.4 3.1	1.4 3.1	2.3 2.4	1.5 3.1	1.4 3.1	1.4 3.1
9	1.4 3.2	1.4 3.2	1.4 3.2	0.6 2.5	1.5 3.2	1.5 3.2	1.5 3.2
10	1.4 3.2	1.4 3.2	1.4 3.3	2.1 3.9	1.4 3.2	1.4 3.2	1.4 3.2
11	1.4 3.2	1.4 3.2	1.4 3.2	2.4 5.3	1.4 3.2	1.4 3.2	1.4 3.2
12	1.4 3.2	1.4 3.2	1.4 3.2	1.4 2.4	1.4 3.2	1.4 3.2	1.4 3.2

Figure 9.13.7 Spectra Obtained from CBF (on left) and MUSIC (on right)

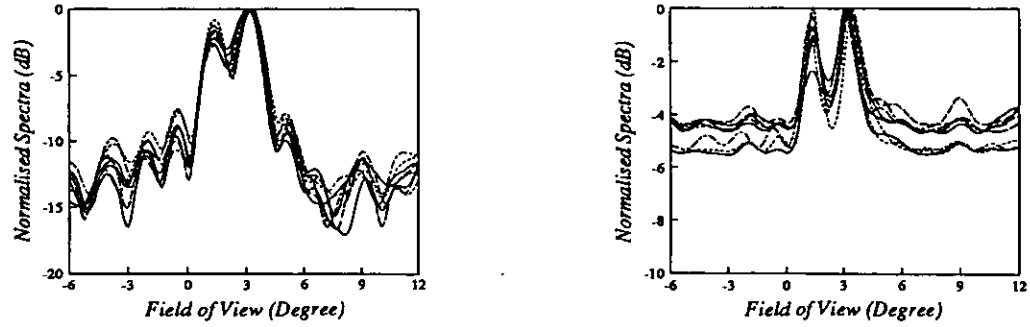

Table 9.5.8 Position of Source 1

No.	CBF	SP-MUSIC	RT-MUSIC	ESPRIT	IMP	ML	WSF
1	2.4	2.4	2.4	2.4	2.4	2.4	3.4
2	2.4	2.4	2.4	2.3	2.4	2.4	2.4
3	2.4	2.4	2.4	2.3	2.4	2.4	2.4
4	2.4	2.4	2.4	2.4	2.4	2.4	2.4
5	2.4	2.4	2.4	2.3	2.4	2.4	2.4
6	2.5	2.5	2.5	2.4	2.5	2.5	2.5
7	2.5	2.5	2.5	2.4	2.5	2.5	2.5
8	2.4	2.4	2.4	2.3	2.4	2.4	2.4
9	2.4	2.4	2.4	2.4	2.4	2.4	2.5
10	2.4	2.4	2.4	2.4	2.4	2.4	2.4
11	2.4	2.4	2.4	2.3	2.4	2.4	2.4
12	2.4	2.4	2.4	2.3	2.4	2.4	2.4

Figure 9.13.8 Spectra Obtained from CBF (on left) and MUSIC (on right)

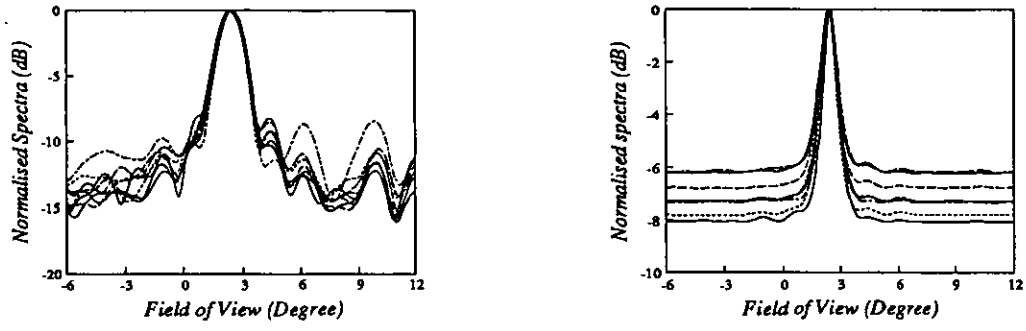

Table 9.5.9 Positions of Both Sources with Separation of 100 mm

No.	CBF	SP-MUSIC	RT-MUSIC	ESPRIT	IMP	ML	WSF
1	2.1	1.8	1.8 2.9	2.1 5.0	2.1	1.8 3.2	1.8 3.2
2	2.1	2.0	2.0	2.2 -10.3	1.8 3.1	1.8 3.2	1.8 3.1
3	2.1	2.0	1.9	2.1 8.3	2.1	1.8 3.2	1.8 3.2
4	2.2	2.1	2.0	2.3 10.5	2.2	1.9 3.3	1.9 3.3
5	2.2	2.1	2.1	2.3 10.3	2.2	1.9 3.2	1.9 3.2
6	2.2	2.1	2.1	2.3 -10.5	2.2	1.9 3.4	1.9 3.4
7	2.1	2.1	2.0	2.3 8.0	2.1	1.8 3.2	1.8 3.2
8	2.0	1.9	1.9	2.1 10.2	1.8 3.2	1.8 3.2	1.8 3.2
9	2.1	2.0	2.0	2.2 0.6	2.1	1.8 3.1	1.8 3.2
10	2.1	1.9	1.9	2.2 5.4	1.8 3.2	1.8 3.1	1.8 3.2
11	2.0	1.9	1.9	2.1 -10.0	2.0	1.8 3.2	1.8 3.2
12	2.1	1.9	1.9	2.2 7.3	2.1	1.8 3.2	1.8 3.2

Figure 9.13.9 Spectra Obtained from CBF (on left) and MUSIC (on right)

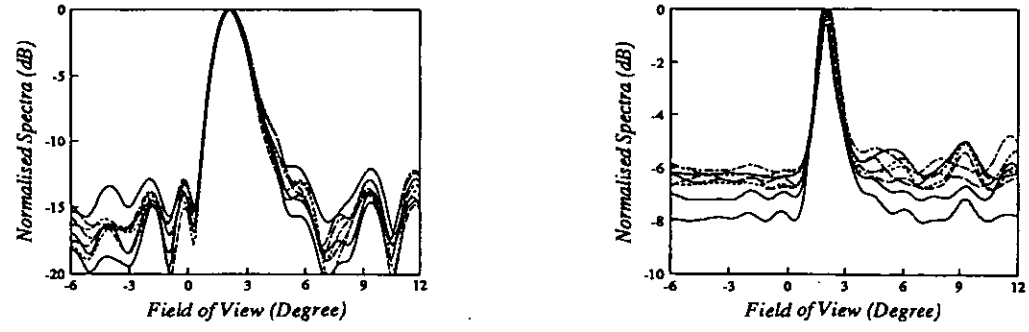

Table 9.5.10 Positions of Both Sources with Separation of 100 mm when the Number of Source was Assumed as 1

No.	SP-MUSIC	RT-MUSIC	ESPRIT	IMP	ML	WSF
1	2.1	2.1	2.2	2.1	2.1	2.1
2	2.1	2.1	2.2	2.1	2.1	2.1
3	2.1	2.1	2.2	2.1	2.1	2.1
4	2.2	2.2	2.3	2.2	2.1	2.2
5	2.2	2.2	2.3	2.2	2.2	2.2
6	2.2	2.2	2.3	2.2	2.2	2.2
7	2.1	2.1	2.2	2.1	2.1	2.1
8	2.1	2.0	2.2	2.0	2.1	2.1
9	2.1	2.1	2.2	2.1	2.1	2.1
10	2.1	2.1	2.2	2.1	2.1	2.1
11	2.0	2.0	2.2	2.0	2.0	2.0
12	2.1	2.1	2.2	2.1	2.1	2.1

Figure 9.13.10 Spectra Obtained from CBF (on left) and MUSIC (on right)

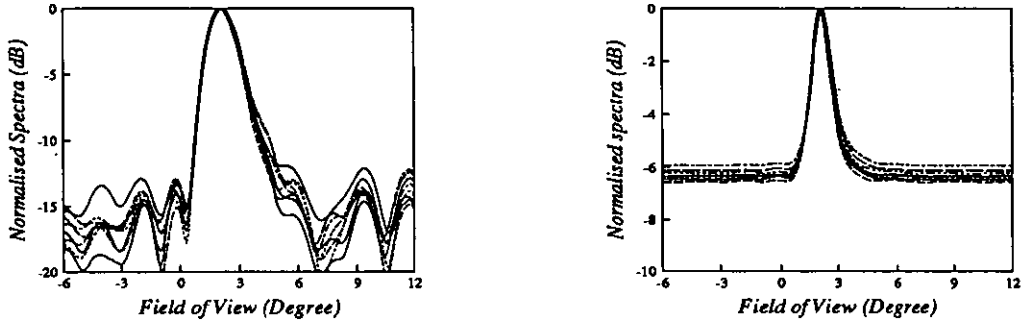

For the separations of 300 *mm* and 200 *mm*, performances from all methods under examination were good, which can be seen from both the tables 9.5.4 to 9.5.7 and the figures 9.13.4 to 9.13.7. This was, however, somehow unexpected from experience in the last section.

As the separation reduced to 100 *mm*, both conventional spectra and the MUSIC spectra depicted a single peak in each of the plots, as shown in figure 9.13.9. RT-MUSIC managed to give two estimates only in one measurement which could be recognized as possible source directions. ESPRIT depicted two estimates but only one of them was acceptable, lying between the two source directions. The IMP algorithm showed three chances of giving two estimates, which were very similar as those given by ML and WSF in the same row. ML and WSF showed two stable estimates in all the 12 measurements.

The last set of measurements was tested under the assumption that only one source was present. The results are presented in table 9.5.10 and figure 9.13.10. All methods show very consistent performance. The CBF spectra plotted in figure 9.13.10 were the same as those in figure 9.13.9, but the MUSIC spectra given in figure 9.13.10 were smoother and the peak positions were more concentrated.

Measurement Groups 2 and 3 were both taken as the responses of the array to the sources which worked as the same frequency. However, only slight difference was shown in the analysed results. Those in the Group 2 were more like the expected results obtained in the situations when the same frequency was used in the two sources; while those in Group 3 were approaching the performance in the situation when the two sources worked at two different frequencies, as discussed in section 9.3.1. Correlation between the two sources needs testing to provide insight into the explanation of the results presented here, which however, is not included in this thesis.

9.3.4 Experiments, Group 4

The experimental results to be presented in this subsection are the results obtained from the target reflections received at the array. Because it was very difficult to put the targets at wanted positions, fewer target separations were considered, compared with the measurements in the passive working mode of the array. For the same reason, the position of the moving target, target #1, was not estimated by removing the other target. Only the cases with both targets present were tested. But the position of the fixed target, target #2, was estimated by taking measurements before adding the second target.

5 target separations were assumed which were 340 *mm*, 270 *mm*, 200 *mm*, 150 *mm*, and 100 *mm*. For each separation, 12 measurements were taken. The corresponding results by applying different algorithm are shown in table 9.6, and the spectra from the conventional beamformer and from the spectral MUSIC method are plotted in figure 9.14 and figure 9.15.

Target #2 was positioned by the estimates given in the first block in table 9.6. All seven methods used in the analysis gave very good estimates which were consistent from method to method and also from measurement to measurement. Only 2 measurements among the 12 failed the IMP algorithm. No peak was found in the spectrum at the first stage of the algorithm. Actually the first stage of the IMP algorithm was the conventional beam-scan, which found peaks in all the 12 measurements as shown in table 9.6 and in figure 9.14. The failure of the IMP algorithm was thought to be caused by the threshold defined in the processing programs, which was related with the number of sensors in the array, number of snapshots, and noise variance estimate. The peak level found in the first stage of IMP was compared with the threshold, and only if this peak was higher would the peak be accepted as an estimate, otherwise the no peak was assumed to be found.

This problem with the IMP algorithm was observed in the case when both targets were on and the target separation was 340 *mm*. Whilst all other methods gave very good estimates of both target positions, the IMP algorithm failed several times by giving only one estimate or even none at all. It seemed an adjustment in defining the threshold was necessary to guarantee the performance of the IMP method to be at least as good as the conventional beamforming method, which was the basis of the high resolution IMP algorithm.

As the separation decreased to 270 *mm*, the situation in the results was similar to the previous separation. CBF, SP-MUSIC, RT-MUSIC, and the two multidimensional approaches, ML and WSF showed very consistent estimates, while the ESPRIT method gave estimates with bigger arbitrary. The performance showed by the IMP algorithm seemed better compared to the case of 340 *mm* separation. Half of the measurements were found to give similar results with ML and WSF, while the other half showed only one estimate in each measurement.

When target #1 was moved nearer to target #2 with a separation of 200 *mm*, the conventional method failed to resolve the two targets. But all other methods showed the ability to separate the two targets. Estimates given by ESPRIT were less convincing for several measurements while those from the other five methods were excellent.

Referred to figure 9.15.4 where the MUSIC spectra were shown, the peaks on the left were not of great enough height above the nulls between the two peaks. Comparing the estimates from CBF and those from ML or WSF, it was found that the estimates given by the conventional beamforming method were almost equal to one of the estimates rather than falling in some direction between the two estimates. It was suspected that one of the targets reflected weak signals which made the conventional beamforming method, the target strength-sensitive method, "ignore" the existence of such a target.

At the even smaller separation of 150 *mm*, the conventional beamforming method surprisingly showed double humps which were of similar heights, as showed in figure 9.14.5. The MUSIC spectra were similar but having a smoother background. IMP, ML, and WSF again depicted very similar results except one measurement where only one estimate was shown by IMP, which was the corresponding CBF estimate with the global maximum value. Estimates from ESPRIT, however, changed a lot between measurements.

At the smallest separation in this group of experiments, 100 *mm*, ML and WSF still managed to give two reasonable estimates in all measurements with good consistency. Most of the

Table 9.6. Results when two targets were in use

Target State	Emitter Separation	CBF	SP-MUSIC	RT-MUSIC	ESPRIT	IMP	ML	WSF
#2 ON #1 OFF		0.5 0.4 0.5 0.6 0.6 0.6 0.6 0.6 0.6 0.5 0.4 0.7	0.5 0.4 0.5 0.6 0.6 0.6 0.6 0.6 0.7 0.5 0.4 0.7	0.4 0.4 0.5 0.6 0.6 0.6 0.6 0.6 0.9 0.5 0.4 0.7	0.5 0.4 0.4 0.5 0.7 0.6 0.5 0.6 0.8 0.4 0.5 0.7	0.5 0.4 0.5 0.6 0.6 0.6 0.6 [] [] 0.5 0.4 0.7	0.5 0.4 0.5 0.6 0.6 0.6 0.6 0.6 0.6 0.5 0.4 0.7	0.5 0.4 0.5 0.6 0.6 0.6 0.6 0.6 0.7 0.5 0.4 0.7
#1 ON #2 ON	340 mm	-3.0 0.0 -3.0 0.3 -3.1 0.3 -2.9 0.0 -3.0 0.3 -3.1 0.2 -3.0 0.3 -3.0 -0.2 -2.9 0.0 -2.7 -0.1 -3.1 0.0 -3.2 0.3	-3.1 0.1 -3.1 0.4 -3.1 0.4 -2.9 0.3 -3.1 0.4 -3.2 0.3 -3.1 0.4 -3.1 -0.2 -3.0 0.6 -2.9 0.3 -3.3 0.0 -3.2 0.3	-3.1 0.1 -3.1 0.3 -3.1 0.4 -2.9 0.3 -3.2 0.4 -3.1 0.3 -3.1 0.4 -3.0 -0.3 -3.0 0.7 -2.9 -0.2 -3.4 0.0 -3.2 0.3	-3.2 0.5 -3.2 1.0 -3.2 0.3 -3.1 0.5 -3.2 0.8 -3.3 0.5 -3.2 0.5 -2.9 0.7 -3.2 0.8 -3.0 0.7 -3.2 0.3 -3.1 0.5	[] -3.0 0.3 -3.1 0.3 -2.9 -3.0 0.3 -3.1 0.2 -3.0 -3.0 -2.9 -2.9 0.2 [] []	-3.0 0.1 -3.0 0.3 -3.1 0.3 -2.9 0.2 -3.0 0.3 -3.0 0.2 -3.0 0.3 -3.1 0.0 -2.9 0.2 -2.8 0.2 -3.1 0.0 -3.2 0.3	-3.0 0.1 -3.0 0.3 -3.1 0.3 -2.9 0.2 -3.0 0.3 -3.1 0.2 -3.0 0.3 -3.1 0.0 -2.9 0.1 -2.8 0.2 -3.1 0.0 -3.1 0.3
#1 ON #2 ON	270 mm	-2.3 0.3 -2.2 0.0 -2.3 0.1 -2.4 0.0 -2.2 0.2 -2.2 0.0 -2.2 0.1 -2.2 0.0 -2.3 0.0 -2.4 0.0 -2.4 -0.1 -2.3 0.1	-2.3 0.7 -2.3 0.3 -2.4 0.2 -2.5 0.2 -2.2 0.3 -2.3 0.1 -2.3 0.2 -2.3 0.1 -2.4 0.1 -2.4 0.2 -2.4 0.3 -2.3 0.3	-2.3 0.7 -2.3 0.1 -2.4 0.2 -2.5 0.2 -2.2 0.1 -2.3 0.0 -2.3 0.1 -2.3 0.0 -2.4 0.1 -2.4 0.1 -2.4 0.0 -2.3 0.1	-2.2 0.8 -2.1 1.0 -2.7 0.2 -2.7 0.4 -1.9 1.3 -2.0 0.4 -2.0 0.8 -2.2 0.9 -2.4 0.6 -2.3 1.1 -2.3 0.8 -2.3 1.1	-2.3 -2.2 -2.5 0.2 -2.6 0.2 -2.2 -2.2 -2.2 -2.2 -2.5 0.1 -2.5 0.1 -2.5 0.2 -2.4 0.3	-2.4 0.6 -2.4 0.2 -2.5 0.2 -2.6 0.2 -2.3 0.4 -2.4 0.3 -2.4 0.2 -2.3 0.1 -2.5 0.1 -2.5 0.1 -2.5 0.1 -2.4 0.3	-2.4 0.6 -2.4 0.2 -2.5 0.2 -2.6 0.2 -2.3 0.4 -2.4 0.3 -2.4 0.2 -2.4 0.1 -2.5 0.1 -2.5 0.1 -2.5 0.1 -2.4 0.3

(to be continued)

(continued)

Target State	Emitter Separation	CBF	SP-MUSIC	RT-MUSIC	ESPRIT	IMP	ML	WSF
#1 ON	200 mm	-0.3	-1.7 -0.2	-1.9 -0.2	-1.8 0.3	-1.8 -0.1	-1.9 -0.1	-1.9 -0.1
#2 ON		-0.5	-2.4 -0.5	-2.5 -0.4	-0.7 0.1	-2.2 -0.4	-2.1 -0.3	-2.1 -0.3
		-0.3	-2.2 -0.3	-2.3 -0.3	0.9 0.7	-2.0 -0.2	-2.0 -0.2	-2.0 -0.2
		-0.3	-2.2 -0.3	-2.2 -0.3	-2.0 0.0	-2.2 -0.3	-2.1 -0.2	-2.1 -0.2
		-0.2	-2.2 -0.1	-2.1 -0.1	0.0 -2.1	-2.0 -0.1	-2.0 -0.1	-2.0 -0.1
		-0.4	-2.1 -0.3	-2.2 -0.3	-0.8 1.1	-2.2 -0.3	-2.1 -0.2	-2.1 -0.2
		-0.2	-2.2 -0.2	-2.2 -0.2	-2.5 0.0	-2.1 -0.2	-2.1 -0.2	-2.1 -0.2
		-0.2	-2.1 -0.2	-2.1 -0.2	-1.1 -0.2	-2.1 -0.2	-2.0 -0.1	-2.0 -0.1
		-0.3	-2.2 -0.2	-2.2 -0.2	-2.2 -0.1	-2.1 -0.2	-2.2 -0.2	-2.2 -0.2
		-0.2	-2.0 -0.1	-2.1 -0.1	-1.9 0.1	-2.0 -0.1	-2.0 -0.1	-2.0 -0.1
		-0.1	-1.8 0.1	-2.0 0.1	-1.9 0.3	-1.8 0.1	-1.7 0.2	-1.7 0.2
		-0.2	-2.0 0.1	-2.0 -0.1	-2.1 0.1	-2.0 -0.1	-2.0 -0.1	-2.0 -0.1
#1 ON	150 mm	-1.4 0.1	-1.5 0.2	-1.5 0.1	-0.8 1.6	-1.5 0.1	-1.5 0.1	-1.4 0.2
#2 ON		-1.5 0.2	-1.5 0.2	-1.5 0.2	-0.8 3.2	-1.5 0.3	-1.5 0.3	-1.5 0.3
		-1.3 0.2	-1.5 0.2	-1.5 0.1	-1.7 0.8	-1.3 0.1	-1.3 0.1	-1.3 0.2
		-1.5 0.1	-1.4 0.2	-1.5 0.1	-1.0 1.4	-1.5 0.1	-1.5 0.1	-1.5 0.1
		-1.4 0.2	- 1.4 0.2	-1.5 0.2	-1.0 0.9	-1.4 0.2	-1.4 0.2	-1.4 0.2
		-1.3 0.3	-1.4 0.3	-1.5 0.3	-0.2 2.9	-1.3 0.3	-1.3 0.3	-1.3 0.3
		-1.4 0.2	-1.4 0.3	-1.5 0.2	-0.6 0.2	-1.3 0.2	-1.3 0.2	-1.2 0.2
		-1.5 0.2	-1.5 0.2	-1.6 0.1	-0.5 3.9	-1.4 0.1	-1.4 0.1	-1.3 0.1
		-1.3 0.2	-1.4 0.3	-1.5 0.3	-0.5 1.9	0.2	-1.4 0.3	-1.3 0.3
		-1.4 0.3	-1.5 0.3	-1.5 0.3	-0.5 3.4	-1.3 0.3	-1.3 0.3	-1.3 0.3
		-1.4 0.2	-1.4 0.3	-1.5 0.2	-1.2 0.6	-1.3 0.2	-1.3 0.2	-1.3 0.2
		-1.2 0.3	-1.6 0.3	-1.6 0.2	-2.5 0.3	-1.3 0.3	-1.2 0.3	-1.1 0.3
#1 ON	100 mm	-0.2	-0.3 1.2	-0.4 1.3	-0.3 1.4	-0.2	-0.4 1.2	-0.4 1.3
#2 ON		-0.3	-0.3	-0.4	-0.2 3.0	-0.3	-0.5 1.0	-0.5 1.0
		-0.2	-0.2	-0.3	0.0 8.2	-0.4 1.1	-0.4 1.1	-0.4 1.1
		-0.2	-0.4	-0.4 1.1	0.0 2.7	-0.3 1.4	-0.4 1.2	-0.4 1.2
		-0.2	-0.2	-0.2 1.3	0.0 6.0	-0.3 1.2	-0.3 1.2	-0.3 1.2
		-0.2	-0.3	-0.3	0.0 9.7	-0.4 1.2	-0.4 1.2	-0.4 1.2
		-0.2	-0.5 1.1	-0.5 1.1	-0.5 1.7	-0.5 1.2	-0.5 1.2	-0.5 1.2
		-0.3	-0.4	-0.4	-0.3 4.7	-0.3	-0.5 1.1	-0.5 1.1
		-0.2	-0.2	-0.2	-0.1 9.8	-0.4 1.1	-0.4 1.1	-0.4 1.1
		-0.1	-0.2	-0.4	0.0 8.9	-0.4 1.1	-0.4 1.0	-0.4 1.1
		-0.1	-0.3	-0.3	0.0 5.2	-0.4 1.2	-0.5 1.1	-0.4 1.1
		-0.2	-0.4	-0.4	-0.1 2.7	-0.3 1.4	-0.4 1.3	-0.4 1.3

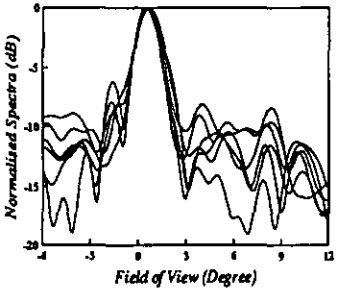

Figure 9.14.1

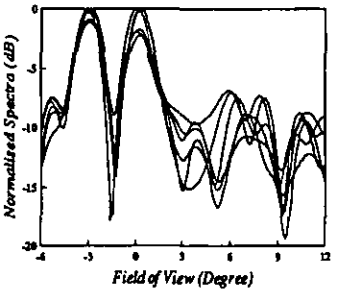

Figure 9.14.2

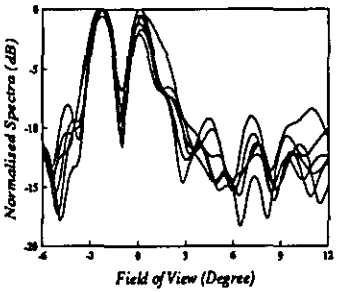

Figure 9.14.3

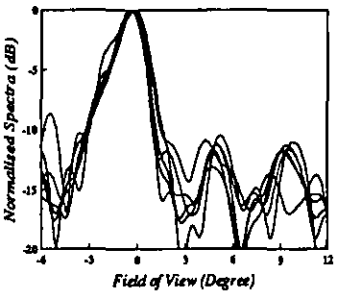

Figure 9.14.4

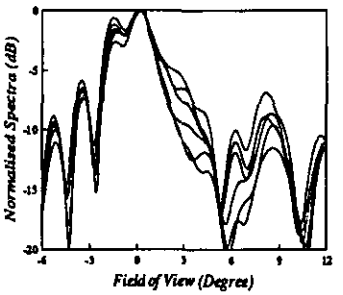

Figure 9.14.5

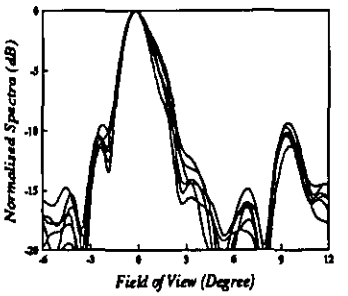

Figure 9.14.6

Figure 9.14 Spectra obtained by the conventional beamforming method

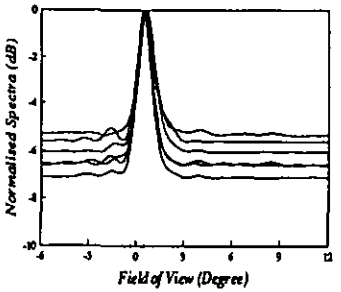

Figure 9.15.1

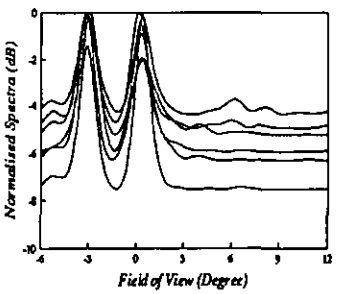

Figure 9.15.2

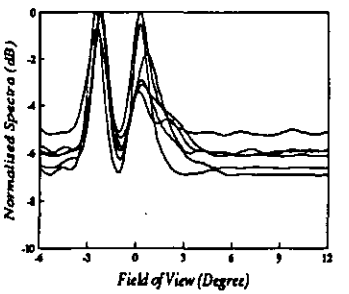

Figure 9.15.3

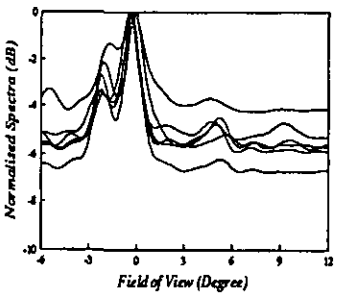

Figure 9.15.4

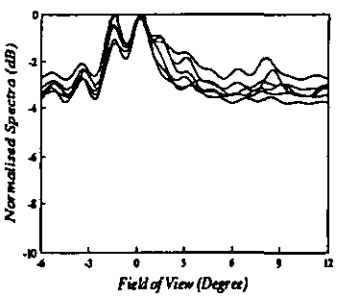

Figure 9.15.5

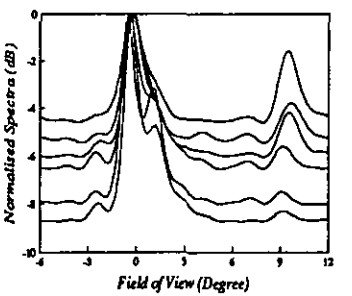

Figure 9.15.6

Figure 9.15 Spectra obtained by the spectral MUSIC method

IMP estimates were also quite good while others were similar to the CBF estimates. Both MUSIC methods showed resolving abilities on only a few occasions. Although two estimates in each measurement were listed for ESPRIT, few of them gave two meaningful estimates.

Through the experimental analysis in this subsection, the RT-MUSIC had the same problem as that explained earlier. Not all the biggest moduli corresponded to the angular estimates which were more likely to be the target position estimates from the "prior knowledge". More than two estimates had similar values of moduli. The results listed in the RT-MUSIC column were chosen mainly according to the values of angular estimates.

9.4 Conclusion

Results from practical measurements have been presented in this chapter. The aim was to investigate the performance of the algorithms, which have been previously analysed and simulated, with practically sampled data rather than the more ideal data in simulations. Situations when sources and targets were used have been considered. A large amount of data was obtained, analysed, and presented in the previous section. The results presented therein showed the superior performance of the multidimensional methods over the more conventional methods such as CBF, MUSIC, and ESPRIT. Especially the ML and the optimal WSF methods depicted stable and reliable abilities to estimate the source / target directions under all the circumstances considered in this thesis.

CHAPTER 10

CONCLUSION AND SUGGESTION FOR FURTHER WORK

The task of the research in this thesis was to investigate the performance of direction finding algorithms applied to sonar signal processing. This has been accomplished mainly by computer simulations and analysis of practical measurements from an air acoustic sonar array, together with some theoretical discussions. The current chapter is devoted to the conclusion of the work and suggestions for further work in this and relevant fields.

10.1 Conclusion of the Work in this Thesis

The algorithms included in the study of this thesis are representatives of each class of methods, which, so far have been either widely used (such as the conventional beamforming method), or extensively studied theoretically (such as the well studied MUSIC technique and the recently proposed Weighted Subspace Fitting (WSF) methods). Computer simulation provides a more visual way for the examination of performance than the mathematical expressions, and more factors that affect the performance of the algorithms can be considered. On the other hand, analysis of practical measurements allows the algorithms to be explored in an environment which is nearer to the "destination".

The simulations in this thesis mainly concern three statistics that are very important in evaluating algorithms: probability of resolution, bias of estimated angles, and their standard deviations. They are studied as functions of the signal to noise ratio and the angular separation between the two sources, respectively. The same set-up of parameters has been used throughout the simulations of all algorithms and, for the multidimensional approaches, more situations were tested. This was motivated by the thought of testing the optimal methods with "bad data".

In the computer simulations, MEM, MVM, MNM, and MUSIC and their root versions were first examined and the MUSIC techniques were chosen as "models" to be compared with the ESPRIT algorithm and the IMP algorithm respectively, because of the lowest standard deviations in both versions as functions of signal to noise ratio and those of angular separations. For the ESPRIT technique, only one subarray displacement vector was considered which was the one with the maximum over lapping subarrays in the uniform linear array with half wavelength spacing. The asymptotic properties of ESPRIT were found to be very similar to those of the MUSIC methods while its probability of resolution is almost the same as the root MUSIC method, which is higher than that of the spectral MUSIC method.

The IMP algorithm provides high resolution ability by re-processing the observed data and is also able to handle coherent sources at the cost of a heavy computation burden. The ability of the IMP algorithm to detect and estimate sources simultaneously is not evident from the simulations since the order of the model was given and the data was rather "ideal". The number of estimates was the same as that of the order of model throughout the computer simulations. However, this is not the same when the IMP algorithm is applied to the practical measurements.

Both ML and optimal WSF methods gave excellent results in the computer simulations. More simulated date was tested, besides that for other methods, to examine the behaviour of these two methods in "bad" simulations. One factor which needs more attention in implementing these multidimensional methods is the computation load.

The analysis of practical measurements gives an idea of the algorithm performance in reality. All the methods under examination show very consistent results with those in the simulations, although some exceptions exist due to the measurement environment and experimental system.

As can be seen from the experimental results, the conventional beamforming method (CBF) provided reasonably good direction estimates. The beam-width of the employed array was very narrow because the aperture of the array was large in the metric of wavelength (15 transducers were used in array with inter-element spacing of 2.7 wavelengths). This allowed the CBF method to separate closely placed sources / targets.

Although the spectral MUSIC technique did not show significant advantages over the CBF method in the experiments shown in this thesis due to the directivity of the array, it still can

be seen that spectral MUSIC was superior in the sense of providing sharper peaks and smoother background. Also, the spectral MUSIC method failed to separate the two sources / targets as a smaller separation compared to the CBF method. It is certain that the advantages of the spectral MUSIC method over the CBF method will be shown when an array with a small aperture is used. However, this advantages can only be achieved at the cost of a heavier computation burden, which was the case in the analysis here.

The root MUSIC showed similar performance to that of the spectral MUSIC. Although it was found in both the theoretical analysis and the computer simulation that the resolution threshold of the root MUSIC is lower than that of the spectral MUSIC, it was not the case in the practical experiment analysis. The processing speed was higher due to the lack of the eigen-decomposition of the sample covariance matrix, but the order of the polynomial were high since the number of sensors in the array was large. The main problem with the root MUSIC was thought to be the selection of the possible direction estimates from all roots of the polynomial, especially when the angular separation of the two sources / targets was small.

Comparatively, the performance of ESPRIT was slightly disappointing. The noise field was suspected to be the main reason for this performance degradation. This method is less appealing than the conventional beamforming method and the MUSIC techniques.

The IMP algorithm consumed more time than other methods in the data processing. For most measurements, the results from the IMP algorithm were excellent and very similar to those from the ML and the optimal WSF methods; while in other cases the results were less satisfying. There were cases where no peak was found by the IMP algorithm when all other methods were able to give very good estimates. The threshold in the processing was believed to be the key for this problem. A more flexible threshold is required to guarantee the IMP algorithm to perform at least as well as the CBF method, which is the basis of the IMP algorithm. The ability of the IMP algorithm to estimate the number of sources / targets simultaneously when estimating their directions was not demonstrated in the experimental results presented here. But several measurements gave some evidence to this ability by providing results that were not dependent on the number of sources / targets.

For all experiments, the ML and the optimal WSF methods gave the most stable and the most consistent results even when the angular separation of the two sources / targets was very

small. The complex computations of the multidimensional search inherent in these two methods were not a big problem in off-line processing. Their excellent performance deserves effort for real-time implementation.

10.2 Suggestion for Further Work

Several aspects need attention in the future work in this field and its possible applications to other relevant research areas.

The algorithm performance as functions of number of snapshots is interesting, since too many snapshots are impractical in real implementation. A trade-off between the number of snapshots and the performance is required in practical systems.

The properties of sources / targets are also helpful in the analysis of practical observations, especially those of the targets. A better way of placing the targets in the experiments is needed so as to eliminate effects which might cause confusion in explaining the results, such as the narrow directivity of the targets and the edges of the targets.

All transducers and the channels in the measurement system were tested before the data acquisition. Good consistency between transducers and between channels was ensured. However, no array calibration has been carried out for the air acoustic array which was used for the practical data collection. The final performance of algorithms might degrade due to the assumption of a perfect array and sensors while faulty sensors are always possible.

The newly suggested WSF methods are quite promising and provide excellent results even when all other methods fail. A disadvantage inherent in this class of methods is the computational complexity, which in not difficult when using off-line processing, but is problematical in real-time implementation. Mathematical algorithms are required and high speed processing technique, such as the parallel structure, is a promising solution. At the same time, new techniques for hardware could also meet some need in the processing.

When applied to other areas, the choice of the available algorithms should be made according to the special needs in that application. Super resolution is not the utmost judgment of an algorithm. To provide a means for this task, more simulations are needed and the variables in the simulations are task subjective. Only after an intensive study of the algorithms, could an appropriate choice be made.

REFERENCES

[And63] Anderson, T.W.
Asymptotic theory for principal component analysis
Ann. Math. Statist., Vol.34, pp.122-148, 1963

[And69] Anderson, V.C.
DICANNE, a realizable adaptive process
J. Acoust. Soc. Amer., Vol.45, pp.398-405, 1969

[Aka73] Akaike, H.
Information theory and an extension of the maximum likelihood principle
Proc. 2th Int. Symp. Inform. Theory, pp.267-281, 1973

[Aka74] Akaike, H.
A new look at the statistical model identification
IEEE Trans. AC-19, pp.716-723, 1974

[Bar83] Barabell, A.J.
Improving the resolution performance of eigenstructure-based direction-finding algorithms
Proc. ICASSP'83, pp.336-339, 1983

[BLP86] Barboy, B., Lomes, A., Perkalski, E.
Cell-averaging CFAR for multiple-target situations
Proc. IEE Vol.133, Pt.F, No.2, pp.176-186, 1986

[Ber75] Berni, A.J.
Target identification by natural resonance estimation
IEEE Trans. AES-11, pp.147-154, 1975

[BK80] Bienvenu, G., Kopp, L.
Adaptivity to background noise spatial coherence for high resolution passive methods
Proc. ICASSP'80, pp.307-310, 1980

[Boh87] Bohme, J.F.
Accuracy of maximum likelihood estimates for array processing
Proc. ICASSP'87, pp.2015-2018, 1987

[BM86] Bresler, Y., Macovski, A.
Exact maximum likelihood parameter estimation of superimposed exponential signals in noise
IEEE Trans. ASSP-34, pp.1081-1089, 1986

[Bri75] Brillinger, D.R.
Time series: data analysis and theory
Holt, Rinehart and Winston, 1975

[BX90a] Buckley, K.M., Xu. X.L.
Recent advances in high resolution spatial-spectrum estimation
Proc. EUSIPCO-90, Fifth European Signal Processing Conference, Barcelona, Spain, pp17-25, 1990

[BX90b] Buckley, K.M., Xu. X.L.
Spatial-spectrum estimation in a location sector
IEEE Trans. ASSP-38(11), pp.1842-1852, 1990

[Bur67] Burg, J.P.
Maximum entropy spectral analysis
Proc. of the 37th Meeting of the Society of Exploration Geophysicists, 1967

[Bur68] Burg, J.P.
A new analysis technique for time series data
NATO Advanced Study Institute on Signal Processing with Emphasis on Underwater Acoustics, pp.12-23, 1968

[Bur72] Burg, J.P.
The relationship between maximum entropy spectra and maximum likelihood spectra
Geophysics 37(2), pp.375-376, 1972

[Cad88] Cadzow, J.A.
A high resolution direction-of-arrival algorithm for narrow-band coherent and incoherent sources
IEEE Trans. ASSP-36(7), pp.965-979, 1988

[Cap69] Capon, J.
High-resolution frequency-wavenumber spectrum analysis
Proc. IEEE Vol.57, pp.1408-1418, 1969

[Cla87] Clarke, I. J.
Robustness of eigen based analysis techniques versus iterative adaptation
RADAR-87 IEE Conference Publication No. 281, pp.84-88, 1987

[Cla88] Clarke, I. J.
High discrimination detection bound and model order control
Proc. SPIE 975, Advanced Algorithms and Architectures for Signal Processing (3), pp.344-351, 1988

[Cla89] Clarke, I. J.
High discrimination target detection algorithms and estimation of parameters
Y.T.Chan(ed.) Underwater Acoustic Data Processing, pp.273-277, 1989

[Cra61] Cramer, H.
Mathematical methods of statistics
Princeton University Press, 1961

[DJ85] De Graaf, S.R., Johnson, D.H.
Capability of array processing algorithms to estimate source bearings
IEEE Trans. ASSP-33(6), pp.1368-1379, 1985

[DS83] Dennis, J.E., Schnabel, R.B.
Numerical methods for unconstrained optimisation and nonlinear equations
Prentice Hall, Englewood Cliffs, NJ., 1983

[Ell81] Elliott, R.S.
Antenna theory and design
Prentice-Hall, Inc., Englewood Cliffs, N.J.07632, 1981

[EJS81] Evans, J.E., Johnson, J.R., Sun, D.F.
High resolution angular spectrum estimation techniques for terrain scattering analysis and angle of arrival estimation
Proc. 1st ASSP workshop on Spectral Estimation, pp.134-139, Aug. 1981

[EJS85] Evans, J.E., Johnson, J.R., Sun, D.F.
Applications of advanced signal processing techniques to angle of arrival estimation in ATC navigation and surveillance systems
M.I.T. Lincoln Lab. Lexington, MA, Tech. Rep. 582 Oct. 1985

[FM86] Farrier, D.R., Mcleod, F.N.
Direct estimation of multipath signals
Proc. ICASSP'86 Vol.4, pp.2827-2830, 1986

[Fri89] Friedlander, B.
Sensitivity analysis of the maximum likelihood direction finding algorithm
Proc. 23rd Asilomar Conf. Signals Syst., Comput., pp.594-598, 1989

[Fri90] Friedlander, B.
A sensitivity analysis of the MUSIC algorithm
IEEE Trans. ASSP-38(10), pp.1740-1751, 1990

[Gab80] Gabriel, W. F.
Spectral analysis and adaptive array superresolution techniques
Proc. IEEE 68(6), pp.654-666, 1980

[Gab82] Gabriel, W. F.
Tracking closely spaced multiple sources via spectral estimation techniques
NRL Report 8603 pp.1-17, 1982

[GMW81] Gill, P.E., Murray, W., Wright, M.H.
Practical optimisation
Academic Press, London, 1981

[God89] Godara, L.C.
Beamforming in the presence of correlated arrivals
Y.T.Chan(ed.), Underwater Acoustic Data Processing, pp.345-349, 1989

[GP73] Golub, G.H., Pereyra, V.
The differentiation of pseudo-inverses and nonlinear least squares problems whose variables separate
SIAM J. Numer. Anal., Vol.10(2), pp.413-432, 1973

[GV80] Golub, G.H., Van Loan, C.F.
An analysis of the total least squares problem
SIAM J. Numer. Anal., Vol.17(6), pp.883-893, 1980

[GV83] Golub, G.H., Van Loan, C.F.
Matrix computations
The Johns Hopkins University Press, 1983

[Gri83] Griffiths, J.W.R.
Adaptive array processing : a tutorial
Proc. IEE Vol.130, Pt.F, pp.3-10, 1983

[Hog74] Hoghom, J.A.
Aperture synthesis with a non-regular distribution of interferometer baselines
Astron. Astrophys. Suppl., Vol.15, pp.417-426, 1974

[HXB90] Hoffman, M.W., Xu, X.L., Buckley, K.M.
Eigenspace based spatial-spectrum estimation for multiple beam antennas
Proc. ICASSP'90, pp.2671-2674, 1990

[JF85] Jeffries, D.J., Farrier, D.R.
Asymptotic results for eigenvector methods
Proc. IEE Vol.132, Pt.F, No.7, Dec., pp.589-594, 1985

[Joh82] Johnson, D.H.
The application of spectral estimation method to bearing estimation problems
Proc. IEEE Vol.70(9), pp.1018 - 1028, 1982

[JD82] Johnson, D.H., DeGraaf, S.R.
Improving the resolution of bearing in passive sonar arrays by eigenvalue analysis
IEEE Trans. ASSP-30(4), pp.638-647, 1982

[Kau75] Kaufman, L.
A variable projection method for solving separable nonlinear least squares problems
BIT 15-4, pp.49-57, 1975

[KB86] Kaveh, M., Barabell, A.J.
The statistical performance of the MUSIC and the minimum-norm algorithms in resolving plane waves in noise
IEEE Trans. ASSP-34(2), pp.331-341, 1986

[Kay84] Kay, S.M.
Accurate frequency estimation at low signal-to-noise ratio
IEEE Trans. ASSP-32(3), pp.540-547, 1984

[KM81] Kay, S.M., Marple, S.L. Jr.
Spectrum analysis - a modern perspective
Proc. IEEE Vol.69(11), pp.1380-1419, 1981

[KT83] Kumaresan, R., Tufts, D.W.
Estimating the angles of arrival of multiple plane waves
IEEE Trans. AES-19(1), pp.134-139, 1983

[KAR83] Kung, S.Y., Arun, K.S., Rao, D.V.B.
State-space and singular-value decomposition-based approximation methods for the harmonic retrieval problem
Journal of the Optical Society of America, Vol.73, Pt.12, pp.1799-1811, 1983

[KLF86] Kung, S.Y., Lo, C.K., Foka, R.
A Toeplitz approximation approach to coherent source direction finding
Proc. ICASSP'86, pp.193-196, 1986

[LH74] Lawson. C.L., Hanson, R.J.
Solving least squares problem
Prentice-hall, 1974

[LeC89] Le Cadre, J.P.
Parametric methods for spatial signal processing in the presence of unknown colored noise fields
IEEE Trans. ASSP-37(7), pp.965-983, 1989

[LW90] Lee, H. B., Wengrovitz, M. S.
Resolution threshold of beamspace MUSIC for two closely spaced emiters
IEEE Trans. ASSP-38(9), pp.1545-1559, 1990

[LW91] Lee, H.B., Wengrovitz, M.S.
Statistical characterization of the MUSIC null spectrum
IEEE Trans. SP-39(6), pp.1333-1347, 1991

[Lig73] Liggest, W.S.
Passive sonar: fitting models to multiple time series
NATO ASI on Signal Processing, pp.327-345, 1973

[Mar84] Martin, G.E.
Degration of angular resolution for eigenvector-eigenvalue (EVEV) high resolution processors with inadequate estimation of noise coherence
Proc. ICASSP'84, pp.19-21, 1984

[Mat89a] Mather, J.L.
Beamforming pre-processing for high discrimination algorithms
Royal signals and Radar Establishment memorandum 4304, 1989

[Mat89b] Mather, J.L
Characterisation of the Iterative Multi-Parameter (IMP) algorithm
Proc. IOA Vol.11, Part 8, pp.189-196, 1989

[MC85] Mather, J.L., Clarke, I.J.
Sequential processing of multiple data domains using SVD
Proc. IOA Vol.7(4), pp.9-15, 1985

[May88] Mayrargue, S.
ESPRIT and TAM are theoretically equivalent
Proc. ICASSP'88, pp.1456-2459, 1988

[Nic88] Nickel, U.
Algebraic formulation of Kumarensan-Tufts superresolution method, showing relation to ME and MUSIC methods
Proc. IEE Vol.135, Pt.F, No.1, pp7-10, 1988

[OS75] Oppenheim, A.V., Schafer, R.W.
Digital signal processing
Prentice-Hall, Inc., Englewood Cliffe, New Jersey, 1975

[Ott89] Ottersten, B.E.
Parametric subspace fitting methods for array signal processing
Ph.D dissertation, Department of Electrical Engineering, Stanford University, Stanford, CA 94305, 1989

[OK90] Ottersten, B., Kailath, T.
Direction-of-arrival estimation for wide-band signals using the ESPRIT algorithm
IEEE Trans. ASSP-38(2), pp.317-327, 1990

[ORK89] Ottersten, B., Roy, R., Kailath, T.
Signal waveform estimation in sensor array processing
Proc. 23rd Asilomar Conf. Signals Syst., Comput., pp.787-791, 1989

[OV88] Ottersten, B., Viberg, M.
Asymptotic results for multidimendional sensor array processing
Proc. 22nd Asilomer Conf. on Signal System & Computers, pp.833-837, 1988

[OV89] Ottersten, B., Viberg, M.
Analysis of subspace fitting based methods for sensor array processing
Proc. ICASSP'89, pp.2807 - 2810, 1989

[OVK89] Ottersten, B., Viberg, M., Kailath, T.
Asymptotic analysis of the total least squares ESPRIT algorithm
SPIE Vol.1152 Advanced Algorithms and Architectures for Signal Processing (4), pp.146-157, 1989

[OVK91] Ottersten, B.; Viberg, M., Kailath, T.
Performance analysis of total least squares ESPRIT algorithm
IEEE Trans. SP-39(5), pp.1122-1135, 1991

[OWVK89] Ottersten, B., Wahlberg, B., Viberg, M., Kailath, T.
Stochastic maximum likelihood estimation in sensor arrays by weighted subspace fitting
Proc. 23rd Asilomar Conf. Signals Syst., Comput., pp.599-603, 1989

[PRK85] Paulraj, A., Roy, R., Kailath, T.
Estimation of signal parameters via rotational invariance techniques - ESPRIT
Proc. 19th Asilomar Conf. on Circuits, Systems and Computers, pp.83-89, 1985

[PRK86] Paulraj, A., Roy, R., Kailath, T.
A subspace rotation approach to signal parameter estimate
Proc. IEEE Vol.74, pp.1044-1045, 1986

[PK86] Pauljar, A., Kailath, T.
Eigenstruture methods for direction of arrival estimate in the presence of unknown noise fields
IEEE Trans. ASSP-34, pp.13-20, 1986

[Pis73] Pisarenko, V.F.
The retrieval of harmonics from a covariance function
Geophys. J. R. Astr. Soc., Vol.33, pp.347-366, 1973

[PF88] Porat, B., Friedlander, B.
Analysis of the asymptotic relative efficiency of the MUSIC algorithm
IEEE Trans. ASSP-36(4), pp.532-544, 1988

[Pro95] Prony, G.R.B.
Essai Experimental et Analytique
Paris, J. de L'Ecole Polytechnique, Vol.1 cahier, 1795

[RH89a] Rao, B.D., Hari, K.V.S.
MUSIC and spatial smoothing: a statistical performance analysis
Proc. 23rd Asilomar Conf. Signals Syst., Comput., pp.935-939, 1989

[RH89b] Rao, B.D., Hari, K.V.S.
Performance analysis of root-MUSIC
IEEE Trans. ASSP-37(12), pp.1939-1949, 1989

[RH89c] Rao, B.D., Hari, K.V.S.
Performance analysis of ESPRIT and TAM in determining the direction of arrival of plane waves in noise
IEEE Trans. ASSP-37(12), pp.1990-1995, 1989

[RH89d] Rao, B.D., Hari, K.V.S.
Statistical performance analysis of the minimum-norm method
Proc. IEE Vol.36, Pt.F, No.3, pp.125-134, 1989

[Red79] Reddi, S.S.
Multiple source location - a digital approach
IEEE Trans. AES-15(1), pp.95-105, 1979

[Ris78] Rissaren, J.
Modeling by shortest data description
Automatica, Vol.14, pp.465-471, 1978

[Ris84] Rissaren, J.
A universal prior for the integer and estimation by minimum description length
Annals of Statistics, Vol.11, pp.417-431, 1984

[RLD87] Roberts, D.H., Lehar, J., Dreher, J.W.
Time series analysis with CLEAN.1 derivation of a spectrum
The Astronomical Journal, Vol.93(4), pp.968-989, 1987

[Roy87] Roy, R.
ESPRIT - estimation of signal parameters via rotational invariance techniques
Ph.D dissertation, Department of Electrical Engineering, Stanford University, U.S.A., Aug, 1987

[RGO89] Roy, R., Goldburg, M., Ottersten, B.
ESPRIT and uniform linear arrays
SPIE Vol.1152 Advanced Algorithms and Architectures for Signal Processing (4), pp.370-380, 1989

[RK87] Roy, R., Kailath, T.
Total least-squares ESPRIT
Proc. 21st Asilomar Conf. Circuits Syst. Computing. Monterey, CA, 1987

[RK89] Roy, R., Kailath, T.
ESPRIT - estimation of signal parameters via rotation invariance techniques
IEEE Trans. ASSP-37(7), pp.984-995, 1989

[RPK85] Roy, R., Paulraj, A., Kailath, T.
Comparative performance of ESPRIT and MUSIC for direction-of-arrival estimation
Proc. 20th Asilomar Conf. Circuits System & Computing, pp.580-584, 1985

[RPK86] Roy, R., Paulraj, A., Kailath, T.
ESPRIT - a subspace rotation approach to estimation of parameters of cisoids in noise
IEEE Trans. ASSP-34(5), pp.1340-1342, 1986

[RW80] Ruhe, A., Wedin, P.A.
Algorithm for separable nonlinear least squares problems
SIAM Review Vol.22(3), pp.318-337, 1980

[Sch79] Schmidt, R.O.
Mulitple emitter location and signal parameter estimation
RADC Spectrum Estimation Workshop, pp.243-258, 1979

[Sch81] Schmidt, R.O.
A signal subspace approach to multiple emitter location and spectral estimation
Ph.D Dissertation, Department of Electrical Engineering, Stanford University, U.S., 1981

[Sch78] Schwatz, U.J.
Mathematical-statistical description of the iterative beam removing technique (method CLEAN)
Astronomy & Astrophysics, Vol.65, pp.345-356, 1978

[SPK86] Shan, T.J., Paulraj, A., Kailath, T.
On smooothed rank profile tests in eigenstructure approach to directions-of-arrival estimation
Proc. ICASSP'86, pp.1905-1908, 1986

[SWK83] Shan, T.J., Wax, M., Kailath, T.
Spatial smoothing approach for location estimation of coherent sources
Proc. 17th Asilomar Conf. Circ. Syst. Comput., pp.367-371, 1983

[SWK85] Shan, T.J., Wax, M., Kailath, T.
On spatial smoothing for direction-of-arrival estimation of coherent signals
IEEE Trans. ASSP-33, pp.806-811, 1985

[Sha88] Sharman, K.C.
Maximum likelihood parameter estimation by simulated annealing
Proc. ICASSP'88, pp.2741-2744, 1988

[SDWK84] Sharman, K., Durrani, T. S., Wax, M., Kailath, T.
Asymptotic performance of eigenstructure spectral analysis methods
Proc. ICASSP'84 pp.45.4.1-45.4.4, 1984

[SM88] Sharman, K.C., McClurkin, G.D.
Estimating the parameters of correlated sources from arbitrary arrays - a simulated annealing solution
IEE Colloquium on "New Trend in Sensor Array Processing", pp.3/1-3/7, 1988

[Spe87] Speiser, J.M.
Some observations concerning the ESPRIT direction finding method
Proc. SPIE-826, Advanced Algorithms and Architectures for Signal Processing (2), pp.178-185, 1987

[SV84] Speiser, J.M., Van Loan, C.
Signal processing computations using the generalized singular value decomposition
Proc. SPIE on Real-Time Signal Processing Vol.495 Int. Symp., pp.47-55, 1984

[SN88] Starer, D., Nehorai, A.
Maximum likelihood estimation of exponential signals in noise using a Newton algorithm
Proc. 4th ASSP Workshop on Spectrum Estimations and Modeling, pp.240-245, 1988

[SN89] Stoica, P., Nehorai, A.
MUSIC, maximum likelihood, and Cramer-Rao bound
IEEE Trans. ASSP-37(5), pp.720-741, 1989

[SN90] Stoica, P., Nehorai, A.
MUSIC, maximum likelihood, and Cramer-Rao bound : further results and comparisons
IEEE Trans. ASSP-38(12), pp.2140-2150, 1990

[SN91] Stoica, P., Nehorai, A.
Performance comparison of subspace rotation and MUSIC methods for direction estimation
IEEE Trans. SP-39(2), pp.446-453, 1991

[SS90a] Stoica, P., Sharman, K.C.
Novel eigenanalysis method for direction estimation
IEE Proc. Vol.137, Pt.F, pp.19-26, 1990

[SS90b] Stoica, P., Sharman, K.C.
Maximum likelihood methods for direction-of-arraival estimation
IEEE Trans. ASSP-38(7), pp.1132-1143, 1990

[Str80] Strang, G.
Linear algebra and its applications
Academic Press, INC., 1980

[SOK89] Swindlehurst, A., Ottersten, B., Kailath, T.
An analysis of MUSIC and root-MUSIC in the presence of sensor perturbations
Proc. 23rd Asilomar Conf. Signals Syst., Comput., pp.930-934, 1989

[SRK89] Swindlehurst, A.L., Roy, R., Kailath, T.
Suboptimal subspace-fitting methods for multidimensional signal parameter estimation
SPIE Vol.1152 Advanced Algorithms and Architectures for Signal Processing (4), pp.197-208, 1989

[Tao89] Tao, K.M.
On generalized spatial smoothing method for coherent sources
Proc. 23rd Asilomar Conf. Signals Syst., Comput., pp.940-944, 1989

[Tew89] Tewfik, A.H.
Direction finding in the presence of colored noise
Proc. SPIE-1152 Advanced Algorithms and Architectures for Signal Processing (4),. pp.358-369, 1989

[UB75] Ulrych, T.J., Bishop, T.N.
Maximum entropy spectral analysis and autoregressive decomposition
Rev. Geophysics and Space Phys. Vol.13, pp.183-200, 1975

[Uri75] Urick, R.J.
Principles of underwater sound
McGraw-Hill Book Company, 1975

[Van76] Van Loan, C.F.
Generalizing the singular value decomposition
SIAM Journal of Numer. Anal., Vol.13, No.1, pp.76-83, 1976

[Van87] Van Loan, C.F.
A unitary method for the ESPRIT direction-of-arrival estimation algorithm
Proc. SPIE-826, Advanced Algorithms and Architectures for Signal Processing (2), pp.170-176, 1987

[VL89] Van Mierlo, G.W.M., Lenstra, A.J.
Spatial array processing by the method CLEAN
Y.T.Chan(ed.), Underwater Acoustic Data Processing, pp.367-372, 1989

[Vib89] Viberg, M.
Subspace fitting concepts in sensor array processing
Ph.D Dissertation, Department of Electrical Engineering, Linkoping University, S-581 83, Linkoping, Sweden, 1989

[VO91] Viberg, M., Ottersten, B.
Sensor array processing based on subspace fitting
IEEE Trans. SP-39(5), pp.1110-1121, 1991

[VOK89] Viberg, M., Ottersten, B., Kailath, T.
Direction-of-arrival estimation and detection using weighted subspace fitting
Proc. 23rd Asilomar Conf. Signals Syst., Comput., pp.604-608, 1989

[VOK91] Viberg, M., Ottersten, B., Kailath, T.
Detection and estimation in sensor arrays using weighted subspace fitting
IEEE Trans.SP-39(11), pp.2436-2449, 1991

[WB84] Wagstaff, R.A., Berrou, J.L.
A fast and simple nonlinear technique for high resolution beamforming and spectral analysis
J. Acoust. Soc. Am., 75(4), pp.1133-1141, 1984

[Wax85] Wax, M.
Detection and estimation of superimposed signals
Ph.D thesis, Stanford University, Stanford, CA, March, 1985

[WK83] Wax, M., Kailath, T.
Determining the number of signals by information theoretic criteria
Proc. ICASSP'83, pp.192-196, 1983

[WK85a] Wax, M., Kailath, T.
Extending the threshold of the eigenstructure methods
Proc. ICASSP'85, pp.556-559, 1985

[WK85b] Wax, M., Kailath, T.
Detection of signals by information theoretic criteria
IEEE Trans. ASSP-33(2), pp.387-392, 1985

[WZ88] Wax, M. & Ziskind, I.
Detection of fully correlated signals by the MDL principle
Proc. ICASSP'88 pp.2777-2780, 1988

[WZ89] Wax, M. & Ziskind, I.
On unique localization of multiple sources by passive sensor arrays
IEEE Trans. ASSP-37(7), pp.996-1000, 1989

[Wei82] Weiss, M.
Analysis of some modified cell-averaging CFAR processors in multiple-target situations
IEEE Trans. AES-18(1), pp.102-114, 1982

[WPMS88] Williams, R.T., Prasad, S., Mahalanabis, A.K., Sibul, L.H.
An improved spatial smoothing technique for bearing estimation in a multipath environment
IEEE Trans.ASSP-36(4), pp.425-432, 1988

[WZG+90] Wood, W.J., Zhang, J., Griffiths, J.W.R., Goodson, A.D., Payne, D.B.
A computer controlled beam plotter
Sonar Group Internal Report No.43, Loughborough University of Technolgy, 1990

[XB90] Xu, X.L., Buckley, K.M.
A comparison of element and beam space spatial-spectrum estimation for multiple source clusters
Proc. ICASSP'90, pp.2643-2646, 1990

[XBM90] Xu, X.L., Buckley, K.M., Marks, J.A.
CLOSEST spatial-spectrum estimation over the field-of-view of an abitrary array
Proc. EUSIPCO-90, 5th European Signal Processing Conference, Barcelona, Spain, pp629-632, 1990

[ZW88] Ziskind, I., Wax, M.
Maximum likelihood localization of multiple sources by alternating projection
IEEE Trans.ASSP-36(10), pp.1553-1560, 1988